ENTRANCE OF MONOMETHYLMERCURY INTO MARINE PHYTOPLANKTON AND MERCURY DYNAMICS AND ACCUMULATION IN THE FOOD WEB ALONG THE WEST ANTARCTIC PENINSULA

by

PHILIP TIGHE SONTAG

A dissertation submitted to the

School of Graduate Studies

Rutgers, The State University of New Jersey

In partial fulfillment of the requirements

For the degree of

Doctor of Philosophy

Graduate Program in Environmental Sciences

Written under the direction of

John Reinfelder

And approved by

_____

_____

_____

_____

New Brunswick, New Jersey

MAY 2018

ABSTRACT OF THE DISSERTATION

ENTRANCE OF MONOMETHYLMERCURY INTO MARINE PHYTOPLANKTON AND MERCURY DYNAMICS AND ACCUMULATION IN THE FOOD WEB ALONG THE WEST ANTARCTIC PENINSULA

By PHILIP TIGHE SONTAG

Dissertation Director:

John Reinfelder Ph.D.

Mercury (Hg) is a contaminant of global concern due to its volatile gas phase (Hg^0) and toxicity both in its inorganic (Hg^{2+}) and most importantly the organic form, monomethylmercury (MeHg), a developmental neurotoxin capable of crossing the blood brain barrier that increases in concentration at higher levels of marine food webs. Although the threat of MeHg upon exposure to humans is well known, knowledge of its behavior and accumulation in temperate marine ecosystems is in early stages of development and the accumulation of MeHg at the base of the West Antarctic Peninsula (WAP) food web lacks even baseline data. To assess the entrance of MeHg into marine food webs and subsequent accumulation and magnification of the toxin, cellular MeHg uptake rates were examined in temperate and polar marine phytoplankton cultures in artificial and natural seawater with varying concentrations of dissolved organic carbon (DOC). Along with lab incubations, Hg concentrations were measured in seawater,

particulate organic matter (POM), and juvenile and adult Antarctic krill (*Euphausia superba*) in coastal, shelf, and slope waters along the WAP, and Hg and stable carbon ($\delta^{13}C$) and nitrogen ($\delta^{15}N$) isotope ratios were measured in feathers of three *Pygoscelis* penguin species (Adélie-*P. adeliae*, gentoo-*P. papua*, and chinstrap-*P. antarctica*) breeding sympatrically near Anver's Island (~65°S).

Results showed that the maximum MeHg uptake rates in temperate (7.9 to 20.6 attmol/cell/hr) and Antarctic (14.3 to 249 attmol/cell/hr) marine phytoplankton were observed at low DOC concentrations. Methylmercury concentrations in northern (~65°S) WAP krill collected near Anver's Island were low (0.3 to 2.9 ng g^{-1}), while high and variable concentrations of dissolved (0.06 to 0.92 pM) and particulate (0.07 to 7.49 ng_{MeHg}/g_{totbio}) MeHg were measured at neighboring sites. Concentrations of total Hg (sum of inorganic and organic forms) and MeHg in northern WAP krill were significantly higher in juveniles than adults ($p < 0.005$ and $p < 0.001$, resp.). Mean concentrations of Hg in feathers were significantly ($p < 0.05$) higher in chinstrap (0.80±0.20 µg g^{-1}) than sympatric breeding Adélie (0.09±0.05 µg g^{-1}) and gentoo (0.16±0.08 µg g^{-1}) penguins. These findings suggest that the WAP ecosystem receives inputs of Hg from ocean water masses and potentially glacial meltwater. Although krill accumulate MeHg at low levels depending on developmental stage and location, such accumulation still has the potential to support much higher MeHg accumulation in WAP top predators.

Dedication

This work is only made possible as a gift given by

my Lord and Savior Jesus Christ. To my bride,

Alexandra Sontag, without her, these efforts would not have moved past infancy.

I look forward to our future research endeavors together.

Team Sontag!

Acknowledgements

I want to extend my heartfelt thanks to Dr. John Reinfelder for his continued counsel, wisdom, and financial support during the difficulties of graduate school. I am especially appreciative of his example of how to serve and love your spouse and want to replicate his sacrificial nature in my life. I will try to carry your creative thought and patience with me. Lastly, I am quite appreciative of all your underway measurements of total gaseous mercury during the 2014 LTER cruise, which contributed to a richer understanding of Hg in this ecosystem.

I extend sincere gratitude to:

My committee members Dr. Jeffra Schaefer, Dr. Nathan Yee, and Dr. Debbie Steinberg for their insight and willingness to serve on my committee and openness towards my research goals.

I am especially grateful to Dr. Jeffra Schaefer for her generosity in the lab both with knowledge and supplies, of which without this work would not be possible.

My labmates during graduate school, Cindy Wang, Xiaoshuai He, Youki Sato, Thomas Wang, and most importantly Sarah Janssen, who taught me more about analytical chemistry and professionalism in the lab than could ever be learned in a classroom.

All the undergraduate students who contributed substantially in work and thought to the success of this project including Avery Lee, Michael Acosta, Harold Ofori, and most

importantly Andrenette Morrison who's hard work and listening ear in the lab kept things sane during troubled times.

All involved in the Palmer-LTER research cruises including Dr. Debbie Steinberg for all the krill samples, Dr. Rob Sherrell for allowing us to sample WAP seawater for mercury, Dr. Jessica Fitzsimmons for compiling trace metal CTD data, all the marine technicians aboard the Lawrence M. Gould permitting us to sample sea ice, and Dr. Oscar Schofield for providing cruise berths in 2014 and 2015.

My mom, dad, sister, and brother for their emotional and financial support, and willingness to come visit here in New Jersey. Special thanks to my mother who babysat little Evelyn while mamá and papá went out into the Raritan Bay to sample.

Mi suegro Apostle Frank Garcia, suegra Lupe Garcia, and Billie Jean ("Tía-tí-tí") for unwavering faith and parenting Evelyn during the writing of this thesis.

Our Church family, especially pastor Scott Jones and Reid Monaghan from Jacob's Well-North Brunswick and other brothers and sisters for their relentless support and prayers creating a new family for us here in New Jersey.

Lastly but most importantly, my family, Alexandra and Evelyn, who are my heart and motivation by their love and faithfulness towards me.

Table of Contents

List of Tables

List of Figures

Chapter I Review of Literature

A. Chemistry, properties, and anthropogenic sources of mercury

Mercury (Hg) is a toxic metal with unique physical, chemical, and bioaccumulative properties separating itself from many other trace metals as a persistent and global contaminant in the geosphere and biosphere. Speciation of Hg in the environment is complex and highly contingent upon a suite of environmental factors. The major forms of Hg are its neutral, gaseous elemental (Hg(0)) species, its inorganic, largely aqueous and oxidized (Hg^{2+}) species, and monomethylmercury (MeHg) (Fitzgerald et al. 2007), the primary organic Hg species, which will be the primary focus of this research.

High industrial demands for Hg are due to it being a "soft" metal and because it has similar wavelengths for absorbance and fluorescence, a high affinity for organic carbon and other metals, and a non-zero vapor pressure. The heaviest of the naturally occurring transition metals, Hg exhibits solubility characteristics similar to the other metals in its group and other metals sharing its number of electron orbitals. Mercury's vapor pressure makes it a sought after resource, but also an environmental problem due to release during activities of coal combustion and small scale gold mining, the two highest producers of anthropogenic mercury emissions (Pacyna et al. 2010, Cordy et al. 2013, Krabbenhoft and Sunderland 2013, Selin 2014).

Global sites of Hg emission and regional, terrestrial deposits provide local and large-scale sources of mercury (Chakraborty et al. 2013, Corbitt et al. 2014, Soerensen et

al. 2014). Mercury is largely released into the troposphere in its elemental form, Hg^0, which is known to have a range of residence times, which can exceed one year (Lindberg et al. 2007, Drevnick et al. 2012). In the atmosphere, Hg^0 is transported globally and can be oxidized to Hg^{2+} through photochemical reactions and subsequently deposited to remote locations (Fitzgerald 1989, Shia et al. 1999, Driscoll et al. 2013). Although the ocean acts a net sink of Hg, emission of Hg^0 from surface waters of the ocean can play a significant role in the global Hg atmospheric budget (Soerensen et al. 2010a). Responses of global ocean basins to anthropogenic mercury vary across geographic regions (Sunderland and Mason 2007) and declines in atmospheric mercury may be observed in ocean water masses (e.g. North Atlantic) (Soerensen et al. 2010b, Soerensen et al. 2012). Declines of Hg in the water column of certain temperate coastal ecosystems have also been observed (Sunderland et al. 2010) showing the response of local ecosystems to regulatory control of mercury emissions, which may lead to decreased toxicity.

B. Mercury toxicity in natural systems and monomethylmercury (MeHg) exposure

Due to the ubiquitous presence of Hg in global ecosystems, and contributions from commercial (e.g., dental amalgam) and concentrated sources of mercury vapor (e.g., small-scale and artisanal gold mining) pathways of human exposure to inorganic Hg^{2+} and Hg^0 vapors are of great concern. Water soluble Hg^{2+}, a highly potent toxin, can cause collapse of kidney function, while the monoatomic Hg^0 gas when inhaled can be easily absorbed into the lung, crossing cell membranes and diffusing throughout body tissues.

Monomethylmercury (CH_3Hg^+, here referred to as MeHg) is the primary organic and neurotoxic form of Hg, which is able to cross the blood-brain barrier. MeHg is not normally produced commercially,but finds its exposure pathway through natural means. MeHg accumulates at the base of aquatic food webs and increases in concentration (biomagnification) with subsequent predator-prey transfers, reaching high concentrations in fish (Bloom 1992), the main route of human exposure (Mergler et al. 2007). The ability of MeHg to bioconcentrate in marine consumers is derived from its lipophilic nature and +1 valence charge, which favors the formation of a neutral inorganic complex (monomethylmercury chloride (CH_3HgCl)) in saline waters (Mason et al. 1996). Permeability of MeHg creates a multitude of adverse health effects in humans including loss of controlled body movement (ataxia), difficulty with speech (dysarthria), and impaired hearing (Grandjean et al. 2010). The severity of MeHg toxicity was prevalent in children and adults exposed to toxic levels through consumption of fish and shellfish in Minamata, Japan where thousands suffered severe neurological disorders (Harada 1995). The redistribution of MeHg within animals is due to its affinity for low molecular weight thiols (e.g. cysteine) in exposed individuals (Thomas and Smith 1982) and its ability to dissociate from these tightly-bound complexes, and absorb through stomach tissue in the lipid soluble CH_3HgCl form (Rabenstein and Evans 1978).

Toxicity of mercury in natural systems differs at varying levels of the food web. At the base, primary producers (phytoplankton), are sensitive to both dissolved Hg^{2+} and MeHg concentrations producing intracellular metal-binding peptides in response to acute exposure (Wu and Wang 2012), as observed previously in phytoplankton exposed to other trace metals (Morelli and Scarano 2001, Kawakami et al. 2006). Strong

extracellular chelators produced and exuded by marine phytoplankton have been shown to decrease the toxic form of metals in solution, with strong binding constants similar to complexing agents in the environment (Lee et al. 1996, Moffett and Brand 1996, Dupont et al. 2004). Intracellular reduction of Hg^{2+} to volatile Hg^0 is a detoxification mechanism in heterotrophic bacteria that is catalyzed by an enzymatic pathway (Barkay et al. 1991), but non-enzymatic Hg reduction is also exhibited by phytoplankton (Ben-Bassat and Mayer 1977, Mason et al. 1995, Kritee et al. 2017).

Biomagnification of MeHg is a worldwide phenomenon (Lavoie et al. 2013) and sensitive to changes in regional atmospheric deposition and freshwater sources over decadal time scales (Hammerschmidt and Fitzgerald 2006c, Cross et al. 2015). In fish, MeHg concentrates in muscle tissue (Bloom 1992), which can pose a risk to birds and mammal predators (Furness et al. 1986, Evers et al. 2007). Upper trophic level fish and predators, such as marine mammals have developed cellular responses such as the accumulation of selenium (Arai et al. 2004, Ikemoto et al. 2004, Burger and Gochfeld 2011) and metallothionein (Jakimska et al. 2011, Kehrig et al. 2015) in the muscle, liver, and kidney as detoxification mechanisms to mercury accumulation. Excretion of MeHg into feather plumage is another known mechanism employed by seabirds and penguins (Furness et al. 1986, Brasso et al. 2013). To understand the causes of MeHg accumulation in biota and subsequent exposure to humans a focus must be placed on its initial entry into the food web by examining MeHg formation, incidence, and accumulation in the water column.

C. Methylmercury formation and cycling in temperate marine ecosystems

Estuarine environments are characterized by a freshwater inputs, a shallow continental shelf, and reducing sediments due to high production of organic matter (McLusky and Elliott 2004). It is here in reducing sediment where the main production of MeHg occurs (Hammerschmidt and Fitzgerald 2006b, Hollweg et al. 2009). A two-gene cluster, hgcA and hgcB, encoding for a corrinoid protein and an Fe-S ferrodoxin, which act as a methyl carrier and electron donor, respectively, are needed for Hg methylation (Parks et al. 2013). The formation of MeHg from inorganic Hg^{2+} is facilitated primarily by sulfate-reducing bacteria within reducing sediments (Compeau and Bartha 1985, Gilmour et al. 1992). Although sulfate is of primary importance in marine sediments, iron-reducing bacteria (Kerin et al. 2006) and methanogenic bacteria (Wood et al. 1968) are also known to methylate mercury. For bacteria living in reducing sediment, increased bioavailability of Hg^{2+} bound to low molecular weight organic compounds (e.g., cysteine) is likely to increase methylation rates (Schaefer and Morel 2009). Simultaneous demethylation of MeHg is also known to occur in sediments, lowering the net formation of MeHg (Marvin-DiPasquale et al. 2000).

In coastal ecosystems, sediment has largely been thought of as a net sink for Hg^{2+} and possibly a net source of MeHg (Mason et al. 1999, Chen et al. 2008). Release of bound-methylmercury from sediments via sediment-water exchange has been identified (Hammerschmidt and Fitzgerald 2008), but its persistence in the water column and availability to the planktonic food web is uncertain. In the NE Atlantic, pelagic feeding fish have higher MeHg concentrations than those feeding in the benthos (Chen et al.

2009) and MeHg concentrations in pelagic seston (particles) has been found to predict MeHg concentration in fish (Chen et al. 2014) illustrating the importance of focused studies on water-column Hg dynamics and MeHg accumulation in the pelagic food web.

D. Mercury in the water column: light-mediated MeHg decomposition, Hg^{2+} reduction, and controls of speciation

Ecosystem responses to Hg loadings may vary but a common response of water column heterotrophic bacteria is the induction of the *mer* operon and increased activities of organomercurial lyase (MerB) and mercuric reductase (MerA) (Barkay et al. 1991, Schaefer et al. 2004). These enzymes catalyze the breaking of the bond between carbon and mercury in MeHg allowing for release of carbon as methane and further reduction of Hg^{2+} to elemental mercury by (Barkay et al. 2003). Abiotic removal of Hg is another key process controlling its cycling in pelagic ecosystems where visible and UV light penetration are important regulators of surface concentrations of dissolved Hg^0 (DEM). Photoreduction of Hg^{2+} allows for the re-release of recently deposited atmospheric mercury (Nriagu 1994, O'Driscoll et al. 2006a) an active component of mercury cycling in coastal marine ecosystems (Rolfhus 1998) and within the marine boundary layer (Soerensen et al. 2010a). These processes dictate the global Hg cycle and

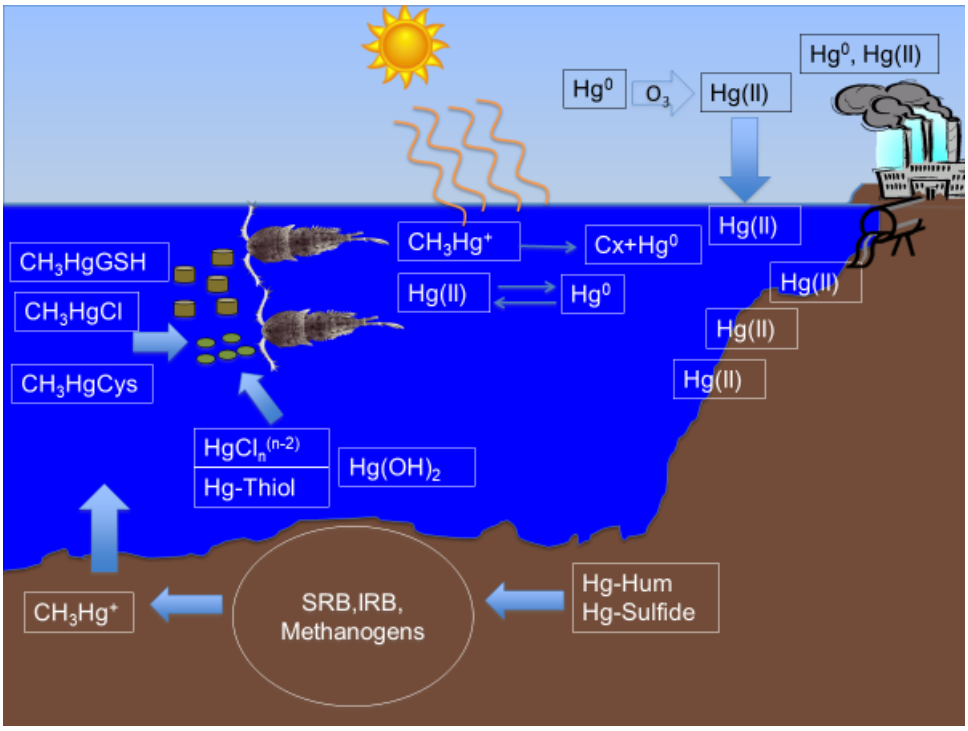

Figure 1.1 Mercury cycling and accumulation in temperate coastal ecosystems. Derived from Gilmour et al. 1992, Krabbenhoft and Sunderland 2013, Mason et al. 1996, Lawson and Mason 1998, Lindberg et al. 2007, Hammerschmidt and Fitzgerald 2006a, Kerin et al. 2006, O'Driscoll et al. 2006, and Hollweg et al. 2009

specifically local Hg budgets in marine ecosystems, allowing for subsequent speciation and accumulation in the pelagic food web (Figure 1.1). Organic matter (OM) complexation of Hg^{2+} and MeHg may inhibit or enhance the kinetics of mercury cycling in pelagic ecosystems. Photoreduction of Hg^{2+} is controlled by the ratio of Hg to dissolved organic carbon (DOC) (Zheng and Hintelmann 2009b) and binding to low molecular weight ligands (Zheng and Hintelmann 2009a). Photodegradation or photodecomposition of MeHg differs between lakes (Sellers et al. 1996, Hammerschmidt and Fitzgerald 2006d, Lehnherr and Louis 2009) and coastal marine systems (Whalin et al. 2007) and is thought to be dictated by MeHg speciation and dominant complexes formed with freshwater organic ligands and the neutral CH_3HgCl complex in marine ecosystems (Zhang and Hsu-Kim 2010).

E. Importance of DOC on MeHg binding and uptake at the base of the pelagic food web

Dissolved organic carbon (DOC) in pelagic ecosystems affects speciation and availability of dissolved trace metals (Ndung'u et al. 2003, Biller and Bruland 2012). Mercury is no exception has a high affinity for natural dissolved organic matter (DOM) and humic acids from coastal ecosystems (Benoit et al. 2001, Amirbahman et al. 2002). With some exceptions seen in contrasting water bodies (Pickhardt and Fisher 2007), increasing DOC concentrations in freshwater ecosystems decrease MeHg uptake in phytoplankton (Gorski et al. 2003, Luengen et al. 2012) and accumulation, biomagnication at the base of aquatic food webs (Watras et al. 1998). Similar trends are observed in marine systems where modeled MeHg concentrations have reproduced measured phytoplankton MeHg enriched in low DOC, ultraoligotrophic conditions of the

open ocean (Schartup et al. 2018). Removing estuarine DOC via UV oxidation increased MeHg internalization in a coastal diatom *Thalassiosira psuedonana* by more than a factor of two (Zhong and Wang 2009). Varying types of DOC may have different effects on MeHg accumulation in marine phytoplankton. Terrestrial organic matter decreased the fraction of MeHg accumulation with increasing concentration relative to marine DOC, where accumulation percentage was consistently higher at the same concentration range (Schartup et al. 2015b). Due to the affinity of MeHg for various functional groups composing natural DOM, especially thiols (containing reduced sulfhydryl groups) (Loux 2007), the availability of these complexes to phytoplankton cells needs to studied.

Concentrations of thiols are lower in coastal systems (≤1 nM), most noticeably near freshwater discharge (Al-Farawati and van den Berg 2001, Tang et al. 2004), than in the open ocean (1-10 nM) in regions of high *chlorophyll a* and oxygen concentrations (Dupont et al. 2006, Swarr et al. 2016). Thiol interactions with trace metals depend on a number of environmental factors including salinity. For example, the apparent stability constants of Cu-thiol complexes decreased with increasing salinity (Laglera and van den Berg 2003), suggesting that thiols were outcompeted by inorganic ligands in more saline waters.

Affinities of dissolved MeHg for inorganic and organic complexes in solution dictates its speciation and potential availability in fresh and saltwater (Loux 2007). Much focus has been placed on the binding of MeHg to the dominant inorganic hydroxide (OH^-) and chloride (Cl^-) and organic thiol complexes, namely cysteine (CYS) and glutathione (GSH) (Rabenstein and Evans 1978, Alderighi et al. 2003) (Table 1.1).

Table 1.1 Apparent binding constants for dominant inorganic and organic ligands and MeHg in seawater

Equation	Log K_{app}	Reference
$CH_3Hg^+ + OH^- \leftrightarrow CH_3HgOH$	9.23	National Institute of Standards and Technology
$CH_3Hg^+ + Cl^- \leftrightarrow CH_3HgCl$	5.18	National Institute of Standards and Technology
$CH_3Hg^+ + CYS^{2-} \leftrightarrow CH_3HgCys^-$	16.60	Alderighi et al. 2003
$CH_3Hg^+ + GSH^{2-} \leftrightarrow CH_3HgGSH^-$	15.70	Rabenstein 1978

My dissertation will aim to assess the bioavailability of MeHg in marine phytoplankton cultures using uptake of the dominant inorganic complex in seawater, monomethylmercury chloride (CH_3HgCl) and an organic ligand complex, monomethylmercury cysteine (CH_3HgCys^-) at varying DOC concentrations. To the best of our knowledge uptake of MeHg has not been studied in polar phytoplankton. Thus uptake experiments with two species of Antarctic phytoplankton will be used to examine possible differences between temperate and polar taxa. These data will be used to provide insight into future examination of MeHg accumulation at the base of Antarctic food webs.

F. Mercury in polar environments and the WAP marine ecosystem

Polar marine ecosystems are distinct from temperate environments as polar regions are removed from local anthropogenic contaminantion and are highly variable seasonally in regard to productivity and surface water dynamics influenced by sea ice conditions. In the Arctic, there is no focal land mass and perennial sea ice exists but is continually being replaced by younger, first-year sea ice (Stein et al. 2017). Southern Ocean dynamics and forcing are dictated by the continental land mass and the Antarctic Circumpolar Current (ACC), which is responsible for horizontal and vertical mixing of all marine waters around the continent. Most of Antarctica's sea ice is created and undergoes melting and retreat each austral year (Knox 2007).

Although Arctic ecosystems are considered sensitive to atmospheric Hg concentrations (Macdonald and Loseto 2010) and future changes due to climate (Stern et al. 2012b), the West Antarctic Peninsula (WAP) may also be a Hg sensitive region and

future monitoring efforts should be considered. Polar ecosystems experience higher net deposition of Hg during springtime atmospheric Hg depletion events (AMDE) where photo-oxidation of the halogens chlorine and bromine lead to thermal oxidation of Hg^0 in the atmosphere (Schroeder et al. 1998, Ebinghaus et al. 2002, Skov et al. 2004, Steffen et al. 2008). Enhanced deposition of Hg in a terrestrial ecosystem was observed along the coast of the Ross Sea, Antarctica (Bargagli et al. 2005), but it is unclear why AMDEs would deposit more Hg nearshore in Antarctic environments following the retreat of annual sea ice exposing areas further offshore first. Anomalously high concentrations of reactive gaseous mercury (RGM) and gaseous elemental mercury (GEM) occur in the atmospheric marine boundary layer near the WAP relative to global values (Soerensen et al. 2010a). Very high concentrations of halogens have been measured in the marine boundary layer at sites near the Antarctic coastline (Saiz-Lopez et al. 2007) and the occurrence of winter depletion events near leads in sea ice (Mastromonaco et al. 2016), suggest more consistent (year-long) sources of mercury deposition near ice and ocean surfaces, which may contribute to high Hg concentrations.

Lacking riverine discharge, a shallow continental shelf, and strongly reducing sediments, continental shelf waters of the West Antarctic Peninsula (WAP) provide a distinct marine habitat lacking conditions typical of temperate or tropical estuaries. Glacial meltwater provides freshwater that can lead to the stratification of surface waters and trigger coastal blooms in the austral summer (Henley et al. 2017). The WAP is a sea ice driven ecosystem, where yearly sea ice conditions drive primary production and recruitment of krill (Saba et al. 2014). The ACC flows in a clockwise direction around the Antarctic continent, mixing newer surface water with older deeper water, known as

Circumpolar Deep Water (CDW), which is drawn from other ocean basins. CDW carries heat, nutrients, and low oxygen (Moffat et al. 2009), and may intrude onto continental shelves via deep canyons associated with complex bottom bathymetry (Martinson and McKee 2012). In this region layering of water masses is primarily driven by salinity as higher temperature CDW forms at intermediate water depths (250-1000 m) below cooler surface waters (Pardo et al. 2017), in contrast to temperature-driven density stratification of the surface mixed layer in other ocean basins.

Circumpolar Deep Water represents a possible source of MeHg to the continental shelf west of the Antarctic Peninsula, but may also be a site of MeHg production, which has been documented in hypoxic marine water columns (Lehnherr et al. 2011). The usual sources of MeHg do not exist in a productive marine ecosystem with a well-mixed and oxygenated water column and weakly reducing sediments (Hartnett et al. 2008), creating a distinct opportunity for alternative pathways of mercury cycling and MeHg production (Figure 1.2).

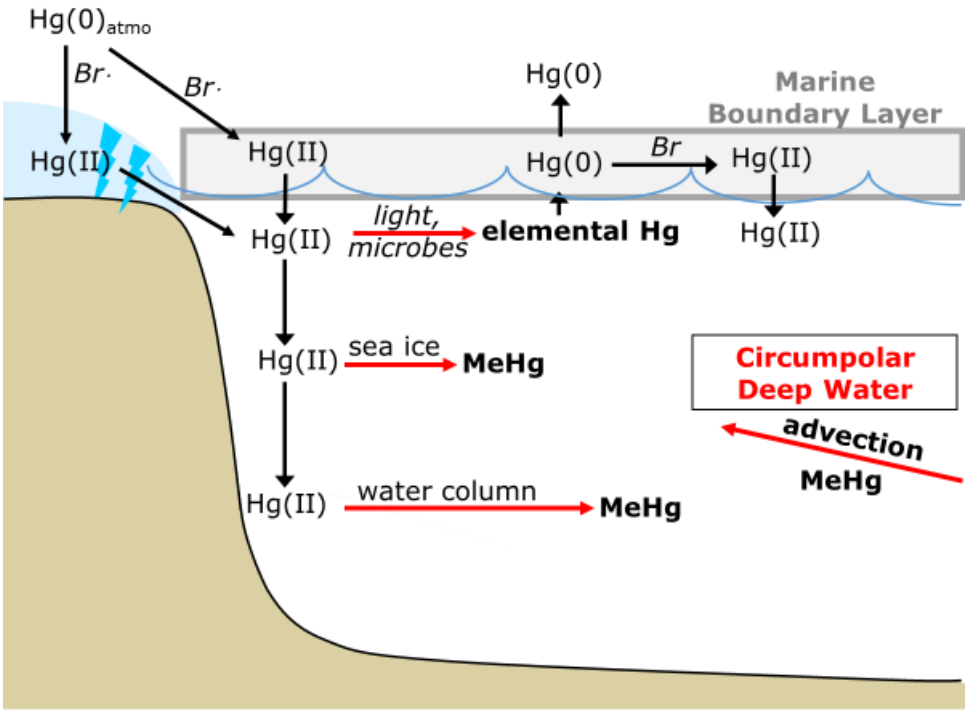

Figure 1.2 Mercury cycling along the WAP. Derived from Ebinghaus et al. 2002, Bargagli et al. 2005, Saiz-Lopez et al. 2007, Gionfriddo et al. 2016, and Mastromonaco et al. 2016.

In recent decades the WAP has become a region undergoing constant changes to its physical environment and pelagic food web (Steinberg et al. 2012). Retreat of glacier fronts and thinning of ice shelves along the Peninsula have been attributed to atmospheric warming (Scambos et al. 2004, Pritchard and Vaughan 2007), but the rapid receding of the majority of glaciers suggests an additional heat source (Cook et al. 2005). Recent studies link locations of higher temperature CDW to glacier retreat as ice shelves terminate in these regions indicating ocean forcing as the main driver in glacier loss along the WAP (Cook et al. 2016). Melting of glaciers may release stored past depositions of atmospheric Hg (Schuster et al. 2002) and may release significant amounts of this Hg and methylated Hg to the WAP coast as seen during the spring freshet in Arctic ecosystems (Loseto et al. 2004, St Louis et al. 2005, Zdanowicz et al. 2013, Douglas et al. 2017). Spring and summer melt of seasonal sea ice may also provide an input of Hg to surface waters, as seen with iron (van der Merwe et al. 2011).

Complex hydrography, a simple food web structure, and a short productive season during times of sea ice retreat make this ecosystem highly susceptible to global and regional warming. Studying shifts in food web structure, using the incidence and accumulation of chemical biomarkers is needed to document ecosystem responses as physical controls on climate continue to fluctuate along the WAP.

G. Structure of the base of the West Antarctic Peninsula (WAP) food web

Positive anomalies in phytoplankton abundance in the coastal WAP are driven by physical and ocean forcing during negative phases of the southern annual mode SAM (Saba et al. 2014). Abundance of WAP zoolplankton was found to be linked to SAM and

Multivariate El Nino Southern Oscillation Index (MEI) (Steinberg et al. 2015). Primary productivity and subsequent transfer of carbon and energy from the base of the WAP food web to top level consumers is primarily through consumption of macrozooplankton (Steinberg et al. 2015) as fish populations are lacking off the WAP (Barrera-Oro 2003). In constrast, food webs with a greater variety of mid-level consumers in pelagic, nearshore, sea ice, and benthic compartments are found in the Arctic Ocean (Douglas et al. 2011). Along the WAP, diatoms dominate phytoplankton assemblages with contributions from cryptophytes and mixed flagellates (Schofield et al. 2017). There exists a highly coupled, but complex relationship between WAP phytoplankton and microbial production despite low activities of planktonic bacteria during the productive austral summer (Ducklow et al. 2012).

Antarctic krill (*Euphausia superba*) are a keystone macrozooplankton species essential for carbon and energy transfer from WAP phytoplankton to upper trophic levels. *E. superba* show positive anomalies about every five years, but no significant decadal trends, and are most abundant in coastal and shelf stations with a spatial separation between them and the gelatinous *Salpa thompsoni* (salps), which are found along the slope in low ice conditions (Ross et al. 2008, Steinberg et al. 2015). The morphologically analogous ice krill (*Euphausia crystallorophias*), occupy the coastal habitat with *E. superba* but are vertically segregated (Daly and Zimmerman 2004). Other abundant pelagic crustaceans in the WAP include the smaller krill species *Thysanoessa macrura*, which is increasing in the northern WAP, along with amphipods and copepods (Steinberg et al. 2015). Other abundant species of zooplankton include free floating pteropods

(pelagic snail), *Limacina helicina*, carnivorous polychaete worms *Tomopteris spp.*, amphipods, and chaetognaths such as *Pseudosagitta sp.* (Steinberg et al. 2015).

Development is essential to understanding the heterogeneity of Antarctic krill along the WAP. A mixotrophic species, Antarctic krill consume primarily phytoplankton but will graze on micro- to macrozooplankton (Martin et al. 2006). Possible ontogenetic niche expansion in diet may occur during development between juvenile and adult stages (Polito et al. 2013) and suggests the importance for delineating bulk sources of krill prey and potential trophic level during krill development. Studying differences in krill development is essential to understanding krill recruitment and future stocks of Antarctic krill. During the harsh first overwintering where water column productivity is low, a significant period during krill development and potential recruitment into adulthood, larval and juvenile krill may be associated with the under-sea ice environment (Daly 1990, 2004). However, a recent study shows the winter pack-ice zone as shelter and marginal sea ice zone as the predominant food source for developing krill (Meyer et al. 2017). Large spatial differences in krill distributions exist with cross-shelf patterns of larger krill located offshore of smaller individuals (Lascara et al. 1999). Krill development begins offshore where spawning females release eggs along the continental shelf and slope that sink to mesopelagic waters (Daly and Zimmerman 2004) known to be sites of remineralization of organic matter and enriched source of dissolved metals, including Hg as discussed above providing a site of early Hg exposure.

H. Use of light stable isotopes (δ^{13}C and δ^{15}N) to identify feeding location and strategies of Antarctic Krill and *Pygoscelis* penguins along the WAP

Stable isotope signatures of carbon (ratio of ^{13}C to ^{12}C) and nitrogen (ratio of ^{15}N to ^{14}N) relative to a known standard have been traditionally been used to identify prey source (or sources) and trophic position, respectively, with a well understood isotopic baseline (Post 2002). Primary producers, phytoplankton, are normally the base of any pelagic food web and traditionally used as an isotopic baseline (Trophic Level (TL) = 1) in aquatic systems (Minagawa and Wada 1984, Post 2002, McCutchan et al. 2003). In the open ocean and polar marine ecosystems, phytoplankton and particulate organic matter (POM) are known to take on large variability in δ^{13}C and δ^{15}N values over small scales during reduced carbon and organic matter formation (Rau et al. 1982, Rau et al. 1991, Gillies et al. 2012b). Ecological studies reveal variation in δ^{13}C and δ^{15}N values within and between seabirds and penguins (Cherel et al. 2005, Tierney et al. 2008, Polito et al. 2011a) necessitating alternative baselines for normalization. This has led to the use of a primary consumer, thought to have integrated variation in δ^{13}C and δ^{15}N values of POM over spatial scales in order to calculate trophic levels of seabirds to complement monitoring studies of metal concentrations in top level predators (Brasso and Polito 2013, Brasso et al. 2015).

Timescales of intrinsic biomarkers such as δ^{13}C and δ^{15}N values and Hg vary and are dependent on sampled tissue (Ramos and Gonzalez-Solis 2012). In the WAP, most abundant top-level predators are *Pygsocelis* penguins, which include Adélie (*P. adeliae*), gentoo (*P. papua*), and chinstrap (*P. antarctica*) species. *Pygoscelis* in the WAP feed predominantly on krill (Trivelpiece et al. 1987), but fish (*Pleuragramma antarcticum* and

myctophids (lanternfish)) can also comprise a significant portion of their diet in northern regions of the WAP (Polito et al. 2011b). These three penguin species breed sympatrically on Anver's Island, near the U.S. Palmer Research Station, at the more northern reaches of the Palmer Antarctica Long-Term Ecological Research (PAL LTER) study region. *Pygoscelis* penguins have varying foraging strategies (Miller et al. 2010) and are known to excrete $\delta^{13}C$ and $\delta^{15}N$ into their feathers during growth. This suggests that these $\delta^{13}C$ and $\delta^{15}N$ values are indicative of a bird's diet during the time period following the previous catastrophic moult (Stonehouse 1967) as feather keratin tissue is inert after synthesis (Pearson et al. 2003). These variables need to be considered when evaluating penguin feather $\delta^{13}C$ and $\delta^{15}N$ values and mercury concentrations. For this study, $\delta^{13}C$ and $\delta^{15}N$ values were used primarily to characterize feeding strategies (epipelagic, mesopelagic, and benthic) and possible differences in foraging locations along with a correction of $\delta^{15}N$ values to POM values to determine a relative trophic position.

Values of $\delta^{13}C$ and $\delta^{15}N$ in Antarctic krill were mainly used to assess developmental differences in foraging locations of juvenile and adult co-populations as previous studies have shown spatial differences in larval krill $\delta^{13}C$ values near our WAP study area (Frazer 1996). Longitudinal and latitudinal differences in $\delta^{13}C$ values of WAP particulate organic matter were also assessed as POM $\delta^{13}C$ values in proximity to Anver's Island tended to differ from offshore samples (Mincks et al. 2008). Prey source may also contribute to $\delta^{13}C$ and $\delta^{15}N$ values as sea ice POM isotope ratios deviate from surface POM in Antarctic seawater (Gillies et al. 2012a). In this study, corrected $\delta^{15}N$

values of Antarctic krill to POM were used to estimate trophic enrichment factors and its relevance to mercury concentrations.

I. Bioaccumulation and biomagnification of MeHg in Antarctic Krill and *Pygoscelis* penguins along the WAP

Heavy metal accumulation has been observed (Bargagli 2001) along with THg accumulation in Antarctic Krill (Honda et al. 1987, Yamamoto et al. 1987), largely composed of inorganic Hg^{2+}, which can be taken up from the water column (Wright et al. 2010). These findings highlight the importance of measuring MeHg concentrations in Antarctic krill as this is the form most efficiently accumulated from prey (Mason et al. 1996). Additionally, MeHg has been shown to increase with a trophic magnification factor of approximately 8.7 in an Arctic food web (Ruus et al. 2015) suggesting the potential for MeHg biomagnification in polar ecosystems to exceed those at lower latitudes (Al-Reasi et al. 2007, Kim et al. 2012).

MeHg in Antarctic krill may come from a variety of sources and be linked to differences in spatial (latitude, distance from shore) distributions and grazing depth. Evaluation of MeHg accumulation in Antarctic krill should consider POM and seawater MeHg concentrations. Large variation in MeHg accumulation in surface POM (Gosnell and Mason 2015) and in vertical distributions of dissolved and particulate MeHg concentrations (Hammerschmidt and Bowman 2012) emphasize the need to consider MeHg accumulation at various depths in the water column. Subsequent transfer of MeHg in phytoplankton to zooplankton and higher trophic level predators can be tracked using assimilated $\delta^{13}C$ and $\delta^{15}N$ values in biota to complement Hg concentrations (Figure 1.3).

A variety of seabirds and penguins accumulate heavy metals (Nygard et al. 2001, Metcheva et al. 2006) and mercury (Furness et al. 1986, Thompson et al. 1998, Carravieri et al. 2013) in their feathers. Near the Antarctic Peninsula, *Pygoscelis spp.* penguins accumulate lower concentrations of Hg in their feathers than those foraging in the South Shetland Islands and Terra Nova Bay in the Ross Sea (Brasso et al. 2015). High Hg concentrations have been measured in the Antarctic prion of the Southern Ocean (Hindell et al. 1999) suggesting potential for high accumulation from prey. A preliminary evaluation of Hg concentrations in *Pygoscelis* penguins near Anver's Island and MeHg and THg concentrations in Antarctic Krill at northern and southern latitudes was conducted to determine bioaccumulation potential of MeHg in the WAP ecosystem.

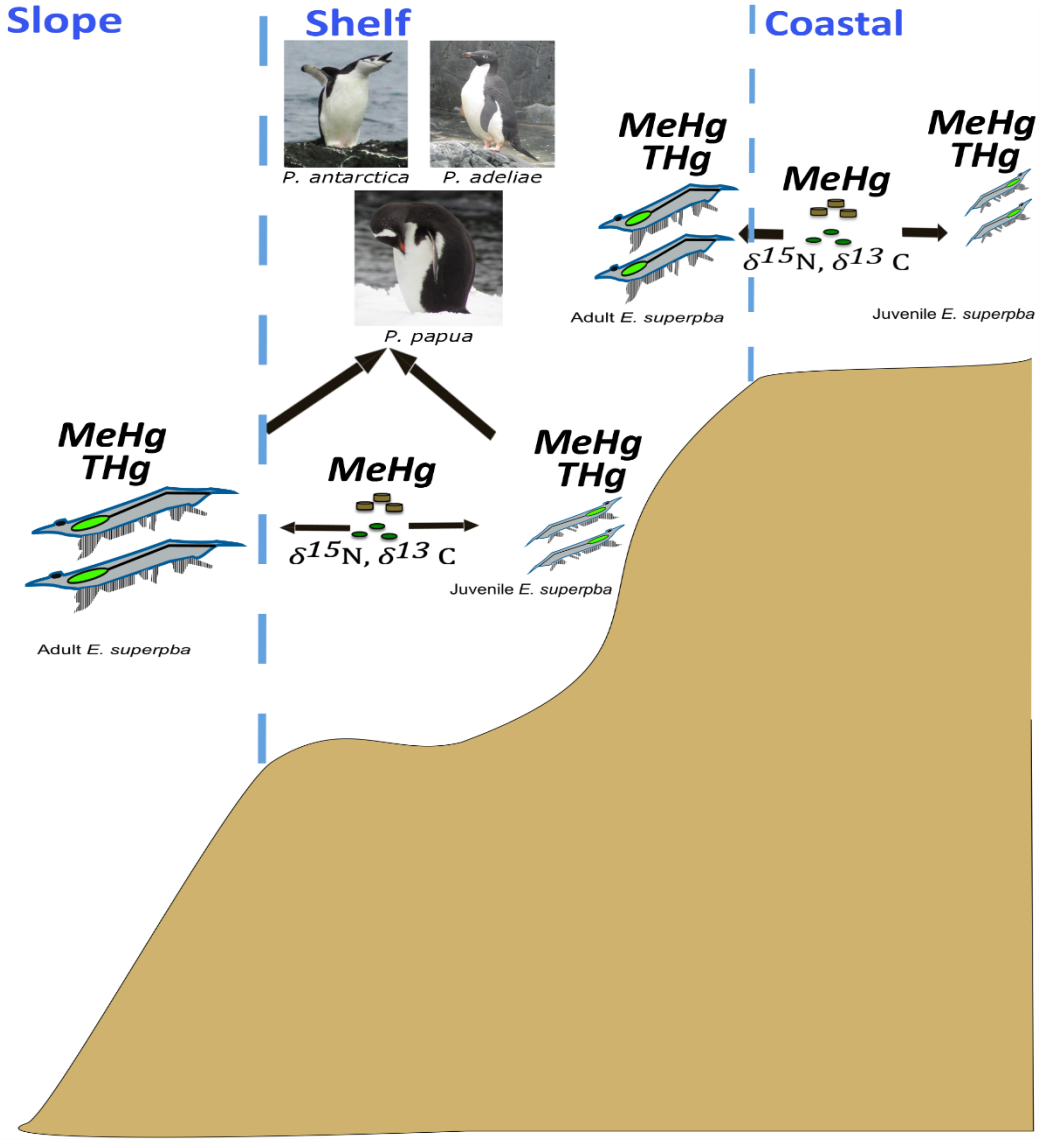

Figure 1.3 Assimilation of δ^{13}C and δ^{15}N values and accumulation of Hg in POM, juvenile and adult Antarctic krill, and *Pygoscelis* penguins along the WAP

J. Conclusions

Mercury is a persistent, global contaminant due to its worldwide use and high in industrial and mining activities resulting in release of anthropogenic Hg primarily as a gas, and with local discharges of liquid waste. The toxicity of this element may occur through gaseous, liquid, and solid exposures with the most pathological form, MeHg, being a neurotoxin in humans, particularly during development. Destructive capabilities of MeHg to cells and living organisms is rooted in its ability to cross cell membranes and attach to functional groups of essential proteins needed for maintaining cell function and metabolism.

Inorganic and organic forms of mercury produce a variety of dose-dependent responses within individual cells and throughout tissues of higher level organisms. These responses may sequester, reduce toxicity, or remove Hg from vital components of the cell or body, and in nature affect the metal's speciation and potential bioavailability. Studying the initial route of MeHg accumulation at the base of the pelagic food web is necessary to determine the ability of organisms to take up or sequester this contaminant and the response of microorganisms to MeHg exposure.

The uptake of MeHg by microorganisms is governed by a variety of factors. Formation, decomposition, and binding to natural organic matter will heavily influence the accumulation of MeHg at the base of the food web and will vary from freshwater to saltwater environments and across latitudes. The central role of DOC to mercury dynamics in pelagic ecosystems cannot be overstated. Binding of MeHg to natural DOC,

especially select functional groups (e.g. thiols), may influence the initial concentration at the base of the food web.

Environmental controls of polar and temperate ecosystems may drive differences in MeHg accumulation and biomagnification. Differences in water depth, bathymetry, hydrology, and light conditions should be considered when evaluating sources and movement of MeHg through an ecosystem. Food web structure plays an integral part in the bioaccumulation of MeHg and ongoing efforts to characterize complex food webs is important. Carbon and nitrogen stable isotopes (δ^{13}C and δ^{15}N) provide short-term tracers of food web structure. The WAP is a sensitive region experiencing great change due to ocean and atmospheric forcing. Documenting any trophic shifts in this environment is essential to understanding the regional food web.

Complementing short-term signals of δ^{13}C and δ^{15}N with Hg concentrations, which turnover more slowly, will help identify regions of high MeHg exposure. Pairing high resolution δ^{13}C and δ^{15}N values for baseline and consumer organisms will help shed light on the trophic transfer efficiency of MeHg following its initial enrichment from seawater at the base of the WAP and other polar food webs.

The overall goals of this dissertation were to establish compare uptake rates of MeHg in marine phytoplankton from temperate and polar environments and document the incidence and bioaccumulation of MeHg in POM, Antarctic krill, and *Pygoscelis* penguins along the continental shelf waters of the WAP ecosystem. These research goals were addressed in the following objectives:

1. Compare short- and long-term MeHg uptake rates in temperate and polar marine phytoplankton;
2. Examine the horizontal and vertical distributions of dissolved total Hg and MeHg, and the horizontal distributions of particulate MeHg in coastal and offshore sites along the WAP;
3. Evaluate total Hg and MeHg concentrations and $\delta^{13}C$ and $\delta^{15}N$ values in juvenile and adult Antarctic krill and three species of *Pygoscelis* penguins in the context of foraging location and strategy.

This work aims to determine key determinants of the entry of MeHg into marine food webs via phytoplankton, Hg incidence, speciation, and accumulation of MeHg in WAP polar shelf waters and MeHg bioconcentration in the keystone prey and predator species of the WAP.

Chapter II Influence of Dissolved Organic Carbon on Monomethylmercury Uptake in Temperate and Polar Marine Diatoms

2.1 Abstract

Entrance of monomethylmercury (MeHg) into global ocean food webs begins with the enrichment from the dissolved phase into phytoplankton, which may likely control MeHg concentrations at upper trophic levels in marine environments. Transport of MeHg into phytoplankton differs from other divalent metals as it is easily able to cross cell membranes due to its lipophilic nature and inorganic chemistry in seawater. The dominant inorganic complex of MeHg, monomethylmercury chloride (CH_3HgCl), can partition and be retained within a cell's cytosolic fraction–a process that may be largely controlled by cell size and cell surface composition. The presence of dissolved organic carbon (DOC) in seawater may compete with the dominant chloride ligand altering bioavailability and passive transport into the cell. These hypotheses regarding MeHg uptake were tested in 4 phytoplankton taxa, the temperate diatoms *Thalassiosira weissflogii* (*Tw*) and *Thalassiosira pseudonana* (*Tp*), the polar diatom *Chaetoceros brevis* (*C. brevis*), and the polar prymnesiophyte *Phaeocystis antarctica* (*Pa*). All four species were grown at varying background DOC concentrations in synthetic ocean water (DOC_{SOW}) at temperate and polar temperatures in short-term incubations with added DOC, and in long-term exposures using DOC produced by phytoplankton cells (DOC_{Cell}). Short-term methylmercury uptake in the temperate species was higher in the

smaller *Tp* than the larger centric diatom *Tw*, with a maximum uptake of 20.6 attomol $cell^{-1}$ hr^{-1} in low DOC seawater. Lowering DOC_{SOW} concentration in short-term exposures resulted in increases of MeHg uptake in all polar and temperate diatom species ranging from 2.5-fold (*Tw*) to an order of magnitude (*Tp*). DOC_{Cell} produced by *Tw* cells in long-term experiments resulted in slower but sustained uptake of MeHg over a 24 h period, suggesting that DOC_{Cell} may alter MeHg speciation. Within (centric) diatom species there was a strong relationship between MeHg uptake rates and cell surface area-to-volume ratios (SA/V) at low DOC concentrations. The highest MeHg uptake rates (249 attomol $cell^{-1}$ hr^{-1}) and normalized uptake amongst all taxa was measured in free-living cells of the polar prymnesiophyte *Phaeocystis antarctica*. These findings emphasize the importance of cell surface composition and size in the uptake of MeHg in open ocean waters and the influence of DOC on inhibiting MeHg uptake across temperate and Antarctic phytoplankton taxa. These baseline uptake rates should be considered when evaluating enrichment of MeHg at the base of pelagic food webs especially the high potential for MeHg uptake in Antarctic phytoplankton species.

2.2 Introduction

Monomethylmercury (MeHg), the dominant and most persistent organic mercury species in the environment (Fitzgerald et al. 2007), is a persistent global contaminant in aquatic and marine ecosystems (Lavoie et al. 2013), and is a developmental neurotoxin in humans (Clarkson and Magos 2006, Grandjean et al. 2010). Production of MeHg from the methylation of inorganic mercury (Hg^{2+}) largely occurs in anaerobic sediments (Hammerschmidt and Fitzgerald 2006b, Hollweg et al. 2009, Schartup et al. 2013), but MeHg may also be formed in biologically active regions of the marine water column

(Lehnherr et al. 2011, Hammerschmidt and Bowman 2012). The concentration of MeHg increases as it is transferred from ecosystem compartments to biota where it continues to increase with subsequent transfers within the food web (Bloom 1992) to potentially harmful levels in upper trophic level vertebrates (Monteiro and Furness 1995, Evers et al. 2007), including humans (Sunderland 2007). The accumulation of MeHg at the base of freshwater and marine food webs is greatly influenced by a water body's aquatic chemistry (Watras and Bloom 1992), particularly the concentration and composition of dissolved organic carbon (DOC) (Lavoie et al. 2013, Schartup et al. 2015a, Schartup et al. 2018).

Phytoplankton are the primary route of entry for MeHg into aquatic and marine food webs and the compartment in which the greatest enrichment of MeHg occurs (Hammerschmidt and Fitzgerald 2006a, Pickhardt and Fisher 2007, Gosnell and Mason 2015, Lee and Fisher 2016). High concentration factors of MeHg in phytoplankton (10^4 to 10^6) are due to the ability of MeHg to cross phytoplankton cell membranes and be retained within the cytosol (Lawson and Mason 1998), whereas inorganic mercury (Hg^{2+}) remains largely attached to cell membranes (Pickhardt and Fisher 2007). Methylmercury chemistry dictates these events as the dominant inorganic complex of MeHg in seawater, MeHgCl, is neutral, lipophilic, and has a higher octanol-water partitioning coefficient than $HgCl_2$ (Mason et al. 1996). Partioning of MeHg into cytosolic fraction increases bioavailability of this compound to higher trophic levels as it has been found to have higher assimilation in copepod zooplankton (Mason et al. 1996). Defining cellular concentrations of Hg is difficult as it includes loosely-bound, tightly-

bound, and intracellular fractions that are defined operationally using various cell-surface wash techniques (Kumar et al. 2002, Schaefer et al. 2011)

The uptake and concentration of MeHg in various species of marine phytoplankton varies with cell surface area-to-volume ratios (SA/V), but is largely independent of seawater temperature consistent with the passive diffusion uptake of MeHgCl (Lee and Fisher 2016, Schartup et al. 2018). Temperature did exhibit a species-specific effect on MeHg uptake in a marine dinoflagellate *Prorocentrum minimum* (Lee and Fisher 2016) suggesting temperature may influence phytoplankton cells differently. Passive uptake may be most pronounced amongst smaller cell sizes where SA/V ratios are highest, however, transport channels may have higher densities per unit surface area of a cell membrane in small cells. Larger cells have lower SA/V, higher per cell biomass, and increased membrane surface area with potentially lower density of bi-directional channels relative to smaller cells where MeHg could be released into the extracellular medium relieving toxic effects of MeHg within the phytoplankton cell. Passive and active MeHg pathways should be considered as previous heat treatment, γ-radiation, and inhibitor studies have lowered MeHg uptake rates suggesting an alternative route of active MeHg uptake (Moye et al. 2002, Pickhardt and Fisher 2007).

Physiological changes during cell growth and responses to trace metals of select phytoplankton taxa and biological morphology (e.g., cell wall structure) may also have an influence on MeHg accumulation and retention at similar SA/V, which was seen in the coccolithophore *Emiliania huxleyi* and chlorophyte *Dunaliella tertiolecta* (Lee and

Fisher 2016). Phytoplankton size and taxa may also be largely influenced by exposure concentration as lower MeHg exposures yield higher uptake rates (Moye et al. 2002).

Differences in regional temperature, light, and metal requirements of phytoplankton taxa could influence the uptake of MeHg if there is any overlap in channels that transport mercury and other trace metals into the cell. Macronutrients may limit phytoplankton growth in temperate estuaries, but polar diatoms may have high iron demands (Timmermans et al. 2001), which may affect MeHg uptake. During favorable conditions, phytoplankton blooms result in higher cell densities and which is known to decrease the concentration of MeHg per unit cell, a process called biodilution (Pickhardt et al. 2002). This is an important feature when considering rates of uptake in phytoplankton cells as initial uptake of MeHg may differ from long-term uptake rates based on fluctuating cell density with time, and the initial exposure concentration gradient following first-order principles (Gorski et al. 2003). Biomass of different phytoplankton species, chemical composition, cleanliness of experimental media (background DOC), and how phytoplankton may affect media composition after exposure to MeHg should be considered when conducting MeHg uptake studies. Phytoplankton exudates are one possible mechanism for altering MeHg chemistry as they contribute increasing proportions of DOC in higher salinity waters (Cuscov and Muller 2015), and are an abundant source of mercury-binding ligand in coastal environments (Lamborg et al. 2004).

In marine ecosystems, contributions to DOC pools includes inputs from rivers, remineralized particulate organic matter (POM), cell exudates, and DOC associated with zooplankton excretion as largely composed of less reactive components with a small

portion of bioreactive materials (Hedges 2002). Reduced sulfhydryl compounds, namely thiols, constitute an even smaller fraction of the bioreactive DOC and are known to have a strong affinity for MeHg in aqueous and biological systems (Rabenstein and Evans 1978, Loux 2007). Binding of dissolved MeHg to thiols, like cysteine, may influence the availability of MeHg and its subsequent concentration into phytoplankton cells (Luengen et al. 2012) with potentially varying contributions of thiols to MeHg availability at different DOC concentrations. At varying DOC concentrations, proportions of MeHg bound to inorganic neutral complexes shifting MeHg speciation slightly change contributions of passive and potentially active uptake based on MeHg bioavailability. Sequestration and subcellular distribution of MeHg within phytoplankton cells seems to also be dictated by intracellular thiols as their production is induced upon MeHg exposure (Wu and Wang 2011, 2012) and may influence internalization or export of MeHg in phytoplankton cells.

In this study, we examined short- and long-term uptake of MeHg in four marine phytoplankton species from temperate and polar environments. The removal of lab-generated DOC in synthetic ocean water (DOC_{SOW}) and its effect on the uptake of the MeHgCl complex was evaluated in efforts to establish baseline MeHg uptake rates in full salinity (low DOC) seawater in temperate and polar environments. The influence of temperature, temperate and polar phytoplankton taxa, and SA/V were assessed. To our knowledge this is the first study examining MeHg uptake in any polar diatom or prymnesiophyte phytoplankton species.

2.3 Materials and Methods

Phytoplankton Culturing

Four phytoplankton species were used to examine MeHgCl short-term uptake rates in synthetic ocean water (SOW): two temperate diatom species–*Thalassiosira weisflogii* (*Tw*) and *Thalassiosira pseudonana* (*Tp*), the polar marine diatom *Chaetoceros brevis* (*C. brevis*), and the polar prymnesiophyte *Phaeocystis antarctica* (*Pa*). Uptake rates of *Tw* and *Tp* in long-term exposures were also determined to provide context for future field studies. Supplemental additions of the thiol cysteine were used to determine the bioavailability and uptake of MeHgCys in comparison to the dominant inorganic complex in seawater at varying DOC_{SOW} levels.

All phytoplankton species were cultured in full strength Aquil media (Morel et al. 1979, Price et al. 1989) with temperate species grown at 18°C under a light:dark cycle (12 h:12 h, 100 µmol quanta m^{-2} s^{-1}) with daylight fluorescence lamps. Polar species were grown in 24h light at 4°C. All culture media was prepared in house using filtered (0.2 µm, Supor Membrane Disc) synthetic ocean water (SOW) (35 psu), which was passed through a column containing an ion exchange (chelex) resin before use in culturing and uptake experiments. Enrichments from chelexed nutrients (N, P, and Si), sterile filtered (0.2 µm, PTFE Acrodisc) vitamins (B_{12}, Biotin, Thiamine), and trace metals (Fe, Zn, Mn, Co, Cu, Mo, and Se) in a 5 µM ethylenediaminetetraacetic acid (EDTA) stock solution prepared separately were added in dilute concentrations (1/1000 (v/v)) to 250 mL of SOW to complete the Aquil media. Specific growth rates (in units of d^{-1}) of temperate and polar species were calculated using *in vivo* chl*a* fluorescence

measured with a handheld fluorometer. Cells were harvested for uptake experiments during late-exponential growth phase.

UV-oxidation of Synthetic Ocean Water

Laboratory prepared SOW was found to contain background levels of contaminant DOC (1.9 to 12 ppm) likely from bottles (phthalic acids) or from chelex (iminodiacetates). This background, lab-generated DOC (DOC_{SOW}) was removed by UV-oxidation of <150 mL volumes of SOW in PTFE bottles for 0.5 to 1.0 hr (Biller and Bruland 2012). UV-oxidized SOW was allowed to degas excess CO_2 overnight before use. UV-oxidation was repeated until <1 ppm of DOC_{SOW} was achieved before SOW was used as experimental media.

Methylmercury Exposure, Cell Wash, and Uptake Experiments

Short-term and long-term MeHg uptake experiments were performed using 10 nM of MeHg from a 1 mg L^{-1} standard solution (Brooks Rand) in 250 mL (short-term) and 500 mL to 1L (long-term) volumes of UV-treated SOW. Additions of 200 nM cysteine were made in selected treatments to evaluate bioavailability and short-term uptake of an organic MeHg complex. Methylmercury was allowed to equilibrate for ~2 hours to allow for the formation of MeHgCl or MeHgCys complexes prior to the addition of phytoplankton cells.

Subsamples of late-exponential phase phytoplankton cells were stained (Lugol's solution) and counted using a hemocytometer to determine culture volume needed to obtain cell densities of 10^4 cells mL^{-1} in experimental media. Filtered cells (1.0 µm, 47 mm Polycarbonate Membrane filter) were washed three times with low DOC SOW to

remove loosely bound metals and DOC from culture media. Cells were resuspended in 30 mL of SOW and then added to pre-equilibrated experimental media and at each time point, 7 to 8 mL samples were filtered (1.0 µm 25 mm, Polycarbonate Membrane) in triplicate every 0.25 h for short-term and 0.25 to 6 h for long-term uptake experiments using a homemade filter manifold and polysulfone filter supports. Following filtration, cysteine-exchangeable MeHg on cell surfaces was removed using a 3-part manifold wash modified from (Zhong and Wang 2009). An initial rinse of 10 mL of low DOC SOW was used to remove MeHg from the filter surface. This was followed by a 1 min cysteine (8mM) "bath" where cells were submerged in 10 mL of cysteine solution (8 mM) before being re-collected on a filter, and a final 10 mL low DOC SOW rinse. All washed cells were stored at -20°C until analysis.

Cell Wash Removal Efficiency

To determine the effectiveness of the 3-part cell wash, the 3-part wash was compared to a seawater rinse in live and dead *Tw* and *C. brevis* cells of short term exposures. A removal efficiency was calculated using the equation below:

$$Removal\ Efficiency = 100 - \frac{[Filtered\ MeHg]_{CysWash}}{[Filtered\ MeHg]_{SOWRinse}} * 100 \qquad \text{Eq. 2-1}$$

where [Filtered MeHg] is the average MeHg concentration of biological triplicates for cysteine washed or SOW rinsed live or heat-killed *Tw* and *C. brevis* cells. Removal efficiencies were 96% for live and 93% for heat-killed *Tw* cells in short term exposures. All filtered samples from uptake experiments are referred to as cellular MeHg, which is composed largely of intracellular MeHg and likely a small fraction (<10%) that is tightly-bound, not removed by competitive cysteine binding.

Due to difficulties arising in filtration of the colony forming *P. antarctica* in culture, all cells were harvested for uptake experiments by centrifugation of semi-continuous batch cultures. Pelleted *Pa* cells were resuspended in low DOC and re-centrifuged to further remove extracellular compounds. Cell densities of 10^3 and 10^4 cells/mL were used in MeHg uptake experiments with *Pa*.

Methylmercury Distillation and Analysis

Methylmercury analysis for all filtered samples followed protocols of US EPA Method 1630 as MeHg was separated from sample matrices by aqueous phase distillation. As stated above, biological triplicates were sampled at each time point and filtered cells distilled and analyzed with two method blanks, and 2-3 matrix spikes composed of pre-filtered (polycarbonate membrane) phytoplankton cultures (MeHg free) spiked with 100 pg of MeHg. Microliter aliquots of 0.1% ammonium 1-pyrrolidinedithiocarbamate (APDC), 50% sulfuric acid, and 2.7 M potassium chloride were used as distillation reagents to rupture cell membranes, digest cells, and convert all MeHg to MeHgCl in a 30 mL total volume and distilled using an automated Tekran 2750 distillation unit. Distillates were stored at 8 C until analysis. Methlymercury in distillates was analyzed with a Tekran Model 2700 using automated direct purge, gas chromatography separation, and detection by cold vapor atomic fluorescence (CVAFS) after addition of 2 M sodium acetate buffer and sodium tetraethylborate and allowing ethylation to proceed for 45 min before analysis. The recovery of MeHg in spiked distillates was 95 ± 14 %, with a range of 71 to 124 %. A methylmercury hydroxide standard (Brooks Rand) was used for spikes and standard curves.

Calculation of MeHg Speciation, Rates, and Rate Constants

Methylmercury speciation calculations were run in MINEQL^{+} 4.6 chemical equilibrium modeling software using binding constants from the National Institute of Standards and Technology (NIST) and (Alderighi et al. 2003). In full SOW and diluted SOW (35, 21 psu resp.) without cysteine, nearly all MeHg was bound as CH_3HgCl (> 98%) and a small percentage as CH_3HgOH (< 2%). In polar conditions (4° C), 97% of MeHg was bound as CH_3HgCl and 3% as CH_3HgOH. In the presence of 200 nM cysteine, the complex CH_3HgCys (-1) accounted for nearly 100% of dissolved MeHg.

All linear regression analyses were performed using the lm function in R 3.3.0. Cellular uptake rates were estimated as the slopes of the line of MeHg concentrations vs. time in units of attomol of MeHg cell^{-1} h^{-1}. Cell-normalized uptake rates were converted to rate constants in units of L g^{-1} hr^{-1} using published dry weights (Fisher and Schwarzenbach 1978, Houde and Roman 1987). Published cell volumes were used to calculate cell surface area:volume ratios (SA/V) in the assessment of normalized uptake rates in *Tw* and *Tp* (Reinfelder 2012) *C. brevis* (van Oijen et al. 2004) and *Pa* (Vogt et al. 2012). Weight and normalized rates were further normalized to exposure concentration in order to compare to uptake and rate constants from other studies.

Experimental Dissolved Organic Carbon Collection and Analysis

DOC_{SOW} samples were collected in muffled glass scintillation vials sealed with aluminum lined caps and frozen (-20°C) until analysis. Excreted DOC from phytoplankton cells (DOC_{Cells}) into SOW was quantified in low DOC SOW experimental media before and after the addition and incubation of unexposed

phytoplankton (positive controls), and MeHg exposed (10 nM) cells to quantify the change in DOC concentrations following MeHg exposure. All DOC measured in experimental media (with cells) was collected using GF/F filters (47 mm), glass filter support, glass side-arm vacuum flask, and glass scintillation vials all muffled at 550°C (>12h) before sampling.

Frozen DOC samples were allowed to thaw overnight and were measured using a Shimadzu TOC-V CSN Total Organic Carbon analyzer with ASI-V autosampler unit. An addition of 5% hydrochloric acid (Fisher, Trace Metal Grade) to aqueous samples was used to convert seawater carbonates to carbon dioxide (CO_2), which was removed from seawater by a sparging with ultra zero compressed air (<0.1 ppm THC) for 3 min. Following sparging, samples were analyzed as non-purgeable organic carbon (NPOC) via tube combustion to carbon dioxide (CO_2) followed by gas chromatography and IR detection. NPOC analysis was performed using ASI-V autosampler unit and TOC-V software Ver 2.2, which reports all values as mass concentration units (mg/L, ppm). Standardization of samples was completed using a potassium hydrogen phthalate standard first prepared in a concentrated (1000 ppm) stock with muffled salts (250°C, 6 h), muffled glassware, and Milli-Q water purged with Ultra-High purity nitrogen (N_2) gas prior to and after addition of salts to remove aqueous CO_2 from sealed glass serum bottles. Milliliter aliquots were removed (via syringe) from serum bottles into muffled volumetric flasks to prepare working standards (25 ppm), which were used within 24 h of sample analysis. Working standards were diluted over a standard range of 25 ppm to 0.50 ppm, and the working detection limit of the instrument as three times the standard

deviation of the blank was 0.11 ppm. All DOC mass concentrations were converted to molar units.

2.4 Results

Cell parameters of two temperate and two polar marine phytoplankton

Cell volumes and SA/V ratios varied from 41 to 626 μm^3 and 0.57 to 1.40 μm^{-1}, respectively, across the four species of phytoplankton examined (Table 2.1). Both properties were similar in *Tp, C. brevis*, and *Pa* cells, but much larger in *Tw*.

Short-term uptake of methylmercury chloride (MeHgCl) in the temperate diatom *Thalassiosira weissflogii* (*Tw*)

Methylmercury chloride (MeHgCl) uptake rates in *Tw* ranged from 0.4 to 7.9 attmol/cell/hr across a DOC_{SOW} concentration range of 28 to 874 µM. A relatively constant percentage of added MeHg (2.4 to 4.2%) was taken up into cells from the dissolved phase (Table 2.2). In DOC_{SOW} concentrations of 158 µM, the cell normalized MeHg uptake rate (3.0 attmol/cell/hr) was linear ($R^2 = 0.966$, $p < 0.05$) (Figure 2.1). A linear trend fitted through the origin (7.9 attmol/cell/hr, $R^2 = 0.997$, $p < 0.05$), was observed in the lower DOC_{SOW} treatment for the first two sampling points as cellular MeHg started to level off after 0.5 hr. The linear trends of the initial sampling points fitted through the origin were used to calculate uptake rates of MeHg for *Tw* in low DOC treatments (Table 2.2). A non-linear trend ($R^2 = 0.990$, $p < 0.05$) was the best fit to the low DOC_{SOW} treatment when considering all sampling points due to the leveling of cellular MeHg concentrations after 0.5 hr approaching saturation in *Tw*.

Table 2.1. Phytoplankton cell parameters including volume (vol), surface area-to-volume (SA/V), and dry weight (dry wt) as calculated or published values.

Phytoplankton	***Ref.***	***vol (μm^3)***	***SA (μm^2)***	***SA/V (μm^{-1})***	***Dry wt (pg)***
Tw	1,2	626	353.9	0.57	503 ± 16
Tp	1,3	41	57.5	1.40	13 ± 1.2
Cb	4	48.7	64.5	1.32	
Pa	5	56	70.8	1.26	

References for cell parameters: [1]Reinfelder 2012 [2]Houde and Roman, 1987 [3]Fisher and Schwarzenback, 1978 [4]van Oijen et al., 2004 [5]Vogt et al., 2012

Table 2.2. Short-term uptake rates and average percent accumulation of methylmercury in the temperate diatom *Thalassiosira weissflogii* (*Tw*) exposed to 10 nM MeHgCl for 1 to 1.5 h in synthetic ocean water (SOW) with various DOC_{SOW} concentrations.

DOC_{SOW} (µM)	***MeHgCl Uptake (attmol/cell/hr)***	***Average $\%MeHg_{Cell}$***
874	0.4	3.7
800	0.7	2.7
158	3.0	3.6
28	6.6	2.4
37	7.9	4.2

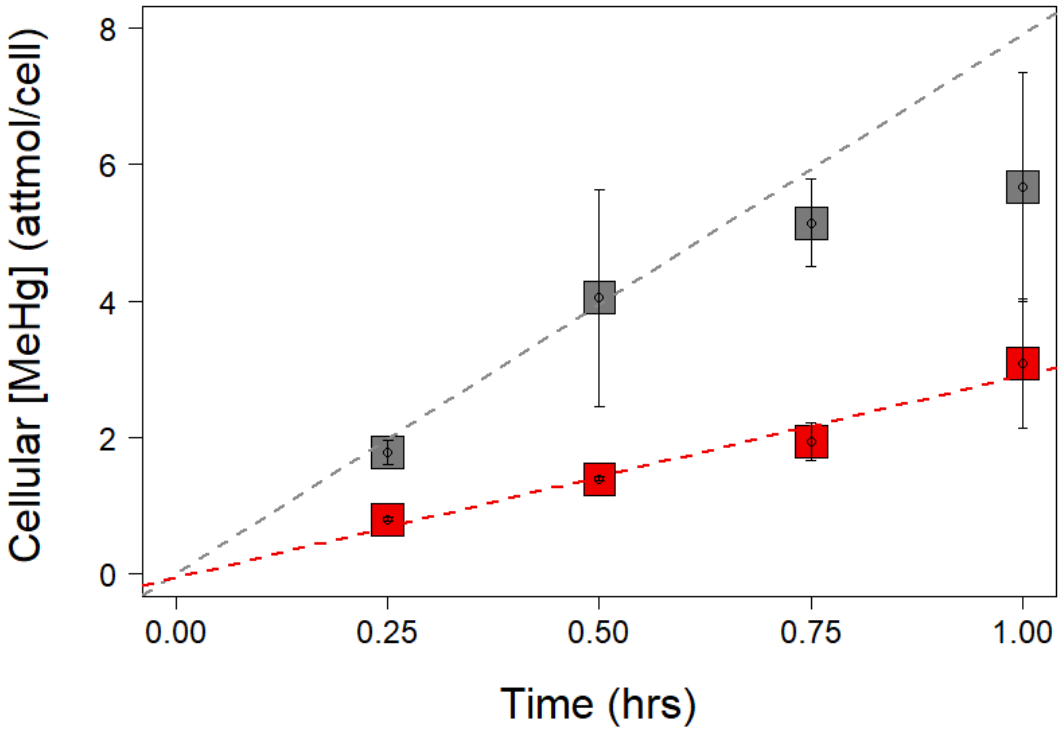

Figure 2.1 Short-term linear uptake rate of MeHgCl in *Thalassiosira weissflogii (Tw)* in mid DOC treatment (red squares) (Cell[MeHg] = 3.0(hr) + 0.0, $R^2 = 0.965$, $p < 0.05$) and linear relationship fitted through the origin using 0.25 and 0.5 hr sampling points in the low (grey squares) (Cell[MeHg] = 7.9(hr); $R^2 = 0.997$, $p < 0.05$) DOC treatment at two initial DOC_{SOW} concentrations (~158 µM, ~37 µM resp.) following UV-oxidation of synthetic ocean water (SOW).

Short-term uptake of methylmercury chloride (MeHgCl) in the temperate diatom *Thalassiosira pseudonana* (*Tp*)

A range of DOC_{SOW} (216 to 13 µM) was used for uptake experiments of MeHgCl in *Tp*, but short term uptake rates varied over a wider range than in Tw (0.79 to 20.6 attmol/cell/hr) (Table 2.3). The percentage of MeHg accumulated from SOW varied greatly (2.2 to 14.1%) and was highest in the low DOC_{SOW} treatment except the anomalously higher accumulation percentages in the 192 µM treatment (Table 2.3). Comparing uptake at a two DOC_{SOW} concentrations revealed a near order of magnitude difference in MeHg uptake (2.4 and 20.6 attmol/cell/hr) between mid (158 µM) and lower (13 µM) DOC_{SOW} concentrations (Figure 2.2). Both trends were highly linear and significant ($R^2 = 0.917$ and 0.997; $p < 0.05$) across a one-hour sampling period.

Effect of DOC_{SOW} on uptake rate of MeHg in *Tw* over a large DOC_{SOW} range

A non-linear relationship was observed between DOC_{SOW} concentrations and corresponding MeHg uptake rates (Figure 2.3). At concentrations below 300 µM, uptake rates increased dramatically until reaching the lowest concentration of DOC_{SOW} at 28 µM (Figure 2.3; Table 2.2). At concentrations >700 µM only a slight increase with decreasing DOC_{SOW} concentration was observed (Figure 2.3).

Table 2.3. Short-term uptake rates, cell surface concentrations (y-intercepts), and average percent accumulation of methylmercury in the temperate diatom *Thalassiosira pseudonana* (*Tp*) exposed to 10 nM MeHgCl for 1 to 1.5 h in synthetic ocean water (SOW) with various DOC_{SOW} concentrations.

DOC_{SOW} (µM)	***MeHgCl Uptake (attmol/cell/hr)***	***Average $\%MeHg_{Cell}$***
216	0.79	5.0
192	11.8	14.1
158	1.06	3.1
158	2.4	2.2
13	20.6	14.1

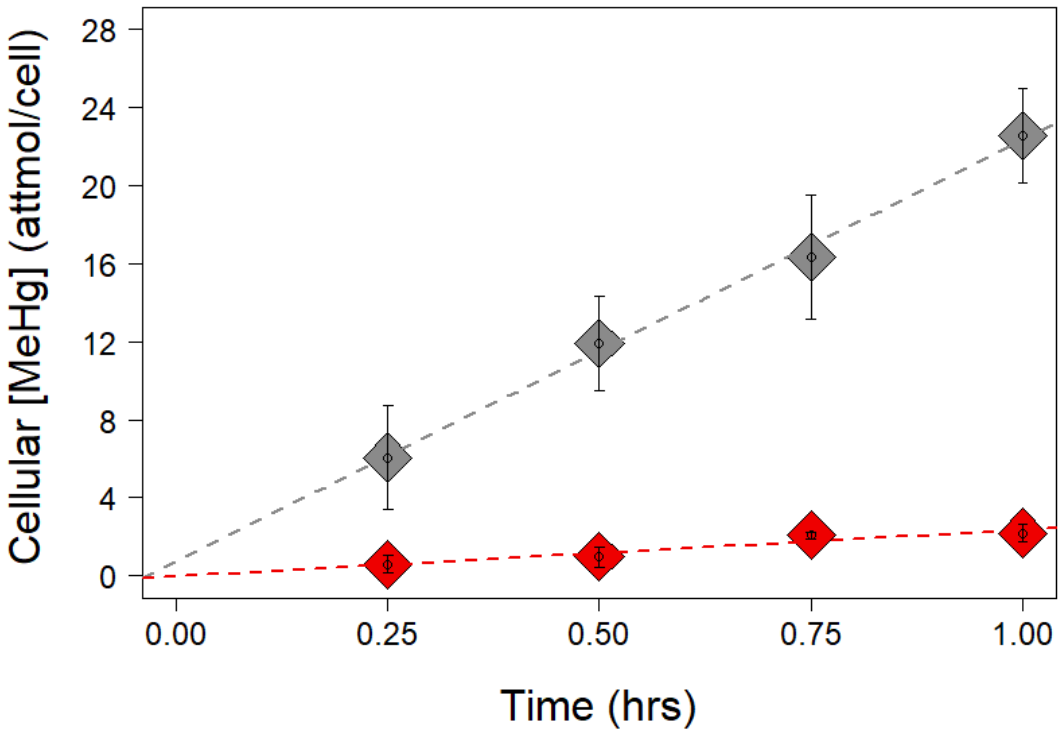

Figure 2.2 Short-term uptake rates of MeHgCl in *Thalassiosira pseudonana (Tp)* in high (red diamonds) and low (grey diamonds) DOC treatments (Cell[MeHg] = 2.4(hr) + 0.0, $R^2 = 0.917$, $p < 0.05$; Cell[MeHg] = 20.6(hr) + 1.2; $R^2 = 0.997$, $p < 0.05$) at two initial DOC_{SOW} concentrations (158 µM, 13 µM resp.) following UV-oxidation of synthetic ocean water (SOW).

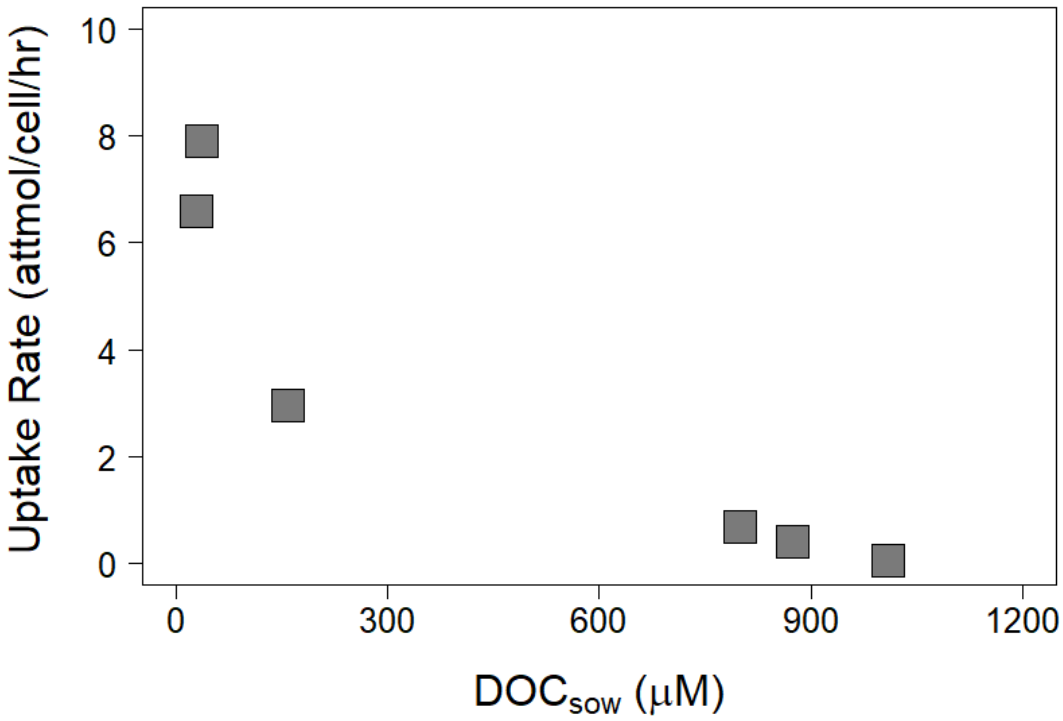

Figure 2.3 Influence of various lab DOC_{SOW} concentrations (<1.2 mM) on short-term uptake rates in temperate *Thallassiosira weissflogii* (*Tw*) (grey square) cells.

Short-term uptake of methylmercury chloride (MeHgCl) in a polar diatom *Chaeotoceros brevis* (*C. brevis*)

Under polar conditions, uptake of MeHgCl in *C. brevis* varied greatly (0.01 to 14.3 attmol/cell/hr) with a markedly higher uptake rate at the low DOC concentration of 16 µM. MeHg accumulation percentage was markedly higher in the low SOW_{DOC} condition (Table 2.4). At 16 µM DOC, uptake of MeHg yielded a high uptake rate (14.3 attmol/cell/hr) relative to the 217 µM condition and all other higher DOC (Table 2.4; Figure 2.4).

Effect of DOC_{SOW} on uptake rate of MeHg in the temperate diatoms *Tw* and *Tp*, and the polar diatom *C. brevis* over a narrow range of DOC_{SOW}

As was found for *Tw* at DOC_{SOW} concentrations >100 µM, there was little change in the MeHg uptake rates in both temperate and polar diatoms (Figure 2.5). However, at concentrations below 100 µM, markedly higher uptake rates were observed in *Tw*, *Tp*, and *C. brevis*, most noticeably in *Tp* and *C. brevis* at DOC_{SOW} concentrations < 20 µM (Figure 2.5; Table 2.3; Table 2.4).

Table 2.4. Short-term uptake rates, cell surface concentrations (y-intercepts), and average percent accumulation of methylmercury in the polar diatom *Chaetoceros brevis* (*Cb*) exposed to 10 nM MeHgCl for 1 to 1.5 h in synthetic ocean water (SOW) with various DOC_{SOW} concentrations.

DOC_{SOW} (μM)	**MeHgCl Uptake (attmol/cell/hr)**	**Average $\%MeHg_{Cell}$**
216	0.49	0.8
270	0.01	0.1
158	0.33	0.6
16	14.3	4.8

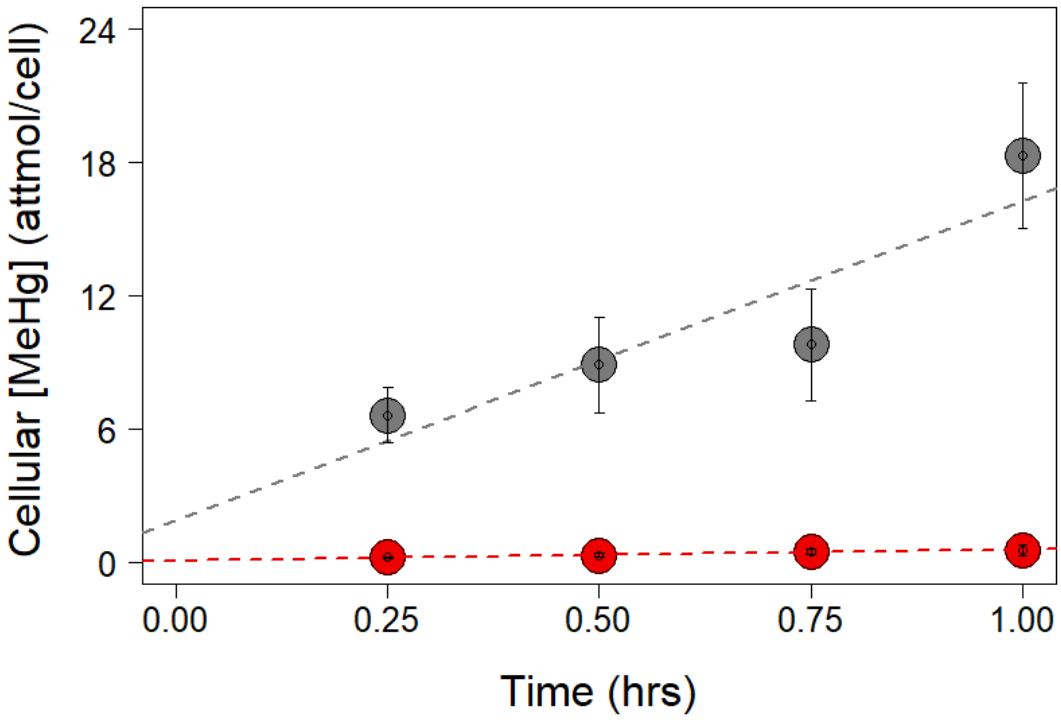

Figure 2.4 Short-term uptake rates of MeHgCl in *Chaetoceros brevis (Cb)* in mid (red circles) and low (grey circles) DOC treatments (Cell[MeHg] = 0.49(hr) + 0.1, R^2 = 0.987, $p < 0.05$; Cell[MeHg] = 14.3(hr) + 1.9; R^2 = 0.824, $p = 0.09$) at two initial DOC_{SOW} concentrations (~217 µM, ~16 µM resp.) following UV-oxidation of synthetic ocean water (SOW).

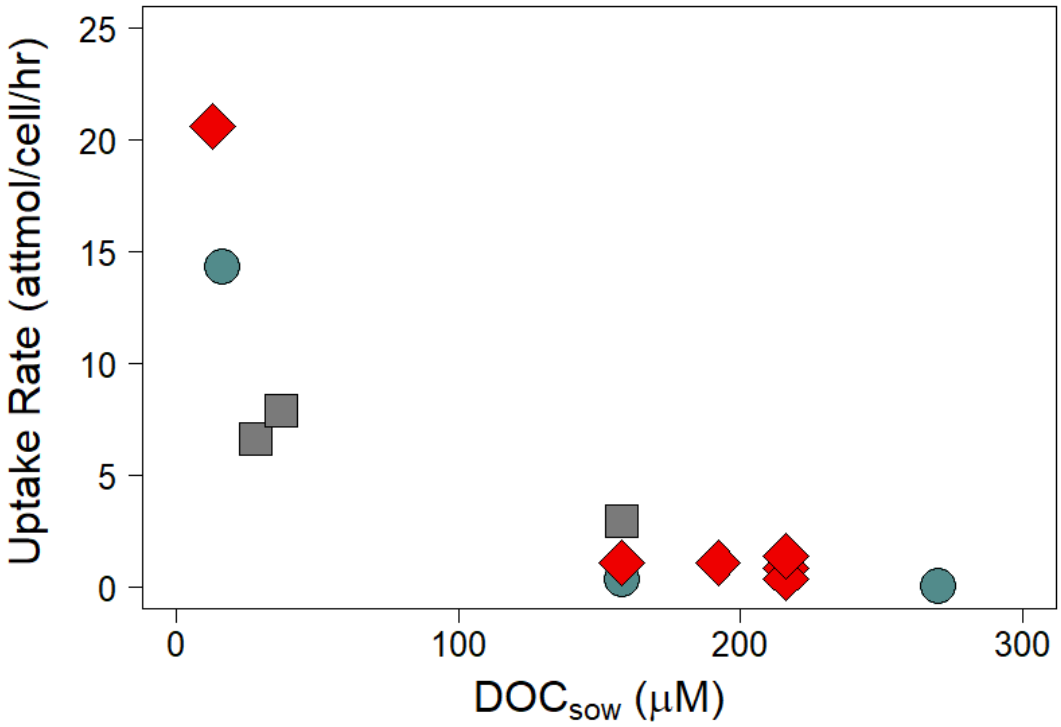

Figure 2.5 Influence of various lab DOC_{SOW} concentrations (<300 µM) on short-term uptake rates in two temperate *Thallassiosira pseudonana* (*Tp*) (red diamond) *Thallassiosira weissflogii* (*Tw*) (grey square) and one polar marine diatom *Chaetoceros brevis* (*Cb*) (green circle).

Influence of cell surface area: volume ratios (SA/V) on the uptake of MeHgCl

In the lowest DOC_{SOW} treatments (< 37 µM), uptake rates of MeHgCl of two temperate diatoms under ambient temperatures (18°C) were found to have a very strong linear relationship ($R^2 = 1.0$, $p < 0.05$, fitted through origin) with SA/V for *Tw* and *Tp* diatom cells (Figure 2.6) at a 10^4 cells/mL density. *Chaeotoceros brevis* had a similar SA/V to *Tp* but lower cellular methylmercury uptake rate incubated at 4°C. The rate for polar *C. brevis* (14.3 attmol/cell/hr) with a SA/V ratio of 1.32 μm^{-1} was between that of temperate *Tw* (0.57 μm^{-1}) and *Tp* (1.40 μm^{-1}) but lower than the expected rate of uptake (19.3 attmol/cell/hr) in temperate conditions for a centric diatom.

Influence of cysteine additions on short-term uptake of methylmercury in temperate diatoms *Thalassiosira weissflogii* (*Tw*) and *Thalassiosira pseudonana* (*Tp*)

A relatively narrow range of MeHg uptake rates were observed during MeHgCys treatments (0.05 to 1.37 attmol/cell/hr) for *Tw* and *Tp* (Table 2.5). Averaged accumulated %MeHg was quite consistent between temperate diatoms (2.1 to 3.9%). Uptake of MeHgCys was linear at a DOC_{SOW} concentration of 216 µM with an almost identical uptake rate in corresponding MeHgCl treatment (Figure 2.7). However, the addition of MeHgCys at this high background DOC concentration lowered the y-intercept of the cellular MeHg linear regression compared to the corresponding MeHgCl treatment.

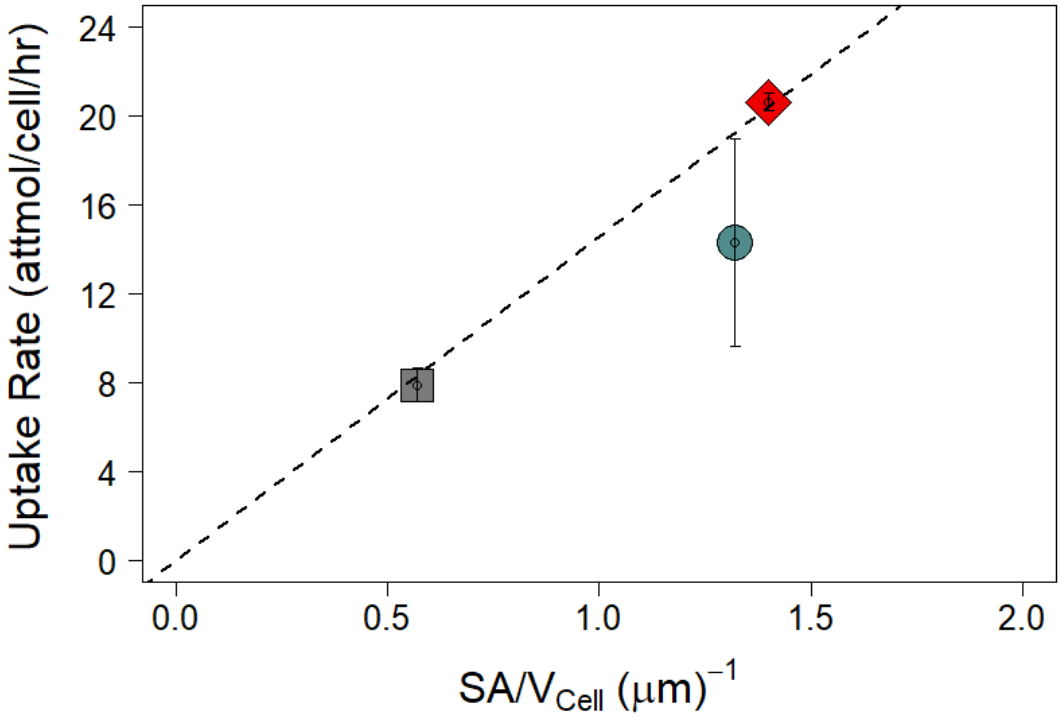

Figure 2.6. Relationship of cell surface area:volume (SA/V) ratios on short-term uptake rates of MeHgCl in two diatoms when fitted through the origin (Cell[MeHg]Uptake = 14.6(SA/V), $R^2 = 1.0$, $p < 0.05$) ±SE of the regression slope in two temperate *Thallassiosira weissflogii* (*Tw*) (grey square) and *Thallassiosira pseudonana* (*Tp*) (red diamond) and one polar marine diatom *Chaetoceros brevis* (*Cb*) (green circle) at a low DOC (< 28 µM) and cell density of 10^4 cells/mL. *Phaeocystis antarctica* (*Pa*) was omitted from analysis due to no linear trend in uptake at 10^4 cells/mL density.

Table 2.5. Short-term uptake rates and average percent accumulation of methylmercury in the temperate diatoms *Thalassiosira weissflogii* (*Tw*) and *Thalassiosira pseudonana* (*Tp*) exposed to 10 nM CH_3HgCys for 1 to 1.5 h in synthetic ocean water (SOW) with various DOC_{SOW} concentrations. Negative y-intercepts (surface concentrations) are reported as zero.

Phytoplankton	DOC_{SOW} (μM)	CH_3HgCys Uptake (attmol/cell/hr)	Average $\%MeHg_{Cell}$
Tw	1009	0.05	2.1
Tp	216	0.83	2.3
Tp	216	1.37	3.9

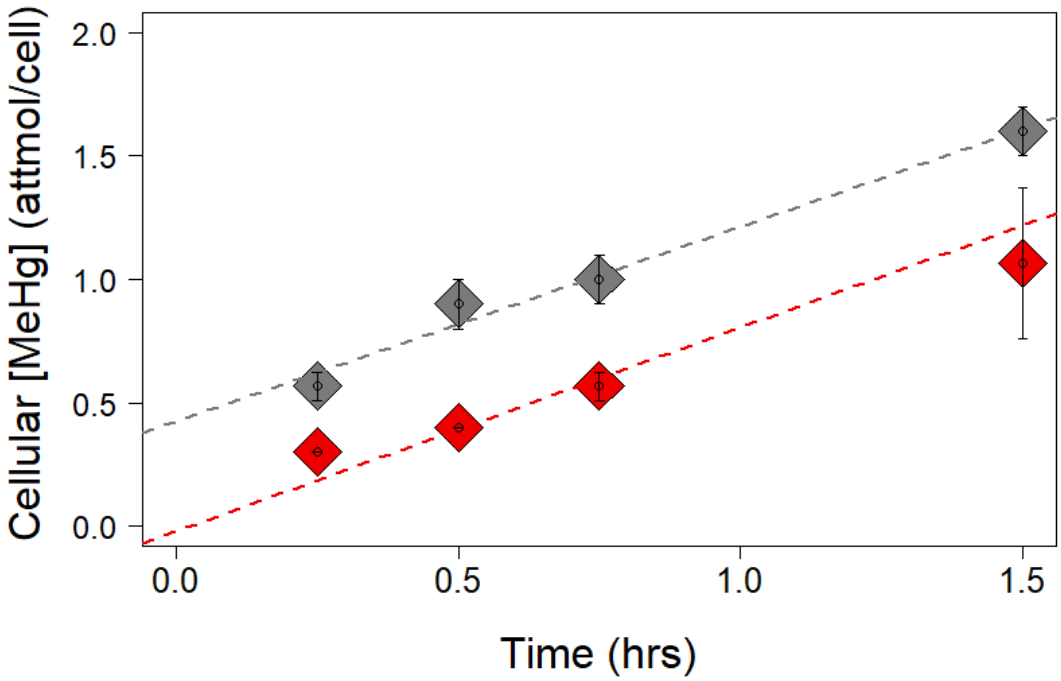

Figure 2.7. Effect of cysteine addition (200 nM) on short-term uptake rates in *Thalassiosira pseudonana (Tp)* of MeHgCys (Cell[MeHg] = 0.83(hr) + 0.0, $R^2 = 0.996$, $p < 0.05$) (red diamonds) and MeHgCl (Cell[MeHg] = 0.79(hr) + 0.42; $R^2 = 0.982$, $p < 0.05$) treatments at a similar DOC_{SOW} concentration (~216 µM).

Removal efficiencies of loosely bound MeHg from *Thalassiosira weissflogii* (*Tw*) and *Chaetoceros brevis* (*C. brevis*) cells

Removal efficiencies of MeHg by the cysteine "bath" (cysteine-exchangeable) were calculated relative to cellular MeHg washed once with SOW (non-cysteine exchangeable) in live and dead *Tw* cells (Table 2.6). Generally, coefficient of variation (CV) in dead cells with both treatments (40.9 and 40.0) were higher than live cells (18.5 and 9.0) with the same technique applied. Averaged MeHg concentrations of cysteine washed live and dead cells (2.2 and 3.5 attmol/cell, respectively) were much lower relative to SOW rinsed cells (59.1 and 48.9 attmol/cell) and removal efficiencies were high, and >90%. Calculated removal efficiencies were slightly higher in live cells (96.3%) than in dead cells (92.7%) (Table 2.6) comparable or exceeding wash efficiencies measured in heat killed *Tp* cysteine washed cells (Zhong and Wang 2009).

Cysteine wash procedures described above were repeated in *C. brevis* cells where cysteine wash was maintained at polar temperatures 4°C. As was seen in *Tw* live and dead cells, cysteine-washed live and dead cells had lower averaged MeHg cellular concentrations (0.8 and 0.5 attmol/cell, respectively) than SOW rinsed cells (4.7 and 6.7 attmol/cell) (Table 2.7). Coefficient of variation of cellular concentrations in dead *C. brevis* cells for both SOW rinse and cysteine wash (19.9 and 3.1, respectively) were lower with higher values calculated in live cells (62.1 and 35.7). In addition, a markedly lower removal efficiency of 83.8% was seen in live *C. brevis* cells compared to 93.1% removal efficiency of MeHg in dead *C. brevis* cells (Table 2.7). This removal efficiency was the lowest seen among all polar and temperate sample treatments (Table 2.6; Table 2.7).

Table 2.6. Efficiencies of 3-part synthetic ocean water (SOW)-8 mM cysteine-SOW washes to remove cell-surface MeHg in live and dead cells of the temperate diatom *Thalassiosira weissflogii* (*Tw*) exposed to 10 nM MeHgCl for 1 h at intermediate DOC_{SOW} concentrations (~150 µM). Values are means ± coefficient of variation (CV) of biological triplicates.

Treatment	Ave [MeHg] (attmol/cell)	%Removal Efficiency
Live_cysteine	2.2 ± 18.5	96.3
Live_SOW	59.1 ± 9.0	
Dead_cysteine	3.5 ± 40.9	92.7
Dead_SOW	48.9 ± 40.0	

Table 2.7. Efficiencies of 3-part synthetic ocean water (SOW)-8 mM cysteine-SOW washes to removal of cell-surface MeHg in live and dead cells of the polar diatom *Chaetoceros brevis* (*C. brevis*) exposed to 10 nM MeHgCl for 1 h at intermediate DOC_{SOW} concentrations (~150 µM). Values are means ± coefficient of variation (CV) of biological triplicates. Notice lower removal efficiencies in live *C. brevis* cells.

Treatment	Ave [MeHg] (attmol/cell)	%Removal Efficiency
Live_cysteine	0.8 ± 62.1	83.8
Live_SOW	4.7 ± 35.7	
Dead_cysteine	0.5 ± 19.9	93.1
Dead_SOW	6.7 ± 3.1	

Short-term uptake rates of MeHgCl in the polar prymnesiophyte *Phaeocystis antarctica* (*Pa*) at two cell densities

Due to complications with the formation of *Pa* cell colonies at a cell density of 10^4 cells mL^{-1}, a cell density of 10^3 cells/mL was used for MeHg uptake in *Pa*. The MeHgCl uptake rate in *Pa* in low DOC waters (<37 µM) at this lower cell density (249 attmol/cell/hr) was two orders of magnitude higher than that for the temperate and polar diatom species at similar cell densities (2.41 attmol/cell/hr) (Table 2.8; Figure 2.8). Indeed, this MeHg uptake rate was higher than all MeHgCl uptake rates for the temperate and polar diatoms incubated at 10^4 cells mL^{-1} (Tables 2.2, 2.3, 2.4, 2.8). At the lower cell density, short-term MeHg uptake was linear ($R^2 = 0.904$, $p < 0.05$) (Figure 2.8). At 10^4 cells/mL, no significant uptake was observed ($R^2 = 0.126$, $p = 0.64$). Although uptake rates and surface MeHg varied greatly between higher and lower cell density treatments of *Pa*, average %MeHg accumulated was similar (7.6, 7.8%) in the two experiments (Table 2.8).

Table 2.8. Short-term uptake rates, cell surface concentrations (y-intercepts), and average percent accumulation of methylmercury in the polar prymnesiophyte *Phaeocystis antarctica* (*Pa*) exposed to 10 nM MeHgCl for 1 h in synthetic ocean water (SOW) with low DOC (<37 µM) concentrations.

DOC_{SOW} (µM)	Cell Density	MeHgCl Uptake (attmol/cell/hr)	Average $\%MeHg_{Cell}$
37	37812	2.41	7.6
13	2031	249	7.8

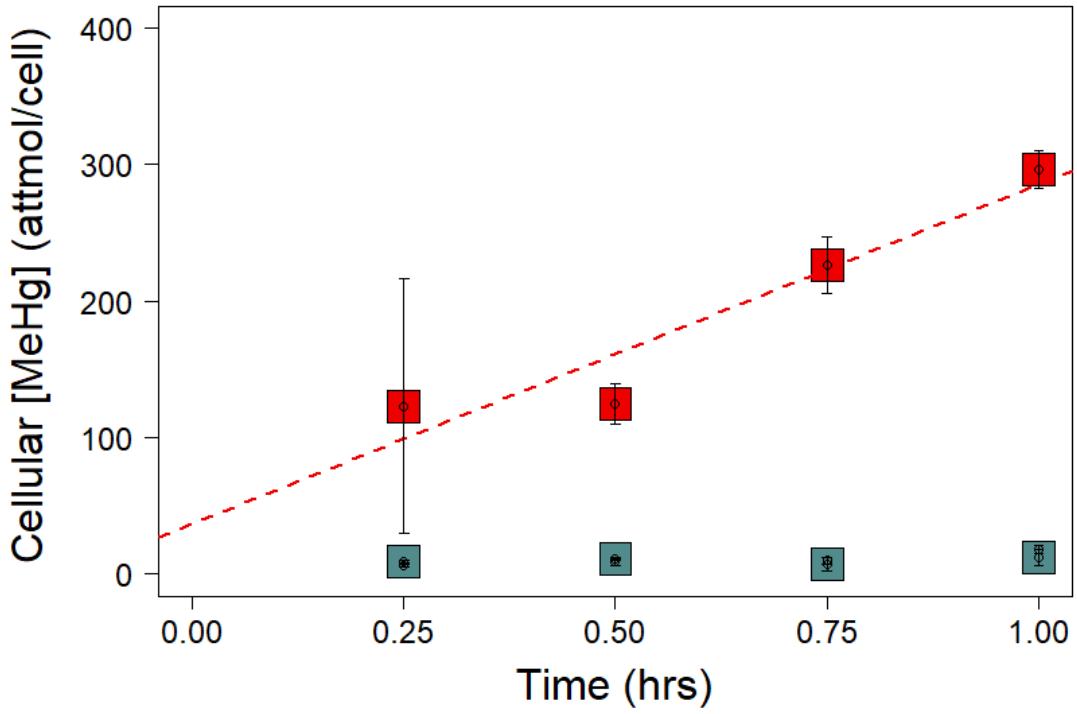

Figure 2.8. Effect of cell density on short-term uptake of MeHgCl in *Phaeocystis antarctica (Pa)* in regular (10^4 cells/mL; green squares) and lower (10^3 cells/mL; red sqaures) cell treatments (regular-no significant MeHg uptake $p = 0.64$; lower - Cell[MeHg] = 249(hr) + 37; $R^2 = 0.904$, $p < 0.05$) in low DOC_{SOW} concentrations (~37 µM, ~13 µM resp.).

Long-term uptake rates of MeHg in two temperate diatom species

Long-term uptake (4-24 hours) of MeHg differed from short-term uptake at low DOC_{SOW} concentrations (<37 µM) (Tables 2.2, 2.3, 2.9) during relatively consistent (~10^4) cell densities (Table 2.10). Methylmercury uptake rates were low (< 0.90 attmol/cell/hr) exhibiting a narrow range from 0.21 to 0.90 attmol/cell/hr between smaller and larger *Tp* and *Tw* cells (Table 2.9). Percent accumulation (8.4 to 13.7%) were high relative to short-term uptake values in low DOC_{SOW} waters. Although the slope of long-term uptake in *Tw* (0.9 attmol/cell/hr) was lower than that for short-term uptake (Figures 2.1 and 2.9) in low DOC_{SOW} treatments, there was a strong linear relationship (R^2 = 0.995, $p < 0.05$). Long-term uptake produced higher maximum cellular MeHg concentrations, upwards of ~25 attmol/cell, similar to those seen in short-term uptake in *Tp* (Figures 2.2) producing higher percent MeHg accumulation (Table 2.9).

Cellular release of dissolved organic carbon (DOC) in long-term MeHg exposures

DOC produced by *Tw* cells in response to MeHg in 2 long-term exposure experiments was assessed relative to unexposed cells in low DOC_{SOW} media (< 34 µM) to verify presence of cell-released DOC (DOC_{Cell}). An initial increase in the DOC_{Cell} of both experiments was observed relative to the background within the first 6 hours of exposure (Figure 2.11). Concentrations then decreased to 100-400 µM levels at 12 and 24 hours while remaining above background DOC levels of positive controls (Figure 2.11).

Table 2.9. Long-term uptake rates, cell surface concentrations (y-intercepts), and average percent accumulation of methylmercury in the temperate diatoms *Thalassiosira weissflogii* (*Tw*) and *Thalassiosira pseudonana* (*Tp*) exposed to 10 nM MeHgCl for 2 to 24 h in synthetic ocean water (SOW) with various DOC_{SOW} concentrations.

Phytoplankton	**DOC_{SOW} (μM)**	**MeHgCl Uptake (attmol/cell/hr)**	**Average $\%MeHg_{Cell}$**
Tw	28	0.21	8.4
Tw	37	0.90	13.7
Tp	13	0.38	10.3

Table 2.10. Duplicate cell counts over 48 hour sampling intervals during *Thalassiosira weissflogii* (*Tw*) long-term MeHg uptake experiment. PRD = percent relative difference.

Time (h)	*Cell Density (cells/mL)*	*Average Cell Density (cells/mL)*	*PRD*
0	35000	37500	7
	40000		
1	46250	46875	1
	47500		
2	100000	96250	4
	92500		
4	81250	60000	35
	38750		
6	67250	61750	9
	56250		
24	32500	47500	32
	62500		
48	42500	58125	27
	73750		

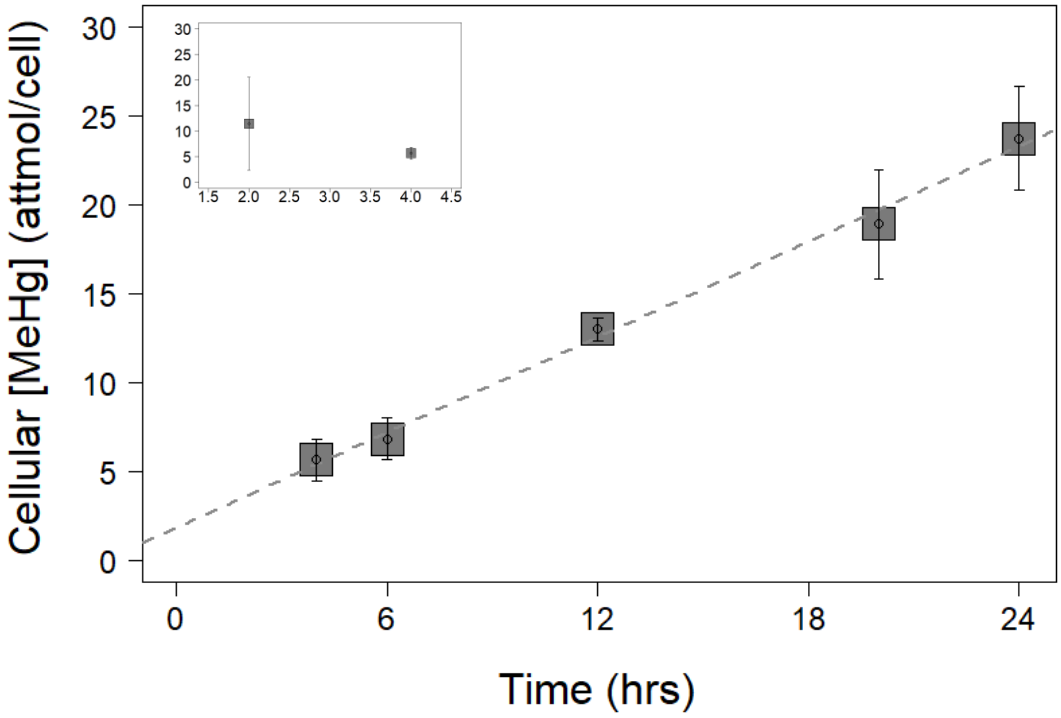

Figure 2.9. Long-term uptake rates of MeHgCl in *Thalassiosira weissflogii (Tw)* in an initial low (37 µM) DOC treatment (Cell[MeHg] = 0.9(hr) + 1.9; $R^2 = 0.995$, $p < 0.05$). Inset graph in upper left corner depicts MeHg release 2 and 4 h before long-term uptake. All points are mean ± 1SD.

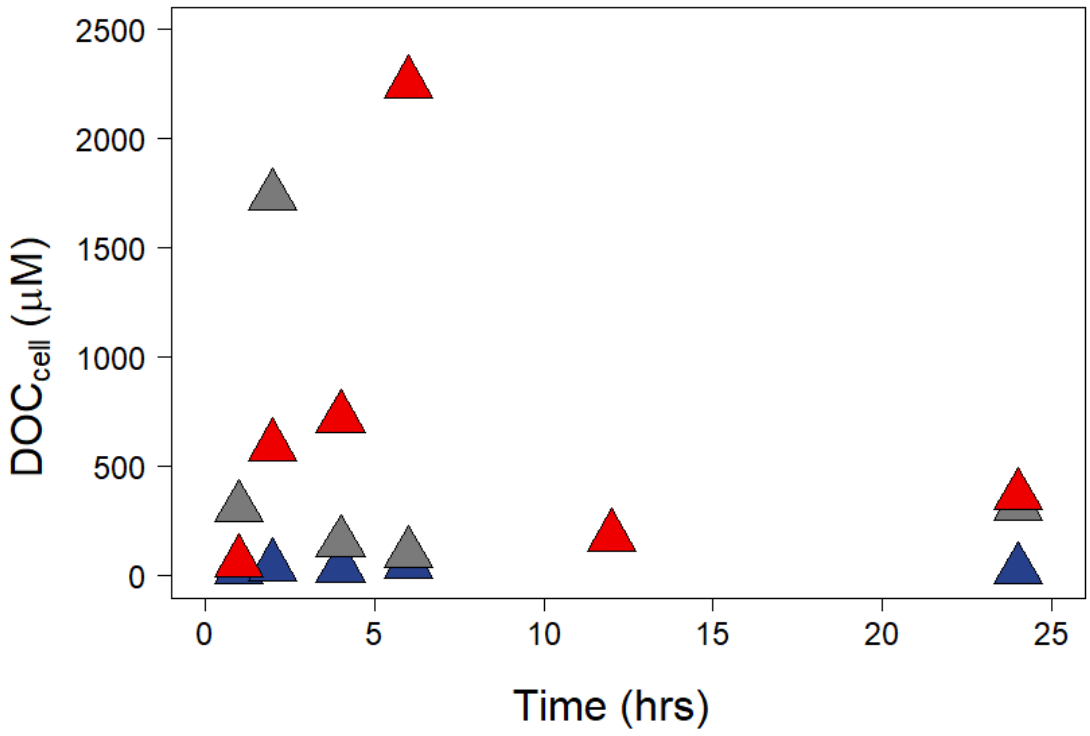

Figure 2.10. Release of cellular DOC by *Thalassiosira weissflogii* (*Tw*) during two 10 nM MeHg long-term exposures (grey triangles, $[DOC]_{SOW}$ = 28 µM; red triangles, $[DOC]_{SOW}$ = 34 µM) above unexposed *Tw* controls (blue triangles, $[DOC]_{SOW}$ = 10 µM).

Normalized MeHg uptake rates in temperate and Antarctic phytoplankton

Low DOC treatments were used to calculate uptake rate constants normalized to cell dimension parameters (volume and surface area) to compare MeHg uptake between temperate and Antarctic phytoplankton taxa. Methylmercury cell SA normalized uptake was higher in *Tp* (0.0358 attmol MeHg μm^{-2} h^{-1} nM^{-1}) than the larger centric diatom *Tw* (0.0022 attmol MeHg μm^{-2} h^{-1} nM^{-1}) and *C. brevis* (0.0222 attmol MeHg μm^{-2} h^{-1} nM^{-1}) (Table 2.11; Figure 2.11). A small difference in volume normalized uptake was seen between *Tp* (0.0502 attmol MeHg μm^{-2} h^{-1} nM^{-1}) and *C. brevis* (0.0294 attmol MeHg μm^{-2} h^{-1} nM^{-1}), but both MeHg normalized uptake rates were greater than one order of magnitude higher than *Tw* (0.0013 attmol MeHg μm^{-2} h^{-1} nM^{-1}) (Table 2.11).

Surface area and volume normalized uptake were approximately 1-2 orders of magnitude higher in *Phaeocystis antarctica* than all other cells (Table 2.11). Findings confirm that *Phaeocystis Antarctica*, a prymnesiophyte, does take up MeHg at higher rates than the polar and temperate diatoms species studied here (Figure 2.12).

Table 2.11. Phytoplankton uptake ± SE of the regression slope normalized to cell and cell parameters including vol (μm^3) and SA (μm^2)

Species	***cell (attmol MeHg cell^{-1} h^{-1})***	***vol (attmol MeHg µm^{-3} h^{-1} nM^{-1})***	***SA (attmol MeHg µm^{-2} h^{-1} nM^{-1})***
Tw	7.9 ± 0.6	0.0013 ± 0.0001	0.0022 ± 0.0002
Tp	20.6 ± 0.8	0.0502 ± 0.0020	0.0358 ± 0.0014
Cb	14.3 ± 4.7	0.0294 ± 0.0097	0.0222 ± 0.0082
Pa	249 ± 57.2	0.4446 ± 0.1021	0.3518 ± 0.0808

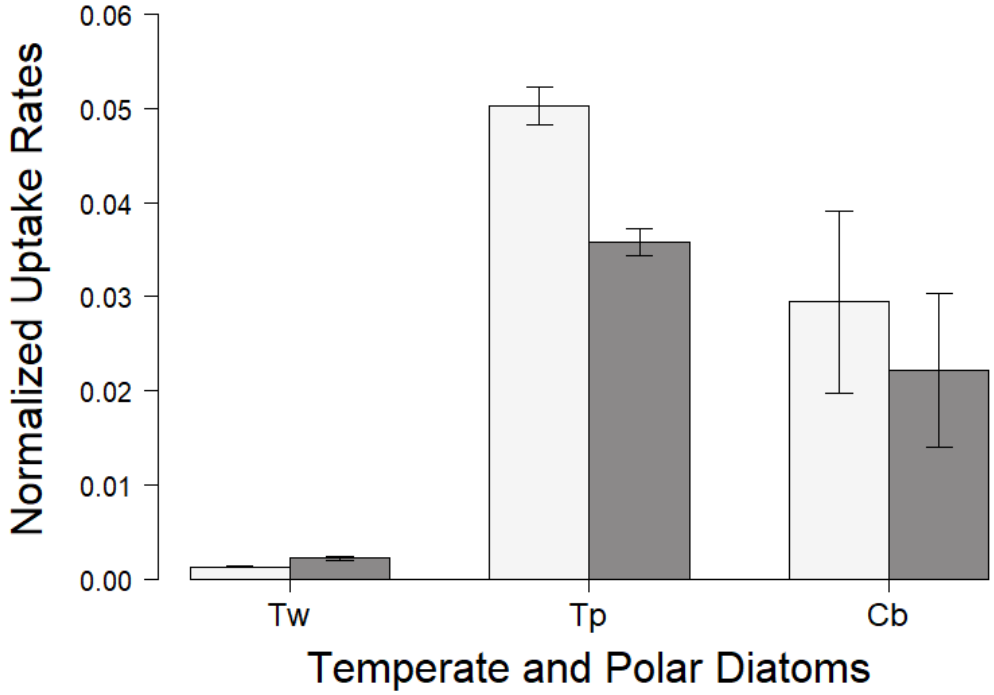

Figure 2.11. Normalized uptake rates in two temperate and one polar diatoms. Uptake rates were normalized to exposure concentrations volume (white bars) and surface area (grey bars). Units normalized uptake are attmol MeHg μm^{-3} h^{-1} nM^{-1} exposure and attmol MeHg μm^{-2} h^{-1} nM^{-1}.

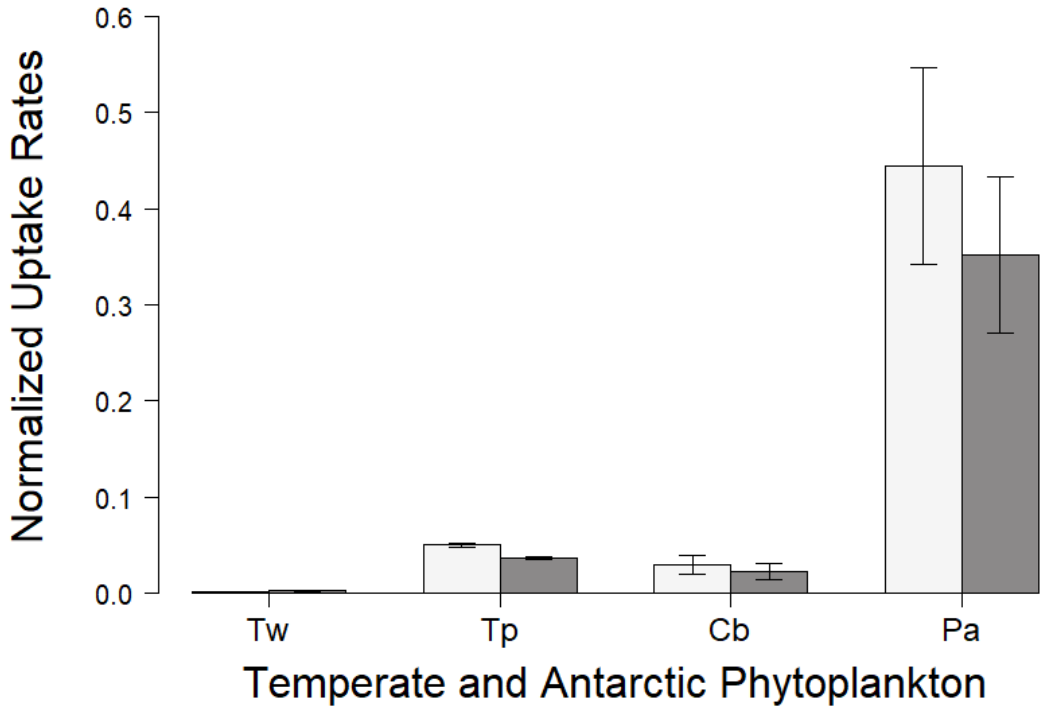

Figure 2.12. Normalized uptake rates in two temperate and one polar phytoplankton. Uptake rates were normalized to exposure concentrations volume (white bars) and surface area (grey bars). Units normalized uptake are attmol MeHg μm^{-3} h^{-1} nM^{-1} exposure and attmol MeHg μm^{-2} h^{-1} nM^{-1}.

2.5 Discussion

Normalized MeHg uptake rates in temperate and Antarctic phytoplankton

Volume and surface area normalized uptake rates of *Pa* fell between those for a temperate cyanobacterium *Synechococcus bacillaris* and *Tp,* and exceeded all other normalized uptake rates for a temperate chlorophyte, cryptophyte, dinoflagellate, and coccolithophore (Lee and Fisher 2016). These results suggest that *Pa* possibly other *Phaeocystis* species may accumule high cellular MeHg at a high rate in temperate and polar ecosystems. Our cellular uptake for *Tp* when normalized to exposure concentration (2.06 attmol MeHg $cell^{-1}$ hr^{-1} nM^{-1}) was lower than those measured in surface water from Southampton, NY as were normalizations to surface area and volume (Lee and Fisher 2016) (Table 2.2) likely due to lower exposure concentrations.

Comparison of MeHg uptake rates in temperate diatoms with other studies

Short-term uptake rates (cellular [MeHg]/cell/hour) in the temperate diatoms *Thalassiosira weissflogii* (*Tw*) and *Thalassiosira pseudonan* (*Tp*) in low DOC SOW from this study and under various conditions in other temperate studies were normalized to known dry weights and to the MeHg exposure producing a rate constant for MeHg uptake (Table 2.12). The rate constant for *Tw* (1.61 $Lg^{-1}hr^{-1}$) was about approximately two orders of magnitude lower than for *Tp* (177 $Lg^{-1}hr^{-1}$). The short-term uptake rate constant for *Tw* was one order of magnitude lower than the other rate constant in the Moye et al. 2012 study, while the weight normalized uptake rate constant for *Tp* was comparable to a measured value in Clearwater Bay seawater with an almost identical DOC concentration. A positive non-linear relationship exists between MeHg uptake and MeHg exposure concentrations (Moye et al. 2002), and all these experiments were performed with ^{14}C-

labeled monomethylmercury iodide or the gamma-emitting ^{203}Hg radioisotopes (Moye et al. 2002, Zhong and Wang 2009). Methylmercury exposures and differences in methods may have produced variation in MeHg uptake rate constants in these two temperate diatoms, especially in *Tw* cells, which had a markedly lower uptake rate at higher exposure concentrations.

Table 2.12. Short-term methylmercury rate constants (L g^{-1} h^{-1}) in two temperate diatoms, *Thalassiosira weissflogii* (*Tw*) and *Thalassiosira pseudonana* (*Tp*). Values were calculated from measured cellular uptake rates (attmol/cell/hr), dry weights per cell (see methods), and exposure concentrations. All studies listed applied some chelating MeHg cell wash technique, and Moye et al. 2012 used media simulating brackish water in which 85% of the MeHg was bound to chloride.

Short-term Uptake Study	***Tp Rate Constant ($L g^{-1} hr^{-1}$)***	***Tw Rate Constant ($L g^{-1} hr^{-1}$)***
MeHgCl_37 (μM) $[DOC]_{sow}$ $[MeHg]_{diss}$ = 10 nM		1.61
MeHgCl_13 (μM) $[DOC]_{sow}$ $[MeHg]_{diss}$ = 10 nM	177.0	
MeHgCl Moye et al. 2012 $[MeHg]_{diss}$ = 1.9 nM		16.7
MeHgCl_17 μM [DOC] Zhong & Wang 2009 $[MeHg]_{diss}$ = 1 nM	204	

Short-term MeHg uptake rates in two temperate diatoms

Methylmercury uptake rates were generally low in *Tw*, especially at higher DOC_{SOW} concentrations (≥800 µM) but increased by almost an order of magnitude at lower (<200 µM) DOC_{SOW} concentrations (Table 2.2) suggesting that DOC has a negative effect on MeHg uptake (Figure 2.1). Lowering DOC concentrations may also influence transport of MeHg into *Tw* cells. In the 37 µM treatment (Figure 2.1), there was a shouldering of cellular MeHg concentrations most noticeable at 0.75 hr and 1 hr suggesting saturation of MeHg into the phytoplankton cell. Saturation of MeHg in *Tw* cells is likely due its low MeHg capacity and potentially low membrane permeability as indicated by low SA and volume-normalized uptake rates relative to all other phytoplankton (Figure 2.12). Lower densities of bi-directional metal transport channels per unit surface area and a large vacuole inside *Tw* cells may influence uptake and potential release of MeHg.

Thalassiosira pseudonana had higher rates of MeHgCl uptake than *Tw* at almost all corresponding DOC_{SOW} concentrations (Tables 2.2 and 2.3). As *Tw* and *Tp* are both coastal centric diatoms, the primary difference between these cells is size, which is an important factor controlling passive diffusion of the neutral MeHgCl and potentially active transport at different DOC concentrations. The high MeHg uptake rate (20.6 attmol/cell/hr) measured in *Tp* cells at a low concentration of DOC_{SOW} is consistent with MeHg passive transport as the primary mechanism in *Tp* cells, especially at low DOC concentrations where MeHg is predominantly bound to the chloride ion. We acknowledge that this assessment is based on one uptake rate experiment at a low DOC_{SOW} and that further studies at DOC conentations between 150-50 µM are needed.

However, the importance of DOC on methylmercury uptake in *Tp* is evident in the lower MeHg uptake rates measured in DOC concentrations typical of coastal waters.

Effect of DOC on MeHg uptake in *Chaetoceros brevis* (*C. brevis*)

At low DOC_{SOW} (16 µM) there was a noticeable increase in uptake, percent accumulated, and surface bound MeHg compared to experiments with > 150 µM DOC_{SOW} (Table 2.4). To the best of our knowledge, MeHg accumulation in *C. brevis*, or any other polar diatom, has not been previously examined. Only one study has looked at inorganic mercury (Hg^{2+}) bioaccumulation in *C. brevis*, but not under polar (4°C) conditions, but at 23°C (Monikh et al. 2013). Here they found that the maximum levels of Hg^{2+} bioaccumulation in *C. brevis* was greater than that in two larger dinoflagellate phytoplankton species (Ceratium *furca*, *C. tripos*), and subsequent transfer of Hg^{2+} to *Daphnia* from exposed phytoplankton was highest for *C. brevis* (Monikh et al. 2013). There was a weak ($p = 0.09$) linear trend in the high DOC_{SOW} treatment (Figure 2.3). At low DOC, MeHg was largely present as the neutral MeHgCl complex. This complex would have had limited competition with DOC_{SOW} organic ligands at active sites near the cell surface, leading to higher initial cell surface concentrations and accumulated MeHg in *C. brevis* than at high DOC.

Non-linear relationship between DOC_{SOW} and MeHg uptake

At high DOC_{SOW} (≥800 µM) there was a slight increase in uptake rate of MeHg starting at negligible values until reaching 0.7 attmol/cell/hr at 800 µM (Figure 2.3; Table 2.2). At DOC_{SOW} concentrations less than 300 µM, a non-linear increase in uptake rates occurred reaching a maximum at 20.6 attmol/cell/hr (Figure 2.5; Table 2.2). Low DOC

concentrations seem to drive a higher initial MeHg uptake rate despite low SA/V (0.57) of *Tw* relative to other diatoms and phytoplankton in this study (Tables 2.1; Figure 2.3). The neutral MeHgCl complex formed at low DOC_{SOW} is known to be taken up via passive diffusion into the cytosolic fraction of this larger marine diatom as a result of MeHgCl being slightly hydrophobic, (Mason et al. 1996). As MeHgCl is not stable within the cell and MeHg will preferentially bind to thiols in biological systems (Rabenstein and Evans 1978). MeHg distributes itself within the cell between varying metal-sensitive (organelles, heat denatured proteins) and biologically detoxified fractions (Wu and Wang 2011). Methylmercury also exists within the cytosolic fraction that makes it more easily assimilated by copepods under conditions were the MeHgCl complex is dominant (Mason et al. 1996). In low DOC marine surface waters, MeHgCl may be accumulated at high rates regardless of cell size. An enrichment of MeHg at the base of offshore food webs may drive high Hg concentrations in upper trophic levels of migratory fish a primary rout of human exposure (Sunderland 2007).

Despite differences in cell size (Table 2.1) and experimental temperatures, decreasing DOC_{SOW} concentrations below about 100 µM increased MeHg uptake non-linearly in two temperate and one polar marine diatom (Figure 2.5). In *Thalassiosira pseudonana*, removing natural DOC concentrations through UV-oxidation to negligible levels (100 µM to 1 µM) increased MeHg internalization rates by more than a factor of 2 (Zhong and Wang 2009). In *Tw*, decreasing DOC_{SOW} from mid (158 µM) to low (28 µM) levels, increased cellular uptake rates by more than a factor of two (Table 2.2) and in *Tp* by a factor of 20 (Table 2.3). A more pronounced increase in uptake rates of MeHg at low DOC_{SOW}, likely composed of phthalic acids from bottles, is not unexpected as

phthalic acids are chelators of heavy metals (Mahmoud et al. 2016) and are known to accumulate as environmental pollutants (phthalic acid esters) in surface sediments of estuarine environments (Weng et al. 2008). DOC_{SOW} is not of biological origin but is representative of carboxylic acid and amine (non-thiol) functional groups in natural DOM. These model compounds are important to determining the influence of nitrogen (amine) and oxygen (carboxylic acid) binding of MeHg in natural systems, a significant portion of the bioreactive pool of DOM (Hedges 2002).

Uptake of MeHgCl is dictated by SA/V ratios in two temperate marine diatoms

A very strong positive relationship between the SA/V ratios and cellular MeHg uptake rates of diatoms in two temperate species indicates the importance of cell size, uniformity of cell structure, and possibly temperature in MeHg concentration per phytoplankton cell. Lower cellular MeHg uptake was seen in the polar diatom *C. brevis* than *Tp* although its SA/V are similar between these smaller centric diatoms species. Differences in the physiology of temperate and polar diatoms did have an affect on MeHg uptake rates per cell, as was observed for one marine dinoflagellate (Lee and Fisher 2016). At lower temperatures, active transport of MeHgCl may occur at a slower rate as would kinetics of MeHgCl passive diffusion through seawater and a phytoplankton cell membrane. Interactions of MeHg with cell shape (cylindrical, spherical) and differing cell wall compositions of phytoplankton should be considered when examining MeHg concentration within a phytoplankton cell as surface composition of the cell wall has been known to greatly affect biosorption capacities of trace metals across phytoplankton taxa (Brinza et al. 2007).

Cysteine does not enhance uptake of MeHg in *Thalassiosira weissflogii* nor *Thalassiosira pseudonana*

In very high DOC_{SOW} treatments (> 850 µM) low uptake of MeHg in *Tw* was observed in the absence of cysteine (0.4 attmol/cell/hr), but in the presence of 200 nM cysteine, uptake of MeHg was essentially negligible (0.05 attmol/cell/hr) (Table 2.5). These results mirrored the effect of a cysteine addition (67 µM) to natural DOC concentrations (204 µM) in marsh freshwaters near the Sacramento River delta (Luengen et al. 2012), but differed from the apparent enhanced MeHgCys uptake rates relative to the neutral complex MeHgCl in a series of seawater Hg accumulation experiments involving *Tw* (Lawson and Mason 1998).

In synchronized uptake experiments at intermediate DOC_{SOW} concentrations (> 200 µM), almost identical MeHg uptake rates were observed in cysteine and cysteine-free treatments (0.83 attmol/cell/hr and 0.79 attmol/cell/hr resp.) with a duplicate MeHgCys experiment yielding similar results (Figure 2.7 and Tables 2.2 and 2.5) in *Tp* cells. Uptake of MeHg bound to cysteine has been postulated to occur through a neutral amino acid transporter (Bridges et al. 2004) or a methionine transporter in brain cells (Aschner and Clarkson 1988) and diatom species (Wang et al. 2004). No affect of methionine additions on MeHg accumulation on the cell wall or in the cytoplasm of the diatom *Cyclotella meneghiniana* was observed (Pickhardt and Fisher 2007).

Our similar MeHg uptake rates of MeHgCys and MeHgCl in synchronized experiments provide some evidence for active uptake of MeHgCl or almost identical passive diffusion rates for the two compounds. The formation of the CH_3HgCys (-1)

complex in the cysteine treatment may be taken up by transporters of charged amino acids as in other diatom species (Liu and Hellebust 1974) and this route of uptake of MeHgCys may be dictated by cellular demand for nitrogen as uptake of MeHgCys was almost negligible at high DOC_{SOW} concentrations containing an abundance of iminodiacetates. A noticeable difference between these intermediate DOC_{SOW} MeHgCl and MeHgCys experiments is the absence of the cellular MeHg concentration calculated from the y-intercept (Figure 2.7 and Tables 2.3 and 2.5). The dissolved cysteine ligand may outcompete surface active sites of diatom cells rendering non-cysteine exchangeable MeHg surface adsorption essentially negligible independent of background DOC_{SOW} concentration.

High MeHg adsorption and cysteine removal of MeHg from cells of *Tw* and *C. brevis* and

High cell associated (SOW rinsed) MeHg in *Tw* and *Cb* cells was observed after one hour in intermediate DOC_{SOW} concentrations. Slighlty higher MeHg concentrations were measured in live SOW rinsed *Tw* cells than dead cells, however lower MeHg concentrations were measured in live cysteine washed cells than dead cysteine washed cells. These results raise the question of whether MeHg sorption or intracellular concentration of MeHg increased over time. Low initial cellular MeHg concentrations calculated from the linear regression in most of the temperate diatom species suggest that most of the initial surface bound MeHg is removed from temperate phytoplankton.

The SOW rinse and cysteine wash removed identical amounts (~93%) of cysteine-exchangeable MeHg from the surfaces of dead *C. brevis* and *Tw* cells.

However, in *C. brevis*, the 3-part cysteine wash efficiency was only 83.8% for live cells, approximately 10% less efficient than for dead cells (Table 2.7) and approximately 12% less effective than for live *Tw* (Tables 2.6 and 2.7). Lower cell wash efficiencies in live than dead *C. brevis* and higher cell surface MeHg concentrations at low DOC_{SOW} (Figure 2.8) than in Tw at low DOC suggest that the cell surface of *Chaetoceros brevis* has a higher reactivity with MeHg than that of *Thalassiosira weissflogii.* Indeed, Fe reactivity experiments showed a light independent enhancement of Fe(II) production in the presence of *C. brevis* and a decrease in the concentration of strongly chelated Fe and its conditional stability constant (Rijkenberg et al. 2008), suggesting that *C. brevis* modified the speciation of strongly complexed Fe through sorption to the cell wall increasing its bioavailability. This effect was not observed in the presence of another Southern Ocean diatom, *Thalassiosira sp.* It is possible that live *C. brevis* may have a somewhat greater capacity to bind metals on its cell surface (Table 2.7). Due to its neutrality CH_3HgCl is bioavailable to the organism through passive transport. However, cell surface chemistry and binding of MeHg may change the speciation and/or charge of MeHg at the cell surface increasing the bound portion. Microscopic examination revealed little to no chain-forming of *C. brevis* cultures, suggesting that this was not a factor in MeHg adsorption.

Colony forming mucous matrix and concentration gradient drives higher cellular MeHg in *Phaeocystis antarctica* (*Pa*)

P. antarctica is known to produce a colony-forming mucous matrix (Schoemann et al. 2005), and colony-forming matrices produced by *Phaeocystis antarctica* and other *Phaeocystis sp.* can accumulate heavy metals like Fe and Mn (Davidson and Marchant

1987, Lubbers et al. 1990, Schoemann et al. 2001) by adsorption and complexation to polysaccharides and precipitation on the cellular mucous matrix (Schoemann et al. 2001). In the high cell density treatment, MeHg was likely adsorbed by colony mucous matrix with limited MeHg taken up into *P. antarctica* cells (Figure 2.9).

At a lower cell density with more free-living cells, a high MeHg uptake rate was observed (249 attmol/cell/hr) (Table 2.8). These results show that the mucous matrix associated with Pa colony formation inhibits cellular uptake of MeHg and among the four species of phytoplankton examined, *Pa* had the highest short-term cell uptake rates of MeHg, when normalized to cell surface area and cell volume (Fig 2.12). Cell normalized uptake rates of *Pa* were well above the linear trend of cellular MeHg uptake rate and SA/V providing evidence for an active route of MeHg uptake through cell membrane channels in this polar prymnesiophyte phytoplankton species.

Cellular release of dissolved organic carbon upon MeHg exposure in *Tw* cells

Tw released dissolved organic carbon upon MeHg exposure (10 nM) at levels well above those in incubations without MeHg. Extracellular release of dissolved organic carbon by phytoplankton at ppm (~100 µM) levels has been observed previously in response to exposures to toxic levels of metals (e.g. Cu) (Herzi et al. 2013, Tonietto et al. 2014). *Thalassiosira weissflogii* rapidly responds to mercury exposure through intracellular production of non-protein thiols (Morelli et al. 2009, Wu and Wang 2012) and a dose dependent relationship has been observed (Morelli et al. 2009). Intracellular concentrations of these non-protein thiols decreased to control levels after extended exposure (96 h) (Wu and Wang 2012). Loss of these intracellular thiols could have been

to the experimental medium through release through cellular membrane and may possibly contribute to the increased DOC_{Cell} concentrations well above background levels in our study (Figure 2.11). Decreases of released DOC following a sharp initial increase within six hours (Figure 2.11) may have been to DOC assimilation by *Tw* as an organic carbon source in long-term dark incubations or could be attributed to build up of DOC on glass frit during sampling. Improved sampling methods using separate in-line filtration for each sampling time point will should be used in future studies.

Role of chemical and biological factors in long-term MeHg uptake in *Tw*

The release of extracellular DOC by *Tw* following MeHg exposure likely modified MeHg speciation over the course of the long-term (48 hr) experiments. Thiols, carbohydrates, proteins, and humic-like compounds have all been identified in phytoplankton exudates following trace metal exposures (Pistocchi et al. 1997, Vasconcelos and Leal 2001, Dupont et al. 2004, Dupont and Ahner 2005, Herzi et al. 2013). These compounds have the potential to change the speciation of aqueous phase MeHg during experimental exposures. The cell density of *Tw* decreased between 2 and 4 h during the experiment (Table 2.10), perhaps resulting in the release of organic material, during cell lysis. After a decrease in cellular MeHg between 2 h and 4 h (Figure 2.10, inset), a slow, but linear ($R^2 = 0.995$, $p < 0.05$) increase in intracellular MeHg concentrations occurred from 4 to 24 hours (Figure 2.10). The rates of long-term uptake (0.2 to 0.9 attmol/cell/hr) in duplicate experiments, were much lower than any *Tw* short-term passive uptake rates (Figure 2.10; Tables 2.2 and 2.9). Slower uptake during this time period may be due to slower diffusion from the bulk media to the surface of the cell of a much smaller concentration of MeHgCl, or relatively slow, active transport of

MeHg. In the long-term experiments, MeHg was likely bound to free thiols (e.g. cysteine, glutathione) or proteins containing amine (NH_3) and reduced sulfhydryl groups, which can outcompete chloride ions at nM concentrations in seawater. For example, based on thermodynamic considerations, if 10 nM cysteine was excreted by cells during the experiment, 98.5% of the dissolved MeHg would have been bound as CH_3HgCys (-1). In this case, active transport would require the exchange of MeHg between dissolved ligands and cell-surface transport sites. This hypothesis is further verified by similar or even lower rates during long-term uptake than in short-term experiments with cysteine in *Tp* and *Tw* (Tables 2.5 and 2.9) as in these treatments ~100% of MeHg was already bound to cysteine, which may be transported at slower rates than MeHg bound to chloride at high DOC_{SOW} concentrations (> 800 µM), similar to DOC_{Cell} concentrations produced by cells throughout long term exposure (Figure 2.9). Slower uptake of MeHg bound to cysteine in these conditions may be due in part to energy dependent transport of cysteine Hg complexes by amino acid transporters seen in other eukaryotic cells (Liu and Hellebust 1974, Bridges et al. 2004).

2.6 Conclusions

Methylmercury uptake and normalized uptake to cell parameters revealed high rates in the polar prymnesiophyte *Phaeocystis antarctica* in a more free-living condition relative to that of other temperate and polar diatoms. Uptake rates in *Tw* and *Tp* were likely driven by cell size as the smaller *Tp* accumulated much higher MeHg than *Tw*, the larger centric diatom. The results of this study confirm previous observations that DOC decreases MeHg uptake in temperate and polar phytoplankton and may alter contributions of passive and active uptake of MeHg in phytoplankton cells. Lowering

DOC_{SOW} concentrations increased short-term MeHg uptake in temperate and polar diatoms and at low DOC, MeHg uptake in temperate diatoms was controlled by cell SA/V ratios. Higher cysteine exchangeable MeHg concentrations were found in polar phytoplankton when compared to temperate species, suggesting that a small fraction of MeHg may be less available for assimilation into zooplankton grazing on polar phytoplankton. Separation of cytoplasmic, cell wall and membrane fractions are needed to further clarify MeHg cell fractions and their influence on trophic transfer assimilation.

Long-term uptake and exposure studies show that *Tw* releases cellular DOC changing the chemistry and potentially MeHg speciation. These results provide explanations for high concentrations of MeHg in open ocean fish that may be accumulating Hg from prey sources which were initially enriched in MeHg due to high uptake in low DOC conditions. Surface area-to-volume observations indicate smaller phytoplankton cell sizes in oligotrophic waters will also drive initial concentration of MeHg at the base of food webs offshore removed from coastal inputs of organic matter.

Chapter III Influence of physical and biological processes on the horizontal and vertical distributions of mercury across the continental shelf of the West Antarctic Peninsula

A. Abstract

Continental shelf waters west of the Antarctic Peninsula (WAP) differ from most coastal marine ecosystems in temperate regions and the Arctic due to the lack of riverine discharge or anoxic sediments, and the presence of a relatively deep continental shelf (500 to 600 m). Given these physical features, atmospheric deposition and release from glaciers and sea ice may play important roles in supplying Hg to this remote coastal ecosystem, while Circumpolar Deep Water may be linked to Hg dynamics further offshore. The analysis of Hg in seawater, surface particulate organic matter, and sea ice throughout the WAP ecosystem revealed coastal vs. offshore differences in surface Hg concentrations and vertical distributions. Dissolved total mercury (d-Hg_T) concentrations (0.8 to 16.6 pM) varied considerably among continental shelf waters, with a subsurface maximum (16.6 pM) in waters underlying sea ice consistent with other polar studies. Total dissolved Hg was also high in surface waters at a sampling location near regions of accelerated glacier melting in the southwest portion of the Peninsula. Dissolved total methylated mercury (d-$MeHg_T$) (0.02 to 0.9 pM) in seawater was highest in the northern WAP with a maximum concentration (0.9 pM) that exceeded all previously measured values in polar regions. This subsurface maximum was observed at intermediate depth in the Palmer Deep Canyon, a region of high primary productivity, and possible site of high Hg remineralization in the water column. Bioconcentration factors of particulate methylmercury (p-MeHg) ($\log_{10}$ 3.7 to 6.2) calculated from dissolved surface seawater and mass concentrations in phytoplankton biomass (pigment

derived) show high enrichment in WAP phytoplankton. Sea ice contained higher unfiltered total methylmercury (T-MeHg) concentrations (0.18 to 0.52 pM) per volume than surface seawater T-MeHg (0.03 to 0.07 pM) (p-MeHg + d-MeHg fractions), revealing a possible pelagic MeHg source to plankton upon release during austral spring and summer seasons and further emphasizing the importance of sea ice, not only as a driver of the WAP food web, but to Hg dynamics.

B. Introduction

Mercury (Hg) is a contaminant of concern in polar regions due to the long range atmospheric transport and deposition of gaseous elemental mercury (Hg^0) (Fitzgerald et al. 1998, Shia et al. 1999), as well as inputs from riverine discharge (Heimburger et al. 2015, Schartup et al. 2015a) and glacial meltwater (Stern et al. 2012a). In addition, Hg is enriched in the thermoclines of both the Arctic and Southern Oceans relative to the pre-industrial background (Lamborg et al. 2014) and methylmercury (MeHg), the neurotoxic form of Hg, biomagnifies in polar food webs (Bargagli et al. 1998, Ruus et al. 2015). The sources and cycling of Hg in the Arctic and Southern Oceans have only been examined in a few oceanographic surveys (St Louis et al. 2007, Cossa et al. 2011, Heimburger et al. 2015, Mastromonaco et al. 2017b), and little is known about the concentrations and speciation of Hg in the coastal waters along the West Antarctic Peninusula (WAP).

The highly biologically productive coastal marine ecosystem west of the Antarctic Peninsula differs from other coastal marine ecosystems in that it has a relatively deep continental shelf and lacks riverine discharge. Over the past 40 years, the WAP marine ecosystem has undergone major changes due to the shortening of its sea ice season and

the nearly complete loss of perennial sea ice (Stammerjohn et al. 2008, Steinberg et al. 2012). At the same time, the retreat of glaciers on the Antarctic Peninsula has accelerated (Cook et al. 2016). The physical and biological responses of the WAP marine ecosystem to these changes have been well characterized through the efforts of the Palmer Antarctica-Long-Term Ecological Research program and other research efforts (Saba et al. 2014, Carvalho et al. 2017). However, an assessment of the effects of accelerated warming on the distributions and transformations of various forms of Hg lacks even baseline data.

Atmospheric deposition, including that associated with atmospheric mercury depletion events (Schroeder et al. 1998, Ebinghaus et al. 2002, Mastromonaco et al. 2016), is likely an important source of inorganic Hg to the entire coastal marine ecosystem along the WAP, while glacial runoff may be particularly important in coastal bays and inlets (Andersson et al. 2008b, Stern et al. 2012a, Zdanowicz et al. 2013). Once deposited or discharged to the sea, oxidized inorganic Hg may undergo a variety of abiotic or biologically-mediated transformations, including reduction and methylation (Barkay et al. 2011).

The reduction of Hg^{2+} to volatile dissolved elemental mercury (DEM) may be photochemically driven (Amyot et al. 1997, O'Driscoll et al. 2006b) during the high light conditions of austral summer or microbially catalyzed (Poulain et al. 2007), but in either case, reduction of Hg^{2+} tends to be spatially and temporally associated with primary production (Vandal et al. 1991, Lanzillotta et al. 2004, Lehnherr et al. 2011). DEM accumulates in seawater under sea ice in the fall and winter (Cossa et al. 2011) and volatilizes to the atmosphere in the spring (Mastromonaco et al. 2017b). Similar

dynamics likely also control the evasion of dimethylmercury (Me_2Hg). Entrapment of volatile forms of Hg could enhance the formation of methylmercury (MeHg) under sea ice. Indeed, higher MeHg concentrations have been measured in seawater under sea ice than open water in polar regions (St Louis et al. 2007, Cossa et al. 2011). The concentrations of Hg in sea ice are higher than in surface seawater in the East Antarctic (Gionfriddo et al. 2016). Hg in sea ice may be associated with high densities of particulate organic matter (POM) and sea ice algae communities (Burt et al. 2013), which are released to surface waters as first-year sea ice melts in the spring and summer.

With no rivers or estuaries and relatively deep (500 to 600 m), weakly reducing sediments (Hartnett et al. 2008, Parapar et al. 2011), coastal Antarctic environments such as the WAP lack the types of anoxic environments that are the primary source of MeHg to Arctic coastal waters (Douglas et al. 2011, Schartup et al. 2015a). Alternative possible sites of MeHg production along the WAP include glacial melt zones (St Louis et al. 2005) and microbially-active layers of the water column (Pongratz and Heumann 1998, Lehnherr et al. 2011) or sea ice (Cossa et al. 2011, Gionfriddo et al. 2016). In addition to methylation rates, rates of MeHg demethylation measured in polar marine waters require the consideration of both processes when evaluating dissolved MeHg concentrations.

Cycling of MeHg in waters may also be driven by phytoplankton uptake, POM scavenging, and photolytic degradation in surface waters exposed to high intensities and long periods of sunlight during austral summers maintaining low dissolved MeHg concentrations. The phytoplankton community within WAP continental shelf waters is dominated by large diatoms, with small contributions from various nanoplankton (Prezelin et al. 2004, Schofield et al. 2017). Both live and decomposing phytoplankton

cells may contribute to the accumulation of MeHg at the base of the food web as live and dead cells are in close association within productive coastal aggregates and can accumulate mercury due its high affinity for cell surfaces. The fate of inorganic mercury and MeHg in WAP surface waters will likely be dictated by WAP phytoplankton production and bacterial dynamics as they are tightly coupled and quite complex (Ducklow et al. 2012). Large interannual differences in productivity and shifts in phytoplankton composition may influence MeHg concentrations at the base of the food web and its subsequent availability to upper trophic levels.

The transport of MeHg with upwelled Upper Circumpolar Deep Water (UCDW) may be a unique and important source of MeHg to the WAP's coastal marine ecosystem. UCDW is a nutrient-rich and relatively oxygen-depleted water mass that is situated above the more saline Lower Circumpolar Deep Water (LCDW). Together these water masses comprise Circumpolar Deep Water (CDW) within the Southern Ocean's Antarctic Circumpolar Current (ACC). The chemical composition of CDW is a result of the decomposition of organic matter accumulated from deep water masses of the Indian and Pacific Ocean basins and is characterized by high apparent oxygen utilization (AOU). The concentration of MeHg is elevated in CDW (Cossa et al. 2011, Mastromonaco et al. 2017a), perhaps indicating that the microbial activity associated with this decomposition also favors the release of MeHg from remineralized particles. As the Antarctic Circumpolar Current (ACC) flows east along the continental rim of the Amundsen-Bellingshausen Seas, CDW intrudes onto the shelf through submarine canyons (Klinck et al. 2004, Martinson and McKee 2012) bringing saline LCDW along the bottom and warmer (~2°C) UCDW into intermediate depths of the shelf (Moffat et al. 2009,

Martinson and McKee 2012). UCDW exchanges heat with overlying (colder) Winter Water (WW) creating modified Circumpolar Deep Water (mCDW) near the Antarctic Peninsula (Couto et al. 2017), and potentially delivers MeHg to the coastal ecosystem of the WAP.

C. Site – WAP Marine Ecosystem

In contrast to other coastal marine ecosystems, the WAP lacks a shallow continental shelf, riverine discharge, and extensive wetlands. Although freshwater Hg inputs from ice melt to WAP coastal waters may be lower than riverine sources of Hg in the Arctic (Heimburger et al. 2015, Schartup et al. 2015b), freshwater contributions along the coast may be more localized due to substantial glacier loss in central and southern areas of the WAP (Cook et al. 2016). Sea ice duration and glacial meltwater at southern latitudes during summer months drives production in coastal areas such as Marguerite Bay (Henley et al. 2017) and meltwater may transport dissolved Hg to surface waters as in the Arctic Ocean (Andersson et al. 2008b).

In this study, we examined the spatial variation in surface seawater concentrations of dissolved elemental mercury (DEM), dissolved total methylated mercury (d-$MeHg_T$), and dissolved total Hg (d-Hg_T) and the enrichment of MeHg in surface particulate organic matter (POM) (p-MeHg) along the continental shelf west of the Antarctic Peninsula. Unfiltered total methylmercury (T-MeHg) was measured in surface sea ice cores while addition of dissolved total methylated mercury and particulate methylmercury were used to calculate a T-MeHg in surface seawater for comparison with sea ice concentrations. In addition, we assessed the vertical distributions of d-MeHg and

d-Hg_T with respect to the physical and chemical characteristics of the dominant water masses in profiles from northern, mid-latitude, and southern stations along the WAP.

D. **Materials and Methods**

Observational Area

Field work was conducted aboard the ARSV *Laurence M. Gould* during the austral summers of 2014 and 2015 from nearshore, continental shelf, and slope waters west of the Antarctic Peninsula. The area sampled, which was within the Palmer Antarctica Long-Term Ecological Research (PAL LTER) sampling grid (Figure 3.1), varied with sea ice conditions and extended from 64 to 68°S and 64 to 74°W in 2014 and 65 to 69°S and 61 to 78°W in 2015. Coastal, shelf, and slope sub-regions along the WAP were assigned using average depths for stations with otherwise complex bathymetry (Steinberg et al. 2012) containing fjords, deeps, bays, submarine canyons, and embayments connected by deep channels or troughs (Anderson 2002). Coastal and shelf waters were designated as those inshore of the shelf break (average depth approximately 430 m), while shelf and slope waters slope were separated as those offshore of the 750 m isobath.

Underway Analysis of Dissolved Elemental Mercury

Underway measurements of dissolved elemental mercury (Hg^0_{aq}) were carried out aboard the ARSV *Laurence M. Gould* along the LTER grid (Figure 3.2) during austral summer (4 January to 2 February) 2014. Surface seawater was drawn off the ship's flowing clean seawater line (intake depth ~ 3 m) with a T fitting and directed through acid-cleaned 0.64 cm OD Teflon tubing to an acid-cleaned, 500 mL flow-through glass stripping bottle with a glass frit air diffuser. Seawater was pumped into and out of the

stripping bottle using a peristaltic pump with acid-cleaned C-flex tubing at rates of 46 to 65 mL min^{-1} giving an average residence time of about 10 min. The water in the stripping bottle was continuously purged with activated charcoal-filtered, Hg-free air at a flow rate of 1.5 L min^{-1} which was sufficient to strip out all Hg^0_{aq} from incoming seawater in less than one minute. Air leaving the stripping bottle was passed through a soda lime trap to remove water and then into a Tekran 2537A continuous mercury vapor analyzer.

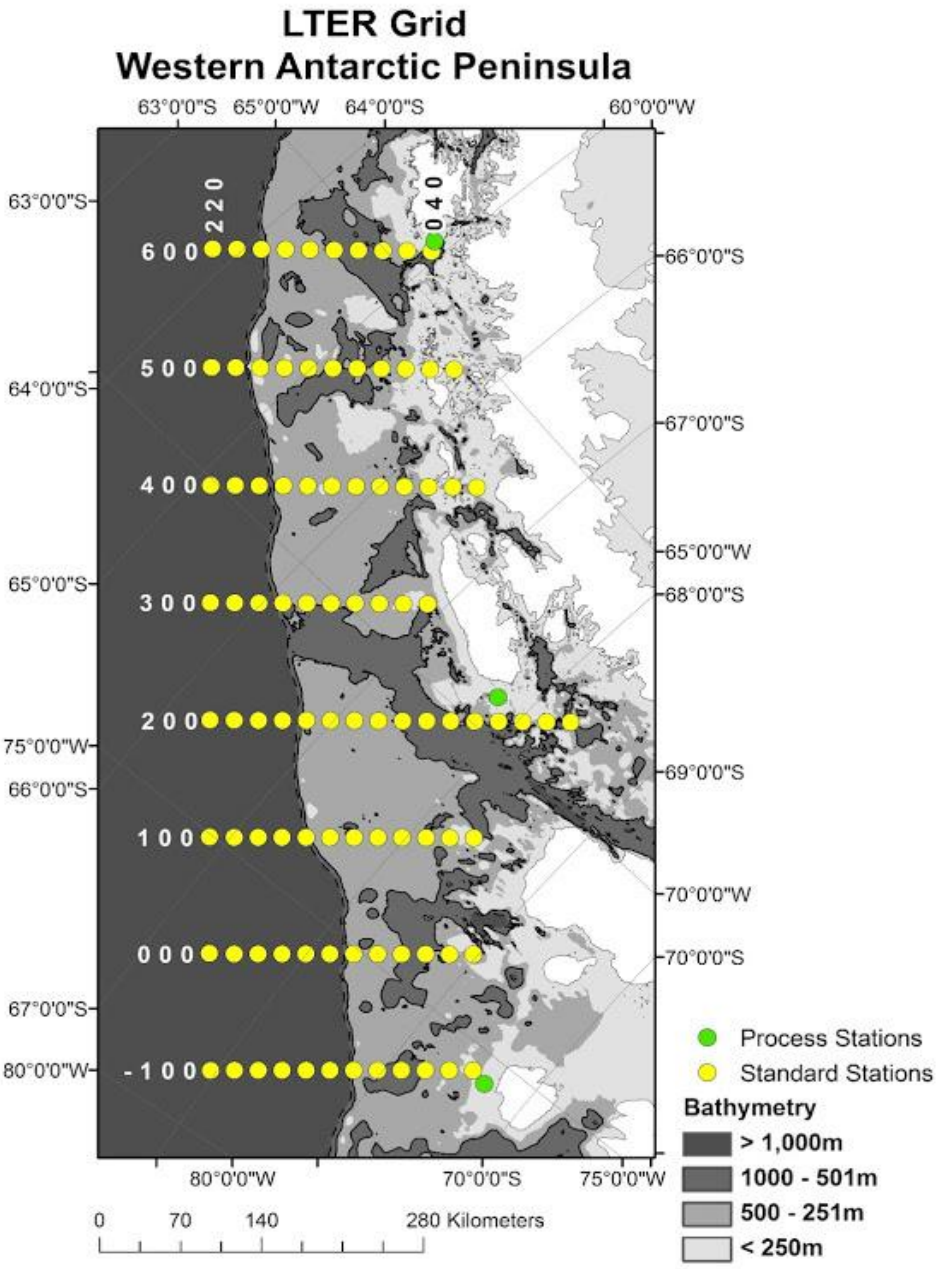

Figure 3.1 Process and standard stations on the Palmer Antarctica Long-Term Ecological Research (PAL LTER) grid along the WAP.

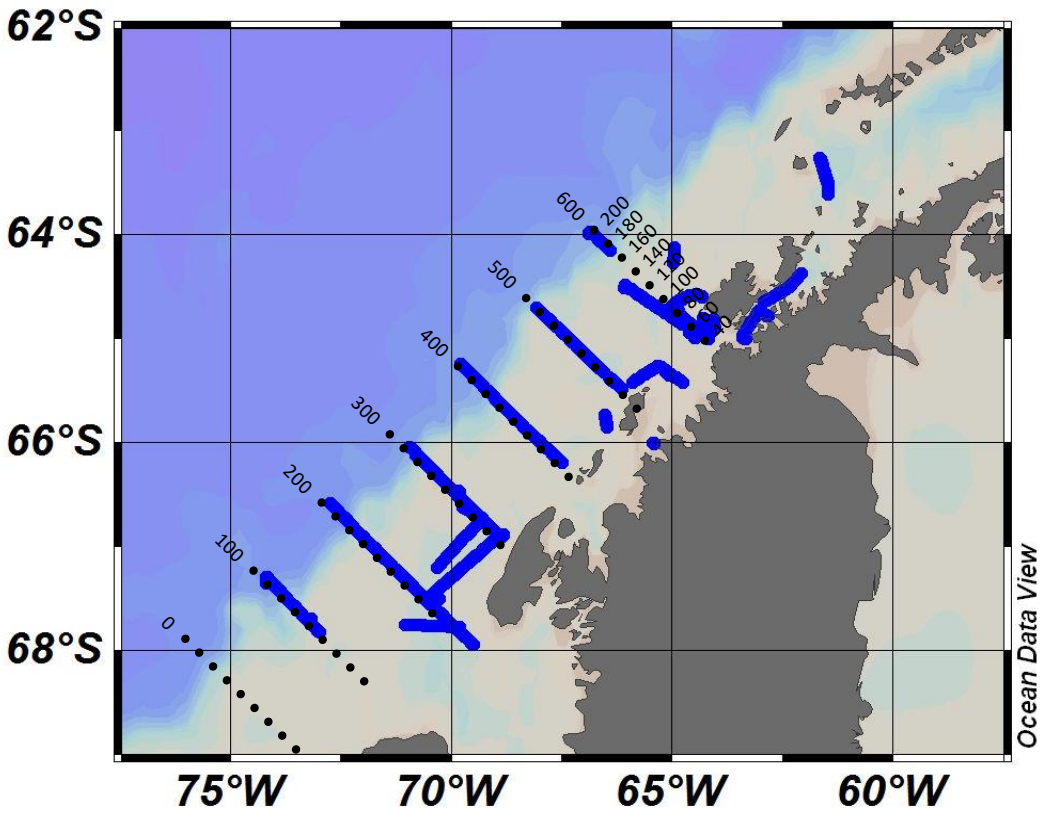

Figure 3.2 Surveyed area of surface measurements within the Palmer Long Term Ecological Research (PAL-LTER) sampling grid ranging from most northern latitudes (600 line) to sea ice edge (100 line) in January 2014.

Elemental mercury in purge air (Hg^0_p, pmol L^{-1}) was measured at five-minute intervals and converted to Hg^0_{aq} (pM) according to:

$$Hg^0_{aq} = \frac{Hg^0_p}{F} \times P \qquad \text{Eq. 3-1}$$

where F is the seawater flow rate into and out of the stripping bottle and P is the purge air flow rate (1.5 L min^{-1}). Pre-cruise calibration of the Tekran 2537A was performed by external injection of gaseous elemental mercury standards. At sea, daily calibrations were run using the Tekran's internal permeation source. Field blanks measured in seawater-filled stripping bottles purged with Hg-free air and with the seawater pump turned off always gave zero peak areas and Hg^0_p concentrations. Based on the stated detection limit of the Tekran 2537A, and the flow rates used here, the detection limit for Hg^0_{aq} was 10 fM. Precision of Hg^0_{aq} analyses estimated as the coefficient of variation of replicate measurements (n = 10) of the same water mass was less than 5%.

Air-sea fluxes of Hg^0 (F, pmol m^{-2} h^{-1}) were estimated according to:

$$F = K_w(Hg^0_{aq} - Hg^0_g/K'_H)*10 \qquad \text{Eq. 3-2}$$

where K_w is the gas exchange transfer velocity, Hg^0_g is the concentration of gaseous elemental mercury in the atmosphere (pmol L^{-1}), and K'_H is the Henry's Law constant for Hg^0 (Andersson et al. 2008a). Gas exchange transfer velocities were parameterized according to:

$$K_w\ (cm\ h^{-1}) = (0.222U_{10}^2 + 0.333U_{10})\ (Sc_{Hg}/600)^{-0.5} \qquad \text{Eq. 3-3}$$

where U_{10} is the wind speed at 10 m, and Sc_{Hg} is the Schmidt number (Nightingale et al. 2000). Schmidt numbers were estimated using temperature-dependent kinematic viscosities of seawater (Thibodeaux 1996) and molecular diffusivities of the gas (Kuss et al. 2009). Concentrations of Hg^0_g varied from 5 to 9 fmol L^{-1} (DL = 0.35 fmol L^{-1}) and

were similar to those previously measured in this region (Soerensen et al. 2010a). Since Hg^0_g was not measured continuously, median Hg^0_g concentrations within sub-regions of the sampling grid were used in flux calculations.

Seawater Collection for Dissolved Total Mercury and Dissolved Total Methylated Mercury

Surface and depth-resolved seawater samples were collected during austral summer 2015 (Figure 1; Table 1) at two northern (64.0-64.9°S; LTER 600 line)), one mid-latitude (67.1-68.1°S; LTER 200 line)), and two southern (~69°S; LTER -100 line)) stations (Figure 3.2) using a trace metal clean rosette equipped with a CTD to measure hydrological parameters of the water column (potential temperature, salinity, and dissolved oxygen). From north to south, these stations were 400 and 300 km apart, respectively, and from east to west, were separated by 160 to 170 km. Stations varied considerably in depth (260 to 2000 m) both transversely across the continental shelf and at different latitudes. Sea ice conditions varied from 0% to 100% ice covered waters and sea ice coverage was not related to proximity to shore.

GEOTRACES protocols (WWW.GEOTRACES.ORG) were followed during the collection of all surface and water-column seawater samples. Water column samples were collected using externally-closing Niskin bottles fitted with Nyco pressed aluminum inserts deployed on a *GEOTRACES* trace-metal-clean rosette with four Kevlar cables. At each station, samples were collected from 7 depths starting at 10 m. Surface seawater was collected at a depth of approximately 1 m using a trace-metal-clean tow-Fish surface sampler and additional surface seawater samples were collected between stations.

Niskin bottles were pressurized using an oil-free air compressor with 0.2 µm filtered lab air and seawater was filtered using acid cleaned Acropak 0.45 µm filters. Filtrate was collected in Teflon (FEP) bottles at northern sites and polycarbonate bottles at mid-latitude and southern sites for dissolved total mercury (d-Hg_T) and dissolved total methylated mercury (d-$MeHg_T$) in a GEOTRACES clean air laboratory. Field blanks of Teflon and polycarbonate bottles filled with ultrapure water were prepared on board at the time of seawater collection at northern and mid-latitude sites. All samples and field blanks were handled with clean-hands-dirty-hands protocol (Fitzgerald et al. 1999), acidified with HCl (0.1% v/v, Fischer Scientific trace metal grade), sealed in two polyethylene bags, and stored at 4°C until analysis at Rutgers University.

Dissolved Total and Dissolved Total Methylated Mercury Analysis

Dissolved total Hg analysis of filtered seawater followed US EPA Method 1631. To oxidize and solubilize all Hg species to Hg^{2+}, seawater samples (150 mL) were pretreated (in duplicate) by addition of 0.1 percent (v/v) acidic 0.2 N bromine monochloride (BrCl). Oxidation reactions were accelerated by heating to 50°C for at least 20 h (Sunderland et al. 2009) in acid-cleaned (8 M HCl for >24 h, then 1.2 M HCl for 12 h) glass bottles. The observation of a faint yellow color indicating the presence of excess BrCl was used to determine complete oxidation. Bottles were allowed to cool to room temperature before a 2 h pre-reduction of BrCl with acidic hydroxylamine hydrochloride (NH_2OH-HCl). Following the reduction of Hg(II) with acidic (10% v/v HCl) stannous chloride ($SnCl_2$), Hg(0) was purged with Hg-free N_2 gas, concentrated by dual-gold amalgamation, desorbed into an argon gas stream and analyzed for total Hg by cold vapor atomic fluorescence spectroscopy (CVAFS) using a Brooks Rand MERX-T

analyzer. Seawater samples were analyzed in duplicate with two method blanks (150 mL MQ and 0.1% v/v 0.2 N BrCl) and Teflon FEP or polycarbonate field blanks (150 mL MQ, 0.1% v/v HCl, and 0.1% v/v 0.2 N BrCl). In addition, seawater samples from various depths at northern, mid-latitude, and southern sites were spiked with 100 pg of reactive mercury (Hg^{2+}) to determine Hg recoveries.

Recoveries of Hg in spiked samples averaged 100 ± 15% and ranged from 84% to 130%. NIST 3133 was used as the analytical standard and for spikes to seawater and NIST 1641d was used for routine calibration. Method blanks were used to determine the average daily detection limit (DDL) of 0.22 pM when Teflon field blanks were below detection. All dissolved total Hg concentrations for filtered seawater samples collected in polycarbonate bottles were corrected to the average (n=4) total Hg concentration in polycarbonate bottle field blanks (0.72 pM). A relative percent difference (RPD) of 15% between analytical duplicates was used as a precision quality criterion, and all samples that had an RPD greater than 15% were run in triplicate.

Previous work has shown that dimethylmercury (Me_2Hg) is not stable when acidified and will decompose into methylmercury (MeHg) (Mason and Sullivan 1999) within a matter of hours (Parker and Bloom 2005). As Me_2Hg was not measured on board in 2015, "methylated Hg" reported here represents dissolved total methylated mercury (d-$MeHg_T$ = d-Me_2Hg + d-MeHg). We analyzed d-$MeHg_T$ by direct ethylation of preserved (0.1% v/v HCl) seawater as it was shown to minimize potential loss or abiotic production of artifact methylmercury and requires minimal amount of sample relative to methylmercury distillation or extraction (Munson et al. 2014). Samples were analyzed manually for d-$MeHg_T$ by CVAFS (Tekran 2500) after gas chromatographic

separation of the ethylated derivative (Liang et al. 1994b) at Rutgers University. In 180 mL aliquots, duplicate preserved (0.1% HCl) seawater samples were further acidified with 0.5% with concentrated (16 N) sulfuric acid (H_2SO_4, Fisher, Trace Metal Grade) in FEP Teflon bottles for 24 h (Bowman and Hammerschmidt 2011). They were then transferred to glass impingers and incubated with 2.5% (wt/vol) ascorbic acid for 15 min. Sample pH was adjusted to 5 with (1 mL) 2 M sodium acetate (Fisher, pH 5) and then neutralized with KOH (45% wt/vol, Fisher). An 85 µL aliquot of just-thawed sodium tetraethylborate (NaTEB, Fisher Chemical) was then added to begin ethylation (Liang et al. 1994a). All reagants were prepared in acid-cleaned Teflon vials.

Along with method blanks (180 mL MQ plus 0.5% v/v 16 N H_2SO_4), field blanks in FEP Teflon or polycarbonate bottles, and dissolved MeHg recovery samples (seawater spiked with 20 pg of methylmercury hydroxide, Brooks Rand), seawater samples were analyzed in duplicate using the RPD precision quality criterion described above for seawater. Methylmercury recoveries ranged from 79% to 107% with an average of 95 ± 10%. As methylmercury in method blanks were below detection, the working detection limit (21 fM) averaged over multiple methylmercury analyses (n=4), was determined as 3 times the standard deviation of the instrument blanks. Field blanks collected in Teflon FEP bottles were below detection. However, the concentrations of d-$MeHg_T$ in all seawater samples collected in polycarbonate bottles were corrected to the average (n=4) methylmercury concentration in polycarbonate bottle field blanks (0.05 pM). As a result of this correction, some d-$MeHg_T$ concentrations for seawater collected in polycarbonate bottles were below detection.

Sea Ice Collection for Unfiltered Total Methylmercury Analysis

First year sea ice was sampled using clean-hands-dirty-hands protocol (Fitzgerald et al. 1999). With a Kovacs MkII corer, 1 m long, 9 cm diameter sea ice cores were collected while wearing arm-length polyethylene gloves. A stainless-steal saw (pre-cleaned) was used to slice each core into 0.25 m sub-cores. Contamination of cores during handling was evaluated in blank ice cores prepared from frozen ultrapure water (0.08 pM). Separated sub-cores were allowed to thaw in polyethylene bags and were then transferred to Teflon and polycarbonate bottles. Sub-cores with high POM were frozen at -20°C while all other samples were acidified with HCl (0.1% v/v, Fischer Scientific trace metal grade), sealed in two polyethylene bags, and stored at 4°C until analysis. We analyzed unfiltered total methylmercury (T-MeHg) by direct ethylation using the seawater extraction methods described above. These unfiltered sea ice samples yielded low MeHg matrix spikes (36%), therefore, all concentrations reported were corrected to account for low recoveries.

Surface Particulate Organic Matter (POM) Collection for Particulate Methylmercury Analysis

A tow-Fish surface sampler was used to collect surface seawater for large volume positive pressure filtration. Surface water was collected in a large volume carboy via double diaphragm pump and acid cleaned plastic tubing. Ten to twenty liters of surface seawater were filtered using by positive pressure through pre-muffled (550°C) 142 mm GF/F filters using appriopriate water sampling bottle procedures for trace metal particulates (Planquette and Sherrell 2012), which were held in Teflon supports using Hg-free, ultra high purity nitrogen gas. Filters were transferred to acid-cleaned 142 mm

petri dishes using trace metal clean Teflon forceps and stored in -20°C until analysis. Field blanks were collected at various latitudes in both sampling years by filtering Milli-Q water to account for any contamination during sampling and handling. Particulate methylmercury (p-MeHg) concentrations were normalized to volume filtered and biomass using chlorophyll *a* (chl*a*) and phaeopigment concentrations measured in separate samples (see below).

In the lab, GF/F filters were transferred to 180 mL Teflon vials with open port caps and were lyophilized for >24 h. Freeze-dried 142 mm GF/F were cut into fourths using stainless steel scalpel blades and Teflon forceps, all acid cleaned using dilute acid (10% HCl) and Milli-Q water prior to use. Cut filters were placed into large volume, Teflon distillation vials, to which 80 mL of Milli-Q water plus microliter aliquots (1-20) of 50% sulfuric acid, 2.7M potassium chloride, and 0.1% ammonium 1-pyrrolidinedithiocarbamate (APDC). Sulfuric acid was added last prior to distillation. Samples were distilled in a custom made 9-place heating block and the Tekran 2750 automated distillation unit at a temperature of 120°C and a gas flow rate of approximately 60 mL/min, until approximately 85% of the total volume was transferred to collection vials following published protocols for large volume distillations (Horvat et al. 1993).

Duplicate subsamples (20-30 mL) of POM distillates were analyzed. Two method blanks, and one matrix spike composed of pre-filtered (GF/F), freeze-dried phytoplankton cultures (MeHg free) spiked with 100 pg of methylmercury were also analyzed. Analysis of methylmercury for all distillates followed US EPA Method 1630 and was carried out using a Tekran Model 2700 automated direct purge, gas chromatography, cold vapor atomic fluorescence (CVAFS) system. Samples were incubated with 2 M sodium acetate

buffer and sodium tetraethylborate for 45 min before analysis. Values reported are averages of duplicates. A relative percent difference (RPD) of <50% was used as a precision quality criterion (QC) for methylmercury concentrations in POM samples, and if exceeded, a third subsample was analyzed.

Methylmercury recovery from spiked samples averaged 95 ± 21% (range 71-126%). A methylmercury hydroxide Brooks Rand standard was used for spikes and standard curves. The average daily detection limit of methylmercury in POM was 0.27 pM, which was estimated based on three times the standard deviation of the distillation blanks. Distilled field blanks were below detection.

Microbial biomass and activity

All data for surface plots of phytoplankton pigments and bacterial measurements were obtained from the PAL LTER DataZoo (http://pal.lternet.edu/data). All bacterial analyses and phytoplankton pigment concentrations were collected from surface water (0-10 m) using the CTD-Rosette system. Bacterial abundances were determined by flow-cytometry of stained bacterial cells on-board, and bacterial production rates were assessed by incorporation of 3H-leucine (Smith 1992, Ducklow et al. 2000, Gasol and Del Giorgio 2000). Chl*a* and phaeopigment concentrations were measured in acetone extracts of GF/F filtered samples using a Turner 10AU fluorometer at Palmer Station. The accessory pigment fucoxanthin was analyzed by High Performance Liquid Chromoatography at Rutgers University.

Calculations for total biomass of particulate organic matter (POM), particulate methylmercury, and bioconcentration factors

A modified approach from Gosnell & Mason 2015 (central Pacific) was used to calculate total biomass for POM along the WAP. Phytoplankton pigment concentrations of Chl*a* and phaeopigments were used to account for contributions of live and dead phytoplankton to the particulate organic carbon (POC) pool (Gosnell and Mason 2015)

$$MeHg\ \left(\frac{ng_{MeHg}}{g_{totbio}}\right) = \frac{ng_{MeHg}/L}{((chla_{\frac{\mu g}{L}} + phaeo_{\frac{\mu g}{L}}) * \text{POC:chl} * \text{POM:POC} * \text{Tot Biomass}) * 10^{-6}} \quad \text{Eq. 3-4}$$

A POC:chl ratio of 210 from a productive, diatom-dominated region of the Ross Sea was used to convert pigment concentrations to POC and an estimate of 30% POC of the total organic matter was used to calculate mass contribution of phytoplankton (DiTullio and Smith 1996). To account for other sources of particulate organic carbon such as bacterial biomass during a time of high bacterial abundance, zooplankton fecal pellets, and other organic materials (Church 2008) during the very productive austral summer, values were scaled by a factor of 5 (Tot biomass) to a final total biomass gram weight. Values are reported as pmol of MeHg per dry weight of total particulate biomass.

Bioconcentration factors (BCFs) were calculated using the equation below and co-located concentrations of dissolved MeHg in WAP surface seawater ($MeHg_d$) and MeHg concentrations in POM ($MeHg_p$).

$$BCF = \frac{MeHg_p\ (\frac{ngMeHg}{gtotbio})}{MeHg_d\ (\frac{ngMeHg}{gseawater})} \quad \text{Eq. 3-5}$$

E. Results

Dissolved elemental mercury (DEM) concentrations and saturation in surface waters

Elevated concentrations of dissolved elemental mercury (DEM) were observed in inner shelf regions and were highest near the coast between the 600 and 400 lines (65°S and 66°S) with an approximate range of 0.15 to 0.25 pM (Figure 3.3). Surface DEM concentrations near the coast were lower south of the 400 line to southern latitudes (range 0.15 to 0.05 pM) and near the sea ice edge in January 2014 (at approximately the 100 line). Coastal waters along the WAP were generally supersaturated in DEM (≥100%) with calculated degrees of saturation reaching up to 300% spanning north of Anvers Island (64°S) to north of Alexander Island (~67°S) (Figure 3.4). Mid-shelf regions had noticeably lower DEM concentrations than coastal sections in the northern regions of the WAP, and DEM decreased on the outer shelf to concentrations below 0.05 pM. Mid-shelf DEM concentrations at latitudes below the 300 line were quite uniform at ~0.075 pM, but decreased on the outer shelf. DEM saturation in coastal, mid-shelf, and outer shelf surface waters followed spatial patterns of DEM concentrations with higher degrees of saturation observed in the north (>250%), and lower, but still saturated concentrations in the south and near the sea ice edge.

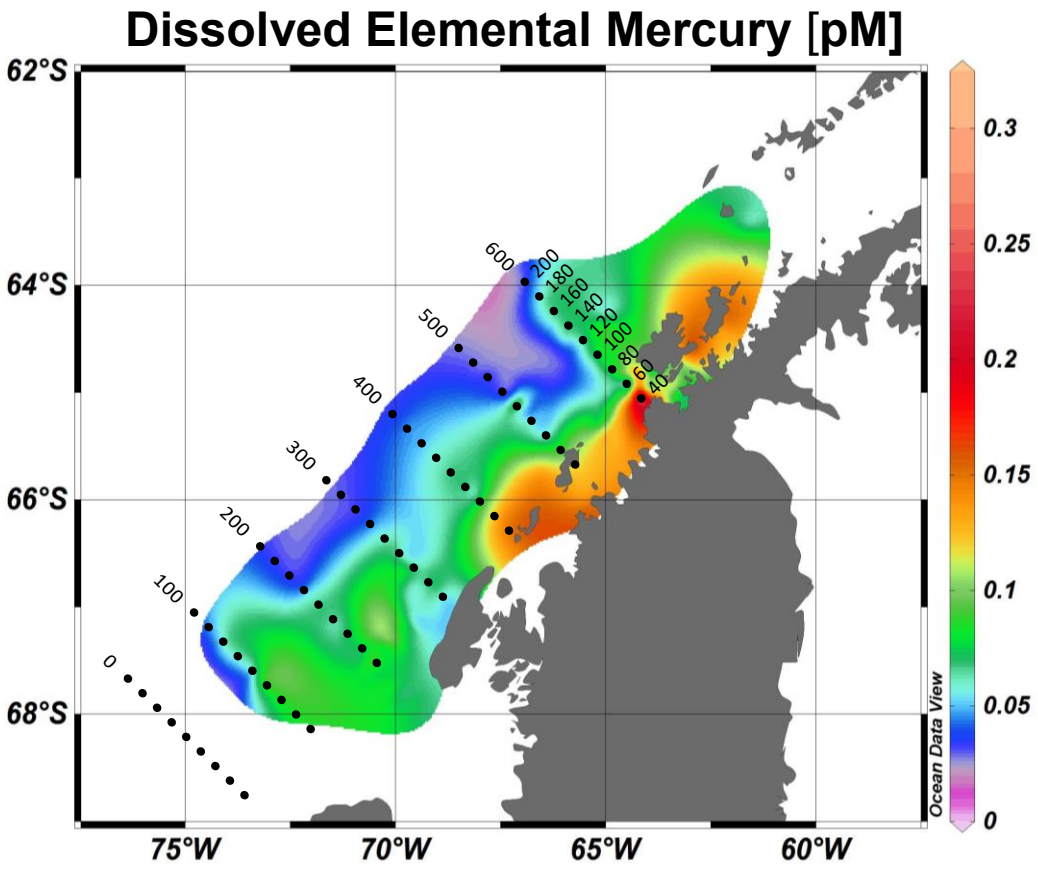

Figure 3.3 Underway surface seawater measurements of dissolved elemental mercury (DEM) concentrations in the Southern Ocean west of the Antarctic Peninsula.

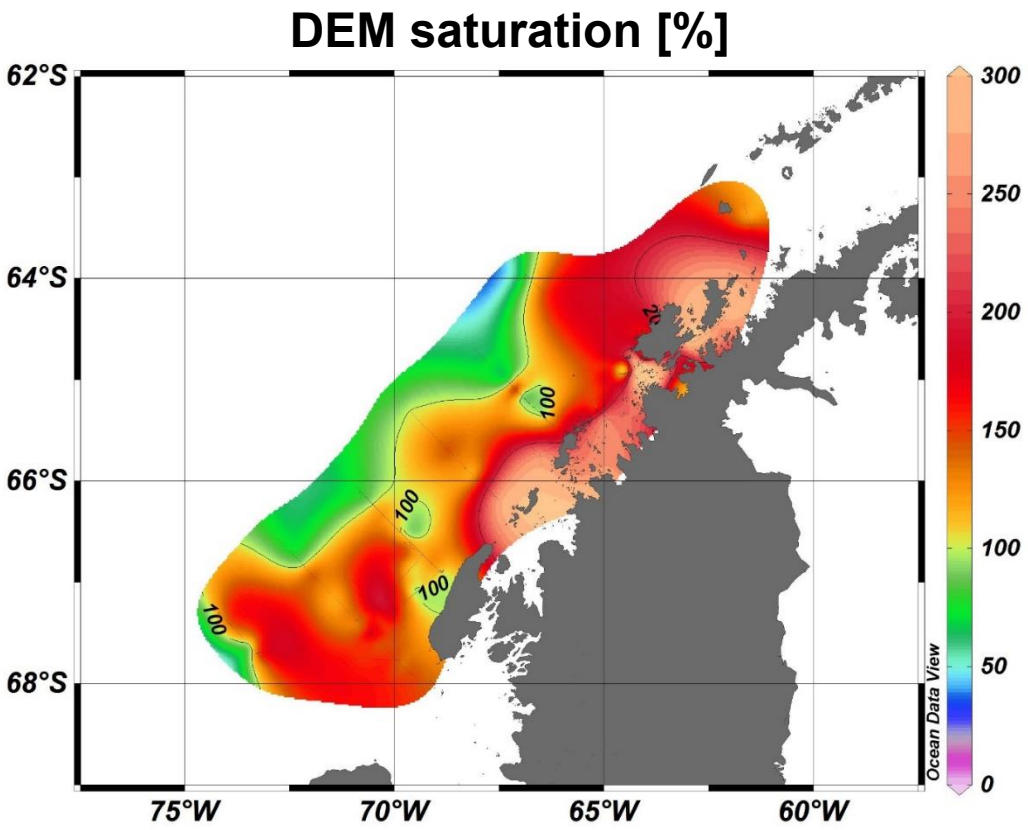

Figure 3.4 Dissolved elemental mercury (DEM) saturation in surface waters along the continental shelf west of the Antarctic Peninsula**.**

Air-sea exchange and flux of DEM

Mercury air-sea exchange fluxes were estimated for nine sub-regions over the continental shelf along the Antarctic Peninsula. These sub-regions were defined by three ranges of LTER grid lines (620-450, 450-250, and 250-100) in the SW-NE direction, and by distance in the SE-NW, nearshore-offshore direction. Thus coastal, shelf, and slope regions were defined as <40 km, 40 to 120 km, 120 to 200 km, respectively. Flux estimates for these nine sub-regions ranged from -0.79 in the slope sub-region of the 620-450 lines to 7.66 pmol m^{-2} h^{-1} in the coastal sub-region along the 250-100 lines (Table 3.1). Fluxes of Hg^0 were highest nearshore except for the coastal sub-region between the 450-250 lines. Total air-sea mercury exchange rates ranged from -0.26 to 1.79 mol/d, and generally mirrored fluxes except for the larger shelf sub-regions between the 450-250 and 620-450 lines (Table 3.2).

Biomass as chlorophyll *a* (chl*a*) and phaeopigments in 2014 surface water

Synchronous measurements of surface chl*a* and phaeopigments were conducted along the LTER grid in 2014. Higher chl*a* was measured nearshore with concentrations reaching as high as 25 µg/L and lowest pigments measured on the slope shelf approaching non-detectable values (Figure 3.5A). Phaeopigment concentrations followed trends of chl*a* closely at nearshore sites with highest values (>4 µg/L) near the coast and lower phaeopigment concentrations offshore (Figure 3.5B)

Bacterial abundance and production in surface waters

In January 2014, bacteria counts were highest near Alexander Island (300 line) and into Marguerite Bay (Figure 3.6A). Bacterial production

Table 3.1 Air-sea flux [pmol m^{-2} h^{-1}] of elemental mercury (Hg^0) from surface waters in sub-regions of the continental shelf west of the Antarctic Peninsula. Fluxes were estimated using the Nightingale et al. 2000 gas exchange transfer velocity (K_w), the Andersson et al. 2000 Henry's Law constant (K'_H), and gaseous elemental mercury concentrations in air from Soerensen et al. 2010. Schmidt numbers were calculated using the kinematic viscosity as in Thibodeaux 1996 and the Kuss et al. 2009 Hg^0 diffusivity.

Station Lines			
Shelf area	**100-250**	**250-450**	**450-620**
slope	0.89	1.14	-0.79
shelf	1.53	1.36	1.70
coastal	7.66	1.23	2.43

Table 3.2 Total air-sea exchange [mol/d] of elemental mercury (Hg^0) from surface waters in sub-regions of the continental shelf west of the Antarctic Peninsula. Air-sea exchange rates were calculated as the products of mercury fluxes from Table 3.1 and sub-region area.

Station Lines			
Shelf area	**100-250**	**250-450**	**450-620**
slope	0.26	0.44	-0.26
shelf	0.44	0.52	0.55
coastal	1.79	0.24	0.45

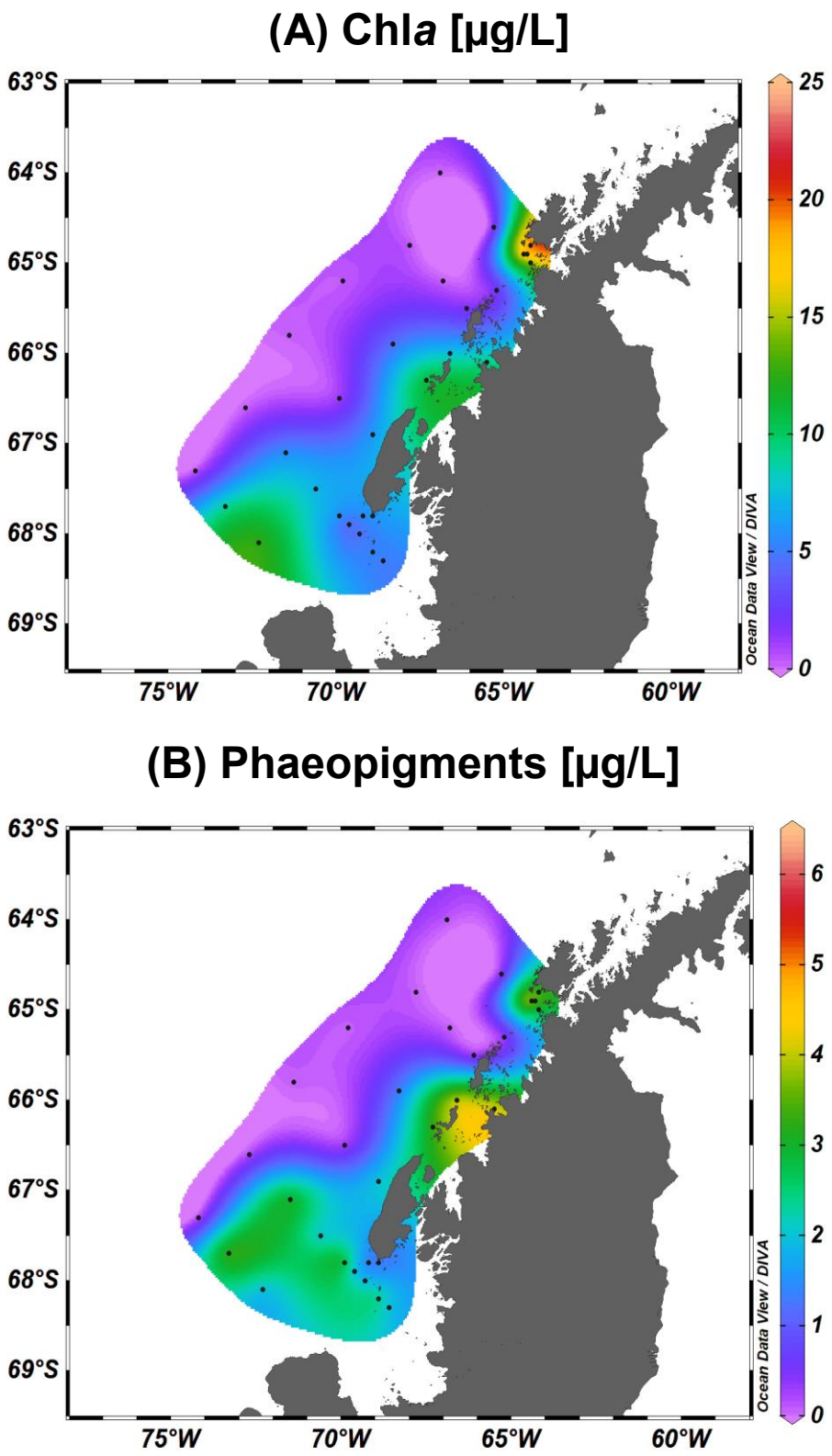

Figure 3.5 Surface measurements of (A) chlorophyll *a* (Chl*a*) and (B) phaeopigments in 2014 surface waters (0-5m) of the Southern Ocean west of the Antarctic Peninsula.

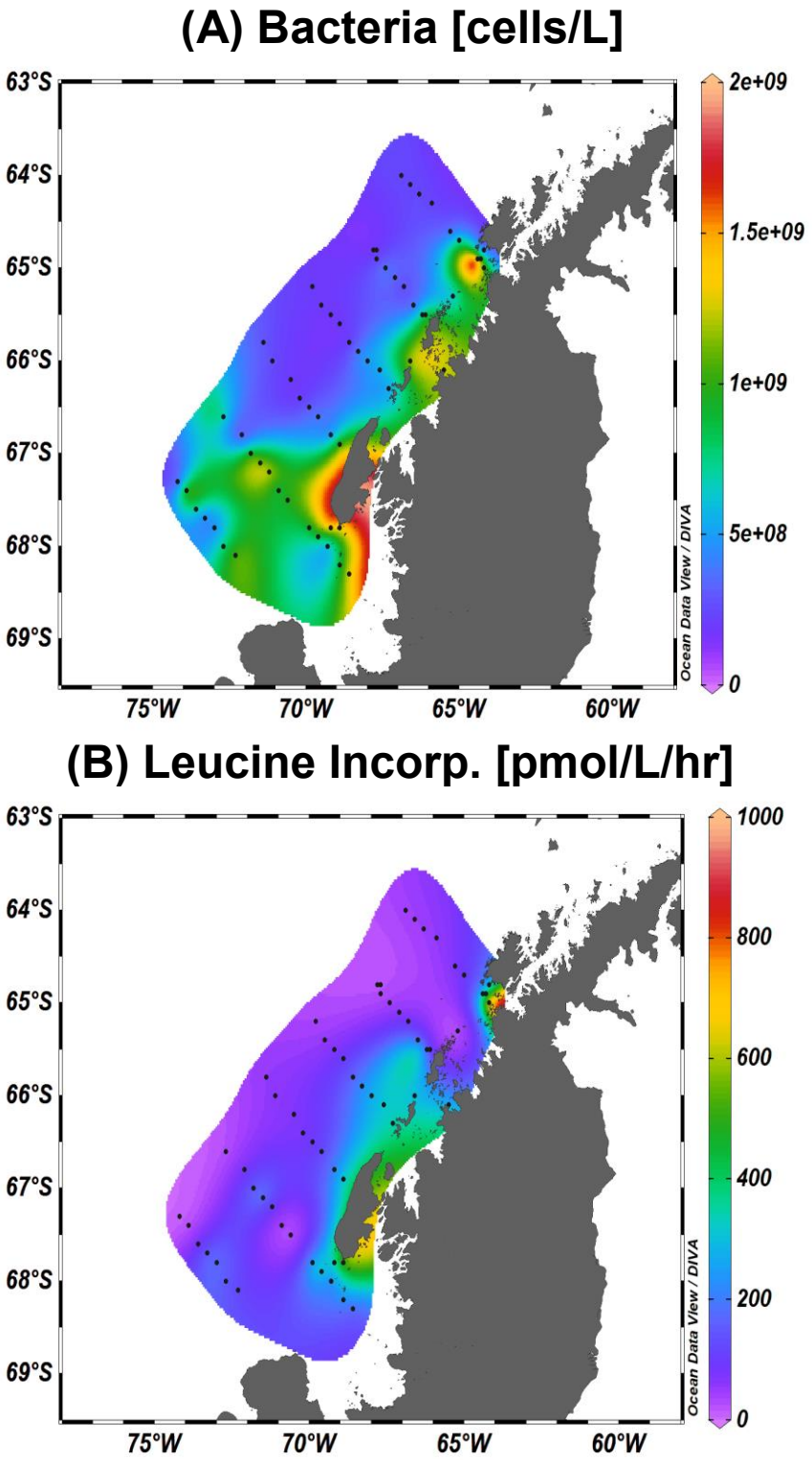

Figure 3.6 Surface measurements of (A) bacterial abundance and (B) leucine incorporation (proxy for bacterial production) in 2014 surface waters (0-5 m) of the Southern Ocean west of the Antarctic Peninsula.

Alexander Island and Marguerite Bay, and south of Anvers Island where bacterial production was high at ~700 pmol/L/hr and >800 pmol/L/hr, respectively (Figure 3.6B).

Hydrography and oxygen in waters offshore of the shelf-slope break in 2015

The warmest waters (>1.7°C) were found mostly in the upper 500 m of the water column offshore of the shelf-slope break lying below cooler surface waters (0 to -1°C) with some higher temperature waters found at ~750 m between the 100 and 000 lines (~67.8°S) (Figure 3.7A). Saline waters (>34.5 psu) were also found at all latitudes in the upper 500 m of the water column but persisted to greater depths (>1000 m) noticeably at northern stations (600 line) and further south at ~67.8°S (Figure 3.7B). Within well oxygenated waters, lowest oxygen concentrations and highest apparent oxygen utilization (AOU) were found in the upper water column and isolated regions with AOU >150 µmol/kg and oxygen concentrations ranging as low as 150 µmol/kg at southern latitude sites (Figures 3.8A and 3.8B).

Hydrography and oxygen along the mid-continental shelf waters in 2015

Winter Water (WW) is the coldest (<-1.5°C) water mass near the Antarctic Peninsula, and is found at depths of approximately 100 m, beneath slightly warmer surface water (>-0.5°C) and extending north-south along the LTER grid. In 2015, the coldest temperatures and thickest depths (~100 m) of WW were found at the most southern stations at ~69°S near the sea ice edge (Figure 3.9A). Modified Circumpolar Deep Water (mCDW) underlies WW with most waters greater than 300 m having temperatures of around 1°C (Figure 3.9A). The warmest temperatures across the shelf (~2°C) were seen at the 400 line (Figure 3.9A) and are similar to temperatures measured

in offshore waters (Figure 3.7A). Salinities along the continental shelf generally followed depth. The most saline waters (>35.5 psu) were found in bottom waters (~500 m) along the shelf with anomalously lower salinity found in the bottom water along the 200 line (Figure 3.9B).

Extensions of mCDW water at depths ≥300 m along the mid-shelf stations had higher AOU (~175) than overlying WW and the lowest (~175 µmol/kg) dissolved oxygen (DO) concentrations. As was the case for salinity, bottom water at the 200 line had relatively high DO and low AOU (Figure 3.10A and 3.10B). Anomalies in DO concentrations and AOU mirrored salinity along the continental shelf (Figures 3.9B and 3.10A) with neighboring lower oxygenated-higher salinity waters (<175 µmol/kg, >35.5 psu respectively) overlying slightly higher oxygen-lower salinity waters.

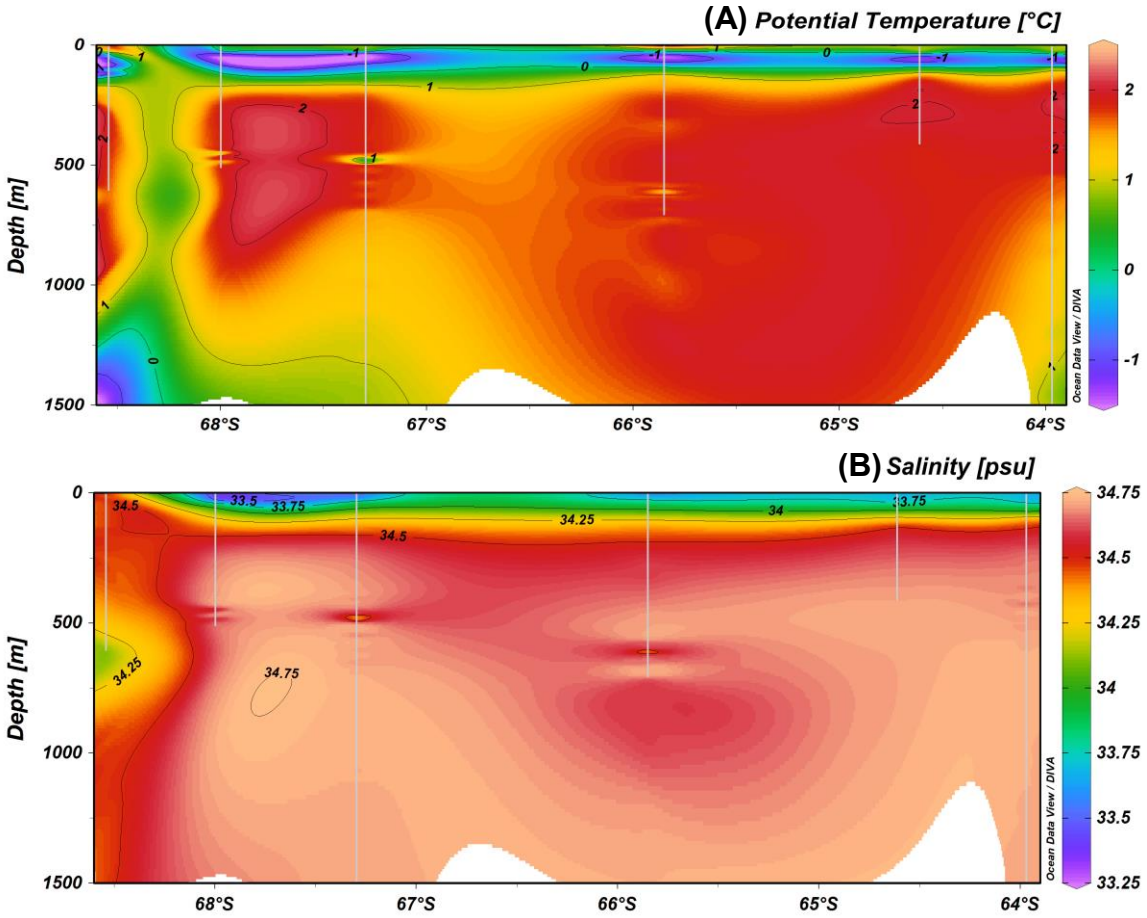

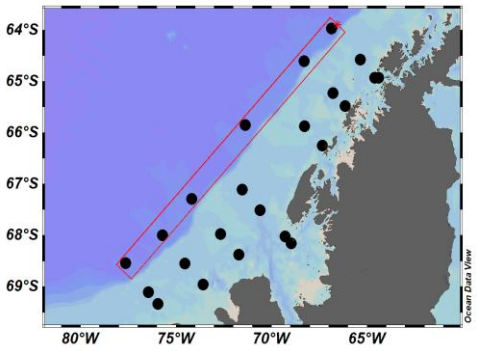

Figure 3.7 Distributions of potential temperature (A) and salinity (B) at six slope sites (section width 49.20 km) offshore of the WAP continental shelf break (boxed points on map) between ~64°S (right side of x-axis) and 69°S near the sea ice edge (left side of x-axis) in 2015. All scale lengths were assigned by Ocean Data View and all poor estimates and outliers were excluded. White lines show depths of CTD casts and the white areas were outside the limits of interpolation.

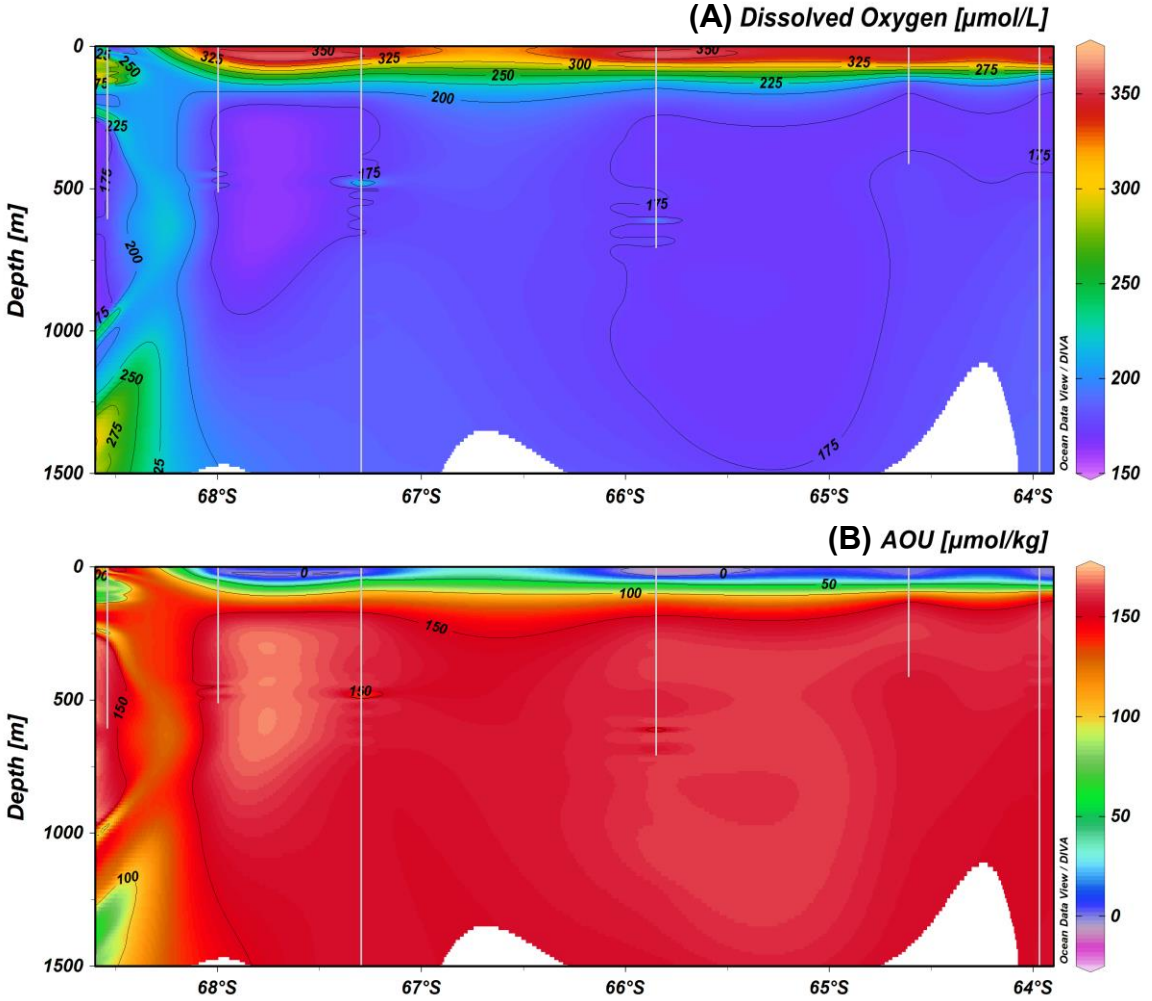

Figure 3.8 Distributions of dissolved oxygen (A) and apparent oxygen utilization (AOU) (B) at slope sites offshore of the WAP continental shelf break (boxed points on map to Figure 3.7) between ~64°S (right side of x-axis) and ~69°S near the sea ice edge (left side of x-axis). Estimates for AOU were calculated in Ocean Data View using measured dissolved oxygen concentrations and calculated neutral density (γn [kg/m^3]) of seawater. White lines show the depths of CTD casts and white areas were outside the limits of interpolation.

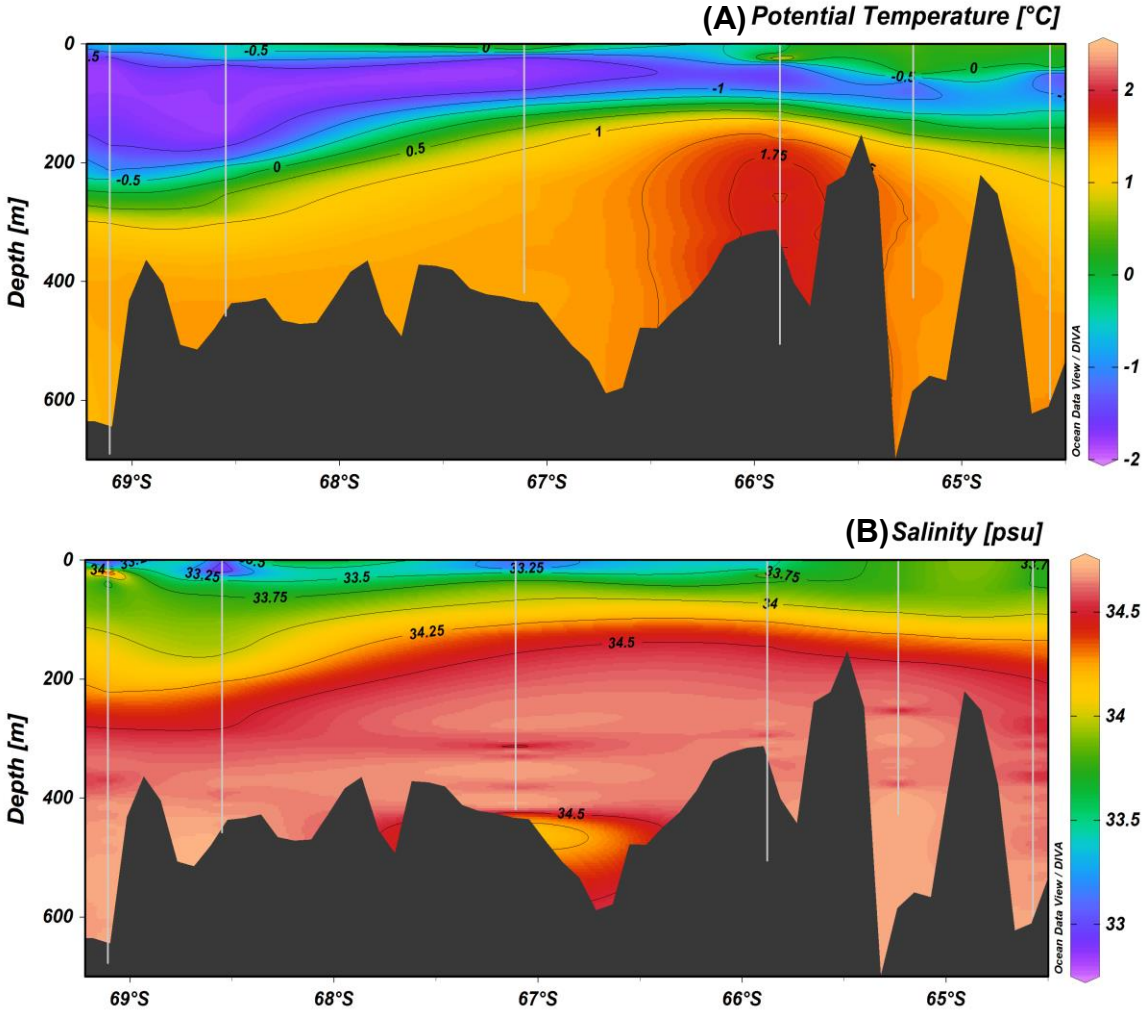

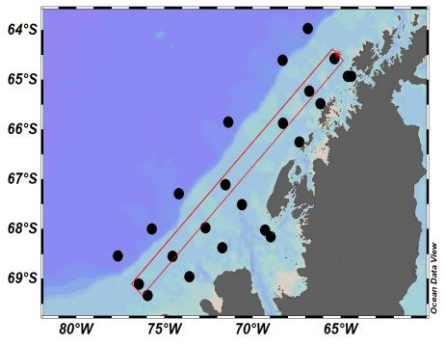

Figure 3.9 Distributions of potential temperature (A) and salinity (B) at six mid-shelf sites (section width 39.3km) along the WAP continental shelf (boxed points on map) between ~65°S (right side of x-axis) and ~69°S near the sea ice edge (left side of x-axis). Bathymetry (IBSCO_v1_1x1min) of continental shelf west of the Antarctic Peninsula is depicted in black. All scale lengths were assigned by Ocean Data View and all poor estimates and outliers were excluded. Temperatures >1.5°C were used to identify UCDW. White lines show depths of CTD casts.

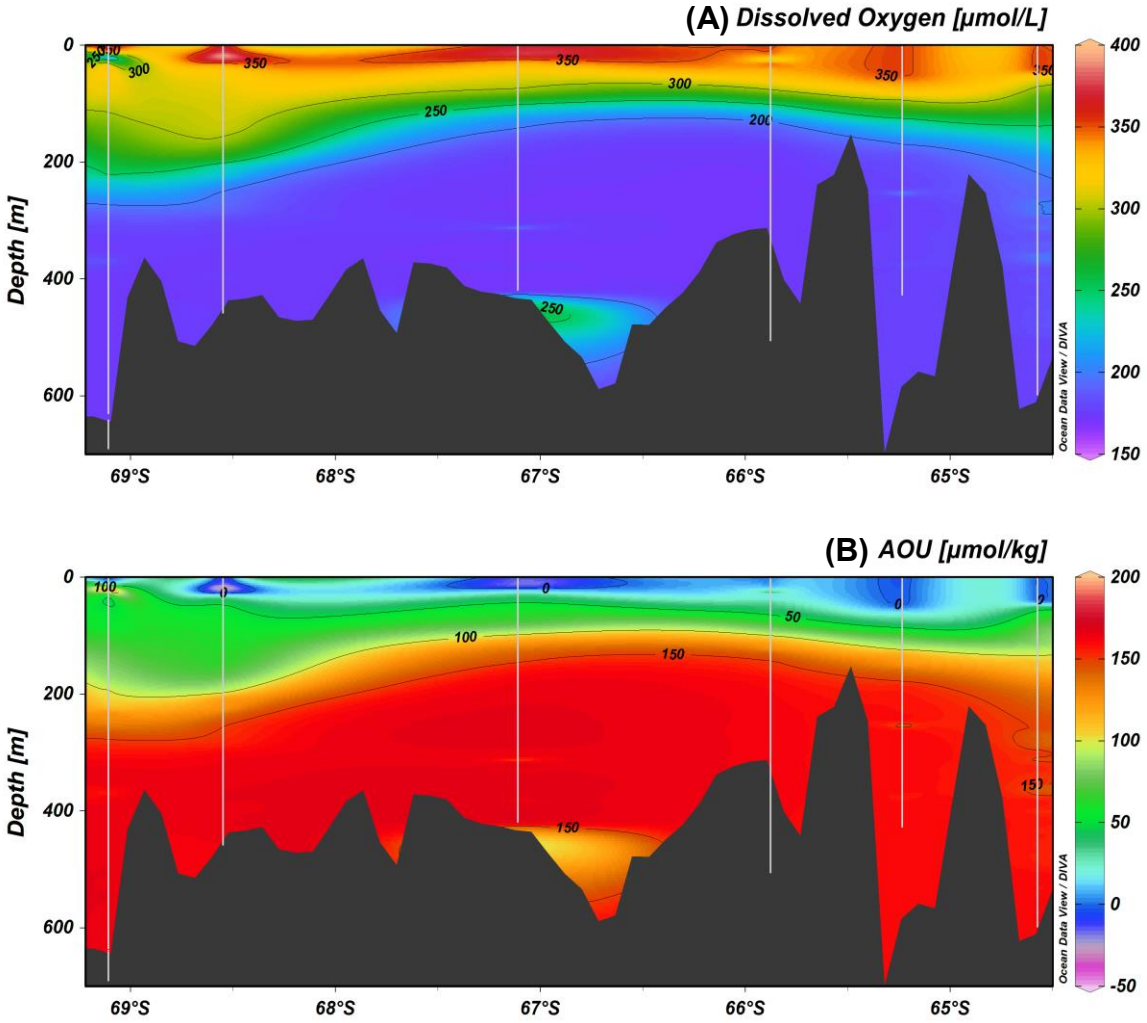

Figure 3.10 Distributions of dissolved oxygen (A) and apparent oxygen utilization (AOU) (B) at mid-shelf sites along the WAP continental shelf (boxed points on map to Figure 3.9) between ~65°S (right side of x-axis) and ~69°S near the sea ice edge (left side of x-axis). Bathymetry of continental shelf west of the Antarctic Peninsula is depicted in black. Estimates for AOU were calculated in Ocean Data View using measured dissolved oxygen concentrations and calculated neutral density (γn [kg/m^3]) of seawater. White lines show depths of CTD casts.

Dissolved total mercury, dissolved total methylated mercury, and percent fraction of total methylated mercury at two northern sites in 2015

Dissolved total mercury (d-Hg_T) and dissolved total methylated mercury (d-$MeHg_T$) were measured at a coastal and a shelf slope site at 65°S and 64°S, respectively, at depths ranging to ~2000 m (Figures 3.11 and 3.12). Within the 14 samples collected at these stations, d-Hg_T ranged from 0.97 to 3.76 pM (Table 3.3). Dissolved total mercury profiles generally exhibited "transient-type" characteristics with enrichment in surface waters, a depletion in sub-surface, underlying waters (≤50 m) and higher concentrations at depth. At the offshore station (600.200), the profile of d-Hg_T followed this pattern except for a minimum (1.16 pmol L^{-1}) at 1000 m. The vertical profile of d-Hg_T at the coastal station (600.040) showed more variability with a sharp increase in bottom waters and subsequent decrease just above the sediment (Figure 3.11).

Dissolved total methylated mercury at the northern coastal and offshore sites exhibited more variability than d-Hg_T and ranged from 0.06 to 0.92 pM (Table 3.3). Dissolved total methylated mercury profiles followed a pattern of low surface levels and increasing concentration at depth. Coastal d-$MeHg_T$ concentrations were low at the surface and increased within the surface mixed layer (1-50 m) to a maximum of 0.92 pM in intermediate waters (500 m). Dissolved total methylated mercury concentrations along the coast decreased noticeably below this subsurface maximum in bottom waters and water above sediment. Slope waters showed similar structure in the upper water column with a subsurface maximum of 0.61 pM at 230 m, and with variable concentrations at greater depths (Figure 3.12).

Fractions of d-$MeHg_T$ as d-Hg_T (%d-$MeHg_T$) ranged from 3 to 40%. Vertical distribution of %d-$MeHg_T$ increased below the surface at both coastal and offshore sampling locations to an average of 22% as %d-$MeHg_T$ below 100 m. However, there were no consistent trends in %d-$MeHg_T$ below this depth (Figure 3.13).

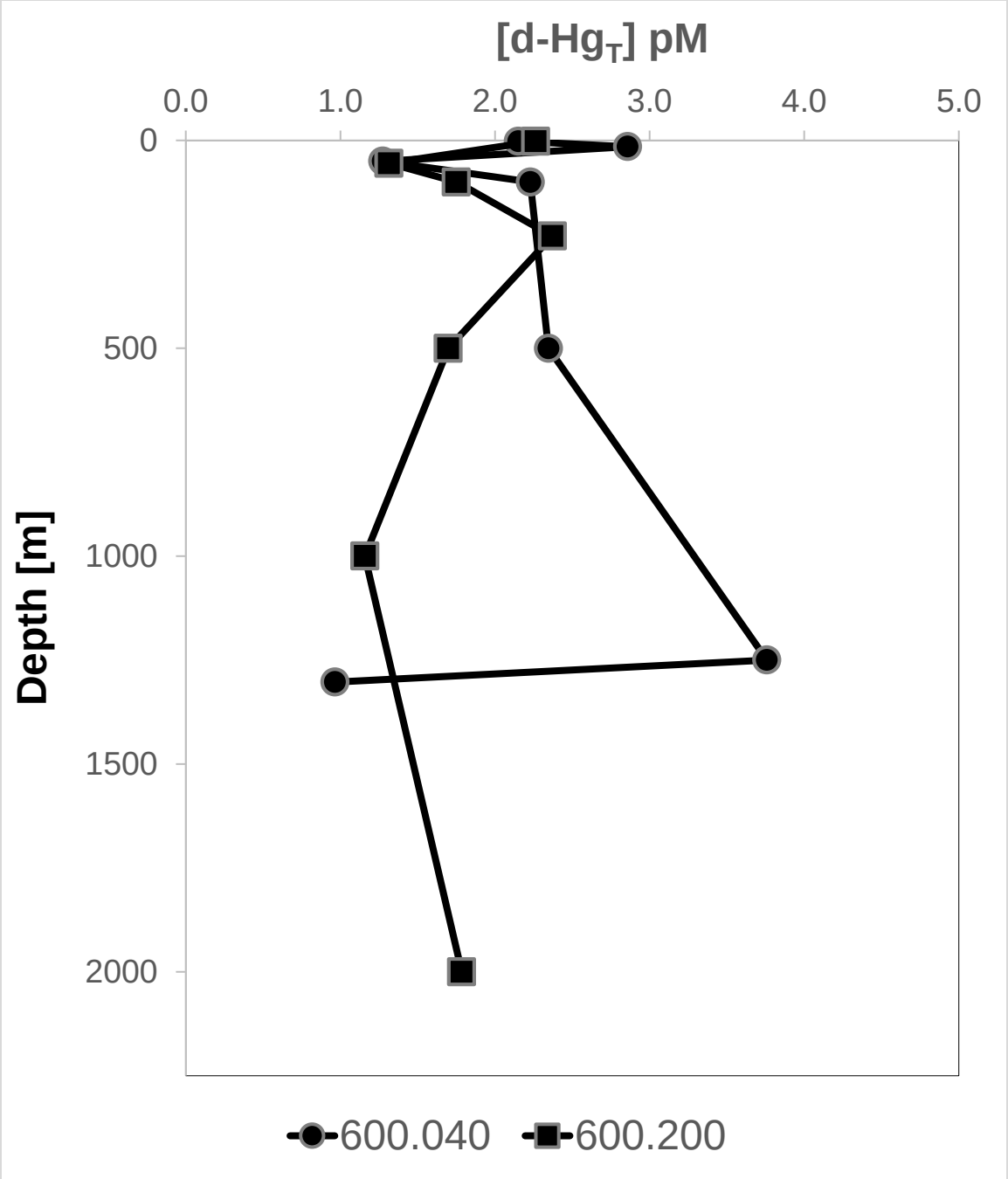

Figure 3.11 Vertical distributions of dissolved total mercury (d-Hg_T) concentrations in seawater from northern latitude coastal (600.040) and slope (600.200) sites at ~65°S.

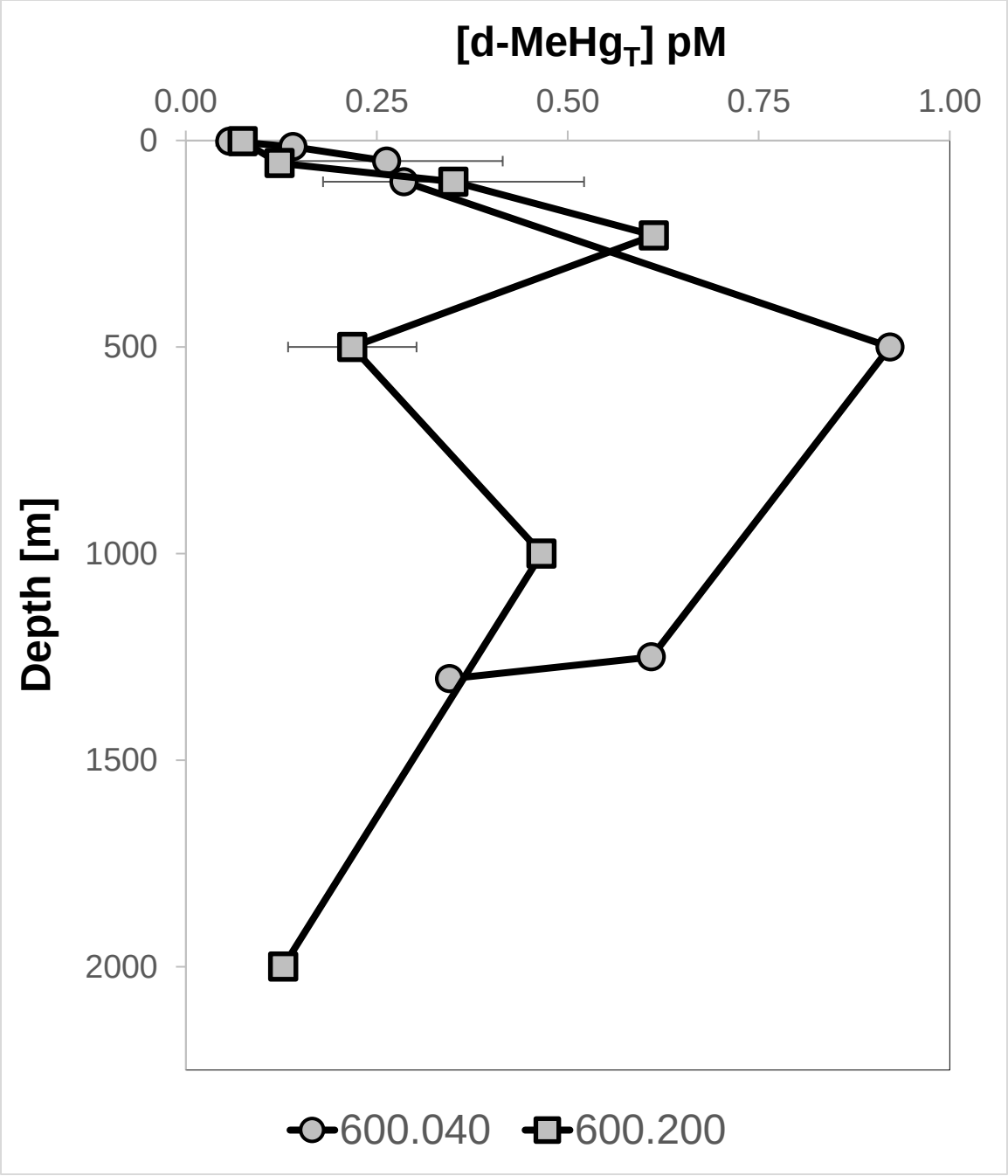

Figure 3.12 Vertical distributions of dissolved totat methylated mercury (d-$MeHg_T$) concentrations in seawater from northern latitude coastal (600.040) and slope (600.200) sites at ~65°S.

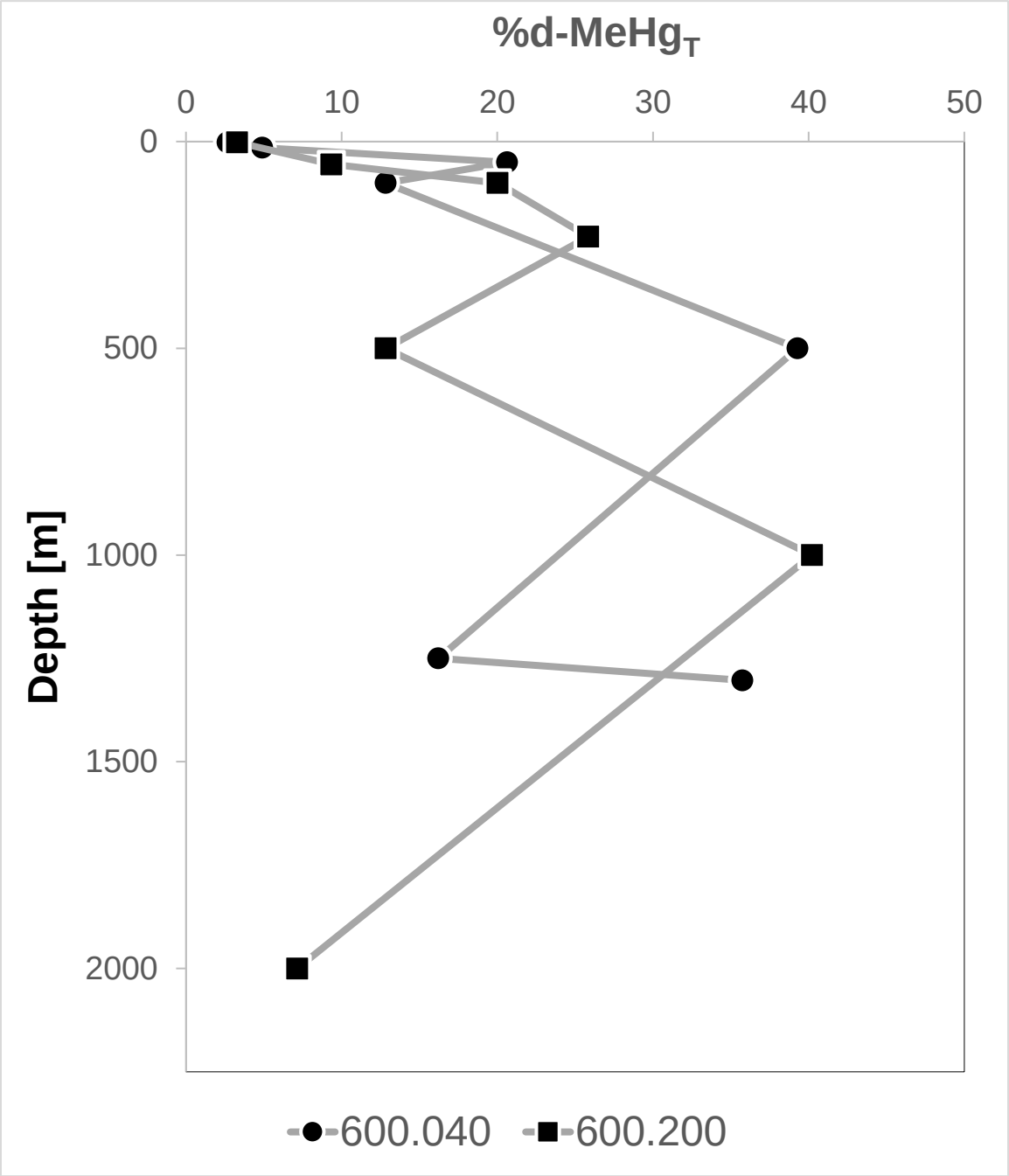

Figure 3.13 Vertical distributions of d-$MeHg_T$ fractions (%d-$MeHg_T$) in seawater from northern latitude coastal (600.040) and slope (600.200) sites at ~65°S.

Table 3.3 Dissolved total methylated mercury mercury (d-$MeHg_T$) and dissolved total mercury (d-Hg_T) concentrations and fractions of d-$MeHg_T$ as d-Hg_T in filtered seawater at ~65°S at coastal (600.040) and slope (600.200) sites west of the Antarctic Peninsula. Bolded values are d-Hg_T and d-$MeHg_T$ maxima in each profile.

Sta.	Depth [m]	[d-$MeHg_T$] ppt	[d-$MeHg_T$] pM	STD ppt	STD pM	[d-Hg_T] ppt	[d-Hg_T] pM	STD pM	d-$MeHg_T$: d-Hg_T
600.040	2	0.01	0.06	0.00	0.02	0.4	2.2		0.03
	15	0.03	0.14			0.6	2.9		0.05
	50	0.04	0.26	0.03	0.15	0.3	1.3		0.21
	100	0.06	0.29			0.4	2.2	1.1	0.13
	500	***0.18***	***0.92***			0.5	2.3		0.39
	1250	0.12	0.61			***0.8***	***3.8***		0.16
	1303	0.07	0.35			0.2	1.0		0.36
600.200	2	0.01	0.07			0.5	2.3		0.03
	55	0.02	0.12			0.3	1.3		0.09
	100	0.07	0.35	0.03	0.17	0.4	1.8		0.20
	230	***0.12***	***0.61***			***0.5***	***2.4***		0.26
	500	0.04	0.22	0.02	0.08	0.3	1.7		0.13
	1000	0.09	0.47			0.2	1.2		0.40
	2000	0.03	0.13			0.4	1.8		0.07

Dissolved total mercury, dissolved total methylated mercury, and percent of dissolved total methylated mercury as total mercury at Marguerite Bay in 2015

Dissolved total mercury concentrations in seawater from the coastal inlet, Marguerite Bay (site 200-.060), ranged from 3.2 to 7.7 pM (Table 3.4). The profile of d-Hg_T showed enrichment in surface waters (≤25 m), a decrease below the mixed layer, and little variation in deeper waters (Figure 3.14). A small increase was also measured in waters overlying the sediment (Figure 3.14).

Dissolved total methylated mercury concentrations in Marguerite Bay were at or near the detection limit (0.02 pM) with a range of 0.05 to 0.09 pM. Dissolved d-$MeHg_T$ was below detection at the surface (~2 m) and at 230 m (Table 3.4). The concentration of d-$MeHg_T$ at this site was highest right below the surface (~15 m) and decreased slightly with depth (Figure 3.15). Percent d-$MeHg_T$ was low, ranging between 0.7 to 1.8% (Table 3.4), which followed d-$MeHg_T$ concentration trends described above (Figure 3.16).

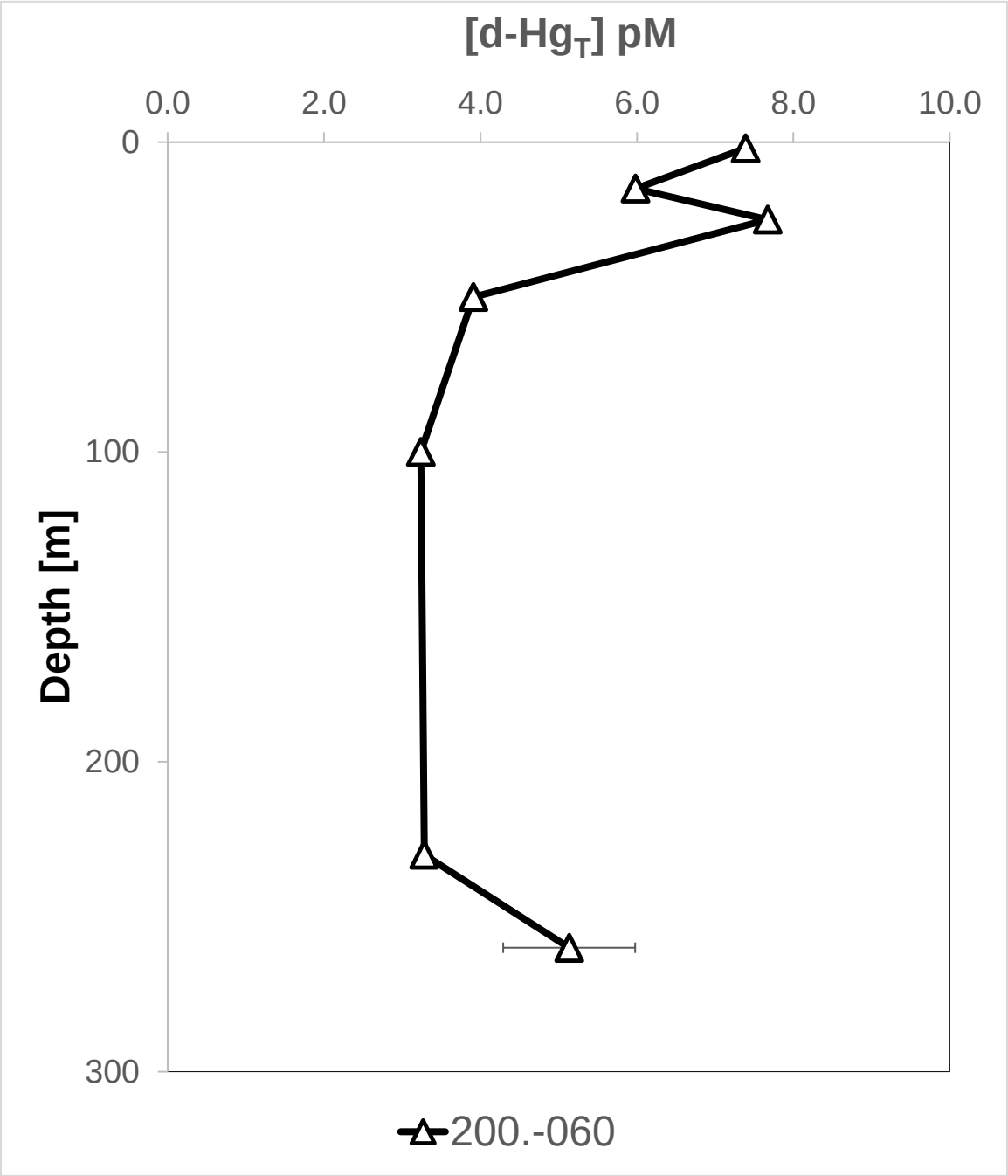

Figure 3.14 Vertical distribution of dissolved total mercury (d-Hg$_T$) concentrations in seawater from Marguerite Bay (200 line), at ~68°S.

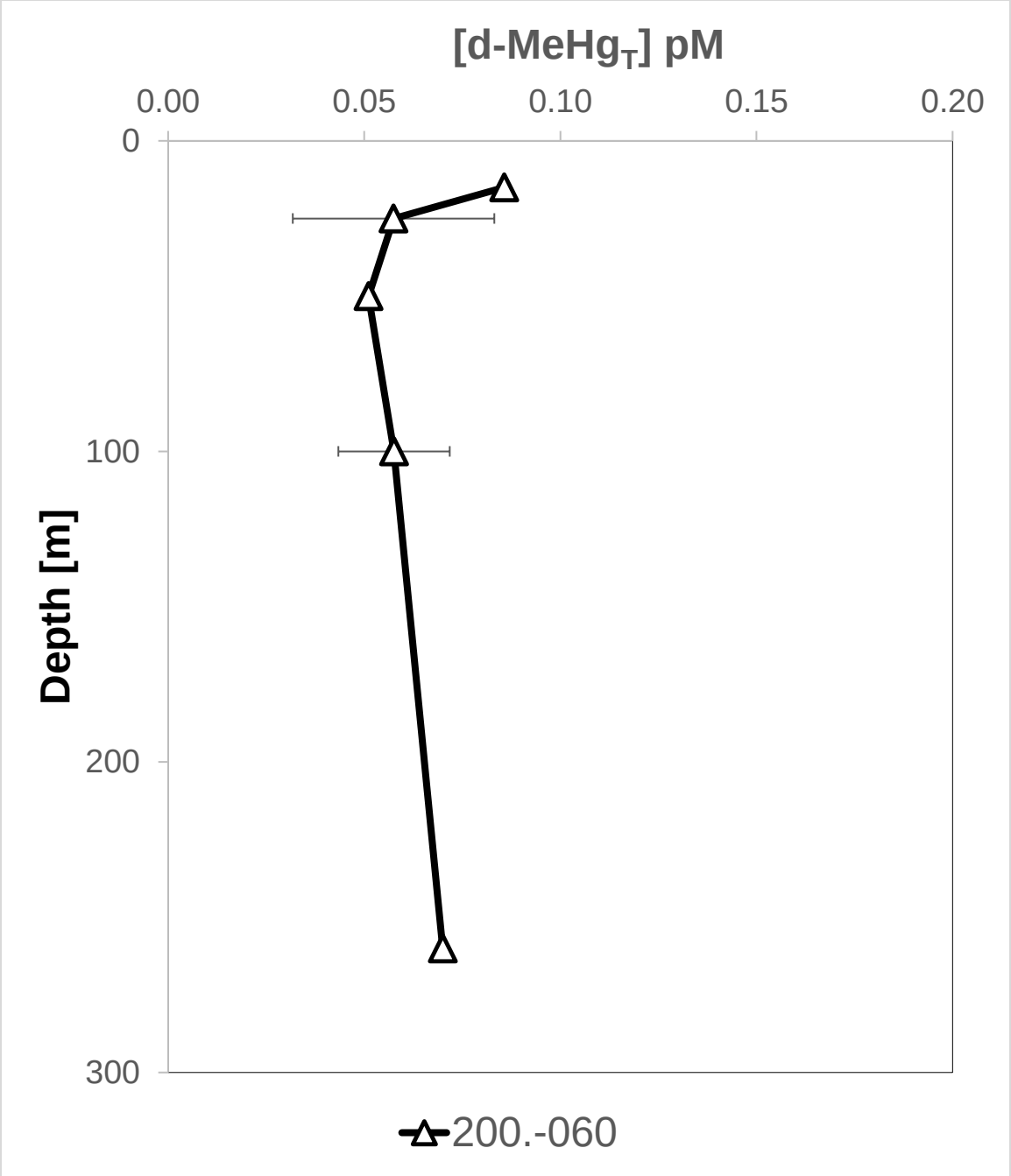

Figure 3.15 Vertical distribution of dissolved total methylated mercury (d-$MeHg_T$) concentrations in seawater from Marguerite Bay (200 line), at ~68°S. Notice smaller x-axis scale compared to that in Figure 3.12.

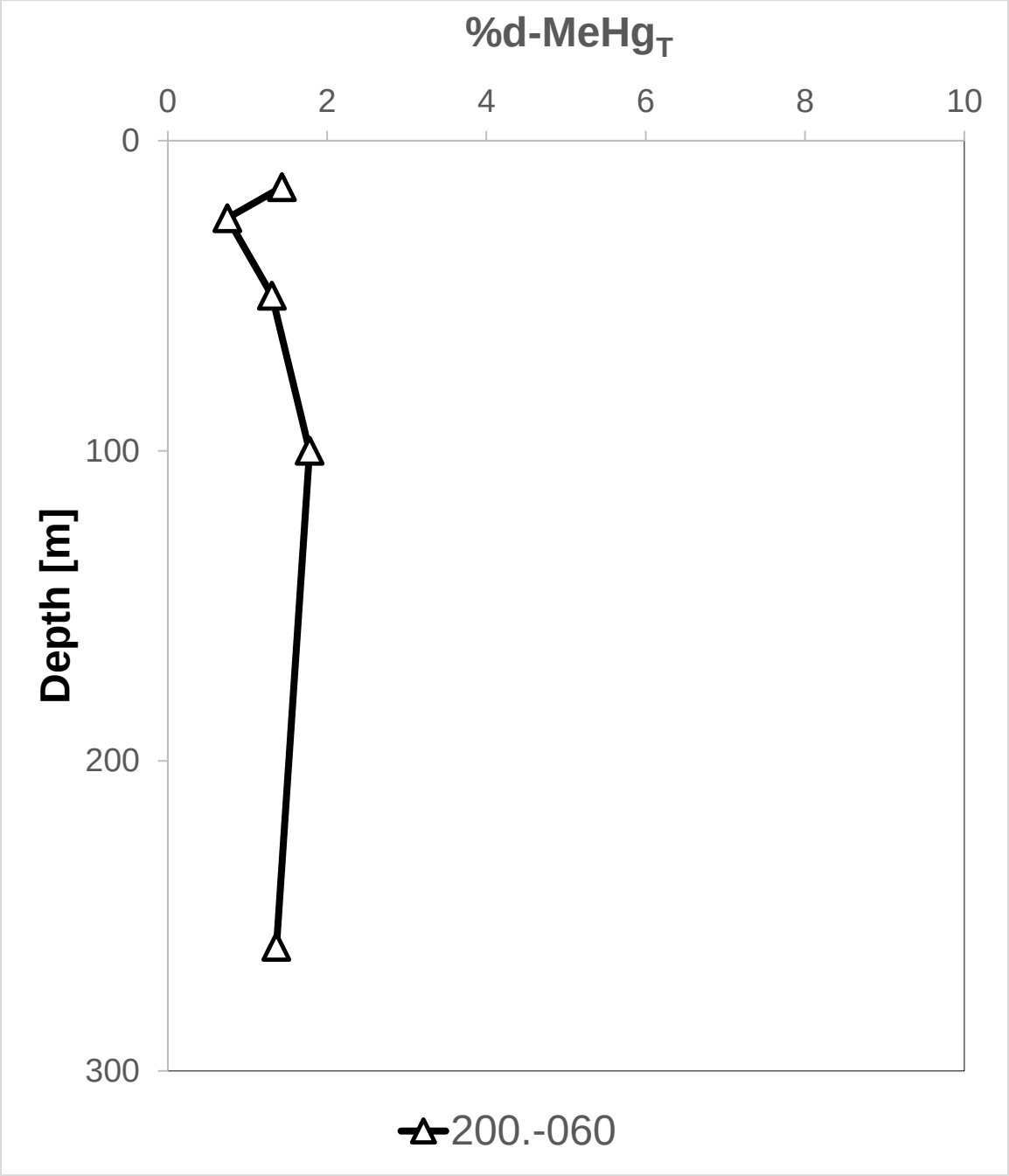

Figure 3.16 Vertical distribution of d-MeHg$_T$ fractions (%d-MeHg$_T$) in seawater from Marguerite Bay (200 line), at ~68°S. Notice smaller (1-10%) x-axis scale compared to that in Figure 3.13.

Table 3.4 Dissolved total methylated mercury (d-$MeHg_T$) and dissolved total mercury (d-Hg_T) concentrations and fractions of d-$MeHg_T$ as d-Hg_T in filtered seawater at ~68°S at a coastal site (200 line) west of the Antarctic Peninsula. Bolded values are d-Hg_T and d-$MeHg_T$ maxima for this profile. BD, below detection limit.

Sta.	Depth [m]	[d-$MeHg_T$] ppt	[d-$MeHg_T$] pM	STD ppt	STD pM	[d-Hg_T] ppt	[d-Hg_T] pM	STD pM	d-$MeHg_T$: d-Hg_T
200.-060	2	BD	BD			1.5	7.4		-
	15	***0.017***	***0.086***			1.2	6.0		0.01
	25	0.012	0.057	0.005	0.03	***1.5***	***7.7***		0.01
	50	0.010	0.051			0.8	3.9		0.01
	100	0.01	0.06	0.00	0.01	0.6	3.2		0.02
	230	BD	BD			0.7	3.3		-
	260	0.01	0.07			1.0	5.1	0.8	0.01

Dissolved total mercury, dissolved total methylated mercury, and percent dissolved total methylated mercury near the seasonal sea ice edge in 2015

Dissolved total mercury in seawater collected at a coastal and a shelf slope station along the -100 line (~69°S) near the seasonal sea ice edge varied from 0.8 to 16.6 pM (Table 3.5). Although both stations had similar low d-Hg_T concentrations in surface waters (≤25 m), they had contrasting d-Hg_T profiles at greater depths (Figure 3.17). At the offshore site, d-Hg_T concentrations increased gradually until 200 m and remained constant to 600 m. However, at the coastal site, d-Hg_T increased sharply from the surface to 75 m, and then decreased sharply from 75 m to 200 m (Figure 3.17).

Dissolved total methylated mercury concentrations at the southern sites ranged from 0.02 to 0.22 pM, but were below detection in the two shallowest samples (Table 3.5). Identical d-$MeHg_T$ concentrations were measured at 25 m at the nearshore and offshore sites (Table 3.5). At the offshore site, the concentration of d-$MeHg_T$ increased to 200 m, but remained at low concentrations (<0.1 pM). From 200 m to 330 m, d-$MeHg_T$ increased sharply, and then declined from 330 m to 600 m to a similar concentration as that in surface waters (Figure 3.18). At the coastal site, d-$MeHg_T$ increased from surface waters to a subsurface maximum at 150 m, declined between 150 m and 200 m, and increased slightly near the bottom (Figure 3.18). Percent d-$MeHg_T$ was low (0.5% to 3.5%) and relatively constant throughout the water column, but did peak at about 330 m at both sites (Figure 3.19).

Dissolved percent fraction of dissolved methylated mercury across all sampling regions of the WAP

Fractions of dissolved total mercury as dissolved total methylated mercury were a factor of 5-20 times higher within subsurface waters of northern latitudes than at Marguerite Bay and other southern latitudes sites (Figure 3.20). Noticebaly increases in %d-$MeHg_T$ was seen in intermediate and deep waters relative to the surface at 600.040 and 600.200 in the north while only small differences in %d-$MeHg_T$ were seen in vertical distributions at the more southern locations. Northern coastal and offshore sampling locations had high d-$MeHg_T$ concentrations, characterized by high subsurface maxima (0.61, 0.92 pM) and all d-$MeHg_T$ concentrations exceeded those at middle and southern sites below 100 m (Figs 3.12, 3.15, and 3.18; Tables 3.3, 3.4 and 3.5) contributing to the high %d-$MeHg_T$ at northern latitudes.

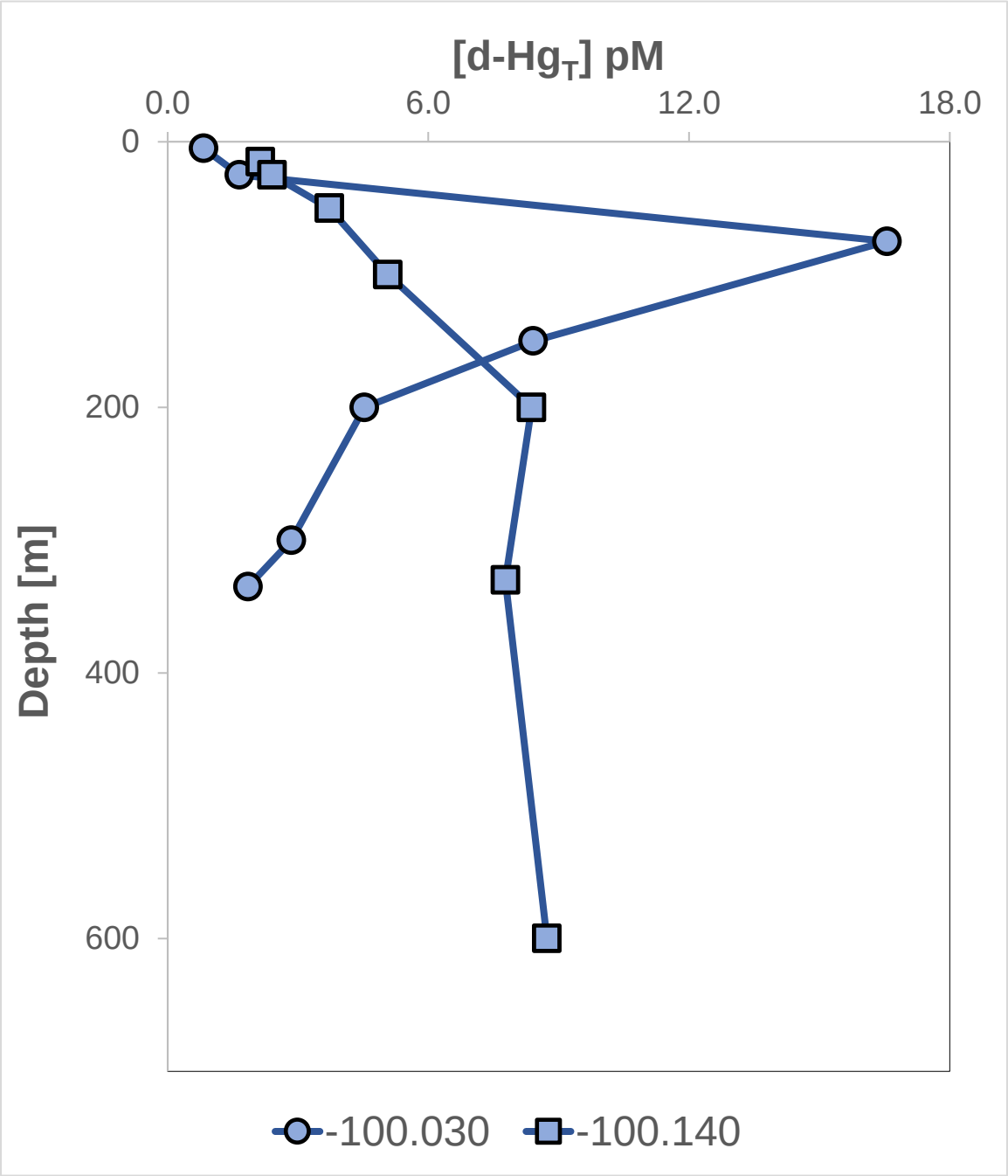

Figure 3.17 Vertical distributions of dissolved total mercury (d-Hg$_T$) concentrations in seawater from southern latitude coastal (100.030) and slope (100.140) sites at ~69°S.

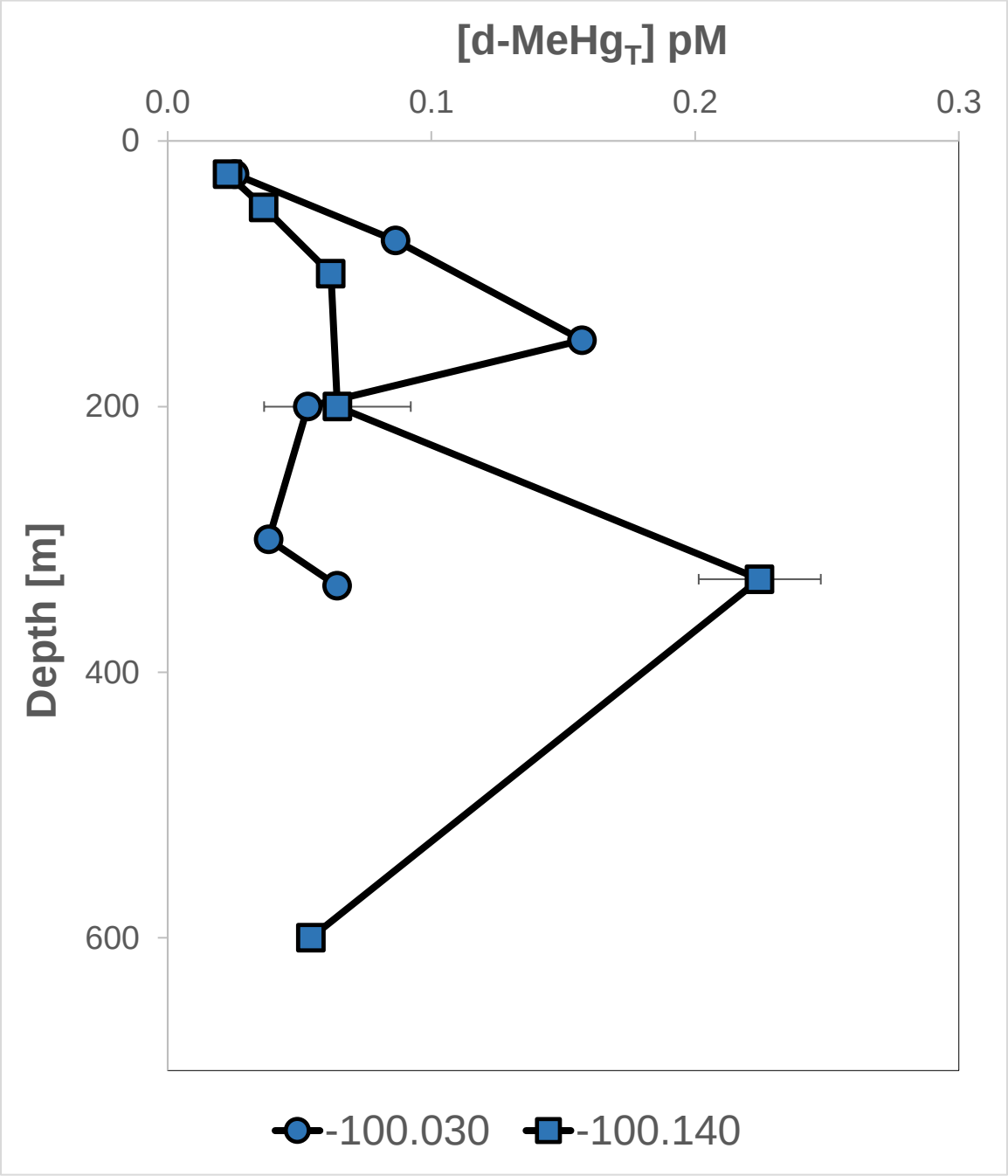

Figure 3.18 Vertical distributions of dissolved total methylated mercury (d-$MeHg_T$) concentrations in seawater from southern latitude coastal (100.030) and slope (100.140) sites at ~69°S.

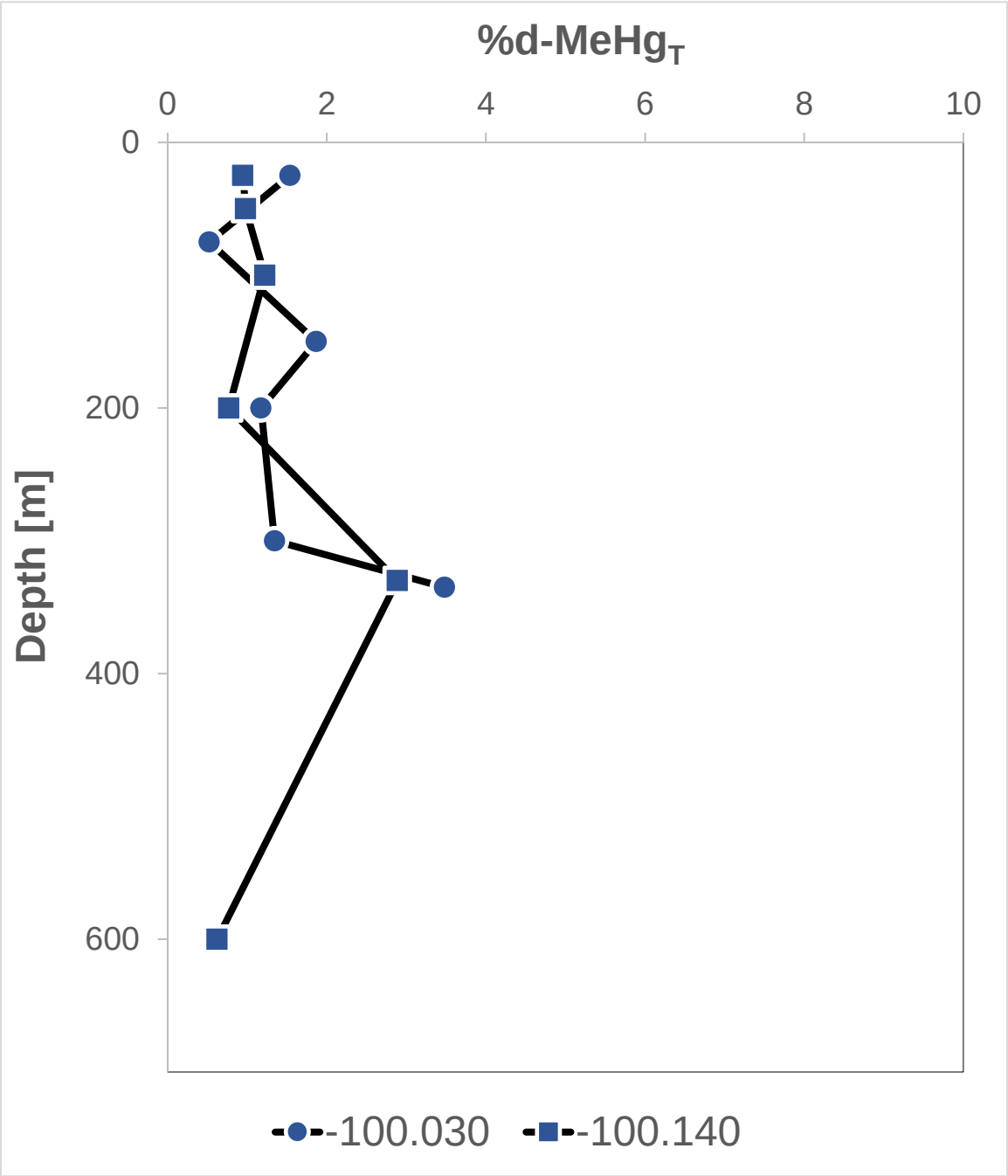

Figure 3.19 Vertical distributions of d-MeHg$_T$ fractions (%d-MeHg$_T$) in seawater from southern latitude (-100 line), coastal and slope sites at ~69°S.

Table 3.5 Dissolved total methylated mercury (d-$MeHg_T$) and dissolved total mercury (d-Hg_T) concentrations and fractions of d-$MeHg_T$ as d-Hg_T in filtered seawater at ~68°S at coastal (100.030) and slope (100.140) sites west of the Antarctic Peninsula. Bolded values are d-Hg_T and d-$MeHg_T$ maxima in each profile. BD, below detection.

Sta.	Depth [m]	[d-$MeHg_T$] ppt	[d-$MeHg_T$] pM	STD ppt	STD pM	[d-Hg_T] ppt	[d-Hg_T] pM	STD pM	d-$MeHg_T$: d-Hg_T
-100.030	5	BD	BD			0.2	0.8		-
	25	0.005	0.025			0.3	1.7		0.02
	75	0.017	0.087			***3.3***	***16.6***		0.01
	150	***0.032***	***0.157***			1.7	8.4		0.02
	200	0.011	0.053			0.9	4.5		0.01
	300	0.008	0.038			0.6	2.9		0.01
	335	0.013	0.064			0.4	1.8		0.03
-100.140	15	BD	BD			0.4	2.1		-
	25	0.005	0.023			0.5	2.4		0.01
	50	0.007	0.036			0.7	3.7		0.01
	100	0.012	0.062	0.006	0.03	1.0	5.1		0.01
	200	0.013	0.064	0.005	0.02	1.7	8.4		0.01
	330	***0.045***	***0.225***			1.6	7.8		0.03
	600	0.011	0.054	0.003	0.01	***1.8***	***8.7***		0.01

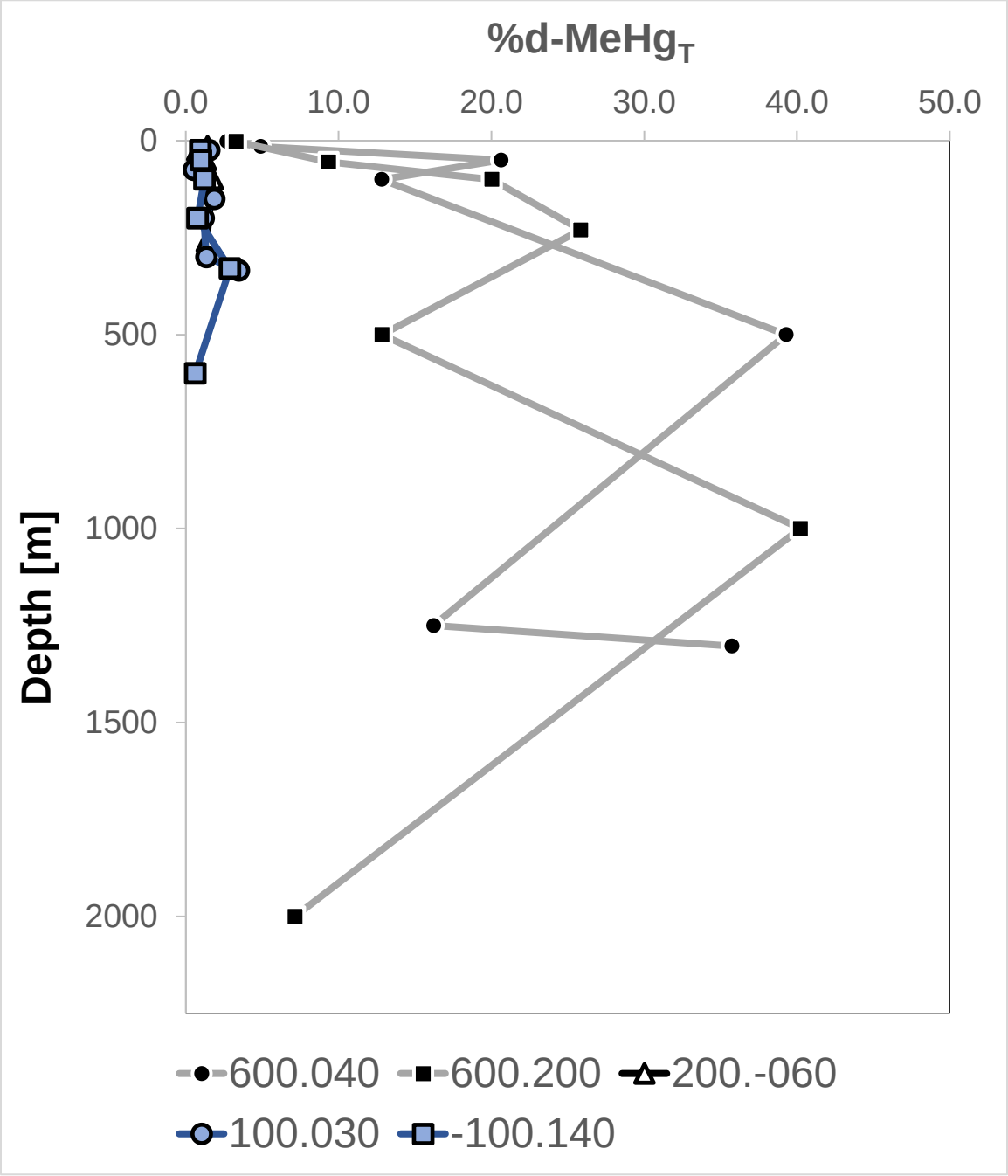

Figure 3.20 Vertical distributions of d-MeHg$_T$ fractions (%d-MeHg$_T$) in seawater along the WAP (65 to 69°S) at coastal and slope sites.

Sea ice in 2014 and 2015

Passive microwave satellite measurements of sea ice extent (km^2) show higher total surface area in austral summer months of December, January, and February during the 2014 LTER compared to the 2015 LTER cruise. The most noticeable differences in sea ice extent were in January and February (Table 3.6).

Biomass as chlorophyll *a* (chl*a*) and phaeopigments in 2015 surface water

Surface concentrations of 2015 chl*a* and phaeopigments were higher near the coast than offshore reaching values of ~7 µg/L and 0.7 µg/L, respectively (Figure 3.21A). Surface water chl*a* was a factor of 4 lower, and phaeopigments were approximately a whole order of magnitude lower, in 2015 compared to 2014 (Figures 3.21A, 3.21B, 3.5A, and 3.5B). In 2015, high chl*a* concentrations were observed near Alexander's Island and into Marguerite Bay while lower levels of phytoplankton biomass where found at northern sites, near Anvers Island Antarctica (Figure 3.21A).

Bacterial abundance and production along shelf surface waters in 2015

Bacterial abundance was high in 2015 reaching densities above 2.0×10^9 cells/L nearshore ~66.5°S (400 line) north of Alexander Island (Figure 3.22A). Bacterial production was non-detectable at most coastal and shelf sites along the WAP in 2015 (Figure 3.22A). Low activity was measured south of Anvers Island and within slope waters but was 2 orders of magnitude lower than 2014 bacterial production (Figures 3.22B and 3.5B). Lower cell densities (5×10^8 cells/L) and no activity of microbes was measured near Anvers Island Antarctica in 2015 (Figure 3.22A and 3.22B).

Table 3.6 Monthly sea ice extents (km^2) west of the Antarctic Peninsula in 2013 through 2015. Months preceding (green), during (red), and following (yellow) LTER 2014 and LTER 2015 cruises are highlighted. Sea ice extents were derived from satellite passive microwave measurements including total surface area within ice edge defined by an ice concentration contour of 15%.

Year	Jul	Aug	Sep	Oct	Nov	Dec
2013	204499	204499	204499	201514	204499	200914
2014	203900	204499	204499	204499	191925	**142295**
2015	204499	204499	204499	204499	204499	**170208**
Year	**Jan**	**Feb**	**Mar**	**Apr**	**May**	**Jun**
2013	34741	4885	3638	3027	87923	168939
2014	**111640**	**34773**	10563	32323	64503	133840
2015	**35457**	**6225**	624	4973	92863	189480

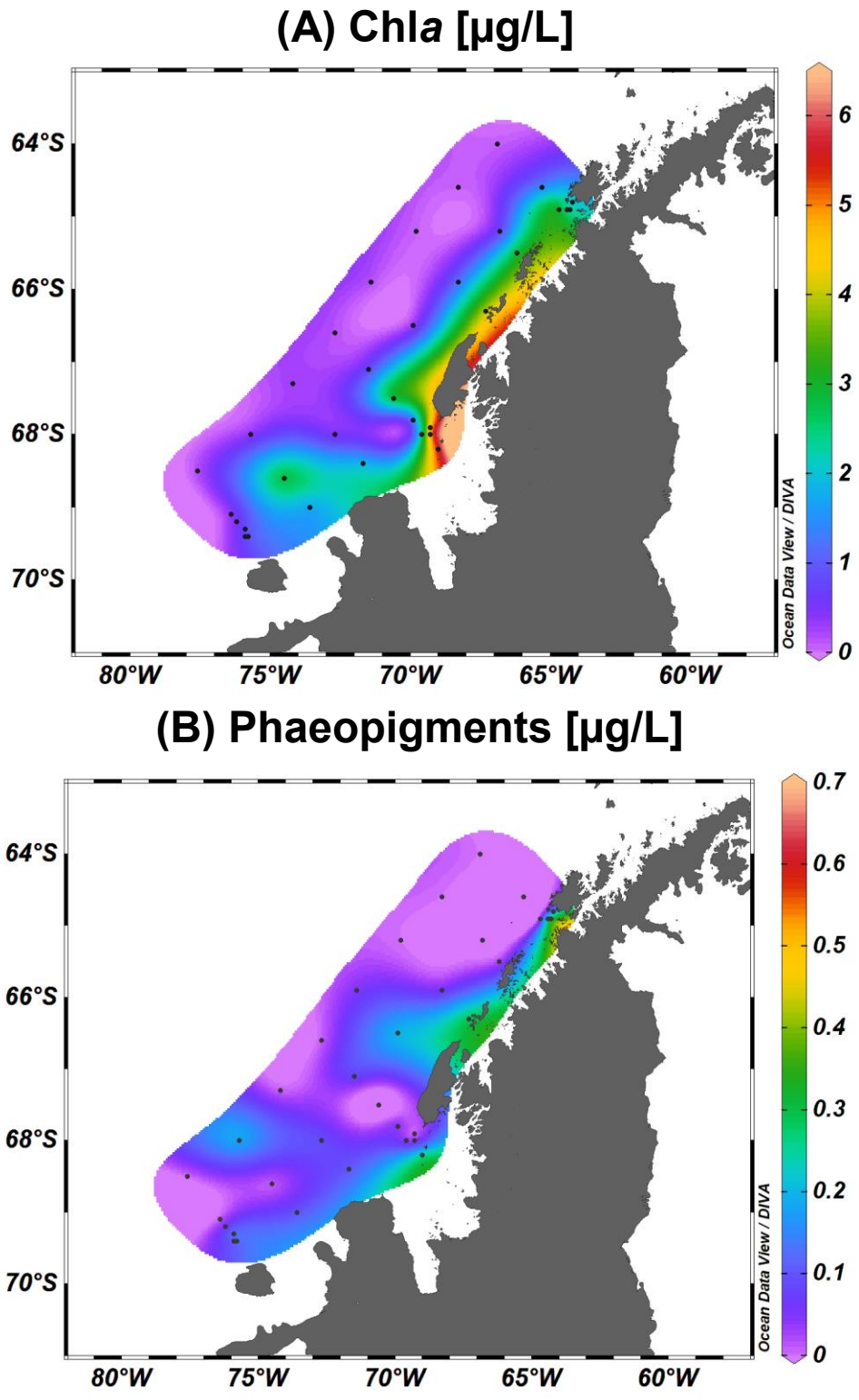

Figure 3.21 Surface measurements of (A) chlorophyll *a* (Chl*a*) and phaeopigments (B) in 2015 surface waters of the Southern Ocean west of the Antarctic Peninsula. Notice differences in Chl*a* [µg/L] scale between 2015 and 2014 (Figure 3.5) sampling years.

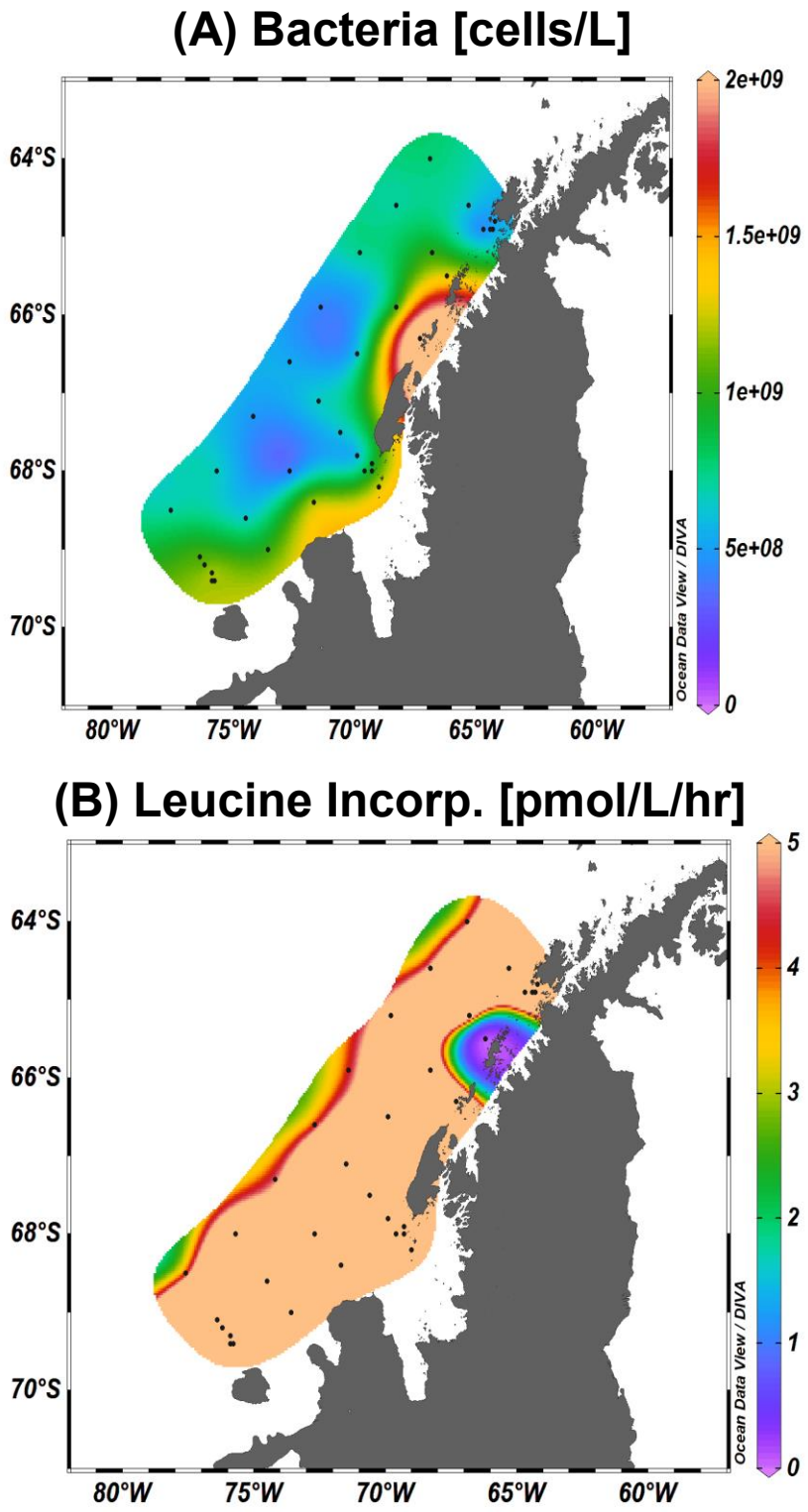

Figure 3.22 Surface measurements of (A) bacterial abundance and leucine incorporation (proxy for bacterial production) (B) in 2015 surface waters of the Southern Ocean west of the Antarctic Peninsula.

Surface dissolved total methylated mercury and dissolved total mercury concentrations in 2015

Dissolved total methylated mercury was low and ranged from non-detectable values to 0.07 pM in surface waters along the WAP. Dissolved total mercury in WAP surface waters ranged from 0.8 to 7.4 pM and only exceeded 2.6 pM in Marguerite Bay. Coastal-offshore differences in surface d-Hg_T concentrations were found at the 400, 200, and -100 lines, while a narrow range (2.2 to 2.3 pM) of d-Hg_T was measured at coastal, shelf, and slope sites along the 600 line (Table 3.7).

Particulate methylmercury, total methylmercury, and percent methylmercury bound to particles in surface waters

A wide range of particulate MeHg concentrations was observed in both 2014 (0.04 to 22.50 $pmol_{MeHg}/g_{totbio}$) and 2015 (0.24 to 20.12 $pmol_{MeHg}/g_{totbio}$) (Tables 3.8 & 3.9). In 2014, higher concentrations of MeHg in POM were found in offshore samples collected along the 600, 500, and 100 lines (Figure 3.23A). The highest MeHg concentrations in 2014 POM (6.35 and 22.48 $pmol_{MeHg}/g_{totbio}$) were found at station 600.080 near Anvers Island (Table 3.8 and Figure 3.23A), while the lowest concentrations of particulate MeHg were found along the 200 line (0.04 to 0.70 $pmol_{MeHg}/g_{totbio}$), with consistently lower concentrations measured near Marguerite Bay than farther offshore. Particulate MeHg increased gradually with distance from shore along the 500 line reaching maximum concentrations of 1.87 and 2.74 $pmol_{MeHg}/g_{totbio}$ at approximately 66°W and 65°S. A small trend with longitude was found along the 100 line where MeHg in nearshore POM was quite low (0.11 $pmol_{MeHg}/g_{totbio}$) while high

MeHg was measured in POM from surface waters of the shelf slope with concentrations reaching 5.95 and 5.07 $pmol_{MeHg}/g_{totbio}$ (Table 3.8 and Figure 3.23A).

Onshore-offshore trends in particulate MeHg were also observed in 2015, most noticeablely along the 200 line (Figure 3.23B). As in 2014, much higher MeHg concentrations were measured offshore of the shelf-slope break in the south at station -100.140 (Figure 3.23B) reaching a local maximum of 20.12 $pmol_{MeHg}/g_{totbio}$ (Table 3.9). Contrary to 2014, all particulate concentrations along the 600 line remained below <5 $pmol_{MeHg}/g_{totbio}$ (Table 3.9) and there was no clear increase in POM associated MeHg offshore of Anvers Island (Figure 3.23B).

In 2015, dissolved surface seawater concentrations of methylmercury and particulate methylmercury concentrations were used to calculate T-MeHg along the WAP (Table 3.9). All surface T-MeHg concentrations fell below 0.08 pM and ranged from 0.0003 to 0.071 pM. Non-dectable values of d-$MeHg_T$ nearshore at 200 and -100 indicate that most of the methylmercury in these surface waters was particle associated. Percent MeHg bound to particles ranged from 8.3 to 24.0% and inshore stations along the 200 and -100 lines suggest higher percentages could be associated with particles, but cannot be directly calculated due to non-dectable d-MeHg concentrations at these sites.

Bioconcentration of MeHg in surface waters

Bioconcentration factors (BCFs) of MeHg in POM varied from $10^{3.5}$ to $10^{6.0}$ (Table 3.10). Bioconcentration of MeHg was highest furthest south at 69°S (-100 line) where logBCFs ranged from 5.2 to 6.0 and lowest at the most coastal 200 line site near

Marguerite Bay. BCFs at the northern coastal sites near Anvers Island were between those at the -100 line and Marguerite Bay.

Fucoxanthin accessory pigment in 2014 and 2015 surface waters

A wide range in values for fucoxanthin pigment concentrations were present within and between years in 2014 and 2015. Fucoxanthin levels in 2014 were high and reached a maximum of ~18 µg/L, while in 2015, fucoxanthin levels in surface waters were two to three orders of magnitude lower, reaching a maximum of 5 µg/L (Figure 3.24A and 3.24B). Spatial distributions of fucoxanthin in 2014 mirrored those of chl*a* (Figure 3.21A) in WAP surface waters with the highest concentrations near Anvers Island and along the furthest south transect at the -100 line (~69°S). Intermediate concentrations of fucoxanthin were measured along the coast between northern and southern sites, and low values were found offshore along the continental slope (Figure 3.24A). While fucoxanthin concentrations were higher in 2014 than 2015, peak values in 2014 were not restricted to Marguerite Bay and were well distributed along the WAP (Figure 3.24A and 3.24B).

Table 3.7 Surface concentrations of dissolved total methylated mercury (d-$MeHg_T$) and surface dissolved total mercury (d-Hg_T) in seawater along the WAP in 2015. NS, not sampled, BD, below the working detection limit.

Station Long/Lat	**[d-$MeHg_T$] pM**	**[d-Hg_T] pM**
600.040 64.4°W/64.9°S	0.06	2.2
600.100 65.3°W/64.6°S	NS	2.3
600.200 66.9°W/64.0°S	0.07	2.3
400.100 68.3°W/65.9°S	0.05	0.9
400.200 69.8°W/65.2°S	0.03	1.7
200.-060 67.0°W/68.2°S	BD	7.4
200.100 72.6°W/68.0°S	0.05	1.9
200.160 72.6°W/68.0°S	0.05	2.6
-100.030 75.9°W/69.3°S	BD	0.8
-100.140 77.6°W/68.5°S	BD	2.1

Table 3.8 Surface concentrations of particulate methylmercury (p-MeHg) in surface waters along the WAP in 2014.

Station Long/Lat	Vol. Filt [L]	[p-MeHg] ppt	[p-MeHg] pM	ng_{MeHg}/g_{totbio}	$pmol_{MeHg}/g_{totbio}$
600.040_1 64.4°W/64.9°S	14.5	0.0398	0.199	0.537	2.683
600.040_2 64.4°W/64.9°S	9	0.0096	0.048	0.129	0.644
600.080_1 65.0°W/64.7°S	14	0.0056	0.028	1.270	6.350
600.080_2 65.0°W/64.7°S	15	0.0199	0.099	4.496	22.480
500.080 66.5°W/65.4°S	15	0.0021	0.010	0.272	1.358
500.060 66.2°W/65.5°S	15	0.0005	0.003	0.070	0.349
500.120 67.1°W/65.1°S	16	0.0010	0.005	0.549	2.744
500.100 66.8°W/65.2°S	16	0.0007	0.003	0.374	1.871
400.040_1 66.1°W/67.1°S	15	0.0013	0.007	0.027	0.133
400.040_2 66.1°W/67.1°S	15	0.0012	0.006	0.025	0.126
400.080 66.0°W/68.0°S	14	0.0016	0.008	0.077	0.384
400.100 65.9°W/68.3°S	13.5	0.0013	0.006	0.062	0.309
200.-040_1 68.8°W/67.8°S	15	0.0005	0.002	0.020	0.100
200.-040_2 68.0°W/69.3°S	17	0.0010	0.005	0.042	0.208
200.-060_1 68.2°W/68.9°S	15	0.0002	0.001	0.008	0.042
200.-060_2 68.2°W/68.9°S	15	0.0006	0.003	0.020	0.100
200.040_1 67.5°W/70.6°S	15	0.0008	0.004	0.026	0.131
200.040_2 67.5°W/70.6°S	16	0.0016	0.008	0.050	0.248
200.140 66.8°W/72.1°S	15	0.0002	0.001	0.141	0.707
200.100 67.1°W/71.5°S	15	0.0003	0.002	0.011	0.053

100.060 68.0°W/72.7°S	8	0.0013	0.007	0.026	0.132
100.040 68.1°W/72.3°S	7	0.0011	0.006	0.022	0.112
100.160_1 67.3°W/74.2°S	17	0.0013	0.007	1.190	5.952
100.160_2 67.3°W/74.2°S	17	0.0011	0.006	1.015	5.074

Table 3.9 Surface concentrations of particulate methylmercury (p-MeHg), total MeHg (T-MeHg = dissolved (nearest site) + particulate MeHg), percent MeHg bound to particulate organic matter (% p-MeHg) in surface waters along the WAP in 2015. Note large volumes (9-17 L) were filtered for p-MeHg, 180 mL was used for d-MeHg analysis. NC, not calculated due to non-detectable values in seawater.

Station Long/Lat	[p-MeHg] ppt	[p-MeHg] pM	ng_{MeHg}/g_{totbio}	$pmol_{MeHg}/g_{totbio}$	[T-MeHg] pM	% p-MeHg
600.040_1 64.3°W/64.9°S	0.0010	0.005	0.173	0.867	0.065	8.3
600.040_1 64.3°W/64.9°S	0.0015	0.008	0.268	1.342	0.068	13.3
600.080_1 65.0°W/64.7°S	0.0023	0.011	0.537	2.685	0.071	18.3
600.080_2 65.0°W/64.7°S	0.0012	0.006	0.286	1.429	0.066	10.0
400.040 67.3°W/66.3°S	0.0010	0.012	0.069	0.344	0.062	24.0
400.100_1 68.3°W/65.9°S	0.0012	0.006	0.402	2.011	0.036	20.0
400.100_2 68.3°W/65.9°S	0.0008	0.004	0.253	1.266	0.034	13.3
200.-060_1 68.9°W/68.2°S	0.0005	0.003	0.047	0.237	~0.003	NC
200.-060_2 68.9°W/68.2°S	0.0010	0.005	0.089	0.445	~0.005	NC
200.080 71.2°W/67.3°S	0.0011	0.005	0.958	4.789	0.055	10.0
200.100 71.5°W/67.1°S	0.0005	0.002	0.439	2.193	0.052	4.0
-100.040_1 75.9°W/69.3°S	0.0011	0.005	0.873	4.364	~0.005	NC
-100.040_2 75.9°W/69.3°S	0.0010	0.005	0.825	4.126	~0.005	NC
-100.040_3 75.9°W/69.3°S	0.0009	0.005	0.758	3.789	~0.005	NC
-100.040_4 75.9°W/69.3°S	0.0008	0.004	0.684	3.419	~0.004	NC
-100.140_1 77.3°W/68.7°S	0.0009	0.005	2.901	14.504	~0.005	NC
-100.140_2 77.3°W/68.7°S	0.0013	0.007	4.023	20.117	~0.007	NC

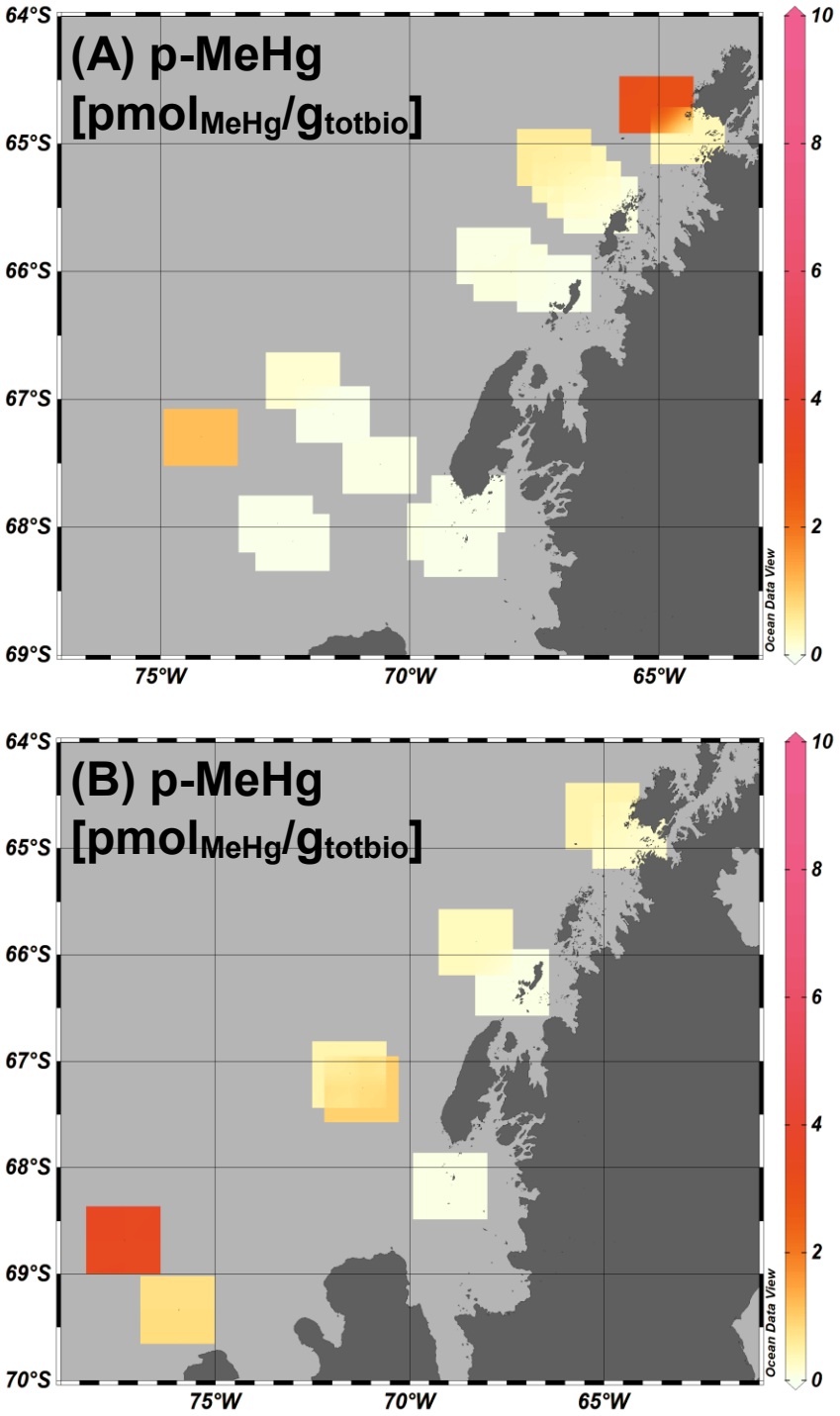

Figure 3.23 Concentrations of MeHg in particulate organic matter (p-MeHg) from surface waters of the WAP in (A) 2014 and (B) 2015. MeHg values were normalized to total biomass using a modified approach of Gosnell & Mason 2015 according to Eq. 3-4.

Table 3.10 Bioconcentration factors (logBCFs) of p-MeHg in particulate organic matter (POM) along the WAP in 2015. Values are for duplicate POM samples and their average. Surface seawater for dissolved MeHg was collected between 2 to 25 m at each station, except for station 600.080 where the concentration of dissolved MeHg from station 600.200 was used.

Station Long/Lat	POM_1	POM_2	AVE BCF
600.040 64.4°W/64.9°S	4.2	4.4	4.3
600.080_1 65.0°W/64.7°S	4.6	4.3	4.4
200.-060 67.0°W/68.2°S	3.5	3.7	3.6
200.100 72.6°W/68.0°S	4.7	5.0	4.8
-100.030 75.9°W/69.3°S	5.3	5.2	5.2
-100.140 77.6°W/68.5°S	5.8	6.0	5.9

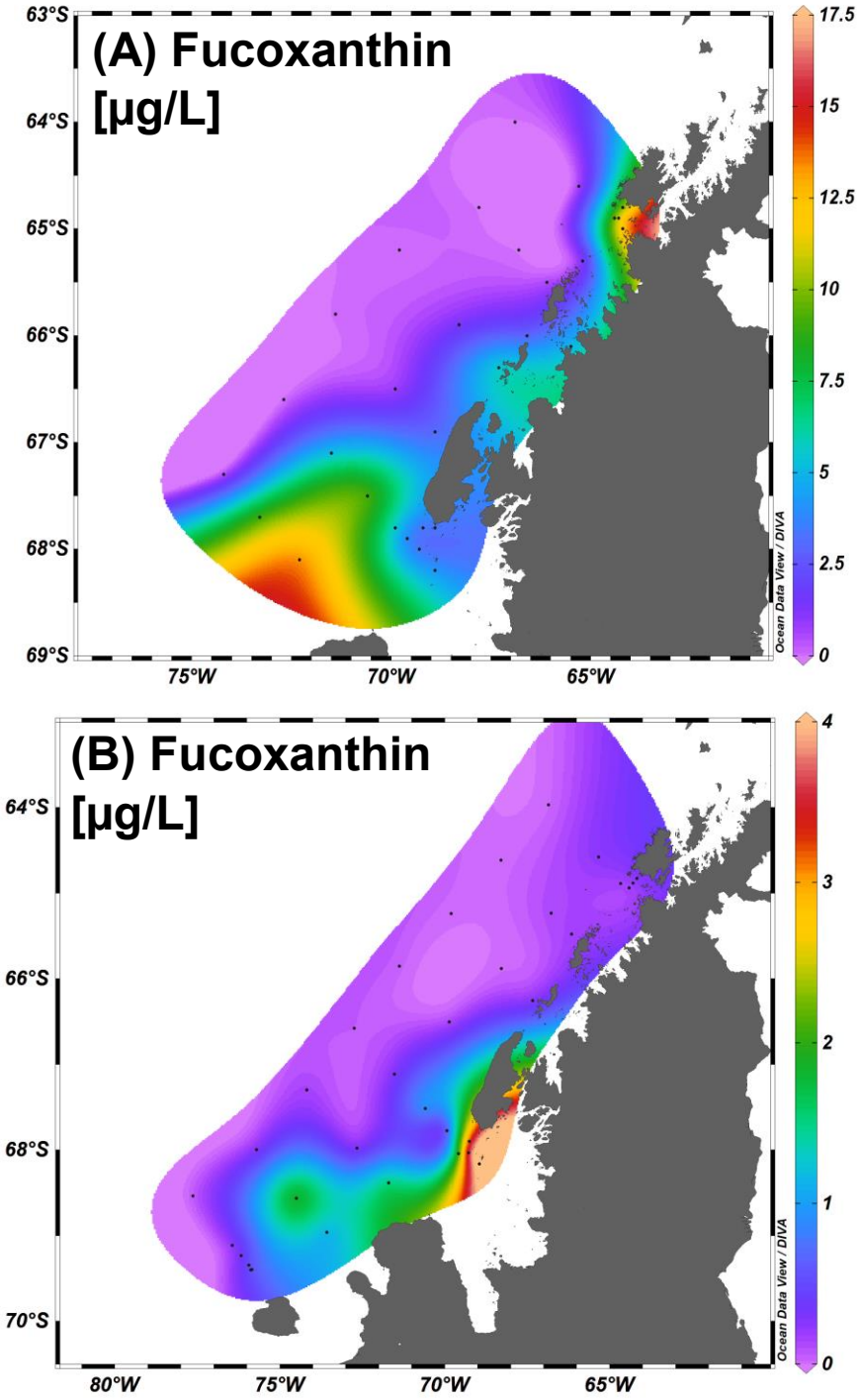

Figure 3.24 Concentrations of fucoxanthin in surface waters of the Southern Ocean west of the Antarctic Peninsula in (A) 2014 and (B) 2015.

Total unfiltered methylmercury (T-MeHg) in sea ice

Nearly identical concentrations of T-MeHg were measured in the upper layers of sea ice in cores collected 400 km apart (Figure 3.25). An increase in T-MeHg concentrations occurred below the snow-sea ice continuum (top 0.25 m) in both cores, and variable T-MeHg concentrations were observed with depth to the sea ice-seawater interface (Figure 3.25). All matrix spike corrected T-MeHg concentrations in surface sea ice were enriched relative to 200 line surface seawater T-MeHg (Figure 3.25; Table 3.9) (surface seawater at -100 line (69°S) was below detection).

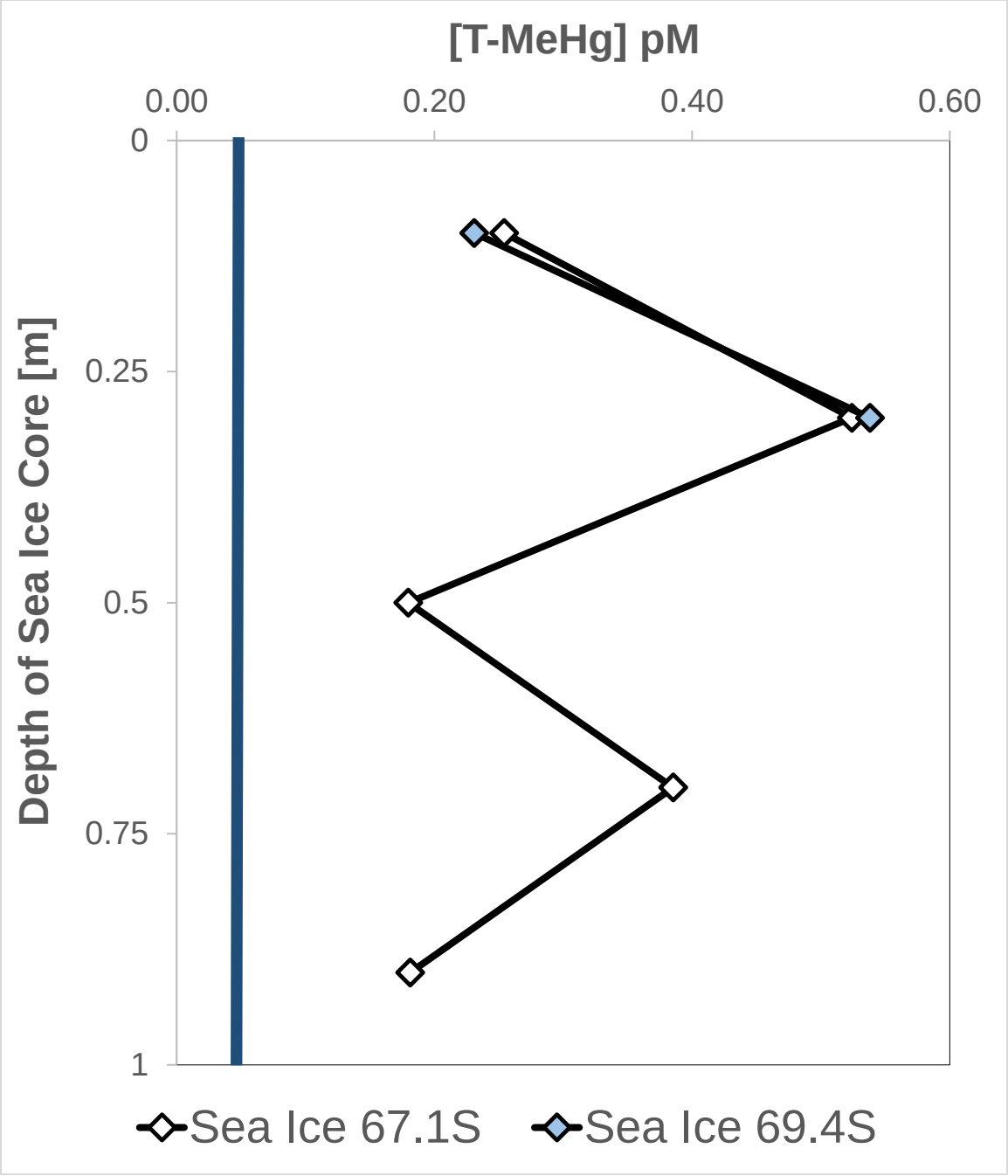

Figure 3.25 Vertical distributions of T-MeHg concentrations within unfiltered samples of 1 m sea ice core. Samples were collected from two locations approximately 400 km appart and were analyzed be direct ethylation. Dark blue line indicates the T-MeHg concentration in surface seawater near the more northern sea ice sampling site (200.100, 72.6°W/68.0°S) as T-MeHg was below detection in surface waters further south.

F. Discussion

The results of this study provide a first look at Hg concentrations in the highly productive continental shelf waters west of the Antarctic Peninsula. They show that dissolved elemental Hg and dissolved total Hg are elevated in coastal surface waters near Anvers Island and in Marguerite Bay, that dissolved MeHg is low in WAP coastal, shelf, and slope surface waters, but increases with depth most noteably in the northernmost region of the WAP. Dissolved total Hg and MeHg concentrations reach subsurface maxima, associated with intrusions of CDW and perhaps the remineralization of sinking particles at depth. Local scale variation in the concentrations of dissolved Hg species reflects the combined effects of various physical and biological inputs and removal processes on the cycling of Hg in this dynamic ecosystem.

Sources of mercury to coastal surface waters west of the Antarctic Peninsula

Net deposition of mercury during springtime atmospheric mercury depletion events is a potential source of inorganic Hg(II) to surface waters near the Antarctic coast (Ebinghaus et al. 2002). Along the Antarctic Peninsula, atmospheric deposition may therefore contribute to higher concentrations of total dissolved mercury in the shallowest surface waters compared to the upper layers of underlying WW, which was most apparent near the coast at station 600.040 (Figure 3.11). Halogens are known to oxidize Hg^0 in the marine boundary layer and iodine and bromine oxides were found in air masses above sea ice and along the Antarctic coast (Saiz-Lopez et al. 2007). These compounds may oxidize gaseous elemental mercury and produce reactive gaseous Hg(II), high concentrations of which were observed in the marine boundary layer near the Antarctic Peninsula (Soerensen et al. 2010a). Dark atmospheric depletion of elemental

mercury over sea ice in the winter, which was recently observed in the marine boundary layer near the Antarctic Peninsula (Mastromonaco et al. 2016), may serve as an additional source of inorganic mercury to underlying surface seawater.

In addition to direct atmospheric deposition, indirect inputs of atmospheric mercury via glacial runoff represents another potential source of mercury to coastal surface waters along the WAP. Glacial ice stores historic atmospheric mercury deposition (Schuster et al. 2002), which could be released to coastal seas during times of melt and ablation. This could be particularly important to the coastal waters west of the Antarctic Peninsula since 90% of glaciers on the western side of the Peninsula are in retreat (Cook et al. 2016), and among those, the greatest areal loss has occurred at southern latitudes (Cook et al. 2014). Greater loss of glacial mass toward the south along the western side of the Antarctic Peninsula may account for higher concentrations of dissolved total mercury throughout the water column at southern latitudes and in Marguerite Bay than in the north (Figures 3.14 and 3.17; Tables 3.3, 3.4, and 3.5).

In Marguerite Bay, which is surrounded by glacier-covered islands and the Antarctic Peninsula, surface dissolved total mercury concentrations were a factor of 2 to 3 higher than in surface waters elsewhere along the WAP (Tables 3.3 and 3.4), indicative of a major local source of inorganic mercury to surface waters in this area. Glacial meltwater supplies nutrients to Marguerite Bayduring the austral summer (Henley et al. 2017), and may also supply a pulse of mercury and other cations as was observed in snowmelt runoff in the Arctic (Douglas et al. 2017). Indeed, glacial meltwater was recently found to be a source of dissolved and particulate Fe to surface waters of the coastal WAP (Annett et al. 2017).

The highest d-Hg_T concentrations were measured below the surface mixed layer and at intermediate depths at the southern coastal station -100.030 (Tables 3.3, 3.4, and 3.5). While sea ice and coastal glaciers may contribute to the subsurface enrichment of d-Hg_T toward the south of the WAP, this area may also receive Hg(II) through advection from more southern latitudes of the Amundsen Sea.

Mercury in Circumpolar Deep Water near the Antarctic Peninsula

As CDW flows around the Antarctic continent, it accumulates dissolved chemicals from the remineralization of sinking biogenic particles. Coastal intrusions of CDW may therefore carry nutrients such as nitrate and silicic acid onto the Southern Ocean's continental shelves (Gordon et al. 2000). Such intrusions may also be a source of Hg to continental shelves as concentrations of dissolved Hg in CDW are elevated compared to other Southern Ocean water masses (Cossa et al. 2011). The co-occurrence of maxima of d-Hg_T and d-$MeHg_T$ within CDW along the continental slope of the Bellingshausen Sea west of the Antarctic Peninsula (Figure 3.26), and previously reported intrusions of Upper Circumpolar Deep Water (UCDW) onto the WAP's continental shelf (Couto et al. 2017), indicate that CDW is a potential source of d-Hg_T and d-$MeHg_T$ to the WAP ecosystem.

Above the continental slope at the northern end of the survey area, maximum concentrations of dissolved total mercury and dissolved total methylated mercury both occurred within UCDW at a depth of 230 m (Table 3.11). The highest concentrations of d-Hg_T and d-$MeHg_T$ also occurred within CDW at the offshore station in the south (Figure 3.27 and Table 3.11) where a sharp d-$MeHg_T$ maximum (0.22 pM) occurred at 330 m and a broad d-Hg_T maximum (7.8 to 8.7 pM) extended from 200 to 600 m (Table

3.5). In contrast to the situation in slope and shelf waters, the contribution of CDW to d-Hg_T and d-$MeHg_T$ in nearshore waters along the WAP may be lower than other sources since near shore maxima were higher than those offshore in the north (Table 3.11) and were within shallower WW in the south (Figure 3.27).

Remineralization of particulate mercury in the near shore water column

The decomposition of sinking particulate matter may also be an important source of dissolved Hg in near shore waters along the Antarctic Peninsula. Within the Palmer Deep Canyon, the concentration of d-Hg_T gradually increased from 100 m to 1250 m (Table 3.3; Figure 3.26). This trend, which followed that of increasing AOU (Figure 3.28), likely reflects the remineralization of mercury bound to sinking biogenic particles produced in the highly productive surface waters south of Anvers Island (Saba et al. 2014, Schofield et al. 2017). Both d-Hg_T and d-$MeHg_T$ decreased by factors of 2 or more within ~50 m of the bottom of the Palmer Deep, indicating possible scavenging by particles just above the sea floor (Table 3.3; Figures 3.11 and 3.12).

Subsurface maxima of dissolved MeHg have been observed in a variety of ocean basins (Hammerschmidt and Bowman 2012, Heimburger et al. 2015, Munson et al. 2015) including the Southern Ocean (Cossa et al. 2011). Near Anvers Island, the northernmost nearshore station in the present study, the subsurface concentration of d-$MeHg_T$ peaked at 0.92 pM (Figures 3.11 and 3.26), the highest d-$MeHg_T$ concentration measured in the Southern Ocean (Cossa et al. 2011, Gionfriddo et al. 2016). Remineralization of biogenic particles may contribute to this subsurface maximum in dissolved d-$MeHg_T$. However, d-$MeHg_T$ had a much larger relative increase in subsurface waters (>10 fold compared to less than a factor of 2 for d-Hg_T) and peaked at a much shallower depth (500 m) than d-

Hg_T. In addition, at both nearshore and offshore northern stations, the fraction of dissolved total Hg present as dissolved methylmercury (%d-$MeHg_T$), increased rapidly with depth below 100 m (Figure 3.13). These observations indicate that there are additional sources of MeHg to the water column at depth, including in situ production. Remineralization was probably a less important source of Hg to the water column at the southern stations than in the north since the proportions of d-Hg_T as d-$MeHg_T$ did not increase very much with depth along the southern (-100) survey line (Figures 3.19 and 3.20).

Particulate accumulation and vertical transport of dissolved mercury in Marguerite Bay

The very high concentrations of d-Hg_T in the surface waters of Marguerite Bay (Figure 3.14) may be due to inputs from snow and glacier meltwater. However, the maximum concentration of d-Hg_T was observed in the center of the WW (Figure 3.29) indicating a slight depletion of d-Hg_T near the surface, possibly as a result of accumulation in suspended particles or biological or photochemical reduction. The decline in d-Hg_T with depth below the mixed layer may result from the intrusion of water masses from elsewhere on the shelf or particle scavenging by sinking phyotplankton in this highly productive ecosystem (Hendry and Rickaby 2008, Henley et al. 2017). High particle export has been measured along continental shelf waters of the WAP (Buesseler et al. 2010). In these productive waters, efficient accumulation and vertical transport of Hg(II) with primarily biogenic particles is likely. The increase in dissolved total mercury by almost 2 pM from 230 m to 260 m near the bottom of Marguerite Bay indicates the

release of Hg from sediments in these relatively low oxygen (<200 µmol/L) waters (Figure 3.14).

Unlike elsewhere along the Peninsula, dissolved total methylated mercury was relatively high toward the surface (15 m) of Marguerite Bay (Figure 3.15), decreased with depth below the mixed layer, and did not accumulate in a subsurface maximum. Efficient particle scavenging may account for the decline in d-$MeHg_T$ with depth and the rapid delivery of biogenic particles to the sediments (Buesseler et al. 2010) may limit particle remineralization and d-$MeHg_T$ production in this relatively shallow water column (~260 m). Relatively constant d-Hg_T and d-$MeHg_T$ concentrations (Figures 3.14 and 3.15) and %d-$MeHg_T$ (Figure 3.16) at depth are consistent with limited water column Hg methylation in Marguerite Bay.

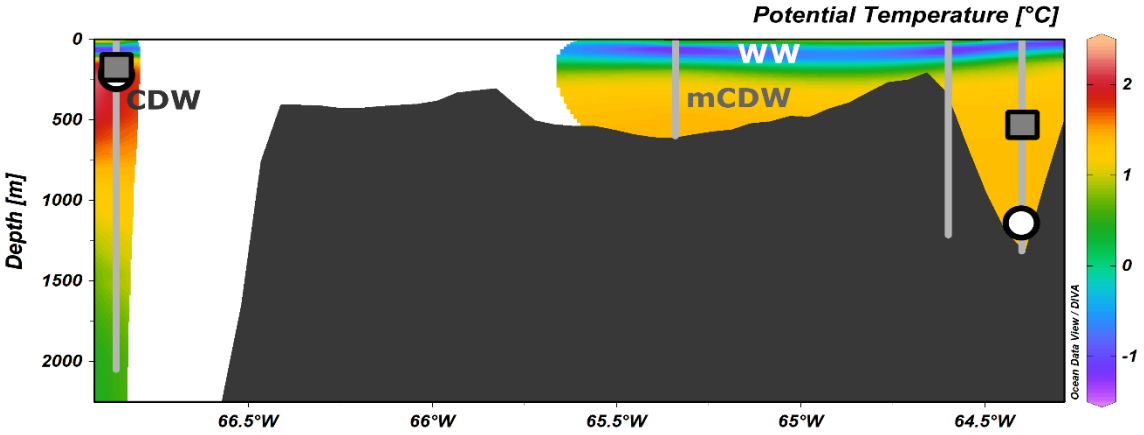

Figure 3.26 Potential temperature and water masses at ~65°S (600 line, boxed points on map). Vertical dissolved total mercury (white circle) and dissolved total methylated mercury (grey square) maxima are indicated at coastal and slope sites sampled for mercury. White area was outside the limits of interpolation. Bathymetry of continental shelf west of the Antarctic Peninsula is depicted in black.

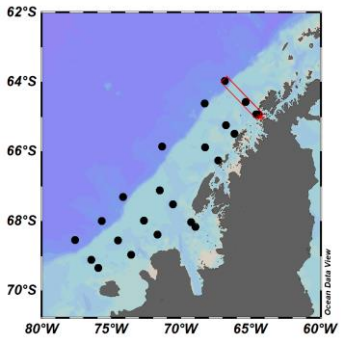

Table 3.11 Vertical dissolved mercury maxima [pM] in seawater along the WAP.

Station Long/Lat	[d-MeHg$_T$]	[d-Hg$_T$]	Depth [m]
600.040 64.4°W/64.9°S	0.92	3.8	500, 1250
600.200 66.9°W/64.0°S	0.61	2.4	230
200.-060 67.0°W/68.2°S	0.09	7.7	15, 25
-100.030 75.9°W/69.3°S	0.16	16.6	150, 75
-100.140 77.6°W/68.5°S	0.22	8.7	330, 600

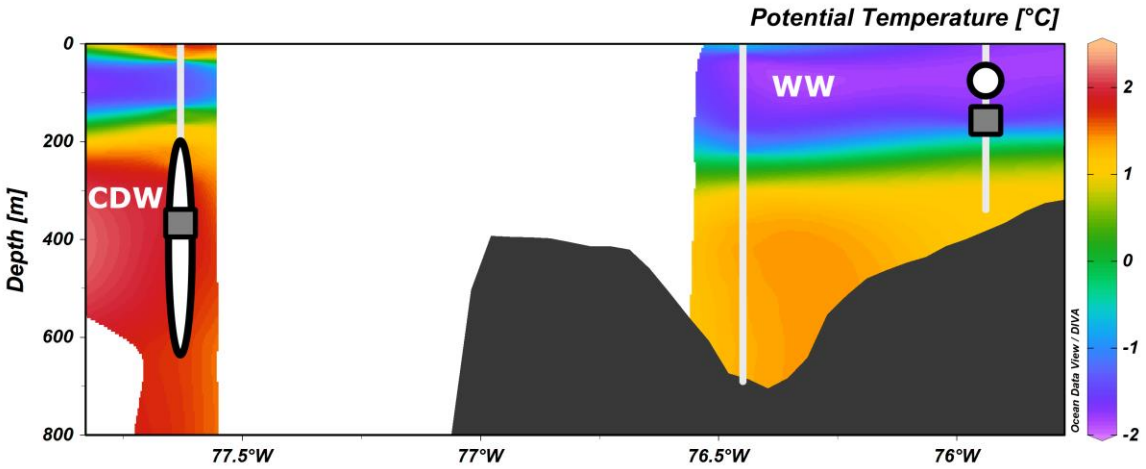

Figure 3.27 Potential temperature and water masses at ~69°S (-100 line, boxed points in map). Vertical dissolved total mercury (white oval) and dissolved methylated mercury (grey square) maxima are indicated at coastal and slope sites sampled for mercury. White areas were outside the limits of interpolation. Bathymetry of continental shelf west of the Antarctic Peninsula is depicted in black.

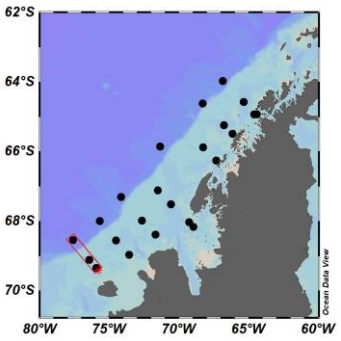

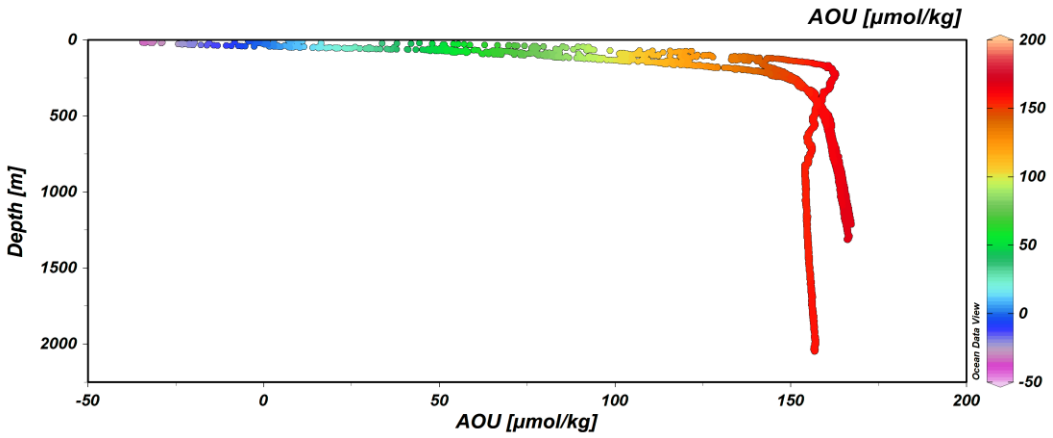

Figure 3.28 Depth profiles of apparent oxygen utilization (AOU) at the 600 line along the WAP continental shelf at ~65°S. Estimates for AOU were calculated in Ocean Data View using measured dissolved oxygen concentrations and calculated neutral density (γn [kg/m^3]) of seawater.

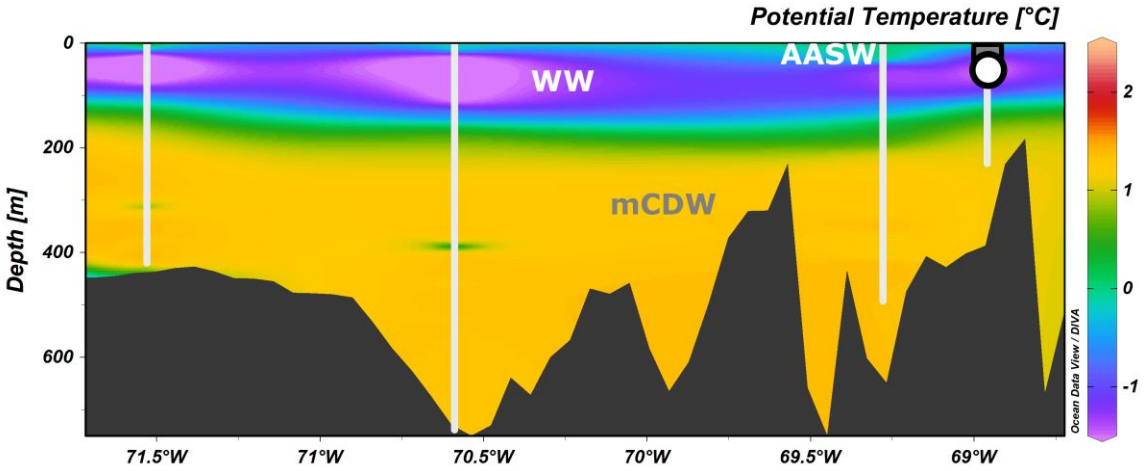

Figure 3.29 Distributions of potential temperature and labeled water masses at ~67°S (200 line, boxed points in map). Vertical dissolved total mercury (white oval) and dissolved methylated mercury (grey square) maxima are indicated at coastal and slope sites sampled for mercury. Bathymetry of continental shelf west of the Antarctic Peninsula is depicted in black.

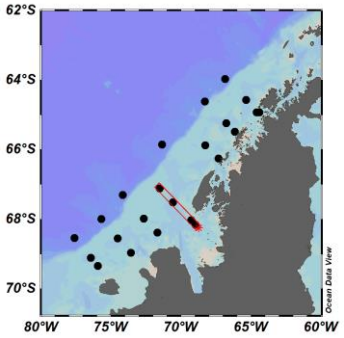

Phytoplankton and bacterioplankton assemblages control on particulate methylmercury of surface waters west of the Antarctic Peninsula

The spatial variability of p-MeHg concentrations along the WAP was similar to that in the central Pacific Ocean (Gosnell and Mason 2015). Less spatial variation in p-MeHg was observed in coastal ecosystems of the northwestern North Atlantic (Hammerschmidt et al. 2013, Schartup et al. 2018) where nearshore p-MeHg concentrations are lower than those in the WAP and similar to those in Arctic estuaries (<10 $pmol_{MeHg}/g_{totbio}$) (Schartup et al. 2015a). In both 2014 and 2015, chl*a* concentrations and bacterial abundances were higher nearshore than offshore (Figures 3.5A, 3.6A, 3.21A, 3.22A) and biodilution of MeHg occur at higher phytoplankton cell densities (Pickhardt et al. 2002) and could be taking place nearshore during the austral summer.

Large diatoms (>20 µm) tend to dominate phytoplankton assemblages during phytoplankton blooms along the WAP (Holmhansen and Mitchell 1991). Fucoxanthin, an accessory pigment produced by diatoms, was highest within regions of higher chl*a* concentrations in both 2014 and 2015 (Figures 3.5A, 3.21A, and 3.24). In 2014, fucoxanthin was generally higher in coastal waters than offshore, but along the 200 line, elevated concentrations of fucoxanthin (>5 µg/L) persisted further out along the continental shelf (Figure 3.24). Within these regions of high fucoxanthin, lower p-MeHg (<5 $pmol_{MeHg}/g_{totbio}$) was measured in surface POM in 2014 (Figure 3.23). In both 2014 and 2015, the highest p-MeHg concentrations (~10-20 $pmol_{MeHg}/g_{totbio}$) were measured in regions of lower fucoxanthin and in waters were fucoxanthin levels began to transition

from higher coastal values to lower levels offshore at northern and southern sites. (Figures 3.23A, 3.23B, 3.24A, and 3.24B).

Biodilution of p-MeHg by diatoms near the coast is likely an important mechanism limiting the biomass-specific accumulation of MeHg at the base of the WAP food web. Further offshore, however, where the highest concentrations of p-MeHg (6-20 $pmol_{MeHg}/g_{totbio}$) were observed (Figures 3.23A and 3.23B), the predominance of smaller nanoplankton (<20 µm) and picoplankton (<2 µm) with higher surface area: volume ratios may lead to higher p-MeHg concentrations per cell, as was seen in the small size fraction of plankton in the central Pacific Ocean (Gosnell and Mason 2015).

Methylmercury in unfiltered sea ice

Preliminary results showing higher T-MeHg concentrations (unfiltered) at all depths in sea ice than in surface seawater (Tables 3.7 and 3.9; Figure 3.25) are consistent with previous observations of an enrichment of mercury in sea ice relative to surface seawater in East Antarctica (Cossa et al. 2011, Gionfriddo et al. 2016) and in seawater directly underlying sea ice relative to adjacent surface waters (St Louis et al. 2007, Wang et al. 2012).

Some of this enrichment may be due to inputs from snow overlying sea ice, which accumulates Hg from the atmosphere and contributes to high total mercury concentrations at the upper boundary of the snow-sea ice continuum (Chaulk et al. 2011, Cossa et al. 2011, Beattie et al. 2014). During melt, inorganic Hg(II) may migrate from surface layers of sea ice down through brine channels, as is the case for iron (van der Merwe et al. 2011). Ice algae and other particles control the distributions of mercury and

other trace metal in sea ice and the release of these metals to surface waters when sea ice melts (Lannuzel et al. 2011, Burt et al. 2013). Microbial activity and abiotic processes may lead to the production of MeHg in sea ice. A microorganism containing a gene related to those involved with Hg methylation has been identified in sea ice (Gionfriddo et al. 2016), although Hg methylation in sea ice has not been directly measured.

Dissolved elemental mercury (DEM) concentrations in WAP surface waters

Once deposited, Hg(II) may be re-reduced to DEM via photochemical reactions (Poulain et al. 2004) during the austral summer or by biological processes (Poulain et al. 2007). Leads in Antarctic sea ice play a role in mercury deposition (Mastromonaco et al. 2016), however, annual sea ice retreat occurs first away from shore exposing slope surface waters which had lower DEM concentrations and degrees of saturation than coastal waters (Figures 3.3 and 3.4). More recent studies show that mercury deposited on surface snow during these events may be remitted with little enhancement of concentrations in snow (Zdanowicz et al. 2013, Obrist et al. 2017).

Surface water DEM concentrations (0.15 to 0.25 pM, Figure 3.3) measured along the WAP were similar to those measured offshore of the shelf-slope break in the Bellinghausen Sea, directly west of our sampling area (Mastromonaco et al. 2017b). However, concentrations of DEM in the WAP are lower than those in the Arctic where particularly high levels were measured near the mouths of large rivers such as the Mackenzie (Andersson et al. 2008b). Sources of freshwater to WAP coastal waters are limited, but glacial meltwater may supply inorganic Hg(II) to coastal ecosystems during the spring and summer as in the Arctic (Loseto et al. 2004, Douglas et al. 2017).

High bacteria densities along the WAP (range 2.5 x 10^8 to 2 x 10^9 cells/mL) (Figures 3.6A and 3.22A) are orders of magnitude higher than those measured in the high Arctic and may be responsible for the reduction of dissolved Hg(II) by means of mercuric reductase (*merA*) (Poulain et al. 2007). The highest concentrations of DEM were observed in coastal productive surface waters with the highest bacteria densities in 2014 (Figures 3.5A and 3.6A). The influence of bacteria-driven Hg(II) reduction may largely be dictated by the bioavailability of Hg(II). Since dissolved organic carbon (DOC) concentrations are low in WAP surface (45-50 µM) and deep (39 µM) waters (H.W. Ducklow 2005, unpublished data), the majority of dissolved inorganic mercury is likely bound to Cl^- as $HgCl_4^{2-}$, which is a bioavailable form of Hg that can readily dissociate within a cell's boundary layer.

Air-sea exchange and fluxes of mercury in coastal, shelf, and slope regions

Estimated air-sea Hg fluxes along the WAP were highest near the coast and are comparable to average fluxes in the Weddell Sea measured during the winter and spring (2.0 pmol m^{-2} hr^{-1}, 5.5 pmol m^{-2} hr^{-1}, respectively) (Mastromonaco et al. 2017b). . The highest flux of Hg^0 (factor of 3 higher than the next highest flux) was observed in the coastal sub-region at the southern edge of our sampling range where in 2014, sea ice persisted well into January. While the magnitude of this flux may be biased by much higher wind speeds during the period of observation than elsewhere along the WAP, the persistence of elevated DEM concentrations during periods of high volatilization fluxes may indicate the presence of Hg^0 that had accumulated under sea ice the previous winter, or the biologically or photochemically-driven reduction of Hg(II) released from melting

sea ice or the more rapidly retreating glaciers toward the Peninsula's southern end as discussed above.

Global context of dissolved total methylated mercury and dissolved total mercury maxima in WAP

The d-Hg_T maxima of 16.6 pM measured in this study is higher than any seawater d-Hg_T value measured in the Arctic (St Louis et al. 2007, Kirk et al. 2008, Chaulk et al. 2011, Lehnherr et al. 2011, Wang et al. 2012, Zdanowicz et al. 2013, Heimburger et al. 2015, Schartup et al. 2015a, Soerensen et al. 2016) or Southern (Cossa et al. 2011, Mastromonaco et al. 2017a) Oceans. Only seawater collected under sea ice (~1 m) in the East Antarctic had a higher total mercury concentration (Gionfriddo et al. 2016). Our data and the latter study suggest the importance of persistent sea ice in the accumulation of inorganic Hg(II) in waters under sea ice during periods of limited exposure to the atmosphere. Subsurface maxima of d-$MeHg_T$ and d-Hg_T in the WAP are some of the highest values in the open ocean (Table 3.11 and 3.12). The only d-$MeHg_T$ value higher than that from station 600.040 was in the anthropogenically impacted North Atlantic (Mason et al. 1998) (Tables 3.11 and 3.12).

Table 3.12 Vertical mercury maxima [pM] in the world's oceans. Data gathered from Lamborg et al. 2014; Hammerschmidt & Bowman 2012; Munson et al. 2015; Mason & Fitzgerald 1993; Sunderland et al. 2009; Mason et al. 1998; Mason & Sullivan 1999; Heimburger et al. 2015; Wang et al. 2012; Cossa et al. 2011; Gionfriddo 2016

Basin	**[$MeHg_T$]**	**[Hg_T]**
Subtropical N. Pacific	0.10	1.60
Central Tropic Pacific	0.16	1.70
Equatorial Pacific	0.92	6.90
North Pacific	0.47	2.39
North Atlantic	1.80	7.10
South and Equatorial Atlantic	0.15	6.10
Central Arctic Ocean	0.35	7.00
Beaufort Sea	0.59	1.54
Southern Ocean	0.86	2.76
East Antarctica	***0.69***	***115***
WAP (this study)	***0.92***	***16.6***

G. Conclusions

Spatial variability in the concentrations of dissolved Hg^0, d-Hg_T, and d-$MeHg_T$, and in particulate MeHg were observed throughout the continental shelf waters of the WAP. Major drivers of mercury dynamics are thought to include: atmospheric deposition, coastal intrusions of CDW, inputs of glacial meltwater to coastal sites, and the timing of annual sea ice retreat. Locally, biological production will affect the mercury reduction and air-sea exchange, particle-water partitioning of d-Hg_T and d-$MeHg_T$, and the possible production of d-$MeHg_T$ during biogenic particle remineralization within the water column. Contributions of methylmercury from sea ice to WAP surface waters needs to be studied further but represents an important potential source during sea ice melt. The results of this study reveal the accumulation of MeHg at the base of the WAP food web, the large and small-scale heterogeneity of mercury distributions in WAP shelf waters, and how these are likely influenced by various physical and biological processes.

Chapter IV Mercury and stable isotopes of carbon and nitrogen in Antarctic krill (*Euphausia superba*) subpopulations and penguins (*Pygoscelis* spp.) near Anvers Island and at the sea ice edge along the WAP

A. Abstract

We examined mercury (Hg) accumulation in Antarctic krill (*Euphausia superba*) subpopulations collected during four Palmer Antarctica Long-Term Ecological Research (PAL LTER) cruises in January during the austral summers of 2011, 2013, 2014, and 2015 and in body feathers from three *Pygoscelis* penguins living near Anvers Island, west of the Antarctic Peninsula in 2011. Mean concentrations of methylmercury (MeHg), the form of Hg that biomagnifies in marine food webs, were significantly higher ($P < 0.001$) in juveniles (0.8 to 2.9 ng g^{-1}) than adults (0.3 to 1.6 ng g^{-1}). Juvenile Antarctic krill also accumulated significantly higher ($P < 0.005$) mean concentrations of THg (4 to 12.6 ng g^{-1}) than adult krill (7.8 to 19.4 ng g^{-1}). Within year pair-wise comparisons revealed significant differences ($P < 0.05$) in MeHg between adults and juveniles in 2011, 2013, and 2014. Greater intra-annual bioaccumulation (BAF) factors of MeHg in juvenile krill (1.5 to 5.3) than adults (0.7 to 2.9 resp.) along with greater distributions of MeHg (60.7±4.7; 54±1.8 juveniles, adults resp.) and THg (28±6.2; 18±3.0 juveniles, adults resp.) in muscle tissue suggest that juvenile krill were likely encountering prey in areas with higher MeHg concentrations or bioavailabilities than adults. Spatial differences in δ^{13}C and δ^{15}N between nearshore and more offshore environments at varying latitudes were measured in krill and particulate organic matter (POM), with 2014 krill enriched in both ^{13}C and ^{15}N relative to all other years, and significant differences ($P < 0.05$) in δ^{13}C and δ^{15}N values between all subpopulations of juvenile and adult krill. MeHg

concentrations in krill were positively correlated with δ^{13}C values (R^2=0.50) but MeHg accumulation could not be explained by δ^{15}N values or trophic position (Δ^{15}N) with respect to particulate organic matter. Higher accumulation of MeHg may be linked to foraging location and the enrichment of ^{13}C at the base of nearshore food webs and perhaps sea ice with lower accumulation of MeHg in krill from shelf and slope waters influencing MeHg transfer to krill-dependent predators. The mean concentration of THg (<95% MeHg) in feathers of chinstrap penguins (*Pygoscelis antarctica*) (0.80±0.20 µg g^{-1}) was significantly higher ($P < 0.001$) than that in either gentoo (*Pygoscelis papua*) (0.16±0.08 µg g^{-1}) or Adélie (*Pygoscelis adeliae)* (0.09±0.05 µg g^{-1}) penguins. All three *Pygoscelis* spp. occupied a relatively narrow trophic niche as defined by C and N stable isotopes. Gentoo penguins, known to have greater flexibility in foraging depth, had slightly, but significantly higher ($P < 0.05$) δ^{15}N values than both chinstrap and *Adélie* penguins. However, gentoos had lower THg concentrations than chinstrap penguins which are known to feed in mesopelagic waters. Accumulation of Hg, δ^{13}C and δ^{15}N values were examined in Antarctic krill at sea ice edge locations along the peninsula in 2013, 2014, and 2015. Higher MeHg concentrations ($P<0.05$) in juvenile than adult krill were observed across all sampling years. Patterns of MeHg accumulation and C and N stable isotopes in krill collected near sea ice suggest that variation of MeHg in adult krill in this region is dictated by sub-population trophic position, while juvenile MeHg is relatively constant across a range of stable C and N isotope values attributed to different feeding patterns at environments where sea ice persists year-round. From plankton to penguins, MeHg concentrations increase by about three orders of magnitude. MeHg accumulation within krill and penguins was not explained by δ^{15}N or trophic position.

Rather developmental stage and feeding near the coast or sea ice were identified as controlling MeHg accumulation in krill, while feeding strategies appear to be important to Hg in penguins. Variation in MeHg accumulation among subpopulations of Antarctic krill and among different species of sympatric penguins, demonstrates the potential use of MeHg as a tracer to identify trophic linkages both across and within organisms of similar trophic position, in this highly productive and tightly coupled, remote marine ecosystem.

B. Introduction

Although remote from anthropogenic sources, Antarctic ecosystems may accumulate mercury (Hg) to very high levels (Bargagli 2008) and Hg concentrations in Antarctic seabirds can be as high as consumers of similar trophic levels from the northern hemisphere (Nygard et al. 2001, Becker et al. 2002). While the accumulation of Hg in zooplankton (Stern and Macdonald 2005, Gantner et al. 2009), and the biomagnification of Hg in higher level consumers (Campbell et al. 2005) are well documented in Arctic marine ecosystems, fewer studies have examined the bioaccumulation of Hg within prey and predators of Antarctica (Bargagli et al. 1998, Sanchez-Hernandez 2000, Bargagli 2001, dos Santos et al. 2006).

In the highly productive coastal waters of the Southern Ocean, food web accumulation of Hg is likely controlled by Antarctic krill (*Euphausia superba*), a keystone species providing a link for carbon, energy, and contaminant transfer between primary producers and upper trophic levels (Szefer et al. 1993, Becker et al. 2002, Chiuchiolo et al. 2004). However, while the concentrations of total mercury (THg), have been measured in Antarctic krill and phytoplankton (Honda et al. 1987, Bargagli et al. 1998), THg in plankton is primarily composed of inorganic Hg, and the accumulation of

monomethylmercury (MeHg), the form of mercury that biomagnifies in marine food webs (Stern and Macdonald 2005, Hammerschmidt and Fitzgerald 2006a), has not been examined.

Krill development begins offshore where spawning females release eggs that sink to mesopelagic waters along the continental shelf and slope and hatch at depth (Daly and Zimmerman 2004). Developing larval krill then undergo an ontogenetic migration vertically to the epipelagic zone and toward the coast (Trathan et al. 1993, Lascara et al. 1999, Daly and Zimmerman 2004). Seasonal sea ice plays an important role in krill recruitment (Saba et al. 2014) as larval and juvenile krill feed under sea ice and within marginal sea ice zones (Daly 1990, Frazer et al. 2002a). Differences in juvenile and adult feeding location during krill development may dictate assimilation in juvenile and adult krill as phytodetritus and trophic structure are known to differ along the continental shelf west of the Antarctic Peninsula (Mincks et al. 2008). Shifts can occur in the proportions of phytoplankton and zooplankton during development (Polito et al. 2013) in the generally omnivorous krill diet (Martin et al. 2006), which could also affect the accumulation of Hg. A previously observed inverse relationship between THg and body length of Antarctic krill (Locarnini and Presley 1995) suggests that Hg concentrations decrease as krill mature. However, the influence of other biological, ecological, and environmental factors on the accumulation of Hg in krill and krill-dependent predators, is not understood.

All three species of *Pygoscelis* penguins, Adélie (*Pygoscelis adeliae*), gentoo (*P. papua*), and chinstrap (*P. antarctica*), reside along the WAP (WAP) during the austral summer and maintain breeding colonies on islands neighboring Anvers Island and U.S.

Antarctic research station Palmer (Fraser and Hofmann 2003, Gorman et al. 2014). These birds occupy separate foraging niches (Miller et al. 2010) with Adélies preferring surface pelagic waters (Kahl et al. 2010) and chinstraps preferring deeper mesopelagic waters (Trivelpiece et al. 2007, Miller and Trivelpiece 2008). Gentoo penguins feed locally nearshore (Williams 1995), but have greater flexibility in their foraging depth than Adélies or chinstraps (Tanton et al. 2004, Cimino et al. 2016). Although fish can account for >50% of the *Pygoscelis* penguin diet during summer months (Polito et al. 2011b), krill are generally the dominant summer prey for all three species (Trivelpiece et al. 1987, Chapman et al. 2010) with chinstraps consuming the highest percentage of krill (Polito et al. 2015) and the highest proportion of juvenile krill (Miller and Trivelpiece 2007, Kokubun et al. 2015).

Penguins are well suited as biomonitors of Hg in the Antarctic ecosystem as they have accessible nesting colonies, accumulate Hg in feathers and eggs (Brasso et al. 2012, Brasso et al. 2014) and undergo an annual (complete) molt where all feathers are removed and regrown over weeks of fasting (Stonehouse 1967). Monomethylmercury is the dominant Hg species in seabird feathers (>95%) (Thompson and Furness 1989, Bond and Diamond 2009), and thus represents a potentially useful long-term (months-year) biomarker of feeding location and diet to complement short-term (weeks-month) signatures of carbon and nitrogen stable isotope ratios(Ramos and Gonzalez-Solis 2012). Carbon and nitrogen isotope ratios in feathers are indicative of a bird's diet during growth as keratin becomes inert after it is synthesized (Hobson and Clark 1992, Pearson et al. 2003). In contrast, Hg in adult *Pygoscelis* penguin feathers represents Hg accumulated throughout the year since the last molt (Anderson et al. 2009), In the summer months,

Pygoscelis penguins are known to forage near breeding grounds (Davis and Renner 2003), as is the case for Adélies living along the southern coast of Anvers Island (Kahl et al. 2010). However, during non-breeding seasons, penguins may forage far from their breeding grounds as has been documented for chinstrap penguins from South Shetland Islands, north of the Antarctic Peninsula (Hinke et al. 2015). Since fish constitute a larger portion of penguin diets in winter[36] and prey fish in the Southern Ocean have large variations in muscle THg concentrations (Sanchez-Hernandez 2000), consumption of fish may be important to the variation of Hg concentrations in penguin feathers.

To examine the factors controlling the accumulation of Hg in the coastal marine food web west of the Antarctic Peninsula, we measured THg and MeHg in whole and dissected adult and juvenile Antarctic krill and THg (>95% MeHg) in body feathers from three species of sympatric *Pygoscelis* penguins living near Anvers Island. We also measured carbon and nitrogen stable isotope ratios in particulate organic matter (POM), krill, and penguin feathers. Variation in Hg accumulation among krill populations was evaluated with respect to spatial distributions (distance from shore) and developmental stage (juvenile, adult), and among penguin species was evaluated in the context of foraging location and diet.

C. Materials and Methods

Collection and mercury analysis of Antarctic krill

Adult and juvenile Antarctic krill (*Euphausia superba*) were collected between the 1st and 14th of January during the austral summers of 2011, 2013, 2014, and 2015 at coastal, shelf, and slope stations (Figure 4.1) along a northern transect (600 line) (Figure

4.2) and at the sea ice edge (100 to -100 line) within the Palmer Antarctica Long-Term Ecological Research (PAL LTER) program sampling grid (Steinberg et al. 2015). Krill were sampled using a 2 m-square frame Metro net (700 µm mesh), towed obliquely to 120 m depth using established PAL LTER protocols (Ross et al. 2008, Steinberg et al. 2015). Coastal, shelf, and slope sub regions along the WAP were assigned using bathymetry (Steinberg et al. 2012, Steinberg et al. 2015). Coastal and shelf waters were designated by the shelf break (at a depth of approximately 431 m), while slope waters were identified as those offshore of the 750 m isobath.

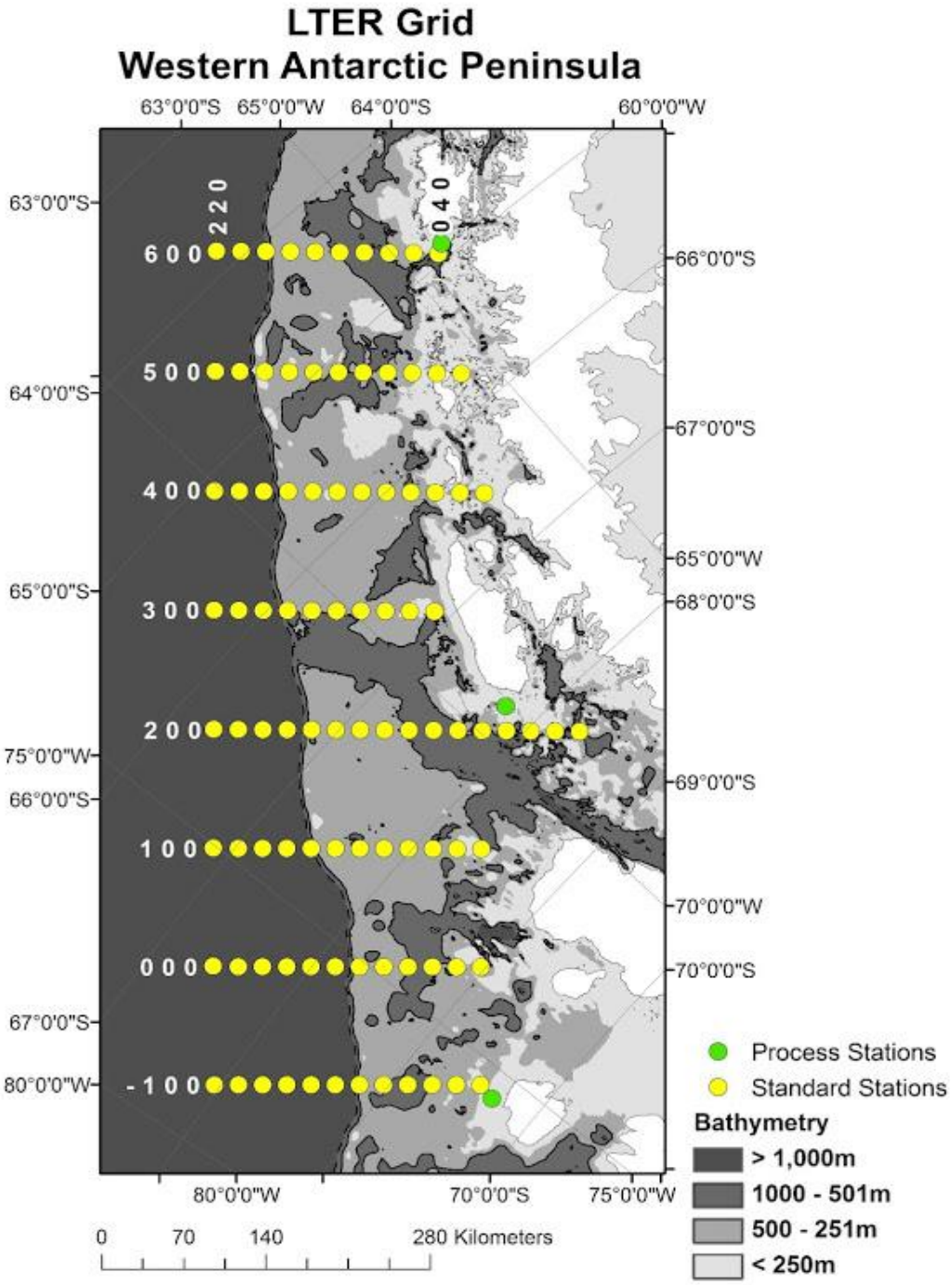

Figure 4.1 Process and standard stations on the Long Term Ecological Research (LTER) grid for Antarctic krill (*E. superba*) and *Pygoscelis* penguins samples collected along the WAP (inset) during the summers of 2011 and 2013-2015.

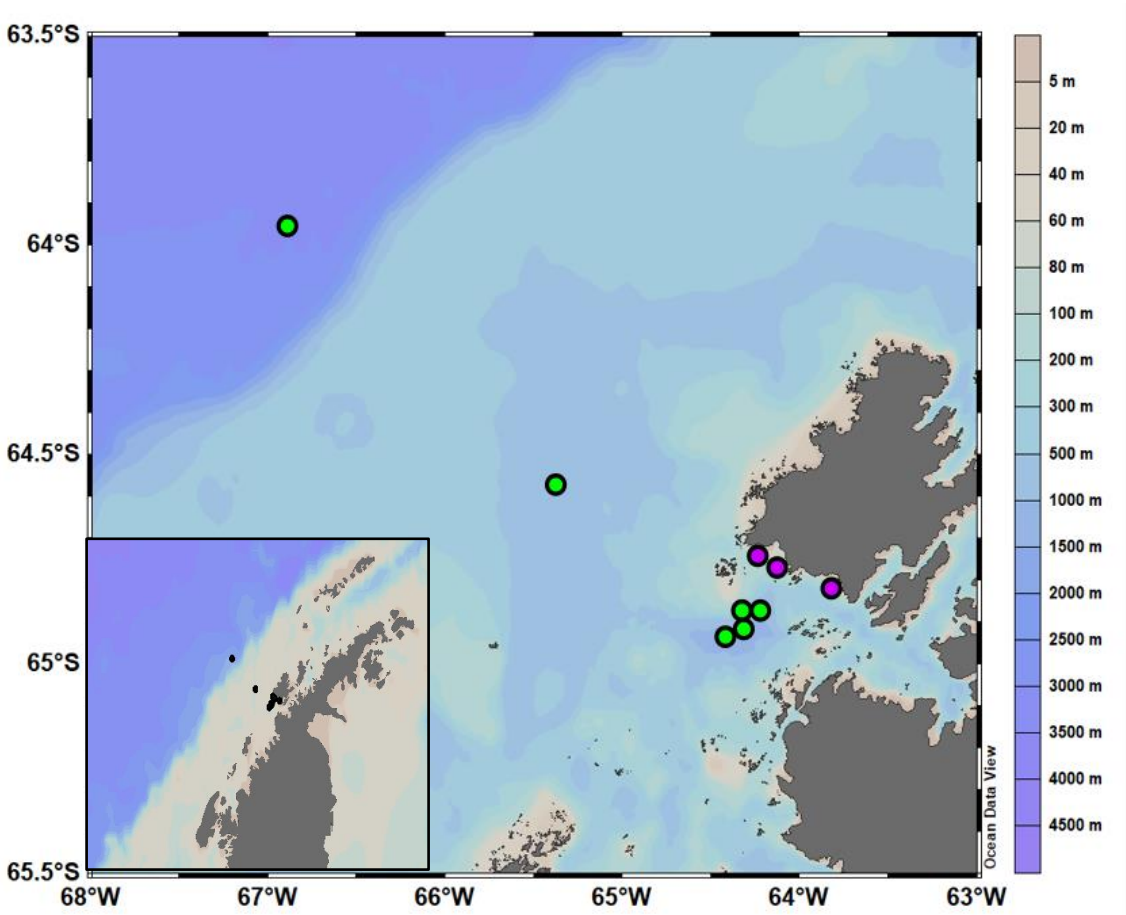

Figure 4.2 Sampling locations near Anvers Island for Antarctic krill (*E. superba*, green circles) and *Pygoscelis* penguins (purple circles) collected along the WAP (inset) during the summers of 2011 and 2013-2015.

Fresh (wet) krill were handled in the field with trace metal clean Teflon forceps and initially separated into juvenile and adult krill by length (Siegel and Loeb 1994) to limit cross-contamination of tissues. Bulk samples (15-20 individuals) were placed in trace metal clean 50 mL polystyrene tubes and frozen at -20°C for shipping back to the Rutgers University laboratory. Prior to analysis, whole krill were partially thawed to separate individual animals, each were lyophilized for 24 hours. After lyophilization, official classification of juvenile krill was designated by dry weights <75 mg, which is consistent with prior studies (Mayzaud et al. 1998, Meyer et al. 2010). Subsamples of adult and juvenile krill were dissected to determine the distributions of THg and MeHg in muscle, soft tissues (hepatopancreas, hindgut), and exoskeleton.

Dry whole individual krill and dissected tissues were homogenized in a 15 mL polystyrene tube, digested in 5 mL of 4 N Trace Metal grade (Fisher) nitric acid (HNO_3) at 55°C for 16 hours (Hintelmann and Nguyen 2005), and stored at 8°C prior to analysis. Krill digests were analyzed in duplicate for MeHg (and THg described below) by cold vapor atomic fluorescence spectroscopy (CVAFS) after gas chromatographic separation of the ethylated derivative (Liang et al. 1994b).

For THg, aliquots (<1 mL) of 4 N HNO_3 krill digests were transferred to acid clean 10 mL glass tubes and oxidized with 1:1 (v/v) 0.2 N bromine monochloride (Hammerschmidt and Fitzgerald 2005) and 5% hydrogen peroxide (H_2O_2). Duplicate aliquots of these digests were analyzed for THg by dual-gold amalgamation CVAFS using a Brooks Rand MERX-T analyzer. All MeHg and THg concentrations for krill are expressed in units of ng g^{-1} (dry wt), and precision as the average relative standard deviation (RSD) of duplicate aliquots of sample digests was 0.14 ng g^{-1} and 0.11 ng g^{-1}

for MeHg and THg, respectfully. Accuracy for both MeHg and THg was assured by analysis of TORT-2 (Lobster Herpatopancreas) standard reference material whose certified values (average ± standard deviation) are 0.152 ± 0.013 μg g^{-1} and 0.27 ± 0.06 μg g^{-1} for MeHg and THg, respectively. The masses of TORT-2 digested (50-200 mg) were similar to those of the krill. Our measured MeHg and THg values for TORT-2 were 0.147 ± 0.034 μg g^{-1} (n=22) and 0.27 ± 0.04 μg g^{-1} (n=24), respectively. Method detection limits based on 3x the standard deviation of blanks were 0.002 ng g^{-1} for MeHg and 0.022 ng g^{-1} for THg.

Collection and mercury analysis of Pygoscelis penguin feathers

Live body feathers from three species of *Pygoscelis* penguins (*P. adeliae*, *P. papua*, and *P. antartica*) were collected beginning in 2010 and during the austral summer of 2011 on three islands (Humble, Biscoe, and Dream) near Anvers Island, WAP (Figure S1). Feathers of Adélie penguins (*P. adeliae*) were collected from seasonal breeding populations living on Humble (n = 15) Island, while those of gentoo (*P. papua*) and chinstrap (*P. antarctica*) penguins were from Biscoe (n = 16) and Dream Islands (n = 15), respectively. While most seabird feathers grow asynchronously, the entire penguin plumage is renewed annually during a 2 to 4 week period after breeding (Stonehouse 1967). As a result, Hg concentrations are fairly uniform among feathers from an individual penguin (Brasso et al. 2013). Mercury in seabird feathers is known to be representative of the internal body burden (Braune and Gaskin 1987, Agusa et al. 2005), over a broad temporal scale (Becker et al. 1993). These feathers, collected at the end of austral summer, are representative of the internal body burden between regrowth in previous austral summer and time of sampling. Body feathers from live penguins were

collected incidentally when handling birds associated with research on foraging ecology using appropriate animal handling procedures under Antarctic Conservation Act permit # 2013-001 to W.R. Fraser. Feathers were stored in zip-top bags at -20°C. Prior to export from Antarctica, feathers were heated at 60° C for 45 min. in accordance with USDA Veterinary Permit 121174 to J.R. Reinfelder.

Penguin feathers were cleaned to remove surface lipids and contaminants by rinsing three times in a 2:1 (v/v) mixture of HPLC grade chloroform/methanol (Carravieri et al. 2013). After cleaning, feathers were dried for 48 h at 50°C. Large feathers were cut into smaller pieces for digestions containing multiple feathers from an individual animal. Composite samples of 2 to 5 feathers (≥10 mg) were digested in 5 mL of a 1:4 (v/v) (Fromant et al. 2016) mixture of Trace Metal grade HCl and HNO_3 and sonicated for 24 h or until all feather tissue was digested.

Aliquots of penguin feather digests were analyzed for THg using dual-Au amalgamation CVAFS as described above. As almost all mercury in seabird feathers (>95%) is present as MeHg (Thompson and Furness 1989, Bond and Diamond 2009), THg was used to estimate MeHg concentrations in penguin feathers. Every set of samples was analyzed in triplicate with two acid blanks, and two method blanks. Precision as standard deviation of all feather THg triplicate runs was <0.02 µg g^{-1} for *P. adeliae* and *P. papua* and <0.16 µg g^{-1} for *P. antarctica*. In addition, three samples (25 to 50 mg) of IAEA-86 (unspiked human hair) certified reference material (0.573 ± 0.039 µg g^{-1} dry wt.) were digested with each set of penguin feathers analyzed. Human hair is a suitable matrix for comparison with bird feathers as both are composed of keratin protein.

Measured THg values were 0.558 ± 0.029 μg g^{-1} (n = 8). The method detection limit (0.0001 μg g^{-1}) was determined using method blanks.

^{13}C and ^{15}N analysis

Freeze-dried, whole krill were homogenized and sub-sampled (100-250 μg) and penguin feather fragments analyzed for carbon (C) and nitrogen (N) stable isotopes and total organic C and N. Suspended particulate organic matter (POM) from surface waters and field blanks during the 2013-2015 LTER summer field seasons were collected on pre-combusted glass-fiber filters (GF/F) lyophilized and analyzed only for δ^{13}C and δ^{15}N. All samples were placed into tin boats, combusted, and analyzed using a Eurovector 3024 Elemental Analyzer coupled to a GVI Isoprime 100 mass spectrometer operated in continuous flow.

Stable isotope ratios presented in δ notation with per-mil units (‰) were calculated as

$$\delta X = \left[\left(R_{sample}/R_{standard}\right) - 1\right] * 1000 \quad \text{Eq. 4-1}$$

where X is ^{13}C or ^{15}N and R is the ratio of either $^{15}N/^{14}N$ or $^{13}C/^{12}C$ in the sample or standard. Isotope ratios were measured relative to the international isotope standards NBS 22 (oil $\delta^{13}C_{VPDB}$ = -30.03‰) (Coplen et al. 2006) and IAEA-N1 (ammonium sulfate, $\delta^{15}N_{ATM}$ = 0.43‰) (Qi et al. 2003) using a single-point normalization run every analysis to calibrate reference gas. Average precisions (1σ), achieved from raw isotope values of standards across all runs was 0.1‰ δ^{13}C for NBS 22 and 0.1‰ δ^{15}N for IAEA-N1. Additional Elemental Microanalysis reference materials (sorghum flour; IAEA-N3,

potassium nitrate), coastal ocean sediment, and an internal laboratory standard (acetanilide) were used to verify the relative differences of C and N isotope ratios between samples and standards.

Total carbon and nitrogen content were calculated using replicate measurements of acetanilide. Carbon and nitrogen content were used to calculate carbon:nitrogen (C:N) ratios of individual penguin feathers and individual juvenile and adult krill. C:N ratios can be used to predict lipid content of marine animals (McConnaughey and McRoy 1979).

Calculations for C isotopes, Trophic Position, and Mercury Bioaccumlation

Variation in C:N ratios (lipid content) exists in marine zooplankton (Post et al. 2007) and among individual Antarctic krill (Table 3.1). Thus C:N was used to normalize measured $\delta^{13}C$ values for variable lipid concentration according to the equation of Post et al. 2007 for aquatic organisms

$$\delta^{13}C_{normalized} = \delta^{13}C_{untreated} - 3.32 + 0.99 + C{:}N \qquad \text{Eq. 4-2}$$

in which $\delta^{13}C_{untreated}$ is the measured $\delta^{13}C$ value, C:N is the element ratio (mol:mol), and $\delta^{13}C_{normalized}$ is the lipid-adjusted $\delta^{13}C$ value of an individual krill within sub-populations containing C:N values above 3.5 (variable lipid content). Penguin feathers $\delta^{13}C$ values were not adjusted as feathers were cleaned to remove surface lipids (described above) and had low variability in C:N ratios within (σ = 0.02, 0.04, 0.05) and across species (σ= 0.04)

Given uncertainty regarding the trophic enrichment factor of ^{15}N in marine zooplankton (McCutchan et al. 2003, Hannides et al. 2009), the trophic positions of krill and penguins ($\Delta^{15}N$) with respect to suspended particulate organic matter (POM) (Table 3.1) were calculated as $\delta^{15}N_{consumer}$ - $\delta^{15}N_{POM}$. The trophic magnification factor of MeHg was estimated from the slope of the $\log_{10}$MeHg-trophic position relationship for POM, krill, and penguins according to Ruus et al. 2015 (Ruus et al. 2015) as follows:

$$\text{Log}_{10} concentration = a + b\ \Delta^{15}N \quad \text{Eq. 4-3}$$

$$Trophic\ magnification\ factor = 10^{b} \quad \text{Eq. 4-4}$$

To assess transfer efficiency of MeHg at the base of the food web west of the Antarctic Peninsula, biomagnification factors (BMFs) were calculated using the equation below with MeHg concentrations in coastal (600.040) WAP POM and subpopulations of adult and juvenile *E. superba* along the 600 line near Anvers Island.

$$BMF = \frac{MeHg_{krill}\ (\frac{ngMeHg}{gtissue})}{MeHg_{p}\ (\frac{ngMeHg}{gtotbio})} \quad \text{Eq. 4-5}$$

Statistical Analysis

All statistical analyses were performed using R 3.3.0. One-way, ANOVA analyses were performed to determine significant differences between calculated means of juvenile and adult krill within all four sampling years. Planned comparisons(Ruxton and Beauchamp 2008) of one-way ANOVA analyses for juvenile and adult krill within each sampling year, were also used to determine sources of variation in mercury concentrations, $\delta^{13}C$ and $\delta^{15}N$ values in krill. The Games-Howell post hoc test was used to identify which sub-populations of krill (juvenile, adult, coastal, shelf, slope) or species

of penguin contributed to variation in mercury concentrations or $\delta^{13}C$ and $\delta^{15}N$ values within each sampling year. Games-Howell pairwise comparisons were chosen as this method does not assume equal variances or sample sizes, which is characteristic of our data set near Anvers Island. A two-tailed Student's t-test was used determine differences between the two juvenile and adult krill populations within each sampling year sampled at the sea ice edge. All tests were conducted using a significance level of $\alpha < 0.05$, and means are presented as ± 1SD.

D. Results

Carbon and nitrogen isotope ratios of particulate organic matter (POM) at northern latitudes

Surface POM $\delta^{13}C$ and $\delta^{15}N$ values during 2013-2015 ranged from -32.3 to -26.6‰ and -2.3 to 3.4‰ respectively. Spatial patterns in $\delta^{13}C$ values were observed within 2013, 2014, and 2015 POM samples with some differences in depth. Coastal POM $\delta^{13}C$ values from 2013 and 2014 tended to be higher with lower $\delta^{13}C$ values in mid-shelf and slope waters (Table 4.1). In 2015, ^{13}C was enriched further offshore in slope waters relative to the coast and continental shelf. No consistent patterns in proximity to shore or depth existed in $\delta^{15}N$ values in the three austral summers (Table 4.1). Overall, $\delta^{13}C$ values were consistent within a 100m depth with slightly higher $\delta^{13}C$ values below epipelagic waters at various sampling sites.

Carbon and nitrogen isotope ratios of particulate organic matter (POM) at latitudes and longitudes along the WAP

Surface POM $\delta^{13}C$ and $\delta^{15}N$ values along the WAP during 2013-2015 ranged from -32.0‰ to -22.3‰ and -3.7 to 4.2‰ respectively. Similar patterns with depth and $\delta^{13}C$ POM values from northern latitudes were seen along the WAP in 2013 and 2014, wtih differences in $\delta^{13}C$ values between depths sampled at the same location in surface, mixed layer POM more depleted in ^{13}C than at depths typical of winter water, except at the sea ice edge station -131.023 where ^{13}C was more depleted at 75m than 10m (Table 4.2). A wide range of $\delta^{13}C$ isotope ratios in 2013 (-31.3 to -21.7‰) spanned the entire range of 2014 (-29.6 to -25.0‰) and 2015 (-31.3 to -25.5‰) POM samples (Table 4.2). Overlap in C and N stable isotope ratios did occur between 2014 and 2015, however, 2014 POM showed higher variation in $\delta^{15}N$ (σ=4.8) than in $\delta^{13}C$ (σ=1.8) values while 2015 was more slightly more varied in $\delta^{13}C$ (σ = 3.7) than in $\delta^{15}N$ (σ = 3.2) values (Figure 4.3). A $\delta^{13}C$ and latitude relationship ($p<0.05$, $R^2=0.52$) existed in POM samples collected along the Peninsula in 2013 (Figure 4.4) with most POM most enriched in ^{13}C at northern latitudes and depleted near the sea ice edge with no $\delta^{13}C$ spatial trend was observed in 2014 and 2015. Additionally, a cross-shelf $\delta^{15}N$ relationship ($p<0.05$, $R^2=0.34$) found slightly lower $\delta^{15}N$ values offshore in slope and shelf waters with coastal waters enriched in ^{15}N, which was consistent across all sample sites at varying latitudes along the WAP (Figure 4.5)

Table 4.1 C and N isotope ratios in particulate organic matter (POM) collected from surface waters of the coastal, shelf, and slope west of the Antarctic Peninsula near Anvers Island at 65°S to 64°S during the austral summers of 2013, 2014, and 2015.

Year	WAP Region	Depth (m)	Lat Long	δ^{13}C (‰)	δ^{15}N (‰)
2013	Coastal	10	-64.9-64.4	-28.8	0.9
	Coastal	90	-64.9-64.4	-26.6	NA
	Shelf	10	-64.6-65.3	-30.6	NA
	Slope	0	-64.0-66.9	-29.0	NA
	Slope	100	-64.0-66.9	-28.3	NA
2014	Coastal	10	-64.9-64.4	NA	3.2
	Coastal	50	-64.9-64.4	-27.8	1.8
	Shelf	10	-64.6-65.3	-28.8	0.6
	Shelf	75	-64.6-65.3	-27.4	3.4
	Slope	20	-64.0-66.9	-28.1	3.0
	Slope	100	-64.0-66.9	-28.1	-2.3
2015	Coastal	5	-64.9-64.4	-31.6	1.3
	Coastal	100	-64.9-64.4	-31.5	0.9
	Shelf	30	-64.6-65.3	-32.3	2.7
	Shelf	100	-64.6-65.3	-32.3	2.8
	Slope	10	-64.0-66.9	-27.9	-0.0
	Slope	100	-64.0-66.9	-28.2	-1.7

Table 4.2 C and N isotope ratios in particulate organic matter (POM) collected from surface waters of the coastal, shelf, and slope west of the Antarctic Peninsula at 66°S to 69°S during the austral summers of 2013, 2014, and 2015,

Year	LTER Grid	WAP Region	Depth (m)	Lat Long	δ^{13}C (‰)	δ^{15}N (‰)
2013	400.040	Coastal	15	-66.3-67.3	-32.0	2.0
	400.040	Coastal	80	-66.3-67.3	-27.4	NA
	400.100	Shelf	10	-65.9-68.3	-29.0	-0.1
	400.200	Slope	10	-65.2-69.8	-31.0	NA
	200.040	Coastal	15	-67.5-70.6	-29.9	1.4
	200.040	Coastal	75	-67.5-70.6	-27.8	NA
	200.100	Shelf	10	-67.1-71.5	-31.2	1.7
	200.100	Shelf	70	-67.1-71.5	-28.0	NA
	200.200	Slope	10	-66.4-73.0	-29.6	NA
	200.200	Slope	75	-66.4-73.0	-27.5	NA
	0.060	Coastal	10	-68.6-74.5	-26.2	NA
	0.060	Coastal	75	-68.6-74.5	-23.5	NA
	0.000	Coastal	15	-69.0-73.6	-24.3	1.7
	0.000	Coastal	55	-69.0-73.6	-22.4	NA
	-131.023	Coastal	10	-69.9-75.8	-22.3	5.3
	-131.023	Coastal	75	-69.9-75.8	-23.1	NA
2014	400.040	Coastal	10	-66.3-67.3	NA	3.0
	400.040	Coastal	75	-66.3-67.3	-25.5	1.8
	400.100	Shelf	15	-65.9-68.3	-25.9	1.1
	400.100	Shelf	80	-65.9-68.3	-25.6	3.2
	400.200	Slope	10	-65.2-69.8	-27.7	-3.7
	400.200	Slope	90	-65.2-69.8	-29.6	2.7
	300.040	Coastal	10	-66.9-68.9	NA	3.4
	300.040	Coastal	100	-66.9-68.9	-25.0	2.1
	200.100	Shelf	25	-67.1-71.5	-26.7	1.7
	200.100	Shelf	100	-67.1-71.5	-25.3	5.8
	200.180	Shelf	10	-66.6-72.7	-28.1	-1.3
	200.180	Shelf	75	-66.6-72.7	-27.4	2.1
	100.040	Coastal	10	-68.1-72.3	NA	4.0
	100.040	Coastal	75	-68.1-72.3	-26.0	4.5

	100.100	Shelf	10	-67.7-73.3	-25.6	3.3
	100.100	Shelf	100	-67.7-73.3	-26.2	4.2
	100.160	Shelf	10	-67.3-74.2	-28.3	0.2
	100.160	Shelf	100	-67.3-74.2	-27.9	3.8
2015	400.040	Coastal	25	-66.3-67.3	-31.3	1.8
	400.040	Coastal	50	-66.3-67.3	-31.3	1.2
	400.100	Shelf	5	-65.9-68.3	-29.6	1.9
	400.100	Shelf	100	-65.9-68.3	-30.2	2.1
	400.200	Slope	15	-65.2-69.8	-28.9	-2.0
	400.200	Slope	80	-65.2-69.8	-30.4	-1.9
	200.100	Shelf	10	-67.1-71.5	-27.9	1.0
	200.100	Shelf	75	-67.1-71.5	-28.0	1.2
	200.160	Shelf	15	-66.6-72.7	-26.0	1.2
	200.160	Shelf	40	-66.6-72.7	-25.5	2.2
	-100.060	Shelf	5	-69.1-76.4	-29.4	-1.1
	-100.060	Shelf	75	-69.1-76.4	-29.1	-1.4
	-100.140	Shelf	15	-68.5-77.6	-29.1	-2.6
	-100.140	Shelf	75	-68.5-77.6	-28.9	-2.0

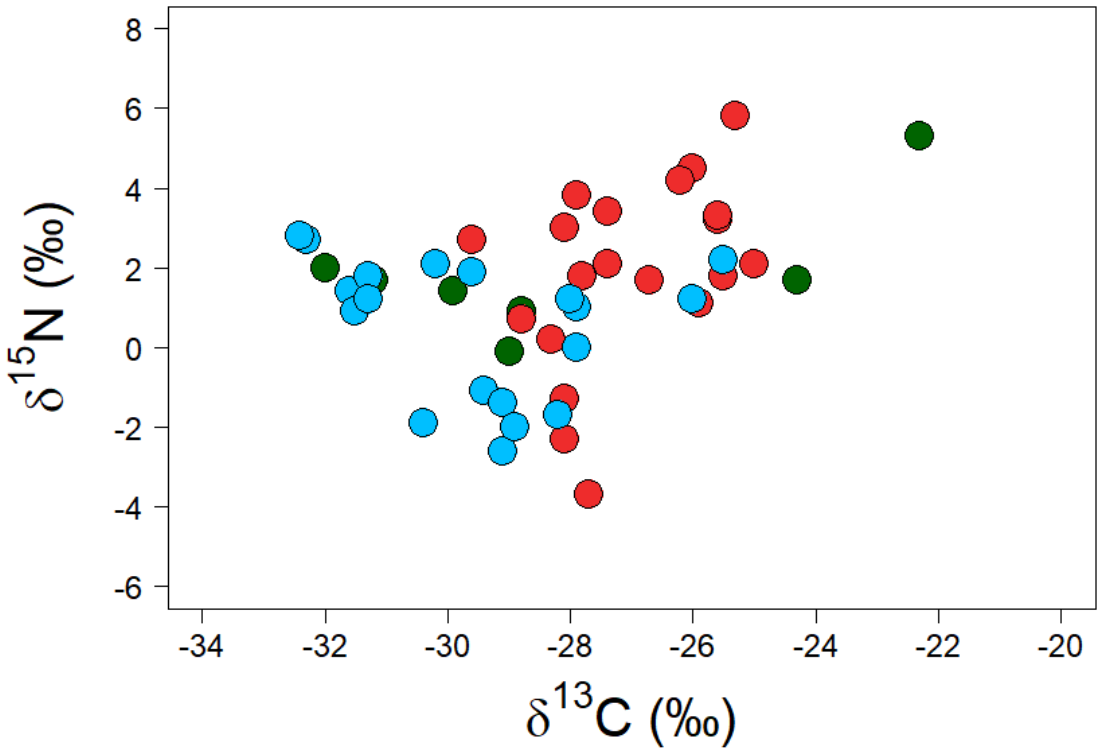

Figure 4.3 C and N stable isotope ratios (δ^{13}C and δ^{15}N; filled circles) in particulate organic matter (POM) sampled from 0-100m depths collected along the WAP (WAP) at 64°S to 70°S in 2013 (dark green), 2014 (red) and 2015 (light blue).

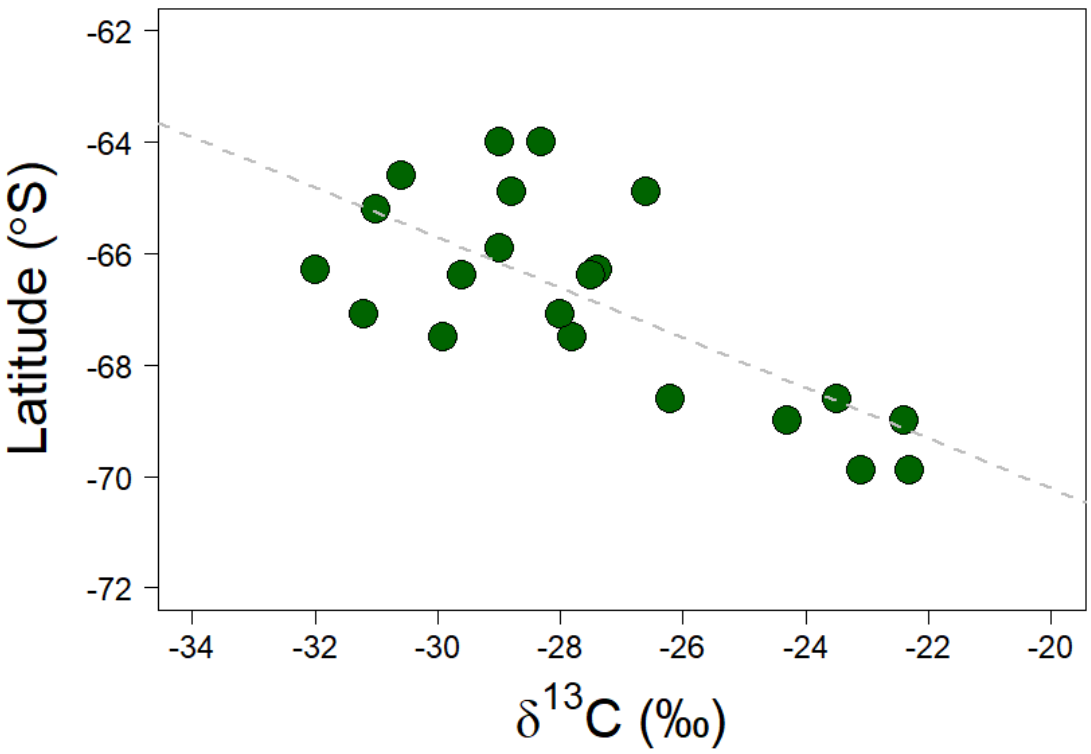

Figure 4.4 Relationship in 2013 particulate organic matter (POM) between latitude at ~64°S closest to Anvers Island (top on y-axis); southward towards ~70°S near sea ice edge (bottom on y-axis) with carbon stable isotope ratios ($\delta^{13}C$) of POM sampled in top 100m waters from 2013 (dark green circles). The dashed line for the POM is [Latitude] = -79.2140 + 0.4501$\delta^{13}C$ ($p<0.05$, $R^2=0.52$).

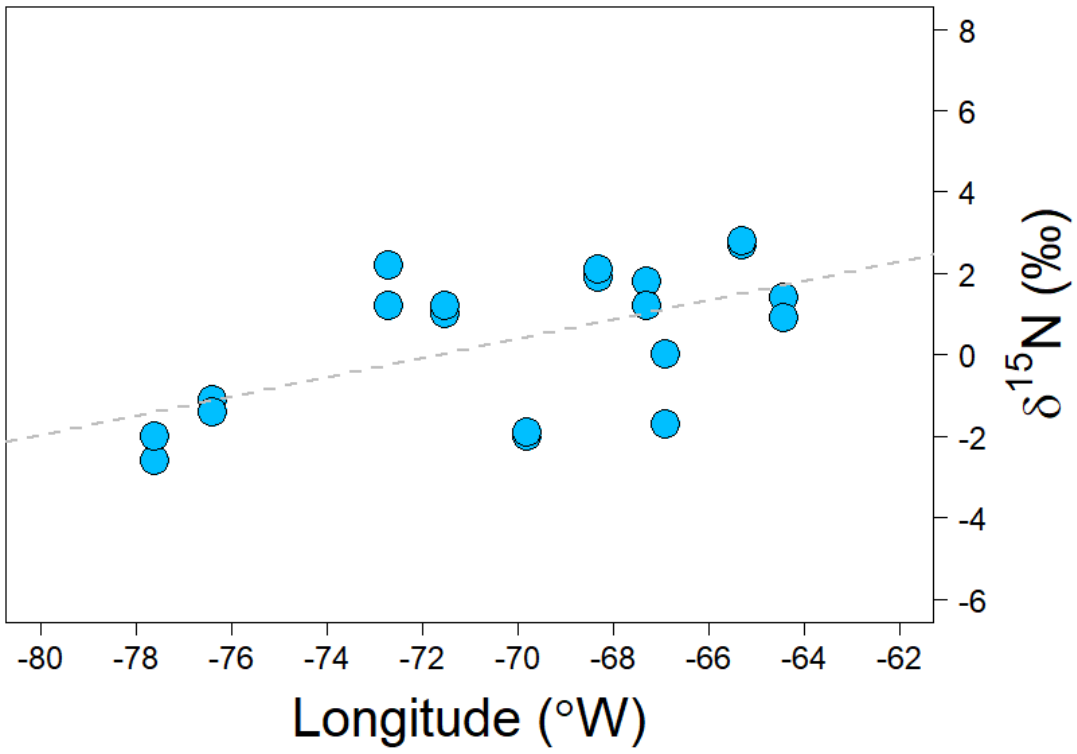

Figure 4.5 Relationship between 2015 nitrogen stable isotope ratios (δ^{15}N) of POM sampled in top 100m waters from 2015 (light blue circles) with varying distances from shore at sites along the WAP (closest to coast is to the right on x-axis; offshore/slope waters to the left). The linear regression of δ^{15}N and longitude is [δ^{15}N] = 17.0117 + 0.2375(°W) ($p<0.05$, $R^2=0.34$).

Carbon and nitrogen content of Antarctic krill (*Euphausia superba*) and in feathers of *Pygoscelis* penguins near Anvers Island, Antarctica

Dissimilarity between the carbon (C) and nitrogen (N) content of juvenile and adult krill was most apparent between sampling years, with small differences observed in carbon and nitrogen content of 2013 mid-shelf juvenile (30±10% carbon, 6±2% nitrogen) and adult (42±3% carbon, 10±1% nitrogen) krill subpopulations. Higher percentages of carbon in juveniles and adults tissue from 2014 led to higher C:N ratios (7.6 to 8.7) than 2011 (5.1±0.6), 2013 (4.3 to 4.9), and 2015 (3.4 to 4.1) krill (Table 4.3). Ultimately, variation in C:N ratios was used to assess lipid content of krill and used to adjust raw krill δ^{13}C values (discussed above). Identical C:N ratios were observed in Adélie (5.9±0.1), gentoo (5.9±0.2), and chinstrap (5.9±0.1) *Pygoscelis* penguin species (Table 4.3).

Table 4.3 C and N content (%) and C:N ratios in Antarctic krill (*Euphausia superba*) collected from coastal, shelf, and slope waters west of the Antarctic Peninsula at 65°S to 64°S during the austral summers of 2011, 2013, 2014, and 2015, and in body feathers from three species of *Pygoscelis* penguins collected during the austral summer of 2011 near Anvers Island, Antarctica where NA, not analyzed.

Year	Organism	WAP Region	Lat	Long	C:N	C Content (%)	N Content (%)
2011	Juvenile *E.superba*	Coastal	-64.9	-64.4	NA	NA	NA
	Adult *E.superba*	Coastal	-64.6	-64.3	5.1±0.6 (3)	44±4 (3)	9±1 (3)
2013	Juvenile *E.superba*	Coastal	-64.9	-64.3	4.9±0.6 (14)	42±3 (15)	8±1 (15)
		Shelf	-64.6	-65.3	4.7±0.2 (6)	30±10 (7)	6±2 (7)
	Adult *E.superba*	Shelf	-64.6	-65.3	4.3±0.5 (14)	42±3 (14)	10±1 (15)
2014	Juvenile *E.superba*	Coastal	-64.9	-64.3	7.8±1.1 (13)	51±2 (13)	7±1 (13)
	Adult *E.superba*	Coastal	-64.9	-64.3	7.6±1.1 (12)	49±3 (12)	7±1 (12)
		Slope	-64.0	-66.9	8.7±0.9 (11)	51±3 (10)	6±1 (10)
2015	Juvenile *E.superba*	Coastal	-64.9	-64.3	4.1±0.2 (5)	36±4 (6)	9±1 (6)
	Adult *E.superba*	Coastal	-64.9	-64.3	3.4±1.0 (12)	35±3 (12)	11±4 (12)
2011	*P. adeliae*	Coastal	-64.8	-64.1	5.9±0.1 (10)	40±1 (10)	7±0 (10)
	P. papua	Coastal	-64.8	-63.8	5.9±0.2 (8)	39±2 (8)	6±0 (8)
	P. antarctica	Coastal	-64.7	-64.2	5.9±0.1 (5)	41±3 (5)	7±0 (5)

Carbon isotope ratios in *E. superba* at northern latitudes

Carbon isotope ratios in Antarctic krill from coastal, shelf, and slope waters west of the Antarctic Peninsula varied spatially, between years, and between co-located populations of juveniles and adults (Table 4.4). We measured higher $\delta^{13}C$ values in juvenile and adult krill from nearshore sites than from mid-shelf or slope waters in 2013 and 2014 (Figure 4.6). This spatial difference was most pronounced in 2014 in which the average $\delta^{13}C$ value of adult krill collected from slope waters was significantly ($P<0.05$) lower than that in either juvenile or adult krill collected closer to shore (Tables 4.4 and 4.5). Note that both coastal and offshore krill collected in 2014, had higher $\delta^{13}C$ values than any other population of krill examined in this study (Figure 4.6). Coastal juvenile krill had significantly ($P<0.05$) higher mean $\delta^{13}C$ values than co-located adult krill in 2014 and 2015 (Tables 4.4 and 4.5; Figure 4.7). However, there was no significant difference between juvenile and adult krill collected from mid-shelf waters in 2013 (Table 4.5). Indeed, the lowest average $\delta^{13}C$ value (-28.2‰) was measured in juvenile krill collected from mid-shelf waters in 2013 (Table 4.4) with greater average dry weight (66 ±4 mg) than juvenile krill collected near the coast in 2013 (43 ±11 mg).

Nitrogen isotope ratios in *E. superba* at northern latitudes

Variations in nitrogen isotope ratios across krill populations from the WAP marine ecosystem did not show clear spatial, ontogenetic, or inter-annual patterns. For example, while $\delta^{15}N$ values were lower in coastal than mid-shelf juvenile krill in 2013, this difference was not significant ($p=0.287$), and 2014 coastal adult krill had higher $\delta^{15}N$ values than adults collected further offshore in slope waters (Tables 4.4 and 4.5). Adult krill had higher $\delta^{15}N$ values than juveniles in 2013 and 2014 (Table 4.4), but the

Table 4.4 Concentrations of total Hg (THg) and methylmercury (MeHg) and C and N isotope ratios in Antarctic krill (*Euphausia superba*) collected from coastal, shelf, and slope waters west of the Antarctic Peninsula at 65°S to 64°S during the austral summers of 2011, 2013, 2014, and 2015, and in body feathers from three species of *Pygoscelis* penguins collected during the austral summer of 2011 near Anvers Island, Antarctica[1]. Note that THg concentrations in penguin feathers are reported as μg g^{-1}. All values are means ± 1SD (n) where NA, not analyzed.

Year	Organism	WAP Region	Lat (°S)	Long (°W)	[THg] (ng g^{-1}, dry wt)	[MeHg] (ng g^{-1}, dry wt)	MeHg/THg (%)	$\delta^{13}C$ (‰)	$\delta^{15}N$ (‰)
2011	Juvenile *E.superba*	Coastal	64.9	64.4	NA	1.7±0.1	NA	NA	NA
	Adult *E.superba*	Coastal	64.6	64.3	4.0±2.7 (3)	0.3±0.2 (3)	9±9 (3)	-26.6±0.4 (3)	4.3±0.4 (3)
2013	Juvenile *E.superba*	Coastal	64.9	64.3	9.2±3.1 (14)	2.3±0.8 (13)	26±9 (13)	-26.7±1.1 (15)	2.2±0.6 (15)
		Shelf	64.6	65.3	7.8±3.2 (9)	0.8±0.4 (7)	10±5 (7)	-28.2±1.8 (6)	2.7±0.6 (7)
	Adult *E.superba*	Shelf	64.6	65.3	6.6±1.9 (13)	0.3±0.2 (11)	5±3 (11)	-27.9±1.7 (14)	3.0±0.5 (15)
2014	Juvenile *E.superba*	Coastal	64.9	64.3	17.1±9.4 (8)	2.9±0.9 (13)	26±20 (8)	-20.1±0.9 (13)	3.4±0.4 (13)
	Adult *E.superba*	Coastal	64.9	64.3	5.5±1.7 (6)	1.6±0.9 (12)	17±13 (6)	-21.8±1.2 (12)	3.8±0.4 (11)
		Slope	64.0	66.9	12.6±3.1 (7)	1.0±0.2 (8)	8±2 (8)	-24.2±1.0 (11)	1.2±0.4 (11)
2015	Juvenile *E.superba*	Coastal	64.9	64.3	19.4±13.5 (8)	1.4±0.9 (8)	11±7 (7)	-25.6±1.4 (5)	3.6±0.6 (6)
	Adult *E.superba*	Coastal	64.9	64.3	8.0±1.8 (9)	0.7±0.5 (8)	10±7 (7)	-27.9±0.4 (10)	3.6±0.6 (12)
2011	*P. adeliae*	Coastal	64.8	64.1	0.09±0.05 (10)	NA	>95%	-25.9±1.0 (9)	8.3±0.2 (9)
	P. papua	Coastal	64.8	63.8	0.16±0.08 (9)	NA	>95%	-25.4±0.8 (8)	8.7±0.3 (8)
	P. antarctica	Coastal	64.7	64.2	0.80±0.20 (10)	NA	>95%	-25.6±0.6 (6)	8.2±0.2 (6)

Table 4.5 Pairwise comparisons (Games-Howell post hoc test) of mercury concentrations and stable isotope ratios within each sampling year between ontogeny (Ad=adult, Ju=juvenile) and region (coast, shelf, slope) of collection for *Euphausia superba* (krill) and *Pygoscelis* penguin species (ADPE= *Adélie*, GEPE=gentoo, and CHPE=chinstrap). Adjusted p-values were chosen at α (0.05). Asterisks (*) indicate significant differences ($p<0.05$).

Comparisons	MeHg p-value	THg p-value	δ^{13}C p-value	δ^{15}N p-value
2011 Krill				
Ad.Coast-Juv.Coast	<0.001*	NA	NA	NA
2013 Krill				
Juv.Coast-Ad.Shelf	<0.001*	0.104	0.250	0.020*
Juv.Shelf-Ad.Shelf	0.040*	1.000	0.905	0.690
Juv.Shelf-Juv.Coast	<0.001*	1.000	0.368	0.287
2014 Krill				
Ad.Slope-Ad.Coast	0.120	0.002*	<0.001*	<0.001*
Juv.Coast-Ad.Coast	0.008*	0.049	0.001*	0.007*
Juv.Coast-Ad.Slope	<0.001*	0.441	<0.001*	<0.001*
2015 Krill				
Juv.Coast-Ad.Coast	0.102	0.050	0.019*	0.898
2011 Penguins				
GEPE-ADPE	--	0.096	1.000	0.016*
GEPE-CHPE	--	<0.001*	1.000	0.027*
CHPE-ADPE	--	<0.001*	1.000	0.988

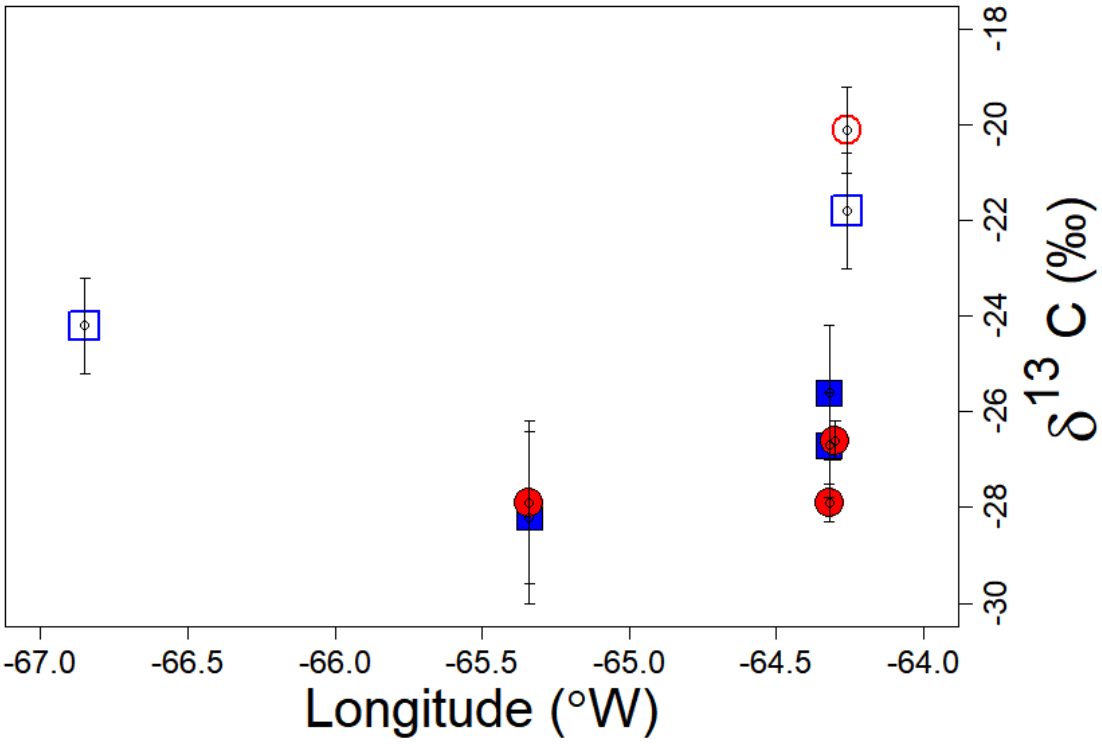

Figure 4.6 Variation in carbon stable isotope ratios (δ^{13}C) of adult (red circles) and juvenile (blue squares) Antarctic krill (*Euphausia superba*), with distance from the WAP shore at ~65°S (closest to coast is to the right on x-axis; offshore/slope waters to the left). Values are mean ± 1SD (see Table 1). Note δ^{13}C values of krill were normalized to C:N ratios to account for lipid concentration and open symbols are 2014 krill.

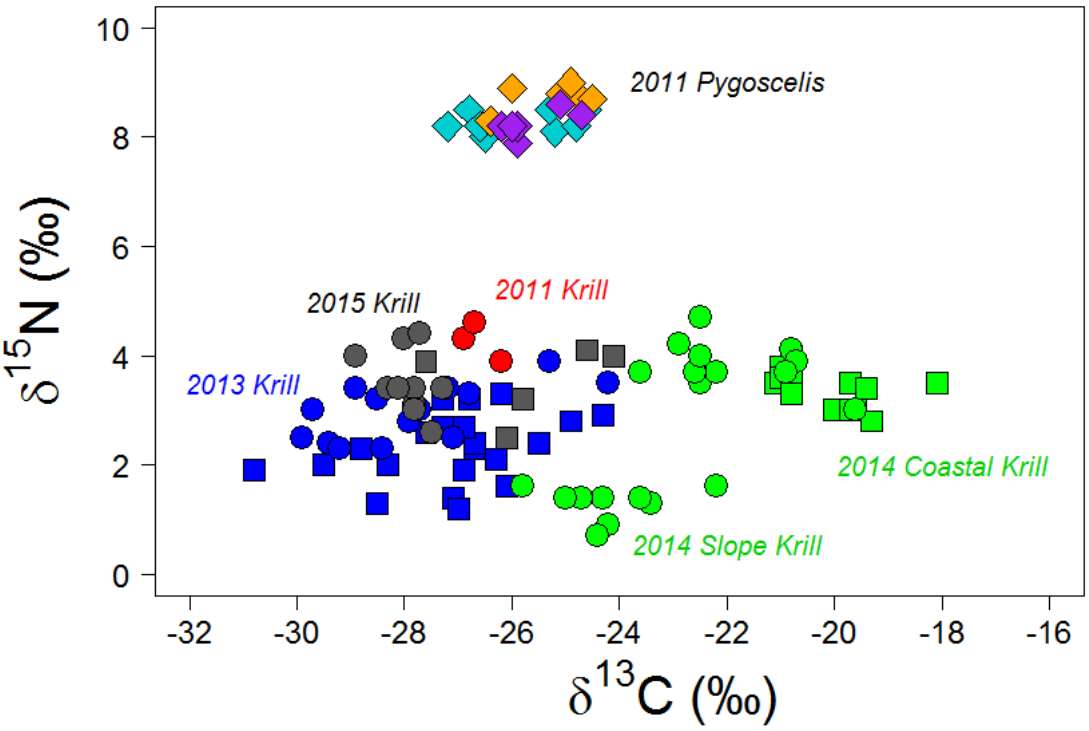

Figure 4.7 C and N stable isotope ratios (δ^{13}C and δ^{15}N; filled symbols) in juvenile (squares) and adult (circles) krill (*Euphausia superba*) collected from coastal, shelf, and slope waters west of the Antarctic Peninsula at 65°S to 64°S in four austral summers, and in *Pygoscelis* penguin feathers (diamonds) from *P. adeliae* (light blue), *P. papua* (orange), and *P. antarctica* (purple) collected near Anvers Island in the austral summer of 2011. Note that δ^{13}C values of krill were normalized for lipid content using C:N ratios (see text).

difference was only significant in 2014 (Table 4.5). No difference in mean δ^{15}N values between juvenile and adult krill was observed in 2015. Among krill collected in coastal waters, δ^{15}N values were not anomalous in 2014 compared to other years, however, krill collected in slope waters in 2014 had the lowest δ^{15}N values of all samples (Table 4.4; Figure 4.7).

Variations in carbon and nitrogen isotope ratios in *Pygoscelis* penguins near Anvers Island, Antarctica

Carbon isotope ratios in body feathers collected in 2010-2011 from the three species of *Pygoscelis* penguins that live along the southern end of Anvers Island varied over a relatively narrow range (24.5 – 27.2‰; Figure 4.7) and were not significantly different between species (p= 1.00 for all comparisons; Tables 4.4 and 4.5). Body feathers of gentoo penguins had slightly, but significantly ($P < 0.05$) higher δ^{15}N values (8.7 ± 0.3‰, range 8.3 – 9.0) than Adélie (8.3 ± 0.2‰, range 8.0 – 8.5) and chinstrap penguins (8.3 ± 0.2‰, range 7.9-8.6) (Tables 4.4 and 4.5).

MeHg and THg concentrations in *E. superba* subpopulations in proximity to Anvers Island

Mean concentrations of total Hg in adult Antarctic krill from the WAP continental shelf varied from 4 to 12.6 ng g^{-1}. THg in juvenile krill from the WAP (7.8 to 19.4 ng g^{-1}) were generally higher than those in adult krill. Mean concentrations of MeHg in *E. superba* varied from 0.7 to 2.9 ng g^{-1} in juvenile krill and from 0.3 to 1.6 ng g^{-1} in adult krill (Table 4.4). Across all four sampling years, juvenile Antarctic krill had significantly higher mean concentrations of THg ($P < 0.005$, $F = 8.77$) and MeHg ($P < 0.001$, $F = 27.06$) than adult krill (Figures 4.8A and 4.8B). Mean concentrations of MeHg were also

higher in juvenile than adult krill within all sampling years, but not significantly higher in 2015 (Figure 4.8C; Table 4.5). Overall, mean concentrations of MeHg juvenile and adult krill in 2014 were relatively higher than all other juveniles and adults in 2011, 2013, and 2015 (Table 4.4). The average fraction of THg in krill present as methylmercury (%MeHg) varied from 10 to 26% and 5 to 17% in juvenile and adult Antarctic krill, respectively (Table 4.4). The concentration of THg in krill from the WAP was strongly correlated ($p<0.001$, $R^2=0.97$) to inorganic Hg, but weakly correlated ($p < 0.005$, $R^2 = 0.12$) to MeHg in krill (Figure 4.9A and 4.9B). Although the relationships between %MeHg and MeHg concentration in individual krill were significant in both juveniles and adults ($p<0.001$), there was considerably more scatter for juveniles, especially in juvenile krill with MeHg concentrations greater than 2 ng g^{-1} (Figures 4.10A and 4.10B). MeHg and THg distribution varied within muscle, soft tissue, and exoskeleton in juvenile and adult krill. Percentages of MeHg and THg distributed in adult soft tissue were higher, while muscle distributions of MeHg (60.7±4.7 juveniles; 54±1.8 adults) and THg (28±6.2 juveniles 18±3.0 adults) were higher in juvenile krill with lowest Hg accumulated, 14 to 19%, in krill exoskeletons for both subpopulations (Table 4.6). The difference in body burdens of THg and MeHg associated with the exoskeleton between juveniles and adults was only 1 to 5% (Table 4.6). Between juveniles and adults, juvenile krill had higher bioaccumulation (BMFs) factors (2.5 to 8.7; 1.1 to 4.8 resp.) within all four years (Table 4.7). These results indicate the importance of developmental differences in mercury biomagnification amongst subpopulations of Antarctic adult and juvenile krill.

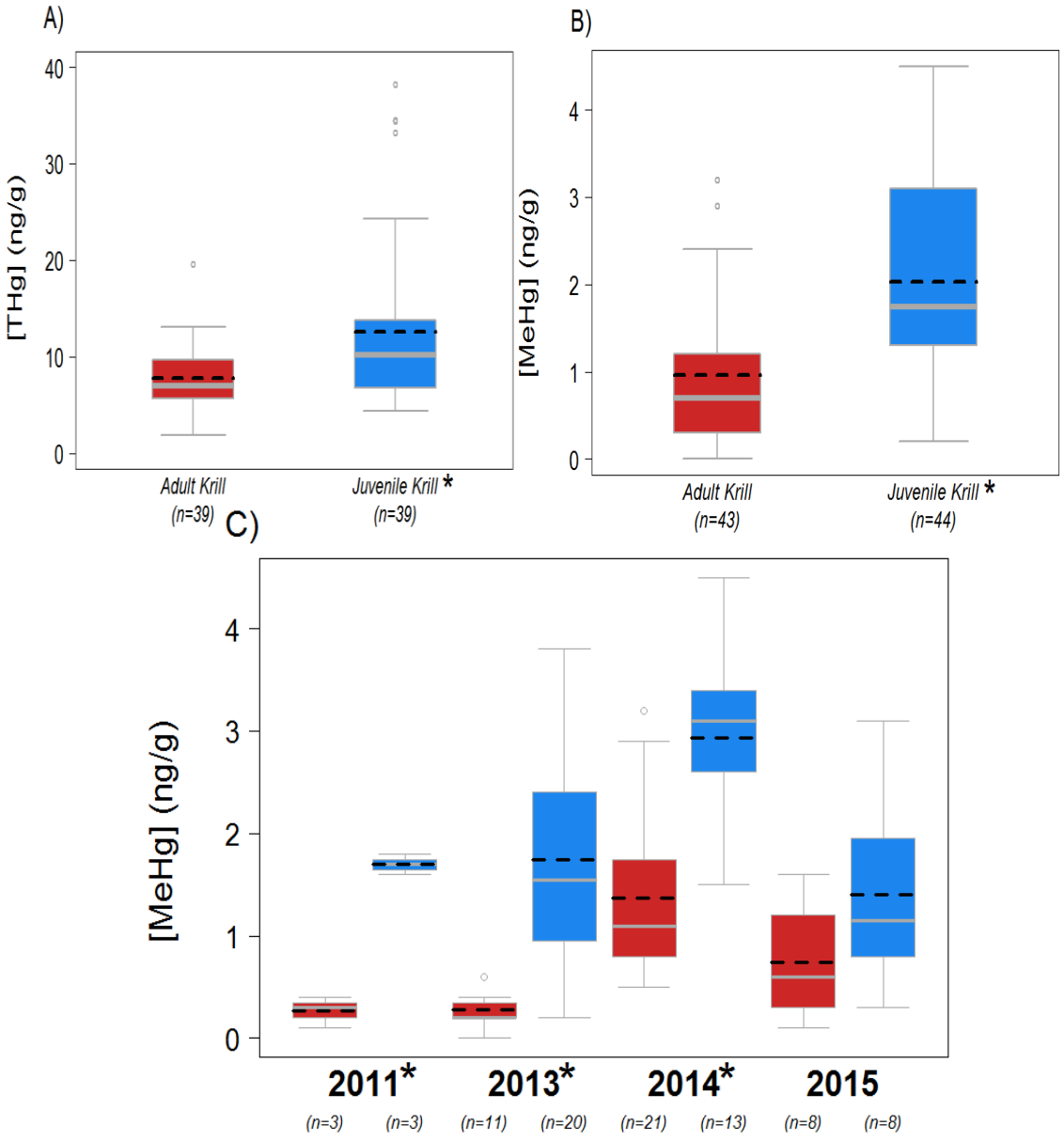

Figure 4.8 Total Hg (THg) and methylmercury (MeHg) concentrations in Antarctic krill (*Euphausia superba*) collected from coastal, shelf, and slope waters west of the Antarctic Peninsula at 65°S to 64°S during the austral summers of 2011, 2013, 2014, and 2015. Box plots show mean (black dashed lines), median (grey lines), minimum, 1st and 3rd quartiles, maximum, and outlier (circles) values for adult (red) and juvenile (blue) krill for all years (A and B) and within each year (C). Asterisks indicate significantly different mean values between adults and juveniles at $P < 0.005$ (I), $P < 0.001$ (II). Significant differences ($p<0.05$) within year pair-wise combinations of juvenile, adult krill, and *Pygoscelis* were done using a Games-Howell post-hoc test (Supplementary Table 1).

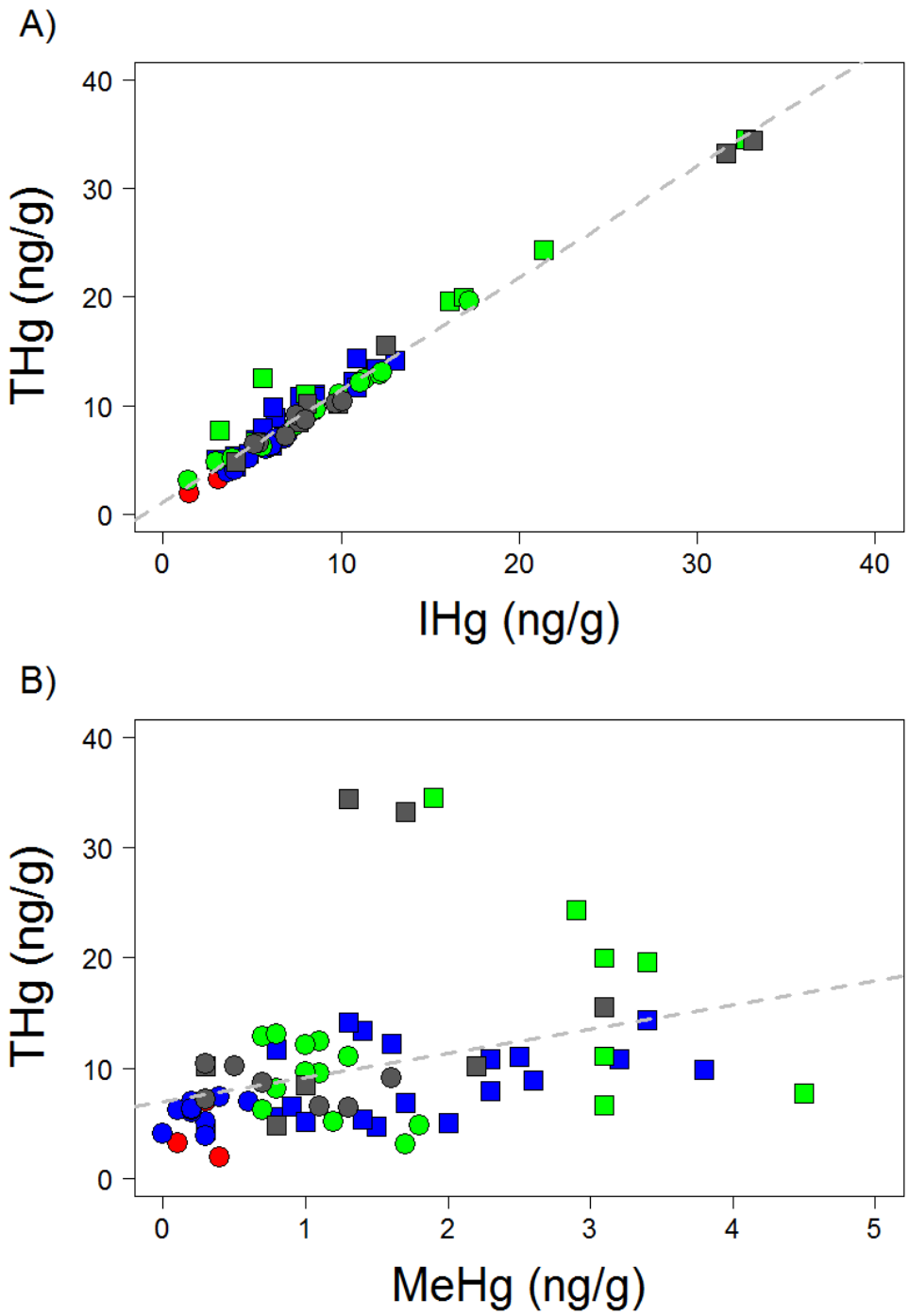

Figure 4.9 Relationships between total mercury (THg) and inorganic Hg (IHg = THg - methylmercury) concentrations (A) and THg and methylmercury (MeHg) (B) in individual juvenile (squares) and adult (circles) krill (*Euphausia superba*) collected from coastal, shelf, and slope waters west of the Antarctic Peninsula at 65°S to 64°S in 2011 (red), 2013 (blue), 2014 (green), 2015 (grey) austral summers. The dashed line is the best fit line for the THg-IHg relationship ([THg]= 1.159 + 1.031[IHg]; $p<0.001$, $R^2=0.97$).

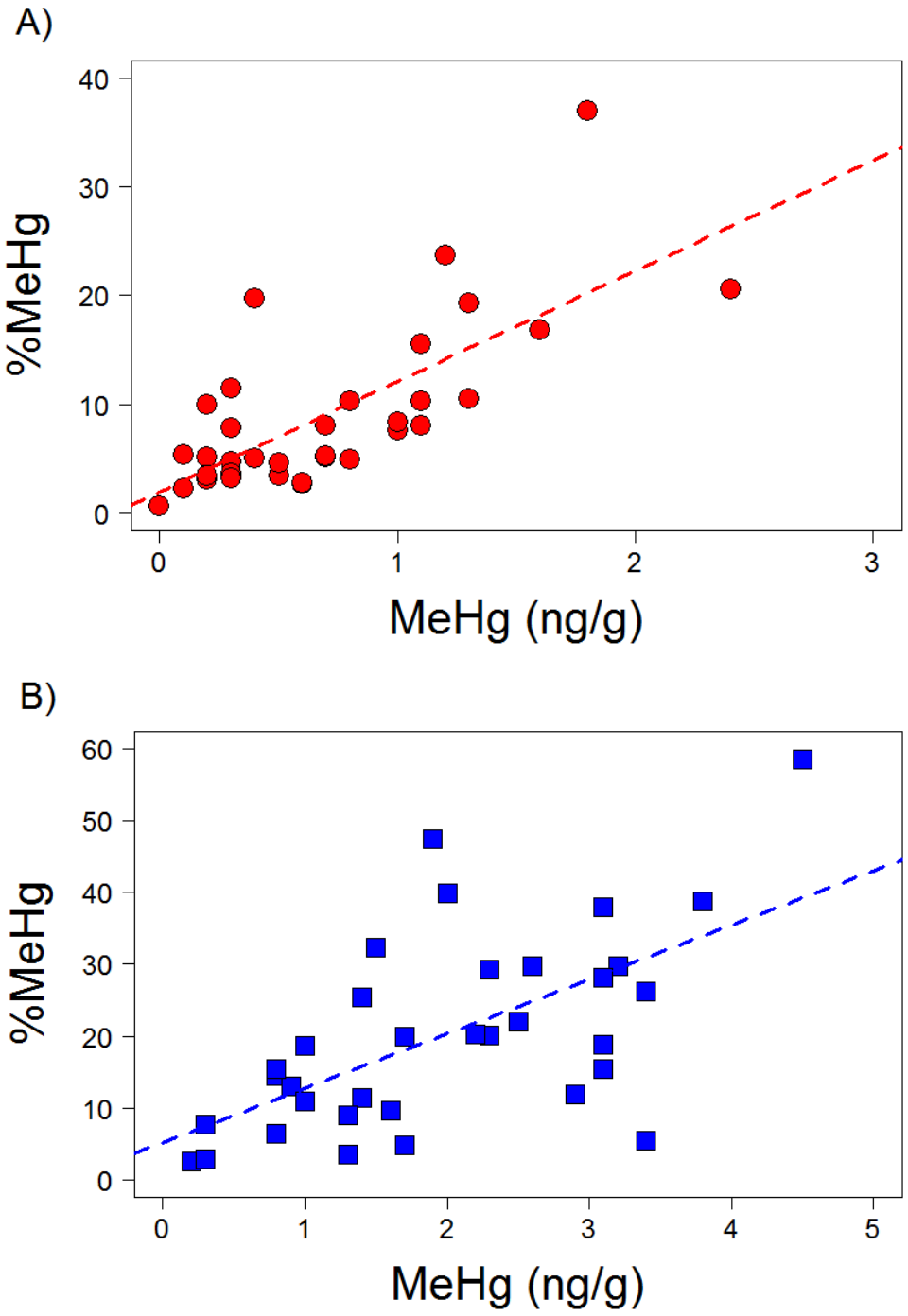

Figure 4.10 Relationships between percent of total mercury as methylmercury (%MeHg) the concentration of methylmercury (MeHg) in adult (A, red circles) and juvenile (B, blue squares) Antarctic krill (*Euphausia superba*). Linear regressions (dashed lines) are %MeHg = 1.939 + 10.153[MeHg] ($p<0.001$, $R^2 = 0.52$) for adults and %MeHg = 5.296 + 7.546[MeHg] ($p<0.001$, $R^2 = 0.38$) for juveniles.

Table 4.6 Subsamples of 30 krill (12 adults, 18 juveniles) were dissected to determine the distributions of THg and MeHg in muscle, soft tissues (hepatopancreas, hindgut), and exoskeleton. An additional dissection of 6 adults and 6 juveniles was needed to determine dry weight percentages of krill tissue. Below are distributions (percent total) of dry weight, total mercury (THg) and methylmercury (MeHg) in tissues of juvenile and adult krill collected from coastal waters west of the Antarctic Peninsula at 65°S in 2014. All values are mean ± 1SD.

		Percent total		
Tissue	**Developmental stage**	**dry weight**	**THg**	**MeHg**
Muscle	Juveniles	43.5	28±6.2	60.7±4.7
	Adults	33	18±3.0	54±1.8
Soft tissue	Juveniles	27.5	53±1.5	22.5±5.8
	Adults	35	69±0.9	28±0.8
Exoskeleton	Juveniles	29.0	19±1.4	16.9±4.4
	Adults	32	14±0.4	18±1.0

Table 4.7 Biomagnification factors (BMF) of MeHg in Antarctic krill (*Euphausia superba*) from coastal, shelf, and slope waters along with POM methylmercury concentrations in 2014 and 2015 surface waters west of the Antarctic Peninsula at 65°S used for BMF calculations.

Year	WAP Region	Adult *E. superba*	Juvenile *E. superba*
		BMF	**BMF**
2011			
	Coastal	1.1	6.1
2013			
	Coastal		8.3
	Shelf	1.1	2.5
2014			
	Coastal	4.8	8.7
	Slope	3.0	
2015			
	Coastal	3.2	6.3
$[MeHg]_{POM}$	Coastal_2014	0.54 ng g^{-1}	
	Coastal_2014	0.13 ng g^{-1}	
	Coastal_2015	0.17 ng g^{-1}	
	Coastal_2015	0.27 ng g^{-1}	

Mercury in feathers of adult *Pygoscelis* penguins from southern Anvers Island

Concentrations of THg (>95% MeHg (Thompson and Furness 1989)) in body feathers from the three species of *Pygoscelis* penguins resident along southern Anvers Island varied over two orders of magnitude (0.02 to 1.02 μg g^{-1}) (Table 4.4). Gentoo penguins had higher THg concentrations in their feathers (0.16±0.08 μg g^{-1}) than Adélie penguins (0.09±0.05 μg g^{-1}), but the difference was not significant (P = 0.10). However, the mean concentration of THg in feathers from chinstrap penguins (0.80±0.20 μg g^{-1}) was significantly higher (P < 0.001) than in feathers from the other two species (Tables 4.4 and 4.5).

Variations in carbon and nitrogen isotopes in relation to mercury accumulation in *Pygoscelis* penguins near Anvers Island, Antarctica

However, nitrogen isotope ratios were not indicative of higher accumulation of Hg as there was no relationship between δ^{15}N values and THg (>95% MeHg) (Bond and Diamond 2009) concentrations in feathers from the three species of *Pygoscelis* penguins (Figure 4.6). Nearly identical δ^{13}C values of gentoo, chinstrap, and Adélie were not indicative of similar Hg accumulation in feathers in the 2011 austral summer with chinstrap penguins having highest Hg concentrations and a mean δ^{13}C value of -25.6‰, lying in between Adélie (-25.9‰) and gentoo (-25.4‰) penguins (Table 4.4).

Northern latitude carbon and nitrogen isotope ratios in relation to mercury accumulation in *E. superba*

Across all years, developmental stages, and sampling locations, mean δ^{13}C values in krill were positively correlated with MeHg (Figure 4.11, R^2=0.50, P<0.05). In contrast to MeHg, THg was not correlated (p=0.19) with δ^{13}C in krill (Figure 4.12). Indeed, in

2014, adult krill from slope waters had significantly ($P<0.05$) lower $\delta^{13}C$ values (Table 4.5) and higher ($P<0.05$) THg concentrations than coastal adult krill. No relationship between $\delta^{15}N$ and MeHg in Antarctic krill from the WAP was observed ($p = 0.76$, Figure 4.13). Krill populations with the highest MeHg concentrations, coastal juveniles collected in 2013 and 2014, had $\delta^{15}N$ values at the low to middle range of observed values, while the krill population with the highest $\delta^{15}N$ value, coastal adults from 2011, had the lowest average concentration of MeHg (Table 4.4).

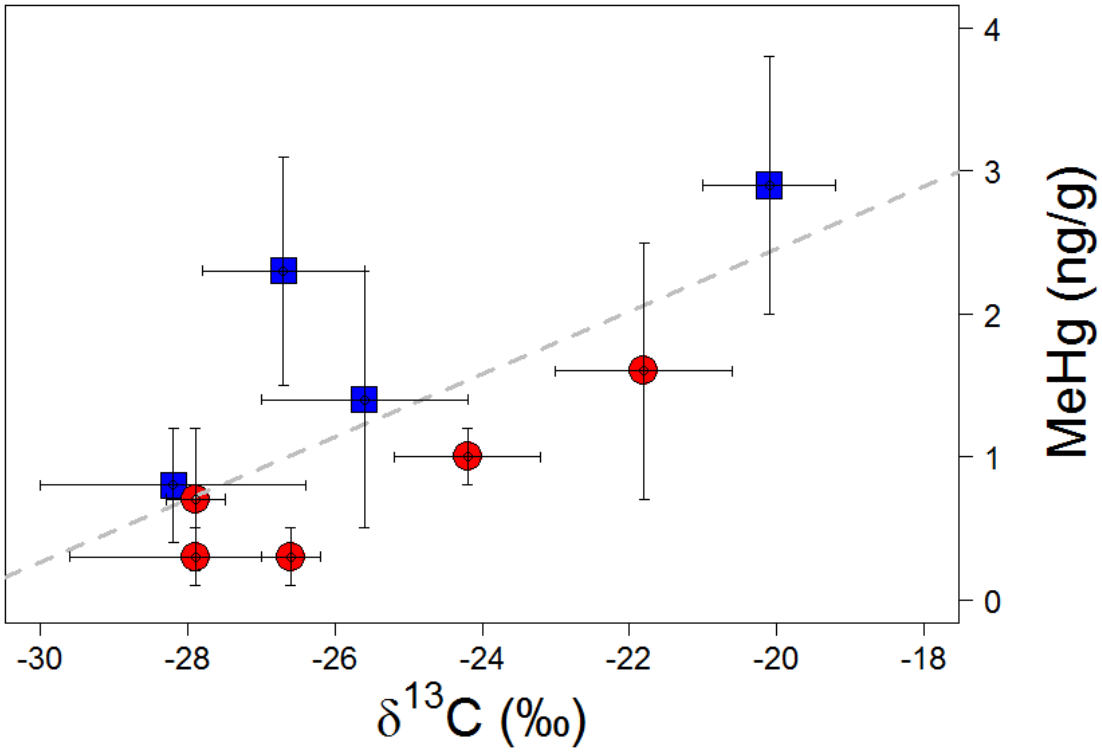

Figure 4.11 Relationship between methylmercury concentrations (MeHg) and δ^{13}C values in adult (red circles) and juvenile (blue squares) Antarctic krill (*Euphausia superba*) from the WAP marine ecosystem. Values are means ± 1SD (see Table 1). The linear regression for this relationship (dashed line) is [MeHg] = 6.8326 + 0.2192δ^{13}C ($p<0.05$, $R^2=0.50$).

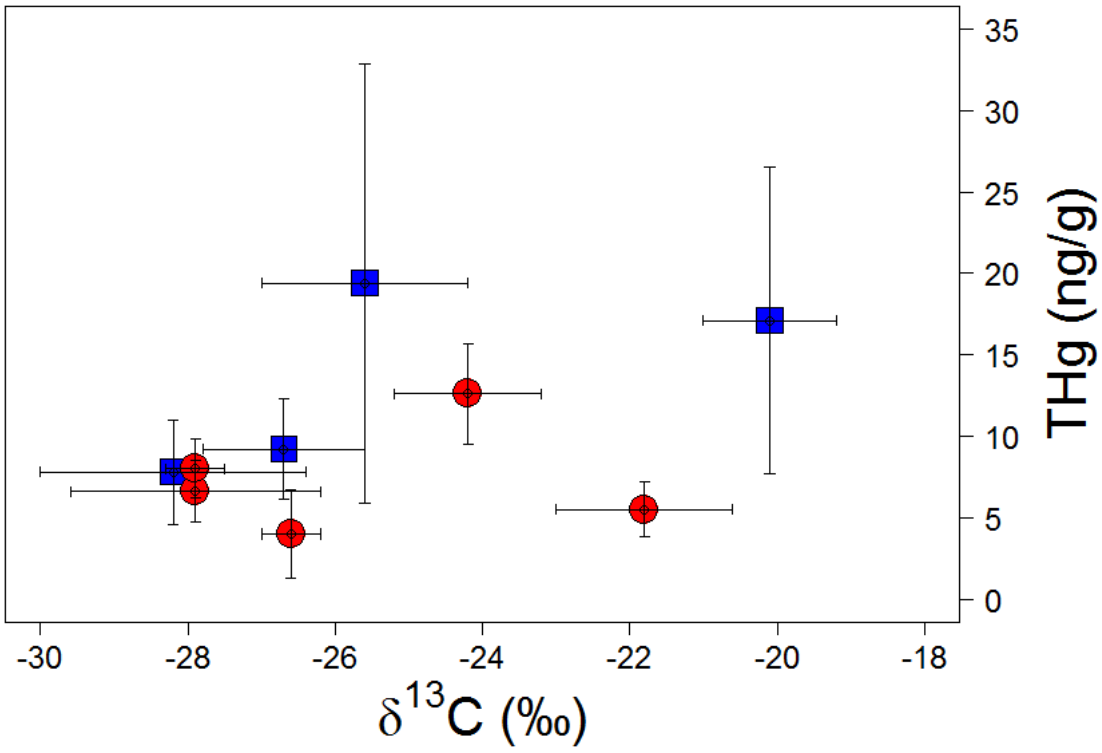

Figure 4.12 THg concentrations of adult (red circles) and juvenile (blue squares) Antarctic krill (*Euphausia superba*) and mean δ^{13}C. Values of THg and δ^{13}C are means ± 1SD (see Table 1).

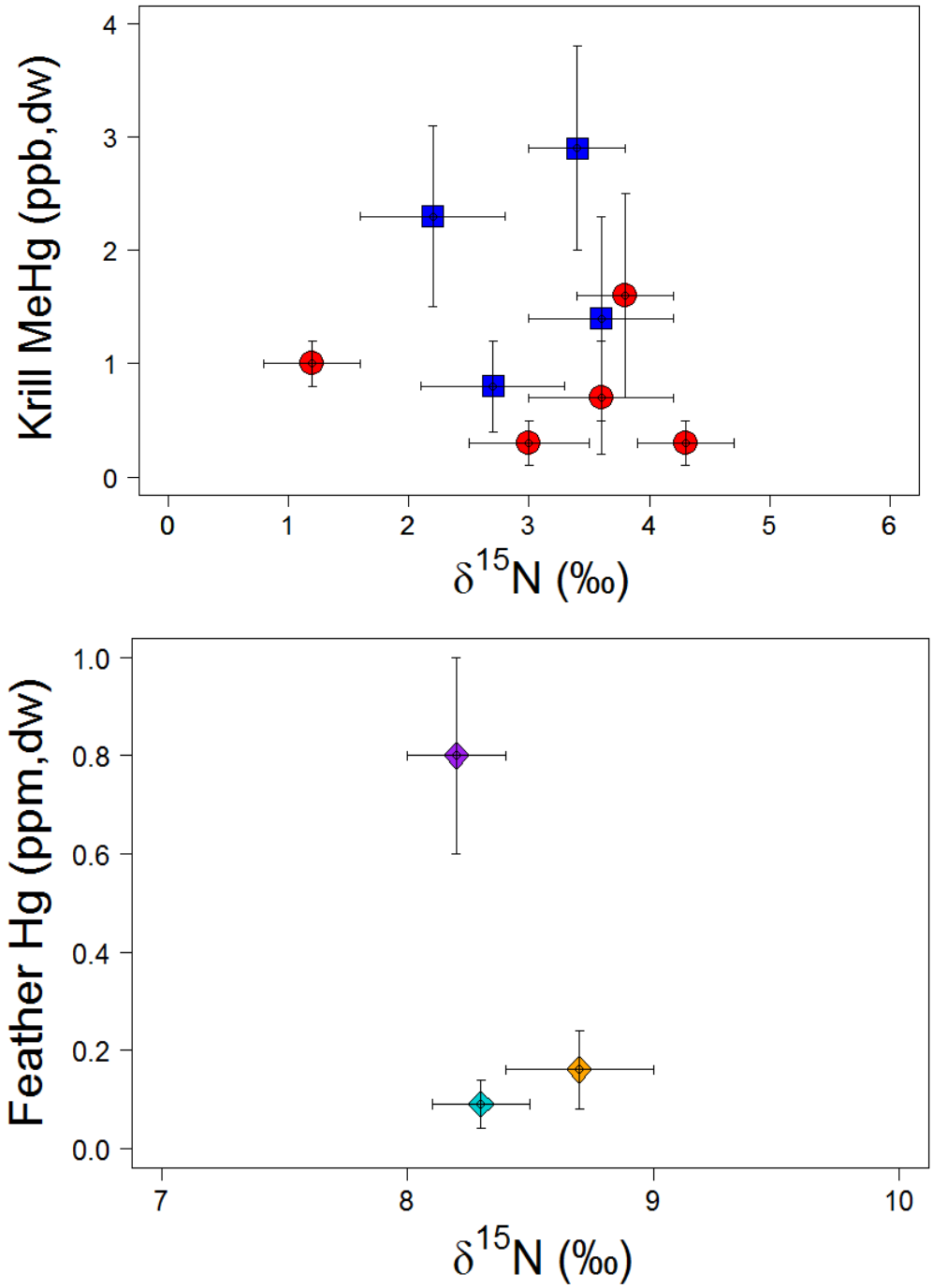

Figure 4.13 Mean Hg concentrations and N stable isotopes (δ^{15}N) in whole adult (red circles) and juvenile (blue squares) krill (top) and in feathers (bottom) of *Pygoscelis* penguins (diamonds) *P. adeliae* (light blue), *P. papua* (orange), and *P. antarctica* (purple) collected along the WAP near Anvers Island. Error bars denote ± 1SD.

Carbon and nitrogen content of Antarctic krill (*Euphausia superba*) at southern stations

In 2013, 2014, and 2015 average carbon:nitrogen (C:N) ratios in adults, from 4.5 to 6.8, were higher than in juvenile krill from 3.6 to 4.5, near the sea ice edge. Greater carbon content in whole adult krill (range 41 to 43%) in 2013 and 2014 was observed relative to juveniles (25 to 41%) at southern latitudes while nitrogen content was almost identical (within 1%) between juvenile and adult krill within sampling years (Table 4.8).

Carbon and nitrogen isotope ratios in *E. superba* at southern latitudes

Carbon isotope ratios in *E. superba* collected at the sea ice edge varied between years and between adults of juveniles in 2013 and 2015. Notably larger variation (σ= 4.0) in C isotope ratios existed in 2013 juvenile and adult krill than 2014 (σ= 1.5) and 2015 (σ= 0.4) krill sampled from more southern latitudes (Figure 4.14). Juvenile krill had significantly higher ($P<0.05$) $\delta^{13}C$ values in 2015, while higher ($P<0.05$) adult $\delta^{13}C$ values were measured in 2013 (Table 4.9). Nearly identical mean $\delta^{13}C$ values in co-located adults (-27.2±1.4‰) and juveniles (-27.2±1.1‰) were measured at the ice edge in 2014. The mean $\delta^{13}C$ values of 2014 juvenile and adult krill (Table 4.9) is not indicative of its individual krill C isotope ratios, which is comprised of two groups of juvenile and adults each with similar $\delta^{13}C$ values, one relatively enriched in ^{13}C (Figure 4.14). Nitrogen isotope ratios in Antarctic krill were less varied, but were significantly ($P<0.05$) different between juvenile and adult krill in 2014, with juveniles enriched in ^{15}N. Carbon isotope ratios of 2013, 2014, and 2015 krill collected near ice edge were positively correlated with N isotopes ($R^2=0.33$, $P<0.001$), with a stronger relationship between 2014 and 2015 ($R^2=0.74$, $P<0.001$) *E. superba*.

Mercury concentrations in *E. superba* subpopulations in proximity to sea ice edge

Total mercury mean concentrations varied from 2.0 to 9.1 ng g^{-1} in adult krill while mean THg in juveniles was 7.2 and 7.9 ng g^{-1} in 2013 and 2014 respectively. In 2013 and 2014, juvenile krill THg concentrations were significantly ($P < 0.05$) higher than adult krill sampled at the same location. Mean MeHg concentrations in juvenile *E. superba* varied from 1.1 to 2.1 ng g^{-1} with a wider range seen in adult MeHg mean concentrations, 0.2 to 1.5 ng g^{-1} (Table 4.9). Across all three years, MeHg concentrations were significantly higher ($P < 0.001$, $F = 18.79$) in juvenile than adult krill sampled near the sea ice edge (Figure 4.15). Within years, only 2014 did juvenile krill have significantly higher ($P < 0.05$) MeHg concentrations than co-located adult krill (Table 4.9). The percentage of THg in krill as methylmercury (%MeHg) varied from 15 and 29% and 6 to 26% in juvenile and adult Antarctic krill, respectively (Table 4.9). Juvenile krill had significantly ($P < 0.05$) higher %MeHg than adults in 2014, however, in 2013 adults MeHg percentages were significantly higher ($P < 0.05$) than juveniles sampled near the sea ice edge (Table 4.9).

Southern latitude carbon and nitrogen isotope ratios in relation to mercury accumulation in *E. superba*

Methylmercury and $\delta^{13}C$ and accumulation seemed to differ for juvenile and adult krill near the sea ice edge along the WAP. A strong correlation ($p<0.05$, $R^2=1.0$) between mean $\delta^{13}C$ values and MeHg concentrations indicate a positive relationship for adult krill sampled at southernmost latitudes along the WAP (Figure 4.16). Although MeHg concentrations did increase with higher $\delta^{13}C$ values in sea ice edge juvenile krill from 2013, 2014, and 2015 (Table 4.9), the trend was weak and insignificant ($P=0.36$).

Mean δ^{15}N values and MeHg concentrations of juvenile krill were scattered across sampling years (Table 3.9), with no trend (Figure 4.17). A tightly-coupled, positive relationship ($p<0.05$, $R^2=1.0$) occurred between mean MeHg concentrations and δ^{15}N values of adult krill sampled at the sea ice edge in 2013, 2014, and 2015.

Enrichment of MeHg near Anvers Island, Antarctica

As a result of trophic enrichment, MeHg concentrations increased by a factor of more than 10^3 from POM to penguins near Anvers Island, Antarctica (Figure 4.18). The trophic magnification factor for this segment of the food web, estimated from the slope of the relationship between logMeHg and relative trophic position (Figure 4.18), therefore indicates that MeHg concentrations increase by about a factor of 3.

Table 4.8 C and N content (%) and C:N ratios in Antarctic krill (*Euphausia superba*) collected from coastal, shelf, and slope waters west of the Antarctic Peninsula at the ice edge around 67°S and 69°S at Cape Sherriff field station at 62°S during the austral summers of 2013, 2014, and 2015.

Year	Krill	LTER Grid	WAP Region	Lat	Long	C:N	C Content (%)	N Content (%)
2013	Juvenile	-100.060	Coastal	-69.1	-76.5	4.3±1.4 (5)	25±3 (6)	6±2 (5)
	Adult	-100.060	Coastal	-69.1	-76.5	6.8±1.3 (11)	43±2 (10)	6±1 (11)
2014	Juvenile	100.100	Shelf	-67.4	-74.2	3.6±0.6 (10)	36±2 (10)	13±4 (11)
	Adult	100.100	Shelf	-67.4	-74.2	4.5±1.6 (9)	41±7 (11)	12±4 (11)
2015	Juvenile	-100.040	Coastal	-69.3	-76.1	4.5±0.3 (8)	41±4 (10)	8±1 (10)
	Adult	-100.040	Coastal	-69.3	-76.1	5.3±0.4 (8)	41±2 (8)	8±1 (8)

Table 4.9 Concentrations of total Hg (THg) and methylmercury (MeHg) and C and N isotope ratios in Antarctic krill (*Euphausia superba*) collected from coastal, shelf, and slope waters west of the Antarctic Peninsula at the ice edge around 67°S and 69°S at Cape Sherriff field station at 62°S during the austral summers of 2013, 2014, and 2015. All values are means ± 1SD (n) where NA, not available.

Year	Krill	LTER Grid	WAP Region	Lat (°S)	Long (°W)	[THg] (ng g^{-1}, dry wt)	[MeHg] (ng g^{-1}, dry wt)	MeHg/THg (%)	$\delta^{13}C$ (‰)	$\delta^{15}N$ (‰)
2013	Juv	-100.060	Coastal	69.1	76.5	**7.2±1.2 (8)	1.1±0.3 (8)	*15±3 (8)	*-28.2±1.7 (5)	4.3±0.2 (5)
	Adult	-100.060	Coastal	69.1	76.5	*4.5±1.1 (9)	1.0±0.2 (8)	**24±4 (7)	**-25.3±1.4 (11)	4.0±0.7 (11)
2014	Juv	100.100	Shelf	67.4	74.2	**7.9±7.8 (6)	**1.8±0.5 (9)	**29±11 (5)	-27.2±1.1 (10)	**3.1±0.6 (11)
	Adult	100.100	Shelf	67.4	74.2	*2.0±0.7 (8)	*0.2±0.1 (7)	*6±3 (5)	-27.2±1.4 (9)	*2.7±0.3 (9)
2015	Juv	-100.040	Coastal	69.3	76.1	NA	2.1±0.7 (10)	NA	**-23.1±0.3 (8)	4.7±0.6 (10)
	Adult	-100.040	Coastal	69.3	76.1	9.1±3.4 (5)	1.5±0.6 (8)	26±16 (5)	*-24.1±0.3 (7)	4.6±0.3 (8)
2015	Juv	Cape Sherriff	Coastal	64.8	64.1	11.3±2.7 (8)	2.5±1.2 (9)	20±7 (7)	-26.9±2.1 (12)	5.2±0.4 (11)

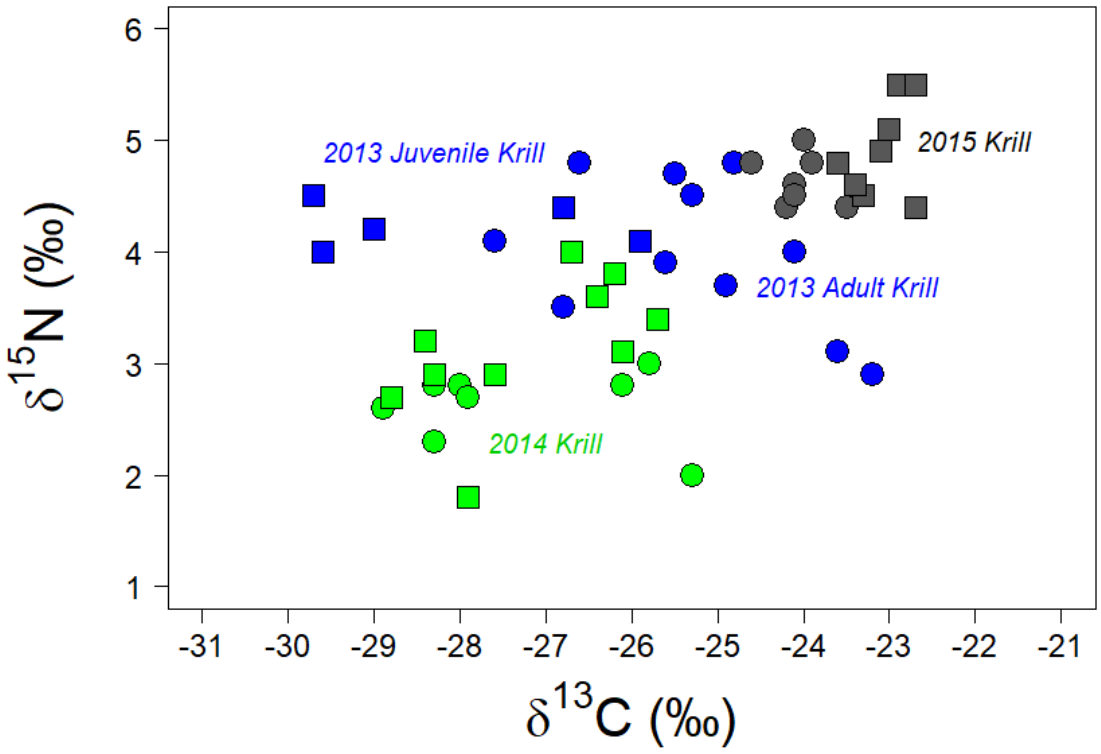

Figure 4.14 C and N stable isotope ratios (δ^{13}C and δ^{15}N; filled symbols) in juvenile (squares) and adult (circles) krill (*Euphausia superba*) collected from the sea ice edge of the WAP at 67°S and 69°S in three austral summers. Note that δ^{13}C values of krill were normalized for lipid content using C:N ratios (see text).

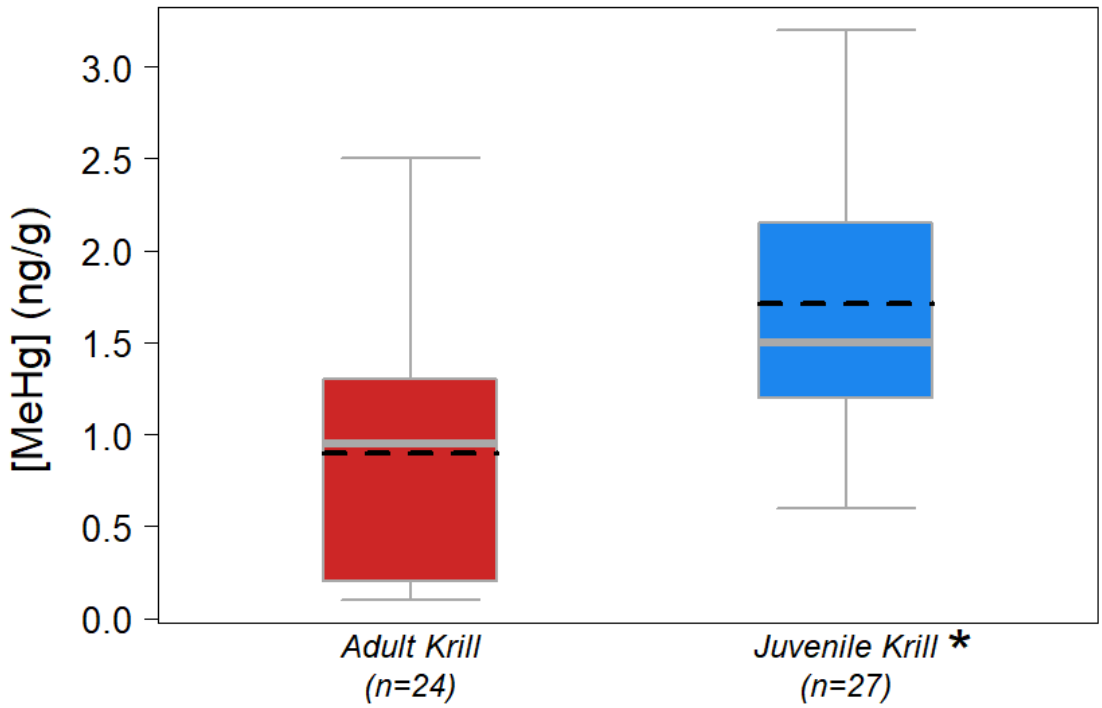

Figure 4.15 Methylmercury (MeHg) concentrations in Antarctic krill (*Euphausia superba*) collected from sea ice edge at coastal and slope waters west of the Antarctic Peninsula at 67°S to 69°S during the austral summers of 2013, 2014, and 2015. Box plots show mean (black dashed lines), median (grey lines), minimum, 1st and 3rd quartiles, and maximum values for adult (red) and juvenile (blue) krill for all years. Asterisks indicate significantly different mean values between adults and juveniles at $P < 0.001$.

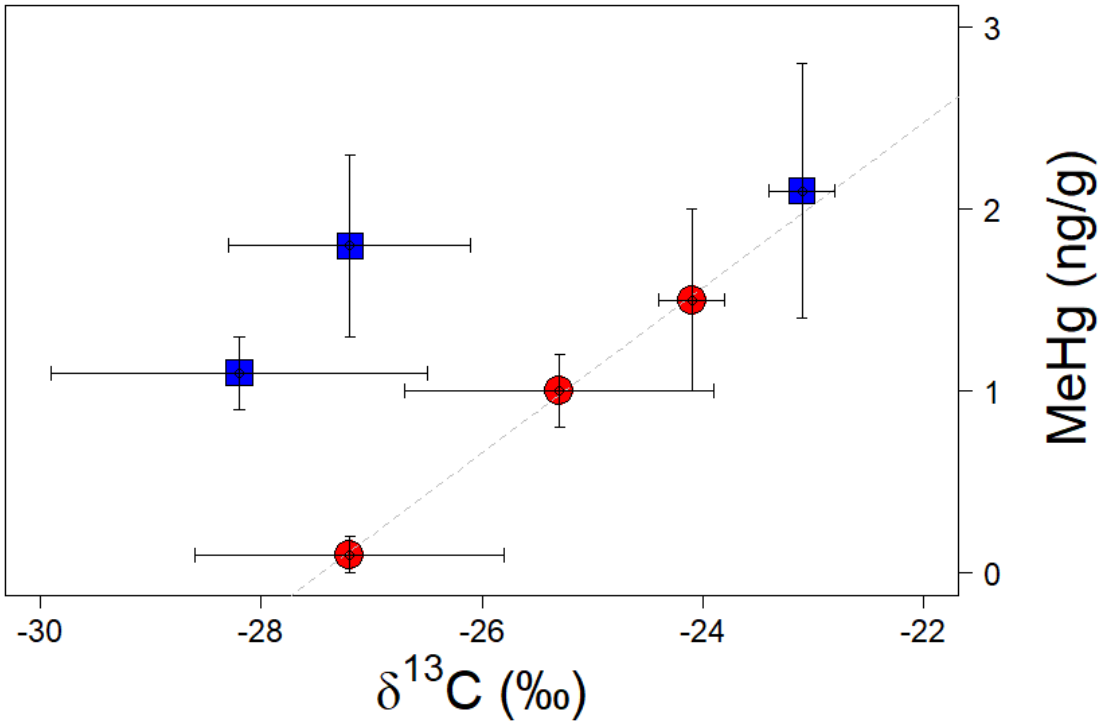

Figure 4.16 Separate accumulation trends between methylmercury concentrations (MeHg) and δ^{13}C values in adult (red circles) and juvenile (blue squares) Antarctic krill (*Euphausia superba*) near the sea ice edge. Values are means ± 1SD (see Table 1). The linear regression for the adult krill (dashed line) is [MeHg] = 12.4490 + 0.4536δ^{13}C ($p<0.05$, $R^2=1.0$), while a trend for MeHg and δ^{13}C mean values of juvenile krill was insignificant (P=0.36).

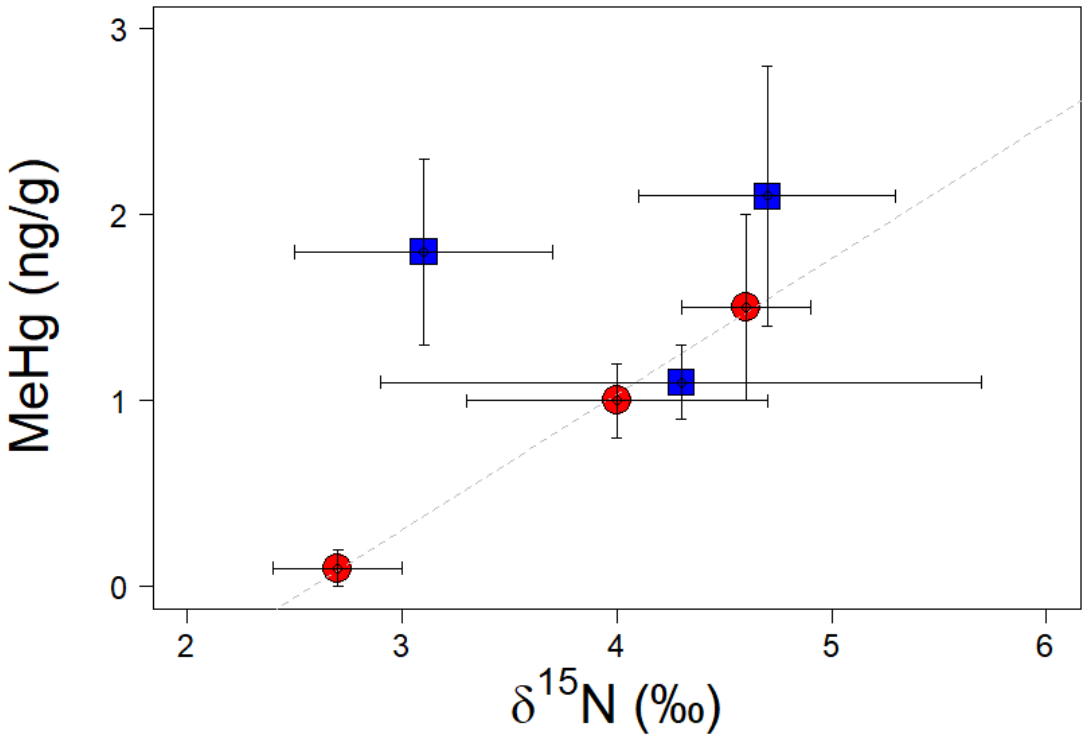

Figure 4.17 Relationship between methylmercury concentrations (MeHg) and δ^{15}N values in adult (red circles) and but not juvenile (blue squares) Antarctic krill (*Euphausia superba*) near the sea ice edge. Values are means ± 1SD (see Table 1). The linear regression for the adult krill (dashed line) is [MeHg] = -1.8818 + 0.72976δ^{15}N ($p<0.05$, $R^2=1.0$).

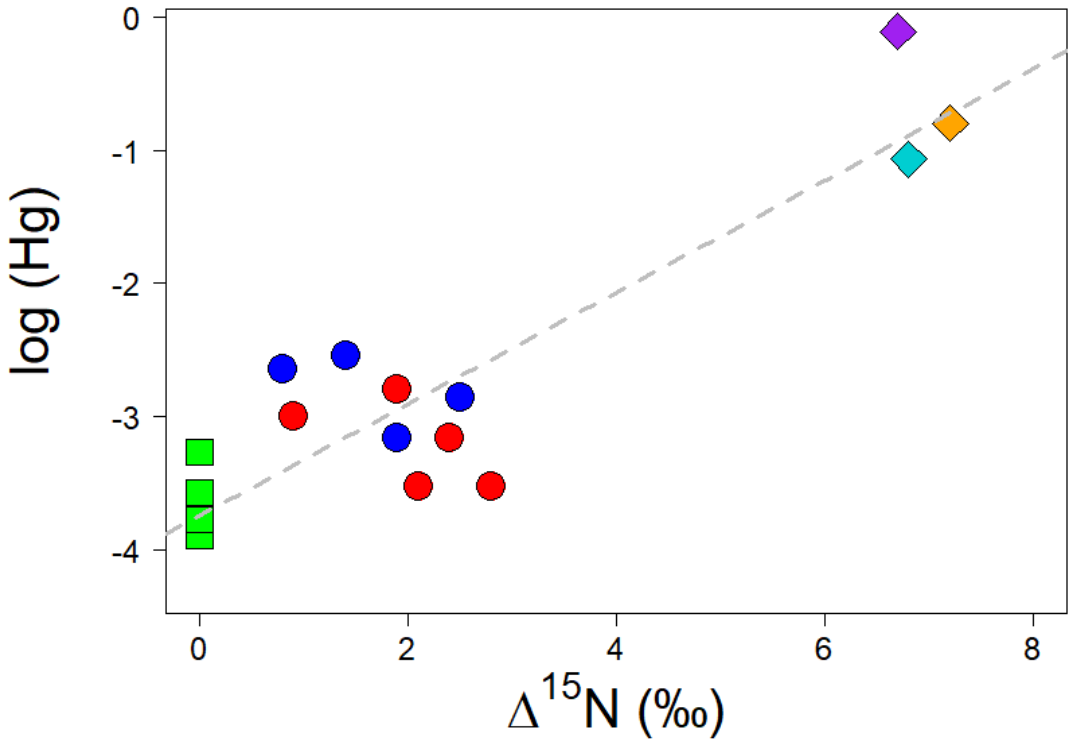

Figure 4.18 Methylmercury concentration (µg g^{-1}) vs. relative trophic position ($\Delta^{15}N$) in coastal particulate organic matter (POM) (squares), Antarctic krill (circles), and *Pygoscelis* penguins (diamonds). Values are for adult (red circles) and juvenile (blue circles) Antarctic krill (*E. superba*) collected at ~65°S, and *P. adeliae* (blue diamond), *P. papua* (orange diamond), and *P. Antarctica* (purple diamond) collected near Anvers Island. Relative trophic positions ($\Delta^{15}N$) for krill and penguins were calculated as $\delta^{15}N_{consumer} - \delta^{15}N_{POM}$. The dashed line ($\log_{10}[MeHg] = -3.744 + 0.419\Delta^{15}N$; $p<0.0001$, $R^2=0.807$) describes the trophic enrichment of MeHg from POM to krill and *Pygoscelis* penguins in this ecosystem.

E. Discussion

Carbon and nitrogen isotope ratios in particulate organic matter (POM) along the WAP

Coastal-offshore variation in surface POM $\delta^{13}C$ and $\delta^{15}N$ values along the WAP are consistent with previously observed patterns. Southern Ocean phytoplankton are typically depleted in ^{13}C due to slow (nutrient limited) growth rates and high dissolved carbon dioxide ($CO_{2(aq)}$) concentrations, which lead to strong carbon isotopic fractionation (Rau et al. 1991). Longitudinal differences in POM $\delta^{13}C$ values at northern latitudes of the WAP (Table 3.2) were similar to those from a previous study which found offshore phytoplankton more depleted in ^{13}C relative to phytoplankton from the highly productive coastal waters near Anvers Island (Mincks et al. 2008). Higher $\delta^{13}C$ values in POM collected at southern latitudes in 2013 (Figure 4.4) may have been influenced by their proximity to sea ice. Ice algae are enriched in ^{13}C during summer months as CO_2 availability in brine channels is depleted (Gibson et al. 1999, Cozzi and Cantoni 2010). During summer months, under-ice erosion and may contribute POM with higher $\delta^{13}C$ values to underlying seawater.

Lighter $\delta^{15}N$ values in POM collected further from the WAP coast (Figure 4.5) are likely due to higher concentrations and utilization of ammonium (NH_4^+) offshore, which has been observed in the Weddell Sea (Smith and Nelson 1990, Rau et al. 1991). In contrast, particulate organic matter enriched in ^{15}N collected near the WAP coast may be attributed to higher utilization of upwelled nitrate by local phytoplankton in coastal waters. Constinently higher $\delta^{13}C$ and $\delta^{15}N$ values in POM from deeper surface waters along the WAP may be attributed to remineralization of organic matter at depth, but

better depth resolution would be needed to examine this mechanism. Wide ranges in C and N isotopes in Antarctic POM are not uncommon and illustrates the importance of fine spatial variation in δ^{13}C and δ^{15}N values when determining trophic structure in waters that vary both geographically and with depth (Gillies et al. 2012b).

Carbon, nitrogen stable isotope ratios and content of Antarctic krill (*Euphausia superba*) at northern latitudes

Previous work over multiple seasons has shown that primary production of organic carbon in offshore WAP Antarctic surface waters tends to be more depleted in ^{13}C than organic carbon in nearshore waters near Anvers Island (Mincks et al. 2008). These observations are consistent with our findings of lower δ^{13}C values in offshore POM (Table 4.1 and 4.2) and juvenile and adult *E. superba* (Figure 4.6) and previously reported spatial trends for δ^{13}C in overwintering larval krill northwest of Adelaide Island (Frazer 1996). In 2014, a year of very high sea ice extent along the WAP (Stammerjohn 2017), krill had higher δ^{13}C values (Figure 4.6) and higher C:N ratios (Table 4.3) than any other population of krill examined in this study. Increased sea ice extent and duration is known to drive primary productivity and positive Chla anomalies in this region (Saba et al. 2014), and annual sea ice conditions may have shifted juvenile and adult krill to a less mixotrophic diet feeding on higher proportions of phytoplankton. Higher δ^{13}C values in 2014 krill likely reflect a greater influence of ^{13}C-enriched sea ice particulate organic matter (POM) (Gillies et al. 2012a, Gillies et al. 2012b) on the carbon isotopic composition of phytoplankton and other prey consumed by krill in 2014 than in other years.

A lack of spatial relationships for $\delta^{15}N$ values in Antarctic krill is not unexpected due variability in N nutrient dynamics and $\delta^{15}N$ at the base of the Antarctic food web. Generally high levels of nitrate exist in deeper water (~33 µm) with significant drawdown of surface nitrate during January phytoplankton blooms (Ducklow et al. 2006), which are found alongside enrichments of ammonium (NH_4^+), suggesting a spatial coupling between primary production and heterotrophy (Serebrennikova and Fanning 2004). This fine-scale heterogeneity in $\delta^{15}N$ values is likely integrated by phytoplankton-dependent grazers such as Antarctic krill. Variability in $\delta^{15}N$ values may be constrained during high sea ice extent years such as 2014 (Stammerjohn 2017), in which $\delta^{15}N$ values for both coastal adults and juveniles were significantly higher ($p<0.05$) than adults sampled offshore from the continental slope. Differences in $\delta^{15}N$ values may also be attributed to developmental differences in diet as significantly ($p<0.05$) heavier $\delta^{15}N$ values (Table 4.4) and higher %N content (Table 4.3) were observed in adults sampled on the continental shelf in 2013, than in co-located juveniles and coastal juveniles (Table 4.5).

Carbon, nitrogen stable isotope ratios and content in feathers of *Pygoscelis* penguins near Anvers Island, Antarctica

The limited range of $\delta^{13}C$ values in the three sampled *Pygoscelis* penguins indicates that all three species feed locally around Anvers Island, as has been documented for resident populations of Adélie penguins in this area (Fraser and Trivelpiece 2013, Oliver et al. 2013). The somewhat elevated $\delta^{15}N$ values in gentoo penguins may have resulted from a greater consumption of fish during the summer months, which are more enriched in ^{15}N than krill (Polito et al. 2011a), as was found at Livingston Island near the

northern end of the Antarctic Peninsula (Polito et al. 2015). Alternatively, higher δ^{15}N values in gentoo penguins may result from their foraging at deeper depths (benthopelagic) (Trivelpiece et al. 1987) than chinstrap (mesopelagic) (Miller et al. 2010) or Adélie (epipelagic) (Cimino et al. 2016) penguins. Differences in δ^{15}N values between sympatric breeding penguins could not be attributed to C:N ratios which were identical in all three *Pygoscelis* penguin species with almost identical %C and %N content.

Mercury concentrations in juvenile and adult *E. superba* at northern latitudes

Total Hg measured in *E. superba* near Anvers, Island are similar to those for *E. superba* collected near the northern tip of the WAP during the austral summer (8 ng g^{-1}) (Brasso et al. 2012) and in feed meal (8 ng g^{-1}) (Moren et al. 2006) and dietary supplements (13 ng g^{-1}) (Leblond et al. 2008) prepared from Southern Ocean *E. superba*. However, they are lower than THg concentrations in *E. superba* collected along the WAP during the fall of 1993 (13 to 49 ng g^{-1}) (Locarnini and Presley 1995) and nearly ten times lower than THg in *E. superba* collected from the Ross Sea (77 ng g^{-1}) (Bargagli et al. 1998).

The concentrations of MeHg we measured in *E. superba* from the WAP bracket the value for the MURST-ISS-A2 krill standard reference material (1.1 ng g^{-1}), the only other reported analysis of MeHg in Southern Ocean krill (Pacheco et al. 2010). Since MeHg is the form of mercury that biomagnifies in marine food webs, this result highlights the importance of determining the concentration of MeHg in krill and the factors controlling MeHg concentrations, to predicting mercury accumulation in higher trophic levels in the WAP marine ecosystem.

Differences in %MeHg between juvenile and adult krill from the WAP suggest that, as the accumulation of MeHg in juvenile krill increased, juveniles were apparently exposed to, and accumulated more variable levels of inorganic Hg than adults. Variability in krill Hg accumulation is likely due to region of exposure as ecosystems nearshore are in proximity to coastal Hg sources such as atmospheric depletion events (Ebinghaus et al. 2002, Bargagli et al. 2005, Mastromonaco et al. 2016). Fluctuations in Hg accumulation attributed to feeding location may be controlled by yearly sea ice conditions. For example, high primary productivity in surface waters in a high sea ice year such as 2014 (Stammerjohn 2017), may lead to greater remineralization of particulate Hg at mesopelagic depths where developing krill reside exposing juvniles to elevated MeHg and THg concentrations.

Developing krill may accumulate MeHg in mesopelagic (>300 m) waters as larvae or during their ascent to the epipelagic zone as juveniles (Daly and Zimmerman 2004). Alternatively, higher MeHg concentrations in juvenile than adult krill may reflect the longer periods of time juveniles spend in the nearshore (coastal) environment along the WAP (Lascara et al. 1999, Daly 2004, Daly and Zimmerman 2004, Siegel et al. 2013). In this case, the accumulation of MeHg by juvenile krill may result from feeding under sea ice or at the sea ice edge (Daly 1990, Frazer et al. 2002b). Elevated levels of MeHg were previously measured in seawater under sea ice in the Arctic (St Louis et al. 2007) and in basal layers of sea ice from East Antarctica (Cossa et al. 2011). Moreover, while the microbial production of MeHg in sea ice has not been demonstrated, an analogous gene to that required for microbial Hg methylation was recently identified in an East Antarctic sea ice microbial community (Gionfriddo et al. 2016).

Our observations of higher THg and MeHg concentrations and BAFs in juvenile than adult krill, and a previous finding that THg was higher in smaller and, presumably, younger krill (Locarnini and Presley 1995), are unexpected since in other aquatic animals, Hg tends to accumulate to higher levels in larger, slower growing adults than smaller, faster growing juveniles (McArthur et al. 2003, Hammerschmidt and Fitzgerald 2006a, Cossa et al. 2012, Lescord et al. 2015). The shorter ecdysis period, or time before shedding a new exoskeleton, in juvenile than adult krill (Daly 1990) may be expected to favor higher turnover and lower concentrations of Hg in juveniles. Based on our results, however, distributions of THg and MeHg in krill exoskeleton are low, emphasizing the importance of tissues where Hg has a longer residence time such as muscle, a tissue compartment with higher body burdens of MeHg in juveniles than adults. If MeHg is accumulated by krill nearly entirely from food, as is the case for other crustacean zooplankton (Wright et al. 2010), higher concentrations and distribution of MeHg in muscle of juvenile than adult krill suggest that juvenile krill living in WAP shelf waters are more efficient at accumulating MeHg from prey than adults. Alternatively, juvenile krill may be selectively consuming prey with higher concentrations of bioavailable MeHg, or forage in areas where prey MeHg concentrations are higher than elsewhere along the WAP.

Mercury in feathers of adult *Pygoscelis* penguins near Anvers Island

The concentrations of Hg in feathers from Adélie and gentoo penguins residing near Anvers Island were a factor of two to three lower than those in feathers from Adélie (0.32 μg g^{-1}) and gentoo (0.28 μg g^{-1}) penguins living near King George Island at the northern tip of the WAP (Brasso et al. 2013). Elevated concentrations of THg in

penguins living near King George Island could be due to greater geothermal activity or the larger human presence associated with the many research stations in this area. Consistent with our results for penguins living near Anvers Island, chinstrap penguins living near King George Island had significantly higher ($p < 0.05$) concentrations of THg in their feathers compared to sympatric Adélie and gentoo penguins (Brasso et al. 2013).

As Hg accumulates in seabird feathers continuously until molt (Becker et al. 1993) including during non-breeding seasons (Anderson et al. 2009), foraging during both winter and summer may contribute to mercury concentrations in penguins along the WAP. During less productive winter months, there may be a shift to higher contributions of fish in the penguin diet as observed in chinstrap and gentoo penguins (Polito et al. 2011b). However, this seasonal shift alone may not explain the significantly higher Hg concentrations in chinstrap than both Adélie and gentoo penguins. Since MeHg concentrations in fish (Monteiro et al. 1996, Choy et al. 2009) and seawater (Cossa et al. 2011) tend to increase at mesopelagic depths (>300 m), chinstrap penguins, which forage in mesopelagic waters may consume fish or krill (Miller and Trivelpiece 2007) with higher MeHg concentrations. Indeed, chinstraps in the northern WAP were found to consume a higher proportion of mesopelagic fish than Adélies or gentoos (Polito et al. 2016) and higher proportions of juvenile krill (Miller and Trivelpiece 2007).

Variations in carbon isotope ratios and relation to mercury accumulation in *E. superba* at northern latitudes

Assimilation of $\delta^{13}C$ and $\delta^{15}N$ values in Antarctic krill are governed by diet source (nearshore, coastal) and grazing depth (Schmidt et al. 2011). While average $\delta^{13}C$ values of *E. superba* may integrate varying prey $\delta^{13}C$ values from different foraging

locations or depths, a positive relationship between MeHg and δ^{13}C values of juvenile and adult krill over all sampling years indicates higher accumulation of MeHg is linked to the enrichment of ^{13}C at the base of nearshore and sea-ice associated food webs along the WAP, with lower accumulation of MeHg in krill from shelf and slope waters. A spatial trend in assimilation of δ^{13}C values and MeHg accumulation within juvenile krill subpopulations is most clearly identified in juveniles from 2013 (Table 4.4). Mid-shelf juveniles had lower MeHg and δ^{13}C values than their coastal counterparts, likely due to migration offshore while nearing adulthood as they were of a greater average dry weight (66 ±4 mg) than juvenile krill collected near the coast (43 ±11 mg).

In contrast to MeHg, THg was not correlated ($p=0.19$) with δ^{13}C in krill (Figure 4.8) indicating that exposures of krill to inorganic mercury were not related to proximity to the Antarctic Peninsula. Indeed, in 2014, adult krill from slope waters had significantly higher ($P<0.05$) THg concentrations than coastal adult krill indicating greater accumulation of inorganic mercury in offshore waters depleted in ^{13}C. In slope waters THg, mostly inorganic Hg, could be accumulated in adult *E. superba* from seawater residing within regions of Circumpolar Deep Water (CDW), which occupies a large portion of the water column (>500m) and is enriched in dissolved Hg concentrations (Cossa et al. 2011).

Nitrogen isotope ratios and mercury accumulation in *E. superba* in the northern WAP

Assimilation of δ^{15}N values in krill have been previously linked to contributions of herbivory and heterotrophy, which may shift during development (Polito et al. 2013). However, a lack of observable patterns in δ^{15}N values and mercury accumulation in

Antarctic krill are not unexpected due to the complexity of the supply, distribution, and biological depletion of macronutrients at the base of the foodweb along the WAP (Prezelin et al. 2004, Serebrennikova and Fanning 2004).

These findings suggest that nitrogen isotope dynamics may be variable, however, more consistent spatial patterns in δ^{15}N values may exist during years of high sea ice as 2014 adult krill had higher δ^{15}N values than co-located juvenile krill near the coast where adults sampled from slope waters had the lowest δ^{15}N values of all krill sampled and comparatively lower MeHg concentrations than coastal krill sampled in 2014 (Tables 4.3 and 4.4). Increased extent and duration of sea ice may provide more contrast in nutrient and food web dynamics and perhaps a lower δ^{15}N baseline in the offshore planktonic food web.

While we cannot infer trophic level of the krill populations we sampled without more spatial and depth resolution in reference POM δ^{15}N values within their food webs, which may vary over space and time (Braune et al. 2014, Kokubun et al. 2015), δ^{15}N values and Hg concentrations in *E. superba* (Figure 4.9) suggest that trophic position is not a primary driver of variation in MeHg accumulation among krill populations of the WAP marine ecosystem.

Variations in carbon and nitrogen isotope ratios and their relation to mercury in *Pygoscelis* penguins

Similar δ^{13}C values for all three species of *Pygoscelis* penguins (Table 4.4; Figure 4.7) is consistent with their overlapping foraging areas in the summer. Higher δ^{15}N values in gentoos, which may be attributed to flexibility in foraging depth, did not result in higher mercury concentrations (Table 4.4, 4.5). As was the case for krill, trophic

position does not appear to exert a strong influence on MeHg accumulation among WAP penguins near Anvers Island (Figure 4.9). Significantly higher ($p<0.05$) THg concentrations in chinstrap feathers therefore is not likely attributed to feeding at a higher trophic level, but accumulation from prey consumed outside of the breeding season, or foraging on krill and/or fish in mesopelagic waters containing higher MeHg concentrations (Cossa et al. 2011). However, δ^{15}N values of fish prey from all depths are known to be equal to or even exceed δ^{15}N values of their *Pygoscelis* predators and have higher measured THg than Antarctic krill (Polito et al. 2011b, Polito et al. 2016). If gentoo penguins were foraging on higher percentages of fish, as is the case at the South Shetland Islands, north of our sampling locations (Polito et al. 2015), an enrichment of both ^{15}N and Hg would be expected in gentoo penguin feathers, which is not seen in multiple data sets, including that of (Polito et al. 2016)

Carbon and nitrogen isotopes and Hg content of Antarctic krill (*Euphausia superba*) at southern stations

At locations along the WAP that are sea ice covered for most or the entire year, isotope dynamics will likely be different than at northern latitudes such as Anvers Island which is free of sea ice during the austral summer. Sea ice may provide more of a constraint on feeding and therefore δ^{13}C and δ^{15}N values in juvenile and adult krill at southern latitudes. Unlike C and N isotope ratios near Anvers Island, krill δ^{13}C and δ^{15}N values near sea ice tended to have a linear relationship within pooled austral years (Figure 4.14). Linearity of sea ice krill C and N isotope ratios across years was attributed to generally increasing δ^{15}N values from 2013 and 2014 to 2015 (Table 4.9), and contrasts with relatively constant δ^{15}N values of krill sampled at northern latitudes (Table 4.4;

Figure 4.7). Values of $\delta^{15}N$ were constant within years, with significantly heavier $\delta^{15}N$ values ($P<0.05$) in juveniles than adult sea ice krill in 2014 (Table 4.9), possibly driven by feeding of juveniles on POM in mesopelagic depths which are enriched in ^{15}N relative to surface waters in Prydz Bay, East Antarctica (Zhang et al. 2017).

Except for 2013, within year sea ice edge krill occupied a relatively narrow isotopic range for $\delta^{13}C$ values relative to krill at northern latitudes (Figure 4.7). Large variation in 2013 sea ice krill $\delta^{13}C$ resulted in significantly lighter ($p<0.05$) $\delta^{13}C$ values in 2013 juveniles than adult krill (Figure 4.14; Table 4.9), a result not seen in 2013, 2014, and 2015 near Anvers Island (Table 4.9; Table 4.4, 4.5). Differences in 2013 $\delta^{13}C$ values could be attributed to higher lipid content as adult krill had a higher mean C:N ratio than juvenile krill (6.8 and 4.3 respectively). The opposite was true in 2015 where juveniles had significantly higher $\delta^{13}C$ values ($p<0.05$) than co-located adult krill, typical of coastal krill feeding nearshore at northern latitudes (Table 4.4; Figure 4.6). Higher $\delta^{13}C$ values in 2015 sea ice juveniles was not due to higher lipid content indicated by a lower mean C:N ratio than coastal adults (Table 4.3), but may be attributed to increased feeding on sea ice POM known to be a food source for Antarctic krill enriched in ^{13}C (Frazer 1996). Two distinct sub-populations of adult and juvenile krill were identified (Figure 4.14) based on $\delta^{13}C$ values that were either all higher or lower than the nearly identical mean $\delta^{13}C$ values for juvenile (-27.2±1.1) and adult (-27.2±1.4) krill. Mean $\delta^{13}C$ values of these two subpopulations (-28.2±0.4 and -26.0±0.4 respectively) were significantly different (Student's t-Test) at $P<0.001$ suggesting that mixed subpopulations of juvenile and adult krill were feeding together at the sea ice edge in 2014.

Mercury concentrations in *E. superba* subpopulations in proximity to sea ice edge

Variations in mercury concentrations in Antarctic krill at the sea ice edge follow some of the trends observed at northern latitudes, but also follow some trends unique to the south. As seen near Anvers Island, significantly higher ($P<0.05$) THg concentrations were measured in co-located juveniles than adult krill from southern stations in 2013 and 2014 (Table 4.9). However, in 2013, %MeHg concentrations in southern krill were higher in adults than juveniles, a result not observed between 2013-2015 sampling years near Anvers Island (Table 4.4, 4.9).

Across three sampling years, juvenile krill MeHg concentrations were significantly higher ($P<0.001$) than adult krill sampled at more southern latitudes (Figure 4.15). Although a similar result was seen in MeHg concentrations in juvenile and adult krill across years near Anvers Island (Figure 4.8), within year comparisons of co-located adult and juvenile krill MeHg concentrations were much more constant (Table 4.9). Only in 2014 were MeHg concentrations juvenile krill near the sea ice edge significantly higher ($P<0.05$) than adults, consistent with higher juvenile $\delta^{15}N$ values. Separation of foraging depths driven by juvenile krill development during a high sea ice year, may have created a new robust recruitment of developing juveniles (Saba et al. 2014) feeding at more mesopelagic depths and accumulating higher MeHg concentrations.

Southern latitude carbon and nitrogen isotope ratios in relation to mercury accumulation in *E. superba*

As a linear correlation between $\delta^{13}C$ and $\delta^{15}N$ values in sea ice krill was observed between years, especially in adult krill (Figure 4.14), any positive relationship of Hg with $\delta^{13}C$, may also have a positive correlation to $\delta^{15}N$ values. Differing accumulation patterns of MeHg were observed at similar ranges of $\delta^{13}C$ values for juvenile and adult krill sampled at the sea ice edge (Figure 4.16). A very strong positive relationship (R^2=1.0) between adult mean MeHg concentrations and $\delta^{13}C$ values demonstrates a strong coupling between these measurements in sea ice edge adult krill. Higher accumulation of MeHg in sea ice juveniles with similar $\delta^{13}C$ values to adults suggests separate accumulation of MeHg feeding under sea ice or at mesopelagic depths at similar foraging locations. Another strong positive correlation (R^2=1.0) between MeHg and $\delta^{15}N$ values, indicates that trophic position of adult krill may dictate MeHg accumulation at the sea ice edge as no spatial trends in $\delta^{13}C$ and $\delta^{15}N$ values from 2014 POM along the WAP were observed. These accumulation patterns of MeHg in sea ice krill differed from juveniles and adult Antarctic krill at northern latitudes, which found a positive relationship between $\delta^{13}C$ and MeHg in juvenile and adult krill across all sampling seasons, while no relationship existed between $\delta^{15}N$ and MeHg (Figures 4.11 and 4.13). During development methylmercury tends to accumulate at higher concentrations within larger, higher trophic level individuals of the same species in aquatic environments (Lescord et al. 2015). The possibility of trophic position having a robust influence on MeHg accumulation in adult and juvenile krill at the sea ice edge is more likely due to

persistence of sea ice year-round at these locations providing year-long stability in food web structure not seen in open ocean waters in the north during the austral summer.

MeHg Enrichment in WAP food web

The enrichment of methylmercury seen here, which is similar to that observed in other temperate marine food webs (Hammerschmidt and Fitzgerald 2006a, Mason et al. 2012), but somewhat lower than that observed in a pelagic food web in the Arctic (Ruus et al. 2015), shows that the accumulation of MeHg in krill has the potential to support much higher MeHg accumulation in top predators of Antarctic food webs, as elsewhere in the ocean.

Biomagnification of MeHg in krill relative to MeHg in surface POM varies considerably between adults and juveniles and differences in feeding location and depth, prey, and differences in internalization of MeHg likely influence the concentration of this compound in krill. Some adult krill had lower MeHg concentrations than POM prey while juveniles have the potential to increase tissue MeHg by up to a factor of 8. Differences in enrichment of MeHg in this keystone species will dictate MeHg concentrations at higher levels of the food web.

The enrichment of MeHg in krill and penguins indicates that MeHg may be used as a tracer of food web connectivity in this highly productive, remote marine ecosystem. In addition, the observed variation in MeHg accumulation among life stages and sub-populations of Antarctic krill and among different species of sympatric penguins, which occupy different ^{13}C and ^{15}N-defined trophic niches, demonstrates the potential use of MeHg to examine trophic linkages not only among, but also within trophic positions.

F. Conclusion

Developmental stage and feeding near the coast or sea ice are important to mercury accumulation in Antarctic krill and feeding depth and diet appear to be important to the accumulation of mercury in three species of *Pygoscelis* penguins living near Anvers Island. Small differences in trophic position between subpopulations of krill or sympatric species of penguins do not strongly affect mercury accumulation within these two groups of consumers. While the biomagnification of MeHg between krill and penguins living near the WAP cannot yet be quantified, our results for MeHg in krill and those for THg in various penguin tissues from this and previous studies (dos Santos et al. 2006) indicate a large trophic enrichment of MeHg in penguin feathers relative to their krill prey from this region. Together our results highlight the importance of quantifying MeHg and its potential use as a chemical tracer of feeding location and diet at the base of coastal Antarctic marine ecosystems.

Chapter V Conclusions and future research

Across multiple phytoplankton taxa and temperate and polar conditions, MeHg uptake increased with decreasing DOC_{SOW} concentrations. At low DOC_{SOW} MeHg uptake was higher in *Thalassiosira pseudonana* (*Tp*) (20.6 attmol/cell/hr) amongst marine diatoms at cell densities ~ 10^4 cells mL^{-1} in the experimental medium, while the highest MeHg uptake rate of all phytoplankton taxa was measured in the polar prymnesiophyte *Phaeocystis antarctica* (*Pa*) (249 attmol/cell/hr) at a free-living cell density (10^3 cells mL^{-1}). The high range of MeHg uptake in Antarctic phytoplankton in low DOC conditions (14.3 to 249 attmol/cell/hr) needs to be considered when evaluating MeHg enrichment in more open ocean, offshore conditions in Antarctic surface waters. A strong relationship of MeHg uptake with SA/V found only in temperate diatom cells suggests that SA/V dictates MeHg entrance into cells in temperate open ocean conditions, where DOC concentrations are low while temperature may affect MeHg uptake between cells with similar size and morphology. Methylmercury chloride uptake rate constants reveal lower values in *Tw* (one order of magnitude) in comparison to other studies. Methylmercury exposure concentration needs to be considered as lower MeHg exposures yield higher uptake rates.

Uptake rates between MeHgCl and MeHgCys treatments at a middle DOC_{SOW} (216 µM) were almost identical (0.79 and 0.83 attmol/cell/hr) in *Tp* and in fact considerably lower (0.4 and 0.05 attmol/cell/hr) in *Tw* at high DOC_{SOW} (> 800 µM) suggesting an amino acid transporter involved in the uptake of MeHgCys possibly dicated by cellular nitrogen demand. Long-term uptake rates in *Tw* and *Tp* were all less

than < 1 attmol/cell/hr and were lower than MeHgCys uptake rates. These results suggest an alternate route of active uptake after speciation of MeHg speciation may have shifted and bound to excreted DOC from phytoplankton cells in response to 10 nM exposure. Future studies should focus on MeHg uptake in additions of natural DOC and clarifying cytoplasm and cell wall, membrane fractions in short-term uptake.

Cb live cells of had noticeably lower wash efficiency (84%) than the temperate diatom *Tw* (96%) contributing evidence that surface MeHg may be an important fraction to consider when assessing bioavailability of this bound MeHg in polar phytoplankton and its subsequent transfer to polar zooplankton, such as Antarctic krill.

Heterogeneity in Hg concentrations was observed in surface waters and within vertical distributions along the WAP at northern, mid, and southern, coastal and offshore sampling sites. Total mercury ranged considerably between lower values at northern sites (0.97 to 3.76 pM) to high concentrations at mid and southern sites containing a subsurface THg concentration higher than any previous THg seawater measurements in the Arctic (16.6 pM). This maximum was sampled in proximity to sea ice in southern latitudes suggesting a concentrated source from melting sea ice in the austral summers to underlying waters.

Vertical distributions of MeHg varied considerably (non-detectable to 0.92 pM) as MeHg concentrations and %MeHg concentrations were at high latidudes ~65°S at a coastal site near Anvers Island with a subsurface MeHg maximium (0.92 pM) measured at intermediate depths within the productive Palmer deep canyon. Remineralization of POM may have resulted in release of Hg within regions of high apparent oxygen utilization following an earlier phytoplankton bloom. Whether there is MeHg associated

with sinking POM or it is released upon remineralization remains unanswered and future vertical POM MeHg distributions would aid in answering these questions. Offshore MeHg maxima were in the center of shoaling circumpolar deep water (CDW) bring high temperatures and nutrients due to age and remineralization known to occur in these older circulated waters from other ocean basins. Measuring methylation rates in CDW and modified CDW to determine the possibility of "in-situ" methylation in continental shelf waters or whether MeHg is largely advected onshore will help aid in understanding of MeHg sources along the WAP.

Surface dissolved elemental concentrations (DEM) exhibited a coastal-offshore gradient with concentrations (0.3 pM) near the shore in northern productive waters while surface POM exhibited an opposite trend with higher tissue concentrations measured offshore at northern and southern sites in less productive waters (2.12 to 7.49 ng_{MeHg}/g_{totbio}, 2014; 0.48 to 4.83 ng_{MeHg}/g_{totbio}) likely attributed to a lesser affect of biodilution of MeHg concentrations per phytoplankton biomass. The lowering of MeHg biodilution producing higher concentrations in 2015 southern surface POM (1.26 to 7.25 ng_{MeHg}/g_{totbio}) may contribute to higher MeHg concentrations in 2015 sea ice edge adult and juvenile krill (1.5±0.6 and 2.1±0.7 ng g^{-1} resp.) than 2015 northern krill sampled near Anvers Island (0.7±0.5 and 1.4±0.9 ng g^{-1}; adult and juvenile).

Near Anvers Island (~65°S) THg and MeHg in northern latitude Antarctic krill were significantly lower in adults (4 to 12.6 ng g^{-1}, THg; 0.3 to 1.6 ng g^{-1}, MeHg) than juveniles (7.8 to 19.4 ng g^{-1}, THg; 0.7 to 2.9 ng g^{-1}, MeHg) across four austral summers ($p < 0.005$ and $p < 0.001$, resp.). Methylmercury concentrations in juvenile and adult krill were found to be positively correlated ($p<0.05$, $R^2=0.50$) with $\delta^{13}C$ values that were

higher near the coast suggesting the importance of MeHg sources in nearshore sites and sea ice POM, known to be enriched in ^{13}C relative to seawater POM. Sea ice dynamics were thought to drive ecosystem processes along the peninsula potentially creating earlier phytoplankton blooms in 2015 than 2014 due to earlier retreat providing forcing on MeHg formation in nearshore environments.

Body feathers were opportunistically sampled from krill-dependent *Pygoscelis* penguin predators (Adélie (*P. adeliae*), gentoo (*P. papua*), and chinstrap (*P. antarctica*)) breeding sympatrically near Anvers Island. Mean concentrations of Hg in feathers was significantly ($p < 0.05$) higher in chinstrap (0.80±0.20 μg g^{-1}) than sympatric breeding Adélie (0.09±0.05 μg g^{-1}) and gentoo (0.16±0.08 μg g^{-1}) penguins. Relative to other regions of the Southern Ocean, these *Pygoscelis* feather Hg concentrations are low and are likely attributed to low MeHg concentrations in Antarctic krill. Although the WAP receives high incidences of Hg from seawater near Anvers Island, accumulated MeHg in POM in this region was lower than POM sampled further offshore. A small range in $\delta^{13}C$ values of *Pygoscelis* (24.5 – 27.2‰) and no significantly difference between species ($p = 1.00$ for all comparisons) suggests these 2011 penguin species were foraging in productive local waters. Anvers Island is a region of high productivity and potentially high MeHg biodilution and surface adsorption to cell surfaces of polar phytoplankton keeping MeHg concentrations generally low in Antarctic krill, as mean MeHg concentrations in our Antarctic krill samples did not exceeded 3 ng g^{-1}. These findings suggest that the WAP ecosystem although receiving high incidences of Hg from the seawater currently accumulate MeHg at low levels with the potential to support much higher MeHg accumulation in WAP top predators.

Work Cited

Agusa, T., T. Matsumoto, T. Ikemoto, Y. Anan, R. Kubota, G. Yasunaga, T. Kunito, S. Tanabe, H. Ogi, and Y. Shibata. 2005. Body distribution of trace elements in black-tailed gulls from Rishiri Island, Japan: Age-dependent accumulation and transfer to feathers and eggs. Environmental Toxicology and Chemistry **24**:2107-2120.

Al-Farawati, R., and C. M. G. van den Berg. 2001. Thiols in Coastal Waters of the Western North Sea and English Channel. Environmental Science & Technology **35**:1902-1911.

Al-Reasi, H. A., F. A. Ababneh, and D. R. Lean. 2007. Evaluating mercury biomagnification in fish from a tropical marine environment using stable isotopes (δ13C AND δ15N). Environmental Toxicology and Chemistry **26**:1572-1581.

Alderighi, L., P. Gans, S. Midollini, and A. Vacca. 2003. Co-ordination chemistry of the methylmercury(II) ion in aqueous solution: a thermodynamic investigation. Inorganica Chimica Acta **356**:8-18.

Amirbahman, A., A. L. Reid, T. A. Haines, J. S. Kahl, and C. Arnold. 2002. Association of Methylmercury with Dissolved Humic Acids. Environmental Science & Technology **36**:690-695.

Amyot, M., G. A. Gill, and F. M. M. Morel. 1997. Production and loss of dissolved gaseous mercury in coastal seawater. Environmental Science & Technology **31**:3606-3611.

Anderson, J. B. 2002. Antarctic Marine Geology. Cambridge University Press, Cambridge, UK.

Anderson, O. R. J., R. A. Phillips, R. A. McDonald, R. F. Shore, R. A. R. McGill, and S. Bearhop. 2009. Influence of trophic position and foraging range on mercury levels within a seabird community. Marine Ecology Progress Series **375**:277-288.

Andersson, M. E., K. Gardfeldt, I. Wangberg, and D. Stromberg. 2008a. Determination of Henry's law constant for elemental mercury. Chemosphere **73**:587-592.

Andersson, M. E., J. Sommar, K. Gardfeldt, and O. Lindqvist. 2008b. Enhanced concentrations of dissolved gaseous mercury in the surface waters of the Arctic Ocean. Marine Chemistry **110**:190-194.

Annett, A. L., J. N. Fitzsimmons, M. J. M. Séguret, M. Lagerström, M. P. Meredith, O. Schofield, and R. M. Sherrell. 2017. Controls on dissolved and particulate iron distributions in surface waters of the Western Antarctic Peninsula shelf. Marine Chemistry **196**:81-97.

Arai, T., T. Ikemoto, A. Hokura, Y. Terada, T. Kunito, S. Tanabe, and I. Nakai. 2004. Chemical forms of mercury and cadmium accumulated in marine mammals and seabirds as determined by XAFS analysis. Environmental Science & Technology **38**:6468-6474.

Aschner, M., and T. W. Clarkson. 1988. UPTAKE OF METHYLMERCURY IN THE RAT-BRAIN - EFFECTS OF AMINO-ACIDS. Brain Research **462**:31-39.

Bargagli, R. 2001. Trace metals in Antarctic organisms and the development of circumpolar biomonitoring networks. Pages 53-110 Reviews of Environmental Contamination and Toxicology. Springer-Verlag New York Inc. {a} , 175 Fifth Avenue, New York, NY, 10010-7858, USA.

Bargagli, R. 2008. Environmental contamination in Antarctic ecosystems. Science of the Total Environment **400**:212-226.

Bargagli, R., C. Agnorelli, F. Borghini, and F. Monaci. 2005. Enhanced deposition and bioaccumulation of mercury in Antarctic terrestrial ecosystems facing a coastal polynya. Environmental Science & Technology **39**:8150-8155.

Bargagli, R., F. Monaci, J. C. Sanchez-Hernandez, and D. Cateni. 1998. Biomagnification of mercury in an Antarctic marine coastal food web. Pages 65-76.

Barkay, T., N. Kroer, and A. J. Poulain. 2011. Some like it cold: microbial transformations of mercury in polar regions. Polar Research **30**:15.

Barkay, T., S. M. Miller, and A. O. Summers. 2003. Bacterial mercury resistance from atoms to ecosystems. Fems Microbiology Reviews **27**:355-384.

Barkay, T., R. R. Turner, A. Vandenbrook, and C. Liebert. 1991. THE RELATIONSHIPS OF HG(II) VOLATILIZATION FROM A FRESH-WATER POND TO THE ABUNDANCE OF MER-GENES IN THE GENE POOL OF THE INDIGENOUS MICROBIAL COMMUNITY. Microbial Ecology **21**:151-161.

Barrera-Oro, E. 2003. The role of fish in the Antarctic marine food web: differences between inshore and offshore waters in the southern Scotia Arc and west Antarctic Peninsula. Antarctic Science **14**:293-309.

Beattie, S. A., D. Armstrong, A. Chaulk, J. Comte, M. Gosselin, and F. Y. Wang. 2014. Total and Methylated Mercury in Arctic Multiyear Sea Ice. Environmental Science & Technology **48**:5575-5582.

Becker, P. H., R. W. Furness, and D. Henning. 1993. THE VALUE OF CHICK FEATHERS TO ASSESS SPATIAL AND INTERSPECIFIC VARIATION IN THE MERCURY CONTAMINATION OF SEABIRDS. Environmental Monitoring and Assessment **28**:255-262.

Becker, P. H., J. Gonzalez-Solis, B. Behrends, and J. Croxall. 2002. Feather mercury levels in seabirds at South Georgia: influence of trophic position, sex and age. Marine Ecology Progress Series **243**:261-269.

Ben-Bassat, D., and A. M. Mayer. 1977. Reduction of Mercury Chloride by Chlorella: Evidence for a Reducing Factor. Physiologia Plantarum **40**:157-162.

Benoit, J. M., R. P. Mason, C. C. Gilmour, and G. R. Aiken. 2001. Constants for mercury binding by dissolved organic matter isolates from the Florida Everglades. Geochimica Et Cosmochimica Acta **65**:4445-4451.

Biller, D. V., and K. W. Bruland. 2012. Analysis of Mn, Fe, Co, Ni, Cu, Zn, Cd, and Pb in seawater using the Nobias-chelate PA1 resin and magnetic sector inductively coupled plasma mass spectrometry (ICP-MS). Marine Chemistry **130**:12-20.

Bloom, N. S. 1992. ON THE CHEMICAL FORM OF MERCURY IN EDIBLE FISH AND MARINE INVERTEBRATE TISSUE. Canadian Journal of Fisheries and Aquatic Sciences **49**:1010-1017.

Bond, A. L., and A. W. Diamond. 2009. Total and Methyl Mercury Concentrations in Seabird Feathers and Eggs. Archives of Environmental Contamination and Toxicology **56**:286-291.

Bowman, K. L., and C. R. Hammerschmidt. 2011. Extraction of monomethylmercury from seawater for low-femtomolar determination. Limnology and Oceanography-Methods **9**:121-128.

Brasso, R. L., S. Abel, and M. J. Polito. 2012. Pattern of Mercury Allocation into Egg Components is Independent of Dietary Exposure in Gentoo Penguins. Archives of Environmental Contamination and Toxicology **62**:494-501.

Brasso, R. L., A. Chiaradia, M. J. Polito, A. R. Rey, and S. D. Emslie. 2015. A comprehensive assessment of mercury exposure in penguin populations throughout the Southern Hemisphere: Using trophic calculations to identify sources of population-level variation. Marine Pollution Bulletin **97**:408-418.

Brasso, R. L., B. E. Drummond, S. R. Borrett, A. Chiaradia, M. J. Polito, and A. R. Rey. 2013. Unique Pattern of Molt Leads to Low Intraindividual Variation in Feather Mercury Concentrations in Penguins. Environmental Toxicology and Chemistry **32**:2331–2334.

Brasso, R. L., and M. J. Polito. 2013. Trophic calculations reveal the mechanism of population-level variation in mercury concentrations between marine ecosystems: Case studies of two polar seabirds. Marine Pollution Bulletin **75**:244-249.

Brasso, R. L., M. J. Polito, and S. D. Emslie. 2014. Multi-tissue analyses reveal limited inter-annual and seasonal variation in mercury exposure in an Antarctic penguin community. Ecotoxicology **23**:1494-1504.

Braune, B. M., and D. E. Gaskin. 1987. MERCURY LEVELS IN BONAPARTES GULLS (LARUS-PHILADELPHIA) DURING AUTUMN MOLT IN THE QUODDY REGION, NEW-BRUNSWICK, CANADA. Archives of Environmental Contamination and Toxicology **16**:539-549.

Braune, B. M., A. J. Gaston, K. A. Hobson, H. G. Gilchrist, and M. L. Mallory. 2014. Changes in Food Web Structure Alter Trends of Mercury Uptake at Two Seabird Colonies in the Canadian Arctic. Environmental Science & Technology **48**:13246-13252.

Bridges, C. C., C. Bauch, F. Verrey, and R. K. Zalups. 2004. Mercuric Conjugates of Cysteine Are Transported by the Amino Acid Transporter System b(0,+): Implications of Molecular Mimicry. Journal of the American Society of Nephrology : JASN **15**:663-673.

Brinza, L., M. J. Dring, and M. Gavrilescu. 2007. Marine micro and macro algal species as biosorbents for heavy metals. Environmental Engineering and Management Journal **6**:237-251.

Buesseler, K. O., A. M. P. McDonnell, O. M. E. Schofield, D. K. Steinberg, and H. W. Ducklow. 2010. High particle export over the continental shelf of the west Antarctic Peninsula. Geophysical Research Letters **37**:5.

Burger, J., and M. Gochfeld. 2011. Mercury and selenium levels in 19 species of saltwater fish from New Jersey as a function of species, size, and season. Science of the Total Environment **409**:1418-1429.

Burt, A., F. Y. Wang, M. Pucko, C. J. Mundy, M. Gosselin, B. Philippe, M. Poulin, J. E. Tremblay, and G. A. Stern. 2013. Mercury uptake within an ice algal community during the spring bloom in first-year Arctic sea ice. Journal of Geophysical Research-Oceans **118**:4746-4754.

Campbell, L. M., R. J. Norstrom, K. A. Hobson, D. C. G. Muir, S. Backus, and A. T. Fisk. 2005. Mercury and other trace elements in a pelagic Arctic marine food web (Northwater Polynya, Baffin Bay). Science of the Total Environment **351**:247-263.

Carravieri, A., P. Bustamante, C. Churlaud, and Y. Cherel. 2013. Penguins as bioindicators of mercury contamination in the Southern Ocean: Birds from the Kerguelen Islands as a case study. Science of the Total Environment **454**:141-148.

Carvalho, F., J. Kohut, M. J. Oliver, and O. Schofield. 2017. Defining the ecologically relevant mixed-layer depth for Antarctica's coastal seas. Geophysical Research Letters **44**:338-345.

Chakraborty, L. B., A. Qureshi, C. Vadenbo, and S. Hellweg. 2013. Anthropogenic Mercury Flows in India and Impacts of Emission Controls. Environmental Science & Technology **47**:8105-8113.

Chapman, E. W., E. E. Hofmann, D. L. Patterson, and W. R. Fraser. 2010. The effects of variability in Antarctic krill (Euphausia superba) spawning behavior and sex/maturity stage distribution on Adelie penguin (Pygoscelis adeliae) chick growth: A modeling study. Deep-Sea Research Part Ii-Topical Studies in Oceanography **57**:543-558.

Chaulk, A., G. A. Stern, D. Armstrong, D. G. Barber, and F. Y. Wang. 2011. Mercury Distribution and Transport Across the Ocean-Sea-Ice-Atmosphere Interface in the Arctic Ocean. Environmental Science & Technology **45**:1866-1872.

Chen, C., A. Amirbahman, N. Fisher, G. Harding, C. Lamborg, D. Nacci, and D. Taylor. 2008. Methylmercury in Marine Ecosystems: Spatial Patterns and Processes of Production, Bioaccumulation, and Biomagnification. Ecohealth **5**:399-408.

Chen, C. Y., M. E. Borsuk, D. M. Bugge, T. Hollweg, P. H. Balcom, D. M. Ward, J. Williams, and R. P. Mason. 2014. Benthic and Pelagic Pathways of Methylmercury Bioaccumulation in Estuarine Food Webs of the Northeast United States. Plos One **9**:11.

Chen, C. Y., M. Dionne, B. M. Mayes, D. M. Ward, S. Sturup, and B. P. Jackson. 2009. Mercury Bioavailability and Bioaccumulation in Estuarine Food Webs in the Gulf of Maine. Environmental Science & Technology **43**:1804-1810.

Cherel, Y., K. A. Hobson, F. R. Bailleul, and R. Groscolas. 2005. Nutrition, physiology, and stable isotopes: New information from fasting and molting penguins. Ecology **86**:2881-2888.

Chiuchiolo, A. L., R. M. Dickhut, M. A. Cochran, and H. W. Ducklow. 2004. Persistent organic pollutants at the base of the Antarctic marine food web. Environmental Science & Technology **38**:3551-3557.

Choy, C. A., B. N. Popp, J. J. Kaneko, and J. C. Drazen. 2009. The influence of depth on mercury levels in pelagic fishes and their prey. Proceedings of the National Academy of Sciences of the United States of America **106**:13865-13869.

Church, M. J. 2008. Resource Control of Bacterial Dynamics in the Sea. Pages 335-382 Microbial Ecology of the Oceans. John Wiley & Sons, Inc.

Cimino, M. A., M. A. Moline, W. R. Fraser, D. L. Patterson-Fraser, and M. J. Oliver. 2016. Climate-driven sympatry may not lead to foraging competition between congeneric top-predators. Scientific Reports **6**:18820.

Clarkson, T. W., and L. Magos. 2006. The toxicology of mercury and its chemical compounds. Critical Reviews in Toxicology **36**:609-662.

Compeau, G. C., and R. Bartha. 1985. Sulfate-Reducing Bacteria - Principal Methylators of Mercury in Anoxic Estuarine Sediment. Applied and Environmental Microbiology **50**:498-502.

Cook, A. J., A. J. Fox, D. G. Vaughan, and J. G. Ferrigno. 2005. Retreating glacier fronts on the Antarctic Peninsula over the past half-century. Science **308**:541-544.

Cook, A. J., P. R. Holland, M. P. Meredith, T. Murray, A. Luckman, and D. G. Vaughan. 2016. Ocean forcing of glacier retreat in the western Antarctic Peninsula. Science **353**:283-286.

Cook, A. J., D. G. Vaughan, A. J. Luckman, and T. Murray. 2014. A new Antarctic Peninsula glacier basin inventory and observed area changes since the 1940s. Antarctic Science **26**:614-624.

Coplen, T. B., W. A. Brand, M. Gehre, M. Groning, H. A. J. Meijer, B. Toman, and R. M. Verkouteren. 2006. New guidelines for delta C-13 measurements. Analytical Chemistry **78**:2439-2441.

Corbitt, E. S., D. J. Jacob, C. D. Holmes, D. G. Streets, and E. M. Sunderland. 2014. Global Source-Receptor Relationships for Mercury Deposition Under Present-Day and 2050 Emissions Scenarios. Environmental Science & Technology **45**:10477-10484.

Cordy, P., M. Veiga, B. Crawford, O. Garcia, V. Gonzalez, D. Moraga, M. Roeser, and D. Wip. 2013. Characterization, mapping, and mitigation of mercury vapour emissions from artisanal mining gold shops. Environmental Research **125**:82-91.

Cossa, D., M. Harmelin-Vivien, C. Mellon-Duval, V. Loizeau, B. Averty, S. Crochet, L. Chou, and J. F. Cadiou. 2012. Influences of Bioavailability, Trophic Position, and Growth on Methylmercury in Hakes (Merluccius merluccius) from Northwestern Mediterranean and Northeastern Atlantic. Environmental Science & Technology **46**:4885-4893.

Cossa, D., L. E. Heimburger, D. Lannuzel, S. R. Rintoul, E. C. V. Butler, A. R. Bowie, B. Averty, R. J. Watson, and T. Remenyi. 2011. Mercury in the Southern Ocean. Geochimica Et Cosmochimica Acta **75**:4037-4052.

Couto, N., D. G. Martinson, J. Kohut, and O. Schofield. 2017. Distribution of Upper Circumpolar Deep Water on the warming continental shelf of the West Antarctic Peninsula. Journal of Geophysical Research: Oceans:n/a-n/a.

Cozzi, S., and C. Cantoni. 2010. Stable isotope (δ13C and δ15N) composition of particulate organic matter, nutrients and dissolved organic matter during spring ice retreat at Terra Nova Bay. Antarctic Science **23**:43-56.

Cross, F. A., D. W. Evans, and R. T. Barber. 2015. Decadal Declines of Mercury in Adult Bluefish (1972-2011) from the Mid-Atlantic Coast of the USA. Environmental Science & Technology **49**:9064-9072.

Cuscov, M., and F. L. L. Muller. 2015. Differentiating humic and algal surface active substances in coastal waters by their pH-dependent adsorption behaviour. Marine Chemistry **174**:35-45.

Daly, K. L. 1990. Overwintering Development, Growth, and Feeding of Larval Euphausia-Superba in the Antarctic Marginal Ice-Zone. Limnology and Oceanography **35**:1564-1576.

Daly, K. L. 2004. Overwintering growth and development of larval Euphausia superba: an interannual comparison under varying environmental conditions west of the Antarctic Peninsula. Deep-Sea Research Part Ii-Topical Studies in Oceanography **51**:2139-2168.

Daly, K. L., and J. J. Zimmerman. 2004. Comparisons of morphology and neritic distributions of Euphausia crystallorophias and Euphausia superba furcilia during autumn and winter west of the Antarctic Peninsula. Polar Biology **28**:72-81.

Davidson, A. T., and H. J. Marchant. 1987. BINDING OF MANGANESE BY ANTARCTIC PHAEOCYSTIS-POUCHETII AND THE ROLE OF BACTERIA IN ITS RELEASE. Marine Biology **95**:481-487.

Davis, L. S., and M. Renner. 2003. Penguins. Pages 1-212 Penguins. T & A D Poyser.

DiTullio, G. R., and W. O. Smith. 1996. Spatial patterns in phytoplankton biomass and pigment distributions in the Ross Sea. Journal of Geophysical Research-Oceans **101**:18467-18477.

dos Santos, I. R., E. V. Silva, C. Schaefer, S. M. Sella, C. A. Silva, V. Gomes, M. Passos, and P. V. Ngan. 2006. Baseline mercury and zinc concentrations in terrestrial and coastal organisms of Admiralty Bay, Antarctica. Environmental Pollution **140**:304-311.

Douglas, T., M. Amyot, T. Barkay, T. Berg, J. Chételat, P. Constant, A. Dommergue, M. Evans, C. Ferrari, N. Gantner, M. Johnson, J. Kirk, N. Kroer, C. Larose, D. Lean, L. Loseto, R. W. Macdonald, D. Muir, T. Nielsen, and C. Zdanowicz. 2011. What is the Fate of Mercury Entering the Arctic Environment?

Douglas, T. A., M. Sturm, J. D. Blum, C. Polashensld, S. Stuefer, C. Hiemstra, A. Steffen, S. Filhol, and R. Prevost. 2017. A Pulse of Mercury and Major Ions in Snowmelt Runoff from a Small Arctic Alaska Watershed. Environmental Science & Technology **51**:11145-11155.

Drevnick, P. E., D. R. Engstrom, C. T. Driscoll, E. B. Swain, S. J. Balogh, N. C. Kamman, D. T. Long, D. G. C. Muir, M. J. Parsons, K. R. Rolfhus, and R. Rossmann. 2012. Spatial and temporal patterns of mercury accumulation in lacustrine sediments across the Laurentian Great Lakes region. Environmental Pollution **161**:252-260.

Driscoll, C. T., R. P. Mason, H. M. Chan, D. J. Jacob, and N. Pirrone. 2013. Mercury as a Global Pollutant: Sources, Pathways, and Effects. Environmental Science & Technology **47**:4967-4983.

Ducklow, H. W., M. L. Dickson, D. L. Kirchman, G. Steward, J. Orchardo, J. Marra, and F. Azam. 2000. Constraining bacterial production, conversion efficiency and respiration in the

Ross Sea, Antarctica, January-February, 1997. Deep-Sea Research Part Ii-Topical Studies in Oceanography **47**:3227-3247.

Ducklow, H. W., W. Fraser, D. M. Karl, L. B. Quetin, R. M. Ross, R. C. Smith, S. E. Stammerjohn, M. Vernet, and R. M. Daniels. 2006. Water-column processes in the West Antarctic Peninsula and the Ross Sea: Interannual variations and foodweb structure. Deep-Sea Research Part Ii-Topical Studies in Oceanography **53**:834-852.

Ducklow, H. W., O. Schofield, M. Vernet, S. Stammerjohn, and M. Erickson. 2012. Multiscale control of bacterial production by phytoplankton dynamics and sea ice along the western Antarctic Peninsula: A regional and decadal investigation. Journal of Marine Systems **98-99**:26-39.

Dupont, C. L., and B. A. Ahner. 2005. Effects of copper, cadmium, and zinc on the production and exudation of thiols by Emiliania huxleyi. Limnology and Oceanography **50**:508-515.

Dupont, C. L., J. W. Moffett, R. R. Bidigare, and B. A. Ahner. 2006. Distributions of dissolved and particulate biogenic thiols in the subartic Pacific Ocean. Deep-Sea Research Part I-Oceanographic Research Papers **53**:1961-1974.

Dupont, C. L., R. K. Nelson, S. Bashir, J. W. Moffett, and B. A. Ahner. 2004. Novel copper-binding and nitrogen-rich thiols produced and exuded by Emiliania huxleyi. Limnology and Oceanography **49**:1754-1762.

Ebinghaus, R., H. H. Kock, C. Temme, J. W. Einax, A. G. Lowe, A. Richter, J. P. Burrows, and W. H. Schroeder. 2002. Antarctic springtime depletion of atmospheric mercury. Environmental Science & Technology **36**:1238-1244.

Evers, D. C., Y. J. Han, C. T. Driscoll, N. C. Kamman, M. W. Goodale, K. F. Lambert, T. M. Holsen, C. Y. Chen, T. A. Clair, and T. Butler. 2007. Biological mercury hotspots in the northeastern United States and southeastern Canada. Bioscience **57**:29-43.

Fisher, N. S., and R. P. Schwarzenbach. 1978. FATTY-ACID DYNAMICS IN THALASSIOSIRA-PSEUDONANA BACILLARIOPHYCEAE IMPLICATIONS FOR PHYSIOLOGICAL ECOLOGY. Journal of Phycology **14**:143-150.

Fitzgerald, W. 1989. Atmospheric and oceanic cycling of mercury. Chemical Oceanography, vol. 10. Academic Press, London, UK, Chemical Oceanography.

Fitzgerald, W. F., D. R. Engstrom, R. P. Mason, and E. A. Nater. 1998. The case for atmospheric mercury contamination in remote areas. Environmental Science & Technology **32**:1-7.

Fitzgerald, W. F., C. H. Lamborg, and C. R. Hammerschmidt. 2007. Marine biogeochemical cycling of mercury. Chemical Reviews **107**:641-662.

Fitzgerald, W. F., C. C. Patterson, T. M. Church, and D. M. Settle. 1999. Clean hands : Clair Patterson's crusade against environmental lead contamination. Nova Scientific Publishers, Inc., Commack, N.Y.

Fraser, W. R., and E. E. Hofmann. 2003. A predator's perspective on causal links between climate change, physical forcing and ecosystem response. Marine Ecology Progress Series **265**:1-15.

Fraser, W. R., and W. Z. Trivelpiece. 2013. Factors Controlling the Distribution of Seabirds: Winter-Summer Heterogeneity in the Distribution of AdéLie Penguin Populations. Pages 257-272 Foundations for Ecological Research West of the Antarctic Peninsula. American Geophysical Union.

Frazer, T. K. 1996. Stable isotope composition (delta C-13 and delta N-15) of larval krill, Euphausia superba, and two of its potential food sources in winter. Journal of Plankton Research **18**:1413-1426.

Frazer, T. K., Quetin L.B., and R. M. Ross. 2002a. Energetic demands of larval krill, Euphausia superba, in winter. Journal of Experimental Marine Biology and Ecology **277**:157–171.

Frazer, T. K., L. B. Quetin, and R. A. Ross. 2002b. Energetic demands of larval krill, Euphausia superba, in winter. Journal of Experimental Marine Biology and Ecology **277**:157-171.

Fromant, A., A. Carravieri, P. Bustamante, P. Labadie, H. Budzinski, L. Peluhet, C. Churlaud, O. Chastel, and Y. Cherel. 2016. Wide range of metallic and organic contaminants in various tissues of the Antarctic prion, a planktonophagous seabird from the Southern Ocean. Science of the Total Environment **544**:754-764.

Furness, R. W., S. J. Muirhead, and M. Woodburn. 1986. USING BIRD FEATHERS TO MEASURE MERCURY IN THE ENVIRONMENT - RELATIONSHIPS BETWEEN MERCURY CONTENT AND MOLT. Marine Pollution Bulletin **17**:27-30.

Gantner, N., H. Hintelmann, W. Zheng, and D. C. Muir. 2009. Variations in Stable Isotope Fractionation of Hg in Food Webs of Arctic Lakes. Pages 9148-9154. Environmental Science Technology.

Gasol, J. M., and P. A. Del Giorgio. 2000. Using flow cytometry for counting natural planktonic bacteria and understanding the structure of planktonic bacterial communities. Scientia Marina **64**:197-224.

Gibson, J., T. Trull, P. Nichols, R. Summons, and A. McMinn. 1999. Sedimentation of 13C-rich organic matter from Antarctic sea-ice algae: A potential indicator of past sea-ice extent.

Gillies, C. L., J. S. Stark, G. J. Johnstone, and S. D. A. Smith. 2012a. Carbon flow and trophic structure of an Antarctic coastal benthic community as determined by delta C-13 and delta N-15. Estuarine Coastal and Shelf Science **97**:44-57.

Gillies, C. L., J. S. Stark, and S. D. A. Smith. 2012b. Research article: small-scale spatial variation of delta C-13 and delta N-15 isotopes in Antarctic carbon sources and consumers. Polar Biology **35**:813-827.

Gilmour, C. C., E. A. Henry, and R. Mitchell. 1992. SULFATE STIMULATION OF MERCURY METHYLATION IN FRESH-WATER SEDIMENTS. Environmental Science & Technology **26**:2281-2287.

Gionfriddo, C. M., M. T. Tate, R. R. Wick, M. B. Schultz, A. Zemla, M. P. Thelen, R. Schofield, D. P. Krabbenhoft, K. E. Holt, and J. W. Moreau. 2016. Microbial mercury methylation in Antarctic sea ice. Nature Microbiology **1**:16127.

Gordon, L. I., L. A. Codispoti, J. C. Jennings, F. J. Millero, J. M. Morrison, and C. Sweeney. 2000. Seasonal evolution of hydrographic properties in the Ross Sea, Antarctica, 1996-1997. Deep-Sea Research Part Ii-Topical Studies in Oceanography **47**:3095-3117.

Gorman, K. B., T. D. Williams, and W. R. Fraser. 2014. Ecological Sexual Dimorphism and Environmental Variability within a Community of Antarctic Penguins (Genus Pygoscelis). Plos One **9**:14.

Gorski, P. R., L. B. Cleckner, J. P. Hurley, M. E. Sierszen, and D. E. Armstrong. 2003. Factors afffecting enhanced mercury bioaccumulation in inland lakes of Isle Royale National Park, USA. Science of the Total Environment **304**:327-348.

Gosnell, K. J., and R. P. Mason. 2015. Mercury and methylmercury incidence and bioaccumulation in plankton from the central Pacific Ocean. Marine Chemistry **177**:772-780.

Grandjean, P., H. Satoh, K. Murata, and K. Eto. 2010. Adverse Effects of Methyl-mercury: Environmental Health Research Implications. Environmental Health Perspectives **118**:1137-1145.

Hammerschmidt, C. R., and K. L. Bowman. 2012. Vertical methylmercury distribution in the subtropical North Pacific Ocean. Marine Chemistry **132**:77-82.

Hammerschmidt, C. R., M. B. Finiguerra, R. L. Weller, and W. F. Fitzgerald. 2013. Methylmercury Accumulation in Plankton on the Continental Margin of the Northwest Atlantic Ocean. Environmental Science & Technology **47**:3671-3677.

Hammerschmidt, C. R., and W. F. Fitzgerald. 2005. Methylmercury in mosquitoes related to atmospheric mercury deposition and contamination. Environmental Science & Technology **39**:3034-3039.

Hammerschmidt, C. R., and W. F. Fitzgerald. 2006a. Bioaccumulation and trophic transfer of methylmercury in Long Island Sound. Archives of Environmental Contamination and Toxicology **51**:416-424.

Hammerschmidt, C. R., and W. F. Fitzgerald. 2006b. Methylmercury cycling in sediments on the continental shelf of southern New England. Geochimica Et Cosmochimica Acta **70**:918-930.

Hammerschmidt, C. R., and W. F. Fitzgerald. 2006c. Methylmercury in freshwater fish linked to atmospheric mercury deposition. Environmental Science & Technology **40**:7764-7770.

Hammerschmidt, C. R., and W. F. Fitzgerald. 2006d. Photodecomposition of methylmercury in an arctic Alaskan lake. Environmental Science & Technology **40**:1212-1216.

Hammerschmidt, C. R., and W. F. Fitzgerald. 2008. Sediment-water exchange of methylmercury determined from shipboard benthic flux chambers. Marine Chemistry **109**:86-97.

Hannides, C. C. S., B. N. Popp, M. R. Landry, and B. S. Graham. 2009. Quantification of zooplankton trophic position in the North Pacific Subtropical Gyre using stable nitrogen isotopes. Limnology and Oceanography **54**:50-61.

Harada, M. 1995. Minamata Disease - Methylmercury Poisoning in Japan Caused by Environmental-Pollution. Critical Reviews in Toxicology **25**:1-24.

Hartnett, H., S. Boehme, C. Thomas, D. DeMaster, and C. Smith. 2008. Benthic oxygen fluxes and denitrification rates from high-resolution porewater profiles from the Western Antarctic Peninsula continental shelf. Deep-Sea Research Part Ii-Topical Studies in Oceanography **55**:2415-2424.

Hedges, J. I. 2002. Chapter 1 - Why Dissolved Organics Matter A2 - Hansell, Dennis A. Pages 1-33 *in* C. A. Carlson, editor. Biogeochemistry of Marine Dissolved Organic Matter. Academic Press, San Diego.

Heimburger, L. E., J. E. Sonke, D. Cossa, D. Point, C. Lagane, L. Laffont, B. T. Galfond, M. Nicolaus, B. Rabe, and M. R. van der Loeff. 2015. Shallow methylmercury production in the marginal sea ice zone of the central Arctic Ocean. Scientific Reports **5**:6.

Hendry, K. R., and R. E. M. Rickaby. 2008. Opal (Zn/Si) ratios as a nearshore geochemical proxy in coastal Antarctica. Paleoceanography **23**:12.

Henley, S. F., R. E. Tuerena, A. L. Annett, A. E. Fallick, M. P. Meredith, H. J. Venables, A. Clarke, and R. S. Ganeshram. 2017. Macronutrient supply, uptake and recycling in the coastal ocean of the west Antarctic Peninsula. Deep-Sea Research Part Ii-Topical Studies in Oceanography **139**:58-76.

Herzi, F., A. S. Hlaili, C. Le Poupon, H. H. Mabrouk, and S. Mounier. 2013. Characterization of exudates released by the marine diatom Skeletonema costatum exposed to copper stress: a 3D-fluorescence spectroscopy approach. Biometals **26**:773-781.

Hindell, M. A., N. Brothers, and R. Gales. 1999. Mercury and cadmium concentrations in the tissues of three species of southern albatrosses. Polar Biology **22**:102-108.

Hinke, J. T., M. J. Polito, M. E. Goebel, S. Jarvis, C. S. Reiss, S. R. Thorrold, W. Z. Trivelpiece, and G. M. Watters. 2015. Spatial and isotopic niche partitioning during winter in chinstrap and Adelie penguins from the South Shetland Islands. Ecosphere **6**:32.

Hintelmann, H., and H. Nguyen. 2005. Extraction of methylmercury from tissue and plant samples by acid leaching. Analytical and Bioanalytical Chemistry **381**:360-365.

Hobson, K. A., and R. G. Clark. 1992. ASSESSING AVIAN DIETS USING STABLE ISOTOPES .1. TURNOVER OF C-13 IN TISSUES. Condor **94**:181-188.

Hollweg, T. A., C. C. Gilmour, and R. P. Mason. 2009. Methylmercury production in sediments of Chesapeake Bay and the mid-Atlantic continental margin. Pages 86-101.

Holmhansen, O., and B. G. Mitchell. 1991. SPATIAL AND TEMPORAL DISTRIBUTION OF PHYTOPLANKTON AND PRIMARY PRODUCTION IN THE WESTERN BRANSFIELD STRAIT REGION. Deep-Sea Research Part a-Oceanographic Research Papers **38**:961-980.

Honda, K., Y. Yamamoto, and R. Tatsukawa. 1987. Distribution of heavy metals in Antarctic marine ecosystem. Proceedings of the NIPR Symposium on Polar Biology:184-197.

Horvat, M., L. Liang, and N. S. Bloom. 1993. COMPARISON OF DISTILLATION WITH OTHER CURRENT ISOLATION METHODS FOR THE DETERMINATION OF METHYL MERCURY-COMPOUNDS IN LOW-LEVEL ENVIRONMENTAL-SAMPLES .2. WATER. Analytica Chimica Acta **282**:153-168.

Houde, S. E. L., and M. R. Roman. 1987. EFFECTS OF FOOD QUALITY ON THE FUNCTIONAL INGESTION RESPONSE OF THE COPEPOD ACARTIA-TONSA. Marine Ecology Progress Series **40**:69-77.

Ikemoto, T., T. Kunito, H. Tanaka, N. Baba, N. Miyazaki, and S. Tanabe. 2004. Detoxification mechanism of heavy metals in marine mammals and seabirds: Interaction of selenium with mercury, silver, copper, zinc, and cadmium in liver. Archives of Environmental Contamination and Toxicology **47**:402-413.

Jakimska, A., P. Konieczka, K. Skora, and J. Namiesnik. 2011. Bioaccumulation of Metals in Tissues of Marine Animals, Part I: the Role and Impact of Heavy Metals on Organisms. Polish Journal of Environmental Studies **20**:1117-1125.

Kahl, L. A., O. Schofield, and W. R. Fraser. 2010. Autonomous Gliders Reveal Features of the Water Column Associated with Foraging by Adelie Penguins. Integrative and Comparative Biology **50**:1041-1050.

Kawakami, S. K., M. Gledhill, and E. P. Achterberg. 2006. PRODUCTION OF PHYTOCHELATINS AND GLUTATHIONE BY MARINE PHYTOPLANKTON IN RESPONSE TO METAL STRESS1. Journal of Phycology **42**:975-989.

Kehrig, H. A., R. A. Hauser-Davis, T. G. Seixas, and G. Fillmann. 2015. Trace-elements, methylmercury and metallothionein levels in Magellanic penguin (Spheniscus magellanicus) found stranded on the Southern Brazilian coast. Marine Pollution Bulletin **96**:450-455.

Kerin, E. J., C. C. Gilmour, E. Roden, M. T. Suzuki, J. D. Coates, and R. P. Mason. 2006. Mercury methylation by dissimilatory iron-reducing bacteria. Applied and Environmental Microbiology **72**:7919-7921.

Kim, E., H. Kim, K. H. Shin, M. S. Kim, S. R. Kundu, B. G. Lee, and S. Han. 2012. Biomagnification of mercury through the benthic food webs of a temperate estuary: Masan Bay, Korea. Environmental Toxicology and Chemistry **31**:1254-1263.

Kirk, J. L., V. L. S. Louis, H. Hintelmann, I. Lehnherr, B. Else, and L. Poissant. 2008. Methylated Mercury Species in Marine Waters of the Canadian High and Sub Arctic. Environmental Science & Technology **42**:8367-8373.

Klinck, J. M., E. E. Hofmann, R. C. Beardsley, B. Salihoglu, and S. Howard. 2004. Water-mass properties and circulation on the west Antarctic Peninsula Continental Shelf in Austral Fall and Winter 2001. Deep-Sea Research Part Ii-Topical Studies in Oceanography **51**:1925-1946.

Knox, G. A. 2007. Biology of the Southern Ocean / George A. Knox. CRC Press/Taylor & Francis, Boca Raton, Fla.

Kokubun, N., E. J. Choy, J. H. Kim, and A. Takahashi. 2015. Isotopic values of Antarctic Krill in relation to foraging habitat of penguins. Ornithological Science **14**:13-20.

Krabbenhoft, D. P., and E. M. Sunderland. 2013. Global Change and Mercury. Science **341**:1457-1458.

Kritee, K., L. C. Motta, J. D. Blum, M. T.-K. Tsui, and J. R. Reinfelder. 2017. Photomicrobial Visible Light-Induced Magnetic Mass Independent Fractionation of Mercury in a Marine Microalga. ACS Earth and Space Chemistry.

Kumar, S. V., S. Maitra, and S. Bhattacharya. 2002. In vitro binding of inorganic mercury to the plasma membrane of rat platelet affects Na+-K+-ATPase activity and platelet aggregation. Biometals **15**:51-57.

Kuss, J., J. Holzmann, and R. Ludwig. 2009. An Elemental Mercury Diffusion Coefficient for Natural Waters Determined by Molecular Dynamics Simulation. Environmental Science & Technology **43**:3183-3186.

Laglera, L. M., and C. M. G. van den Berg. 2003. Copper complexation by thiol compounds in estuarine waters. Marine Chemistry **82**:71-89.

Lamborg, C. H., W. F. Fitzgerald, A. Skoog, and P. T. Visscher. 2004. The abundance and source of mercury-binding organic ligands in Long Island Sound. Marine Chemistry **90**:151-163.

Lamborg, C. H., C. R. Hammerschmidt, K. L. Bowman, G. J. Swarr, K. M. Munson, D. C. Ohnemus, P. J. Lam, L. E. Heimburger, M. J. A. Rijkenberg, and M. A. Saito. 2014. A global ocean inventory of anthropogenic mercury based on water column measurements. Nature **512**:65-+.

Lannuzel, D., A. R. Bowie, P. C. van der Merwe, A. T. Townsend, and V. Schoemann. 2011. Distribution of dissolved and particulate metals in Antarctic sea ice. Marine Chemistry **124**:134-146.

Lanzillotta, E., C. Ceccarini, R. Ferrara, F. Dini, E. Frontini, and R. Banchetti. 2004. Importance of the biogenic organic matter in photo-formation of dissolved gaseous mercury in a culture of the marine diatom Chaetoceros sp. Science of the Total Environment **318**:211-221.

Lascara, C. M., E. E. Hofmann, R. M. Ross, and L. B. Quetin. 1999. Seasonal variability in the distribution of Antarctic krill, Euphausia superba, west of the Antarctic Peninsula. Deep-Sea Research Part I-Oceanographic Research Papers **46**:951-984.

Lavoie, R. A., T. D. Jardine, M. M. Chumchal, K. A. Kidd, and L. M. Campbell. 2013. Biomagnification of Mercury in Aquatic Food Webs: A Worldwide Meta-Analysis. Environmental Science & Technology **47**:13385-13394.

Lawson, N. M., and R. P. Mason. 1998. Accumulation of mercury in estuarine food chains. Pages 235-247.

Leblond, C., J. Mephara, and S. Sauve. 2008. Trace metals (Cd, Co, Cr, Cu, Hg, Ni, Pb, and Zn) in food supplements of marine origin. Human and Ecological Risk Assessment **14**:408-420.

Lee, C. S., and N. S. Fisher. 2016. Methylmercury uptake by diverse marine phytoplankton. Limnology and Oceanography **61**:1626-1639.

Lee, J. G., B. A. Ahner, and F. M. M. Morel. 1996. Export of cadmium and phytochelatin by the marine diatom Thalassiosira weissflogii. Environmental Science & Technology **30**:1814-1821.

Lehnherr, I., and V. L. S. Louis. 2009. Importance of Ultraviolet Radiation in the Photodemethylation of Methylmercury in Freshwater Ecosystems. Environmental Science & Technology **43**:5692-5698.

Lehnherr, I., V. L. St Louis, H. Hintelmann, and J. L. Kirk. 2011. Methylation of inorganic mercury in polar marine waters. Pages 298-302.

Lescord, G. L., K. A. Kidd, J. L. Kirk, N. J. O'Driscoll, X. W. Wang, and D. C. G. Muir. 2015. Factors affecting biotic mercury concentrations and biomagnification through lake food webs in the Canadian high Arctic. Science of the Total Environment **509**:195-205.

Liang, L., N. S. Bloom, and M. Horvat. 1994a. SIMULTANEOUS DETERMINATION OF MERCURY SPECIATION IN BIOLOGICAL-MATERIALS BY GC/CVAFS AFTER ETHYLATION AND ROOM-TEMPERATURE PRECOLLECTION. Clinical Chemistry **40**:602-607.

Liang, L., M. Horvat, and N. S. Bloom. 1994b. AN IMPROVED SPECIATION METHOD FOR MERCURY BY GC CVAFS AFTER AQUEOUS-PHASE ETHYLATION AND ROOM-TEMPERATURE PRECOLLECTION. Talanta **41**:371-379.

Lindberg, S., R. Bullock, R. Ebinghaus, D. Engstrom, X. Feng, W. Fitzgerald, N. Pirrone, E. Prestbo, and C. Seigneur. 2007. A Synthesis of Progress and Uncertainties in Attributing the Sources of Mercury in Deposition. AMBIO: A Journal of the Human Environment **36**:19-33.

Liu, M. S., and J. A. Hellebust. 1974. Uptake of amino acids by the marine centric diatom Cyclotella cryptica. Canadian Journal of Microbiology **20**:1109-1118.

Locarnini, S. J. P., and B. J. Presley. 1995. Trace-Element Concentrations in Antarctic Krill, Euphausia-Superba. Polar Biology **15**:283-288.

Loseto, L. L., D. R. S. Lean, and S. D. Siciliano. 2004. Snowmelt sources of methylmercury to high arctic ecosystems. Environmental Science & Technology **38**:3004-3010.

Loux, N. T. 2007. An assessment of thermodynamic reaction constants for simulating aqueous environmental monomethyl mercury speciation. Chemical Speciation and Bioavailability **19**:183-196.

Lubbers, G. W., W. W. C. Gieskes, P. Delcastilho, W. Salomons, and J. Bril. 1990. MANGANESE ACCUMULATION IN THE HIGH PH MICROENVIRONMENT OF PHAEOCYSTIS-SP (HAPTOPHYCEAE) COLONIES FROM THE NORTH-SEA. Marine Ecology Progress Series **59**:285-293.

Luengen, A. C., N. S. Fisher, and B. A. Bergamaschi. 2012. Dissolved organic matter reduces algal accumulation of methylmercury. Environmental Toxicology and Chemistry **31**:1712-1719.

Macdonald, R. W., and L. L. Loseto. 2010. Are Arctic Ocean ecosystems exceptionally vulnerable to global emissions of mercury? A call for emphasised research on methylation and the consequences of climate change. Environmental Chemistry **7**:133-138.

Mahmoud, M. E., A. E. H. Abdou, S. M. S. Mohamed, and M. M. Osman. 2016. Engineered staphylococcus aureus via immobilization on magnetic Fe3O4-phthalate nanoparticles for biosorption of divalent ions from aqueous solutions. Journal of Environmental Chemical Engineering **4**:3810-3824.

Martin, D. L., R. M. Ross, L. B. Quetin, and A. E. Murray. 2006. Molecular approach (PCR-DGGE) to diet analysis in young Antarctic krill Euphausia superba. Marine Ecology Progress Series **319**:155-165.

Martinson, D. G., and D. C. McKee. 2012. Transport of warm Upper Circumpolar Deep Water onto the western Antarctic Peninsula continental shelf. Ocean Science **8**:433-442.

Marvin-DiPasquale, M., J. Agee, C. McGowan, R. S. Oremland, M. Thomas, D. Krabbenhoft, and C. C. Gilmour. 2000. Methyl-mercury degradation pathways: A comparison among three mercury-impacted ecosystems. Environmental Science & Technology **34**:4908-4916.

Mason, R. P., A. L. Choi, W. F. Fitzgerald, C. R. Hammerschmidt, C. H. Lamborg, A. L. Soerensen, and E. M. Sunderland. 2012. Mercury biogeochemical cycling in the ocean and policy implications. Environmental Research **119**:101-117.

Mason, R. P., N. M. Lawson, A. L. Lawrence, J. J. Leaner, J. G. Lee, and G. R. Sheu. 1999. Mercury in the Chesapeake Bay. Marine Chemistry **65**:77-96.

Mason, R. P., F. M. M. Morel, and H. F. Hemond. 1995. THE ROLE OF MICROORGANISMS IN ELEMENTAL MERCURY FORMATION IN NATURAL-WATERS. Water Air and Soil Pollution **80**:775-787.

Mason, R. P., J. R. Reinfelder, and F. M. M. Morel. 1996. Uptake, toxicity, and trophic transfer of mercury in a coastal diatom. Pages 1835-1845. Environmental Science & Technology.

Mason, R. P., K. R. Rolfhus, and W. F. Fitzgerald. 1998. Mercury in the North Atlantic. Marine Chemistry **61**:37-53.

Mason, R. P., and K. A. Sullivan. 1999. The distribution and speciation of mercury in the South and equatorial Atlantic. Deep-Sea Research Part Ii-Topical Studies in Oceanography **46**:937-956.

Mastromonaco, M. G. N., K. Gardfeldt, K. M. Assmann, S. Langer, T. Delali, Y. M. Shlyapnikov, I. Zivkovic, and M. Horvat. 2017a. Speciation of mercury in the waters of the Weddell, Amundsen and Ross Seas (Southern Ocean). Marine Chemistry **193**:20-33.

Mastromonaco, M. G. N., K. Gardfeldt, and S. Langer. 2017b. Mercury flux over West Antarctic Seas during winter, spring and summer. Marine Chemistry **193**:44-54.

Mastromonaco, M. N., K. Gardfeldt, B. Jourdain, K. Abrahamsson, A. Granfors, M. Ahnoff, A. Dommergue, G. Mejean, and H. W. Jacobi. 2016. Antarctic winter mercury and ozone depletion events over sea ice. Atmospheric Environment **129**:125-132.

Mayzaud, P., E. Albessard, and J. Cuzin-Roudy. 1998. Changes in lipid composition of the Antarctic krill Euphausia superba in the Indian sector of the Antarctic Ocean: influence of geographical location, sexual maturity stage and distribution among organs. Marine Ecology Progress Series **173**:149-162.

McArthur, T., E. C. V. Butler, and G. D. Jackson. 2003. Mercury in the marine food chain in the Southern Ocean at Macquarie Island: an analysis of a top predator, Patagonian toothfish (Dissostichus eleginoides) and a mid-trophic species, the warty squid (Moroteuthis ingens). Polar Biology **27**:1-5.

McConnaughey, T., and C. P. McRoy. 1979. Food-Web structure and the fractionation of Carbon isotopes in the bering sea. Marine Biology **53**:257-262.

McCutchan, J. H., W. M. Lewis, C. Kendall, and C. C. McGrath. 2003. Variation in trophic shift for stable isotope ratios of carbon, nitrogen, and sulfur. Oikos **102**:378-390.

McLusky, D., and M. Elliott. 2004. The Estuarine Ecosystem. Ecology, Threats and Management.

Mergler, D., H. A. Anderson, L. H. M. Chan, K. R. Mahaffey, M. Murray, M. Sakamoto, and A. H. Stern. 2007. Methylmercury exposure and health effects in humans: A worldwide concern. Ambio **36**:3-11.

Metcheva, R., L. Yurukova, S. Teodorova, and E. Nikolova. 2006. The penguin feathers as bioindicator of Antarctica environmental state. Science of the Total Environment **362**:259-265.

Meyer, B., L. Auerswald, V. Siegel, S. Spahic, C. Pape, B. A. Fach, M. Teschke, A. L. Lopata, and V. Fuentes. 2010. Seasonal variation in body composition, metabolic activity, feeding, and growth of adult krill Euphausia superba in the Lazarev Sea. Marine Ecology Progress Series **398**:1-18.

Meyer, B., U. Freier, V. Grimm, J. Groeneveld, B. Hunt, S. Kerwath, R. King, C. Klaas, E. Pakhomov, K. Meiners, J. Melbourne-Thomas, E. Murphy, S. Thorpe, S. Stammerjohn, D.

Wolf-Gladrow, L. Auerswald, A. Götz, L. Halbach, S. Jarman, and I. N. Yilmaz. 2017. The winter pack-ice zone provides a sheltered but food-poor habitat for larval Antarctic krill.

Miller, A. K., M. A. Kappes, S. G. Trivelpiece, and W. Z. Trivelpiece. 2010. Foraging-Niche Separation of Breeding Gentoo and Chinstrap Penguins, South Shetland Islands, Antarctica The Condor **112(4)**:683-695.

Miller, A. K., and W. Z. Trivelpiece. 2007. Cycles of Euphausia superba recruitment evident in the diet of Pygoscelid penguins and net trawls in the South Shetland Islands, Antarctica. Polar Biology **30**:1615-1623.

Miller, A. K., and W. Z. Trivelpiece. 2008. Chinstrap penguins alter foraging and diving behavior in response to the size of their principle prey, Antarctic krill. Marine Biology **154**:201-208.

Minagawa, M., and E. Wada. 1984. STEPWISE ENRICHMENT OF N-15 ALONG FOOD-CHAINS - FURTHER EVIDENCE AND THE RELATION BETWEEN DELTA-N-15 AND ANIMAL AGE. Geochimica Et Cosmochimica Acta **48**:1135-1140.

Mincks, S. L., C. R. Smith, R. M. Jeffreys, and P. Y. G. Sumida. 2008. Trophic structure on the West Antarctic Peninsula shelf: Detritivory and benthic inertia revealed by delta C-13 and delta N-15 analysis. Deep-Sea Research Part Ii-Topical Studies in Oceanography **55**:2502-2514.

Moffat, C., B. Owens, and R. C. Beardsley. 2009. On the characteristics of Circumpolar Deep Water intrusions to the west Antarctic Peninsula Continental Shelf. Journal of Geophysical Research-Oceans **114**:16.

Moffett, J. W., and L. E. Brand. 1996. Production of strong, extracellular Cu chelators by marine cyanobacteria in response to Cu stress. Limnology and Oceanography **41**:388-395.

Monikh, F. A., O. Karami, M. Hosseini, N. Karami, A. A. Bastami, and A. F. Ghasemi. 2013. The effect of primary producers of experimental aquatic food chains on mercury and PCB153 biomagnification. Ecotoxicology and Environmental Safety **94**:112-115.

Monteiro, L. R., V. Costa, R. W. Furness, and R. S. Santos. 1996. Mercury concentrations in prey fish indicate enhanced bioaccumulation in mesopelagic environments. Marine Ecology Progress Series **141**:21-25.

Monteiro, L. R., and R. W. Furness. 1995. SEABIRDS AS MONITORS OF MERCURY IN THE MARINE-ENVIRONMENT. Water Air and Soil Pollution **80**:851-870.

Morel, F. M. M., J. G. Rueter, D. M. Anderson, and R. R. L. Guillard. 1979. AQUIL: A CHEMICALLY DEFINED PHYTOPLANKTON CULTURE MEDIUM FOR TRACE METAL STUDIES12. Journal of Phycology **15**:135-141.

Morelli, E., R. Ferrara, B. Bellini, F. Dini, G. Di Giuseppe, and L. Fantozzi. 2009. Changes in the non-protein thiol pool and production of dissolved gaseous mercury in the marine diatom Thalassiosira weissflogii under mercury exposure. Pages 286-293.

Morelli, E., and G. Scarano. 2001. Synthesis and stability of phytochelatins induced by cadmium and lead in the marine diatom Phaeodactylum tricornutum. Marine Environmental Research **52**:383-395.

Moren, M., J. Suontama, G. I. Hemre, O. Karlsen, R. E. Olsen, H. Mundheim, and K. Julshamn. 2006. Element concentrations in meals from krill and amphipods, - Possible alternative protein sources in complete diets for farmed fish. Aquaculture **261**:174-181.

Moye, H. A., C. J. Miles, E. J. Phlips, B. Sargent, and K. K. Merritt. 2002. Kinetics and untake mechanisms for monomethylmercury between freshwater algae and water. Environmental Science & Technology **36**:3550-3555.

Munson, K. M., D. Babi, and C. H. Lamborg. 2014. Determination of monomethylmercury from seawater with ascorbic acid-assisted direct ethylation. Limnology and Oceanography-Methods **12**:1-9.

Munson, K. M., C. H. Lamborg, G. J. Swarr, and M. A. Saito. 2015. Mercury species concentrations and fluxes in the Central Tropical Pacific Ocean. Global Biogeochemical Cycles **29**:656-676.

Ndung'u, K., R. P. Franks, K. W. Bruland, and A. R. Flegal. 2003. Organic complexation and total dissolved trace metal analysis in estuarine waters: comparison of solvent-extraction graphite furnace atomic absorption spectrometric and chelating resin flow injection inductively coupled plasma-mass spectrometric analysis. Analytica Chimica Acta **481**:127-138.

Nightingale, P. D., G. Malin, C. S. Law, A. J. Watson, P. S. Liss, M. I. Liddicoat, J. Boutin, and R. C. Upstill-Goddard. 2000. In situ evaluation of air-sea gas exchange parameterizations using novel conservative and volatile tracers. Global Biogeochemical Cycles **14**:373-387.

Nriagu, J. O. 1994. MECHANISTIC STEPS IN THE PHOTOREDUCTION OF MERCURY IN NATURAL-WATERS. Science of the Total Environment **154**:1-8.

Nygard, T., E. Lie, N. Rov, and E. Steinnes. 2001. Metal dynamics in an Antarctic food chain. Marine Pollution Bulletin **42**:598-602.

O'Driscoll, N. J., S. D. Siciliano, D. R. S. Lean, and M. Amyot. 2006a. Gross photoreduction kinetics of mercury in temperate freshwater lakes and rivers: Application to a general model of DGM dynamics. Environmental Science & Technology **40**:837-843.

O'Driscoll, N. J., S. D. Siciliano, D. R. S. Lean, and M. Amyot. 2006b. Gross Photoreduction Kinetics of Mercury in Temperate Freshwater Lakes and Rivers: Application to a General Model of DGM Dynamics. Environmental Science & Technology **40**:837-843.

Obrist, D., Y. Agnan, M. Jiskra, C. L. Olson, D. P. Colegrove, J. Hueber, C. W. Moore, J. E. Sonke, and D. Helmig. 2017. Tundra uptake of atmospheric elemental mercury drives Arctic mercury pollution. Nature **547**:201-+.

Oliver, M. J., A. Irwin, M. A. Moline, W. Fraser, D. Patterson, O. Schofield, and J. Kohut. 2013. Adelie Penguin Foraging Location Predicted by Tidal Regime Switching. Plos One **8**:9.

Pacheco, P. H., A. Spisso, S. Cerutti, P. Smichowski, and L. D. Martinez. 2010. Non-chromatographic screening method for the determination of mercury species. Application to the monitoring of mercury levels in Antarctic samples. Talanta **82**:1505-1510.

Pacyna, E. G., J. M. Pacyna, K. Sundseth, J. Munthe, K. Kindbom, S. Wilson, F. Steenhuisen, and P. Maxson. 2010. Global emission of mercury to the atmosphere from anthropogenic sources in 2005 and projections to 2020. Atmospheric Environment **44**:2487-2499.

Parapar, J., E. Lopez, M. C. Gambi, J. Nunez, and A. Ramos. 2011. Quantitative analysis of soft-bottom polychaetes of the Bellingshausen Sea and Gerlache Strait (Antarctica). Polar Biology **34**:715-730.

Pardo, P. C., B. Tilbrook, C. Langlais, T. W. Trull, and S. R. Rintoul. 2017. Carbon uptake and biogeochemical change in the Southern Ocean, south of Tasmania. Biogeosciences **14**:5217-5237.

Parker, J. L., and N. S. Bloom. 2005. Preservation and storage techniques for low-level aqueous mercury speciation. Science of the Total Environment **337**:253-263.

Parks, J. M., A. Johs, M. Podar, R. Bridou, R. A. Hurt, S. D. Smith, S. J. Tomanicek, Y. Qian, S. D. Brown, C. C. Brandt, A. V. Palumbo, J. C. Smith, J. D. Wall, D. A. Elias, and L. Y. Liang. 2013. The Genetic Basis for Bacterial Mercury Methylation. Science **339**:1332-1335.

Pearson, S. F., D. J. Levey, C. H. Greenberg, and C. M. del Rio. 2003. Effects of elemental composition on the incorporation of dietary nitrogen and carbon isotopic signatures in an omnivorous songbird. Oecologia **135**:516-523.

Pickhardt, P. C., and N. S. Fisher. 2007. Accumulation of inorganic and methylmercury by freshwater phytoplankton in two contrasting water bodies. Pages 125-131.

Pickhardt, P. C., C. L. Folt, C. Y. Chen, B. Klaue, and J. D. Blum. 2002. Algal blooms reduce the uptake of toxic methylmercury in freshwater food webs. Pages 4419-4423.

Pistocchi, R., F. Guerrini, V. Balboni, and L. Boni. 1997. Copper toxicity and carbohydrate production in the microalgae Cylindrotheca fusiformis and Gymnodinium sp. European Journal of Phycology **32**:125-132.

Planquette, H., and R. M. Sherrell. 2012. Sampling for particulate trace element determination using water sampling bottles: methodology and comparison to in situ pumps. Limnology and Oceanography-Methods **10**:367-388.

Polito, M. J., R. L. Brasso, W. Z. Trivelpiece, N. Karnovsky, W. P. Patterson, and S. D. Emslie. 2016. Differing foraging strategies influence mercury (Hg) exposure in an Antarctic penguin community. Environmental Pollution **218**:196-206.

Polito, M. J., H. J. Lynch, R. Naveen, and S. D. Emslie. 2011a. Stable isotopes reveal regional heterogeneity in the pre-breeding distribution and diets of sympatrically breeding Pygoscelis spp. penguins. Marine Ecology Progress Series **421**:265-277.

Polito, M. J., C. S. Reiss, W. Z. Trivelpiece, W. P. Patterson, and S. D. Emslie. 2013. Stable isotopes identify an ontogenetic niche expansion in Antarctic krill (Euphausia superba) from the South Shetland Islands, Antarctica. Marine Biology **160**:1311-1323.

Polito, M. J., W. Z. Trivelpiece, N. J. Karnovsky, E. Ng, W. P. Patterson, and S. D. Emslie. 2011b. Integrating Stomach Content and Stable Isotope Analyses to Quantify the Diets of Pygoscelid Penguins. Plos One **6**:10.

Polito, M. J., W. Z. Trivelpiece, W. P. Patterson, N. J. Karnovsky, C. S. Reiss, and S. D. Emslie. 2015. Contrasting specialist and generalist patterns facilitate foraging niche partitioning in sympatric populations of Pygoscelis penguins. Marine Ecology Progress Series **519**:221-237.

Pongratz, R., and K. G. Heumann. 1998. Determination of concentration profiles of methyl mercury compounds in surface waters of polar and other remote oceans by GC-AFD. International Journal of Environmental Analytical Chemistry **71**:41-56.

Post, D. M. 2002. Using stable isotopes to estimate trophic position: Models, methods, and assumptions. Ecology **83**:703-718.

Post, D. M., C. A. Layman, D. A. Arrington, G. Takimoto, J. Quattrochi, and C. G. Montana. 2007. Getting to the fat of the matter: models, methods and assumptions for dealing with lipids in stable isotope analyses. Oecologia **152**:179-189.

Poulain, A. J., J. D. Lalonde, M. Amyot, J. A. Shead, F. Raofie, and P. A. Ariya. 2004. Redox transformations of mercury in an Arctic snowpack at springtime. Atmospheric Environment **38**:6763-6774.

Poulain, A. J., S. M. Ni Chadhain, P. A. Ariya, M. Amyot, E. Garcia, P. G. C. Campbell, G. J. Zylstra, and T. Barkay. 2007. Potential for mercury reduction by microbes in the high arctic. Applied and Environmental Microbiology **73**:2230-2238.

Prezelin, B. B., E. E. Hofmann, M. Moline, and J. M. Klinck. 2004. Physical forcing of phytoplankton community structure and primary production in continental shelf waters of the Western Antarctic Peninsula. Journal of Marine Research **62**:419-460.

Price, N. M., G. I. Harrison, J. G. Hering, R. J. Hudson, P. M. V. Nirel, B. Palenik, and F. M. M. Morel. 1989. Preparation and Chemistry of the Artificial Algal Culture Medium Aquil. Biological Oceanography **6**:443-461.

Pritchard, H. D., and D. G. Vaughan. 2007. Widespread acceleration of tidewater glaciers on the Antarctic Peninsula. Journal of Geophysical Research-Earth Surface **112**:10.

Qi, H. P., T. B. Coplen, H. Geilmann, W. A. Brand, and J. K. Bohlke. 2003. Two new organic reference materials for delta C-13 and delta N-15 measurements and a new value for the delta C-13 of NBS 22 oil. Rapid Communications in Mass Spectrometry **17**:2483-2487.

Rabenstein, D. L., and C. A. Evans. 1978. The mobility of methylmercury in biological systems. Bioinorganic chemistry **8**:107-101,104.

Ramos, R., and J. Gonzalez-Solis. 2012. Trace me if you can: the use of intrinsic biogeochemical markers in marine top predators. Frontiers in Ecology and the Environment **10**:258-266.

Rau, G. H., C. W. Sullivan, and L. I. Gordon. 1991. DELTA-C-13 AND DELTA-N-15 VARIATIONS IN WEDDELL SEA PARTICULATE ORGANIC-MATTER. Marine Chemistry **35**:355-369.

Rau, G. H., R. E. Sweeney, and I. R. Kaplan. 1982. PLANKTON C-13-C-12 RATIO CHANGES WITH LATITUDE - DIFFERENCES BETWEEN NORTHERN AND SOUTHERN OCEANS. Deep-Sea Research Part a-Oceanographic Research Papers **29**:1035-1039.

Reinfelder, J. R. 2012. Carbon dioxide regulation of nitrogen and phosphorus in four species of marine phytoplankton. Marine Ecology Progress Series **466**:57-67.

Rijkenberg, M. J. A., L. J. A. Gerringa, K. R. Timmermans, A. C. Fischer, K. J. Kroon, A. G. J. Buma, B. T. Wolterbeek, and H. J. W. de Baar. 2008. Enhancement of the reactive iron pool by marine diatoms. Marine Chemistry **109**:29-44.

Rolfhus, K. R. 1998. The production and distribution of elemental mercury in a coastal marine environment. Ph.D. Dissertation. University of Connecticut.

Ross, R. M., L. B. Quetin, D. G. Martinson, R. A. Iannuzzi, S. E. Stammerjohn, and R. C. Smith. 2008. Palmer LTER: Patterns of distribution of five dominant zooplankton species in the epipelagic zone west of the Antarctic Peninsula, 1993-2004. Pages 2086-2105.

Ruus, A., I. B. Overjordet, H. F. V. Braaten, A. Evenset, G. Christensen, E. S. Heimstad, G. W. Gabrielsen, and K. Borga. 2015. Methylmercury biomagnification in an Arctic pelagic food web. Environmental Toxicology and Chemistry **34**:2636-2643.

Ruxton, G. D., and G. Beauchamp. 2008. Time for some a priori thinking about post hoc testing. Behavioral Ecology **19**:690-693.

Saba, G. K., W. R. Fraser, V. S. Saba, R. A. Iannuzzi, K. E. Coleman, S. C. Doney, H. W. Ducklow, D. G. Martinson, T. N. Miles, D. L. Patterson-Fraser, S. E. Stammerjohn, D. K. Steinberg, and O. M. Schofield. 2014. Winter and spring controls on the summer food web of the coastal West Antarctic Peninsula. Nature Communications **5**:8.

Saiz-Lopez, A., A. S. Mahajan, R. A. Salmon, S. J. B. Bauguitte, A. E. Jones, H. K. Roscoe, and J. M. C. Plane. 2007. Boundary layer halogens in coastal Antarctica. Science **317**:348-351.

Sanchez-Hernandez, J. C. 2000. Trace element contamination in Antarctic ecosystems. Reviews of Environmental Contamination and Toxicology, Vol 166 **166**:83-127.

Scambos, T. A., J. A. Bohlander, C. A. Shuman, and P. Skvarca. 2004. Glacier acceleration and thinning after ice shelf collapse in the Larsen B embayment, Antarctica. Geophysical Research Letters **31**:4.

Schaefer, J. K., and F. M. M. Morel. 2009. High methylation rates of mercury bound to cysteine by Geobacter sulfurreducens. Nature Geoscience **2**:123-126.

Schaefer, J. K., S. S. Rocks, W. Zheng, L. Y. Liang, B. H. Gu, and F. M. M. Morel. 2011. Active transport, substrate specificity, and methylation of Hg(II) in anaerobic bacteria.

Proceedings of the National Academy of Sciences of the United States of America **108**:8714-8719.

Schaefer, J. K., J. Yagi, J. R. Reinfelder, T. Cardona, K. M. Ellickson, S. Tel-Or, and T. Barkay. 2004. Role of the bacterial organomercury lyase (MerB) in controlling methylmercury accumulation in mercury-contaminated natural waters. Environmental Science & Technology **38**:4304-4311.

Schartup, A. T., P. H. Balcom, A. L. Soerensen, K. J. Gosnell, R. S. D. Calder, R. P. Mason, and E. M. Sunderland. 2015a. Freshwater discharges drive high levels of methylmercury in Arctic marine biota. Proceedings of the National Academy of Sciences of the United States of America **112**:11789-11794.

Schartup, A. T., R. P. Mason, P. H. Balcom, T. A. Hollweg, and C. Y. Chen. 2013. Methylmercury Production in Estuarine Sediments: Role of Organic Matter. Environmental Science & Technology **47**:695-700.

Schartup, A. T., U. Ndu, P. H. Balcom, R. P. Mason, and E. M. Sunderland. 2015b. Contrasting Effects of Marine and Terrestrially Derived Dissolved Organic Matter on Mercury Speciation and Bioavailability in Seawater. Environmental Science & Technology **49**:5965-5972.

Schartup, A. T., A. Qureshi, C. Dassuncao, C. P. Thackray, G. Harding, and E. M. Sunderland. 2018. A Model for Methylmercury Uptake and Trophic Transfer by Marine Plankton. Environmental Science & Technology **52**:654-662.

Schmidt, K., A. Atkinson, S. Steigenberger, S. Fielding, M. C. M. Lindsay, D. W. Pond, G. A. Tarling, T. A. Klevjer, C. S. Allen, S. Nicol, and E. P. Achterberg. 2011. Seabed foraging by Antarctic krill: Implications for stock assessment, bentho-pelagic coupling, and the vertical transfer of iron. Pages 1411-1428. LIMNOLOGY AND OCEANOGRAPHY.

Schoemann, V., S. Becquevort, J. Stefels, W. Rousseau, and C. Lancelot. 2005. Phaeocystis blooms in the global ocean and their controlling mechanisms: a review. Journal of Sea Research **53**:43-66.

Schoemann, V., R. Wollast, L. Chou, and C. Lancelot. 2001. Effects of photosynthesis on the accumulation of Mn and Fe by Phaeocystis colonies. Limnology and Oceanography **46**:1065-1076.

Schofield, O., G. Saba, K. Coleman, F. Carvalho, N. Couto, H. Ducklow, Z. Finkel, A. Irwin, A. Kahl, T. Miles, M. Montes-Hugo, S. Stammerjohn, and N. Waite. 2017. Decadal variability in coastal phytoplankton community composition in a changing West Antarctic Peninsula. Deep-Sea Research Part I-Oceanographic Research Papers **124**:42-54.

Schroeder, W. H., K. G. Anlauf, L. A. Barrie, J. Y. Lu, A. Steffen, D. R. Schneeberger, and T. Berg. 1998. Arctic springtime depletion of mercury. Nature **394**:331-332.

Schuster, P. F., D. P. Krabbenhoft, D. L. Naftz, L. D. Cecil, M. L. Olson, J. F. Dewild, D. D. Susong, J. R. Green, and M. L. Abbott. 2002. Atmospheric mercury deposition during the last 270 years: A glacial ice core record of natural and anthropogenic sources. Environmental Science & Technology **36**:2303-2310.

Selin, N. E. 2014. Global Change and Mercury Cycling: Challenges for Implementing a Global Mercury Treaty. Environmental Toxicology and Chemistry **33**:1202-1210.

Sellers, P., C. A. Kelly, J. W. M. Rudd, and A. R. MacHutchon. 1996. Photodegradation of methylmercury in lakes. Nature **380**:694-697.

Serebrennikova, Y. M., and K. A. Fanning. 2004. Nutrients in the Southern Ocean GLOBEC region: variations, water circulation, and cycling. Deep-Sea Research Part Ii-Topical Studies in Oceanography **51**:1981-2002.

Shia, R. L., C. Seigneur, P. Pai, M. Ko, and N. D. Sze. 1999. Global simulation of atmospheric mercury concentrations and deposition fluxes. Journal of Geophysical Research-Atmospheres **104**:23747-23760.

Siegel, V., and V. Loeb. 1994. LENGTH AND AGE AT MATURITY OF ANTARCTIC KRILL. Antarctic Science **6**:479-482.

Siegel, V., C. S. Reiss, K. S. Dietrich, M. Haraldsson, and G. Rohardt. 2013. Distribution and abundance of Antarctic krill (Euphausia superba) along the Antarctic Peninsula. Deep-Sea Research Part I-Oceanographic Research Papers **77**:63-74.

Skov, H., J. H. Christensen, M. E. Goodsite, N. Z. Heidam, B. Jensen, P. Wahlin, and G. Geernaert. 2004. Fate of elemental mercury in the arctic during atmospheric mercury depletion episodes and the load of atmospheric mercury to the arctic. Environmental Science & Technology **38**:2373-2382.

Smith, D. C. 1992. A simple, economical method for measuring bacterial protein synthesis rates in seawater using 3H-leucine. Mar. Microb. Food Webs **6**:107-114.

Smith, W. O., and D. M. Nelson. 1990. PHYTOPLANKTON GROWTH AND NEW PRODUCTION IN THE WEDDELL SEA MARGINAL ICE-ZONE IN THE AUSTRAL SPRING AND AUTUMN. Limnology and Oceanography **35**:809-821.

Soerensen, A. L., D. J. Jacob, A. T. Schartup, J. A. Fisher, I. Lehnherr, V. L. St Louis, L. E. Heimburger, J. E. Sonke, D. P. Krabbenhoft, and E. M. Sunderland. 2016. A mass budget for mercury and methylmercury in the Arctic Ocean. Global Biogeochemical Cycles **30**:560-575.

Soerensen, A. L., D. J. Jacob, D. G. Streets, M. L. I. Witt, R. Ebinghaus, R. P. Mason, M. Andersson, and E. M. Sunderland. 2012. Multi-decadal decline of mercury in the North Atlantic atmosphere explained by changing subsurface seawater concentrations. Geophysical Research Letters **39**:6.

Soerensen, A. L., R. P. Mason, P. H. Balcom, D. J. Jacob, Y. X. Zhang, J. Kuss, and E. M. Sunderland. 2014. Elemental Mercury Concentrations and Fluxes in the Tropical Atmosphere and Ocean. Environmental Science & Technology **48**:11312-11319.

Soerensen, A. L., H. Skov, D. J. Jacob, B. T. Soerensen, and M. S. Johnson. 2010a. Global Concentrations of Gaseous Elemental Mercury and Reactive Gaseous Mercury in the Marine Boundary Layer. Environmental Science & Technology **44**:7425-7430.

Soerensen, A. L., E. M. Sunderland, C. D. Holmes, D. J. Jacob, R. M. Yantosca, H. Skov, J. H. Christensen, S. A. Strode, and R. P. Mason. 2010b. An Improved Global Model for Air-Sea Exchange of Mercury: High Concentrations over the North Atlantic. Environmental Science & Technology **44**:8574-8580.

St Louis, V. L., H. Hintelmann, J. A. Graydon, J. L. Kirk, J. Barker, B. Dimock, M. J. Sharp, and I. Lehnherr. 2007. Methylated mercury species in Canadian high arctic marine surface waters and snowpacks. Environmental Science & Technology **41**:6433-6441.

St Louis, V. L., M. J. Sharp, A. Steffen, A. May, J. Barker, J. L. Kirk, D. J. A. Kelly, S. E. Arnott, B. Keatley, and J. P. Smol. 2005. Some sources and sinks of monomethyl and inorganic mercury on Ellesmere island in the Canadian high arctic. Environmental Science & Technology **39**:2686-2701.

Stammerjohn, S. 2017. Average monthly sea ice coverage for the PAL LTER region West of the Antarctic Peninsula derived from passive microwave, 1978 - 2016. Environmental Data Initiative, http://dx.doi.org/10.6073/pasta/428c1ac4c851bda811076a2a56c19ca7

Stammerjohn, S. E., D. G. Martinson, R. C. Smith, and R. A. Iannuzzi. 2008. Sea ice in the western Antarctic Peninsula region: Spatio-temporal variability from ecological and climate change perspectives. Deep-Sea Research Part Ii-Topical Studies in Oceanography **55**:2041-2058.

Steffen, A., T. Douglas, M. Amyot, P. Ariya, K. Aspmo, T. Berg, J. Bottenheim, S. Brooks, F. Cobbett, A. Dastoor, A. Dommergue, R. Ebinghaus, C. Ferrari, K. Gardfeldt, M. E. Goodsite, D. Lean, A. J. Poulain, C. Scherz, H. Skov, J. Sommar, and C. Temme. 2008. A synthesis of atmospheric mercury depletion event chemistry in the atmosphere and snow. Atmospheric Chemistry and Physics **8**:1445-1482.

Stein, R., K. Fahl, P. Gierz, F. Niessen, and G. Lohmann. 2017. Arctic Ocean sea ice cover during the penultimate glacial and the last interglacial. Nature Communications **8**:13.

Steinberg, D. K., D. G. Martinson, and D. P. Costa. 2012. TWO DECADES OF PELAGIC ECOLOGY OF THE WESTERN ANTARCTIC PENINSULA. Oceanography **25**:56-67.

Steinberg, D. K., K. E. Ruck, M. R. Gleiber, L. M. Garzio, J. S. Cope, K. S. Bernard, S. E. Stammerjohn, O. M. E. Schofield, L. B. Quetin, and R. M. Ross. 2015. Long-term (1993-2013) changes in macrozooplankton off the Western Antarctic Peninsula. Deep-Sea Research Part I-Oceanographic Research Papers **101**:54-70.

Stern, G. A., and R. W. Macdonald. 2005. Biogeographic provinces of total and methyl mercury in zooplankton and fish from the Beaufort and Chukchi seas: Results from the SHEBA drift. Environmental Science & Technology **39**:4707-4713.

Stern, G. A., R. W. Macdonald, P. M. Outridge, S. Wilson, J. Chételat, A. Cole, H. Hintelmann, L. L. Loseto, A. Steffen, F. Wang, and C. Zdanowicz. 2012a. How does climate change influence arctic mercury? Science of the Total Environment **414**:22-42.

Stern, G. A., R. W. Macdonald, P. M. Outridge, S. Wilson, J. Chetelat, A. Cole, H. Hintelmann, L. L. Loseto, A. Steffen, F. Y. Wang, and C. Zdanowicz. 2012b. How does climate change influence arctic mercury? Science of the Total Environment **414**:22-42.

Stonehouse, B. 1967. The general biology and thermal balances of penguins. Advan Ecol Resadvances in Ecological Research **4**:131-196.

Sunderland, E. M. 2007. Mercury Exposure from Domestic and Imported Estuarine and Marine Fish in the U.S. Seafood Market. Environmental Health Perspectives **115**:235-242.

Sunderland, E. M., J. Dalziel, A. Heyes, B. A. Branfireun, D. P. Krabbenhoft, and F. Gobas. 2010. Response of a Macrotidal Estuary to Changes in Anthropogenic Mercury Loading between 1850 and 2000. Environmental Science & Technology **44**:1698-1704.

Sunderland, E. M., D. P. Krabbenhoft, J. W. Moreau, S. A. Strode, and W. M. Landing. 2009. Mercury sources, distribution, and bioavailability in the North Pacific Ocean: Insights from data and models. Global Biogeochemical Cycles **23**:14.

Sunderland, E. M., and R. P. Mason. 2007. Human impacts on open ocean mercury concentrations. Global Biogeochemical Cycles **21**:15.

Swarr, G. J., T. Kading, C. H. Lamborg, C. R. Hammerschmidt, and K. L. Bowman. 2016. Dissolved low-molecular weight thiol concentrations from the US GEOTRACES North Atlantic Ocean zonal transect. Deep-Sea Research Part I-Oceanographic Research Papers **116**:77-87.

Szefer, P., W. Czarnowski, J. Pempkowiak, and E. Holm. 1993. MERCURY AND MAJOR ESSENTIAL ELEMENTS IN SEALS, PENGUINS, AND OTHER REPRESENTATIVE FAUNA OF THE ANTARCTIC. Archives of Environmental Contamination and Toxicology **25**:422-427.

Tang, D. G., M. M. Shafer, D. A. Karner, J. Overdier, and D. E. Armstrong. 2004. Factors affecting the presence of dissolved glutathione in estuarine waters. Environmental Science & Technology **38**:4247-4253.

Tanton, J. L., K. Reid, J. P. Croxall, and P. N. Trathan. 2004. Winter distribution and behaviour of gentoo penguins Pygoscelis papua at South Georgia. Polar Biology **27**:299-303.

Thibodeaux, J. L. 1996. Environmental Chemodynamics: Movement of chemicals in Air, Water, and Soil. Page 593 *in* I. John Wiley & Sons, editor.

Thomas, D. J., and J. C. Smith. 1982. Effects of coadministered low-molecular-weight thiol compounds on short-term distribution of methyl mercury in the rat. Toxicology and Applied Pharmacology **62**:104-110.

Thompson, D. R., and R. W. Furness. 1989. Comparison of the Levels of Total and Organic Mercury in Seabird Feathers. Marine Pollution Bulletin **20**:577-579.

Thompson, D. R., R. W. Furness, and L. R. Monteiro. 1998. Seabirds as biomonitors of mercury inputs to epipelagic and mesopelagic marine food chains. Science of the Total Environment **213**:299-305.

Tierney, M., C. Southwe, L. M. Emmerson, and M. A. Hindell. 2008. Evaluating and using stable-isotope analysis to infer diet composition and foraging ecology of Adelie penguins Pygoscelis adeliae. Marine Ecology Progress Series **355**:297-307.

Timmermans, K. R., L. J. A. Gerringa, H. J. W. de Baar, B. van der Wagt, M. J. W. Veldhuis, J. T. M. de Jong, P. L. Croot, and M. Boye. 2001. Growth rates of large and small Southern Ocean diatoms in relation to availability of iron in natural seawater. Limnology and Oceanography **46**:260-266.

Tonietto, A. E., A. T. Lombardi, A. A. H. Vieira, C. C. Parrish, and R. B. Choueri. 2014. Cylindrospermopsis raciborskii (Cyanobacteria) exudates: Chemical characterization and complexation capacity for Cu, Zn, Cd and Pb. Water Research **49**:381-390.

Trathan, P. N., J. Priddle, J. L. Watkins, D. G. M. Miller, and A. W. A. Murray. 1993. SPATIAL VARIABILITY OF ANTARCTIC KRILL IN RELATION TO MESOSCALE HYDROGRAPHY. Marine Ecology Progress Series **98**:61-71.

Trivelpiece, W. Z., S. Buckelew, C. Reiss, and S. G. Trivelpiece. 2007. The winter distribution of chinstrap penguins from two breeding sites in the South Shetland Islands of Antarctica. Polar Biology **30**:1231-1237.

Trivelpiece, W. Z., S. G. Trivelpiece, and N. J. Volkman. 1987. Ecological Segregation of Adelie, Gentoo, and Chinstrap Penguins at King-George-Island, Antarctica. Ecology **68**:351-361.

van der Merwe, P., D. Lannuzel, A. R. Bowie, and K. M. Meiners. 2011. High temporal resolution observations of spring fast ice melt and seawater iron enrichment in East Antarctica. Journal of Geophysical Research-Biogeosciences **116**:18.

van Oijen, T., M. A. van Leeuwe, W. W. C. Gieskes, and H. J. W. de Baar. 2004. Effects of iron limitation on photosynthesis and carbohydrate metabolism in the Antarctic diatom Chaetoceros brevis (Bacillariophyceae). European Journal of Phycology **39**:161-171.

Vandal, G. M., R. P. Mason, and W. F. Fitzgerald. 1991. CYCLING OF VOLATILE MERCURY IN TEMPERATE LAKES. Water Air and Soil Pollution **56**:791-803.

Vasconcelos, M., and M. F. C. Leal. 2001. Antagonistic interactions of Ph and Cd on Cu uptake, growth inhibition and chelator release in the marine algae Emiliania huxleyi. Marine Chemistry **75**:123-139.

Vogt, M., C. O'Brien, J. Peloquin, V. Schoemann, E. Breton, M. Estrada, J. Gibson, D. Karentz, M. A. Van Leeuwe, J. Stefels, C. Widdicombe, and L. Peperzak. 2012. Global marine plankton functional type biomass distributions: Phaeocystis spp. Earth System Science Data **4**:107-120.

Wang, F. Y., R. W. Macdonald, D. A. Armstrong, and G. A. Stern. 2012. Total and Methylated Mercury in the Beaufort Sea: The Role of Local and Recent Organic Remineralization. Environmental Science & Technology **46**:11821-11828.

Wang, W.-X., R. S. K. Wong, J. Wang, and Y.-f. Yen. 2004. Influences of different selenium species on the uptake and assimilation of Hg(II) and methylmercury by diatoms and green mussels. Aquatic Toxicology **68**:39-50.

Watras, C. J., R. C. Back, S. Halvorsen, R. J. M. Hudson, K. A. Morrison, and S. P. Wente. 1998. Bioaccumulation of mercury in pelagic freshwater food webs. Pages 183-208.

Watras, C. J., and N. S. Bloom. 1992. MERCURY AND METHYLMERCURY IN INDIVIDUAL ZOOPLANKTON - IMPLICATIONS FOR BIOACCUMULATION. Pages 1313-1318.

Weng, H. X., Y. M. Zhu, Y. C. Qin, J. Y. Chen, and X. H. Chen. 2008. Accumulation discrepancy of heavy metal and organic pollutants in three near-shore depositional environments, southeastern China. Journal of Asian Earth Sciences **31**:522-532.

Whalin, L., E. H. Kim, and R. Mason. 2007. Factors influencing the oxidation, reduction, methylation and demethylation of mercury species in coastal waters. Marine Chemistry **107**:278-294.

Williams, T. D. 1995. The penguins. Spheniscidae. The penguins. Spheniscidae.:i-xiv, 1-295.

Wood, J. M., F. S. Kennedy, and C. G. Rosen. 1968. Synthesis of Methyl-mercury Compounds by Extracts of a Methanogenic Bacterium. Nature **220**:173.

Wright, D. D., T. K. Frazer, and J. R. Reinfelder. 2010. The influence of river plume dynamics on trace metal accumulation in calanoid copepods. Limnology and Oceanography **55**:2487-2502.

Wu, Y., and W. X. Wang. 2011. Accumulation, subcellular distribution and toxicity of inorganic mercury and methylmercury in marine phytoplankton. Environmental Pollution **159**:3097-3105.

Wu, Y., and W. X. Wang. 2012. Thiol compounds induction kinetics in marine phytoplankton during and after mercury exposure. Journal of Hazardous Materials **217**:271-278.

Yamamoto, Y., K. Honda, and R. Tatsukawa. 1987. Heavy metal accumulation in Antarctic krill Euphausia superba. Proceedings of the NIPR Symposium on Polar Biology:198-204.

Zdanowicz, C., E. M. Krummel, D. Lean, A. J. Poulain, E. Yumvihoze, J. B. Chen, and H. Hintelmann. 2013. Accumulation, storage and release of atmospheric mercury in a glaciated Arctic catchment, Baffin Island, Canada. Geochimica Et Cosmochimica Acta **107**:316-335.

Zhang, T., and H. Hsu-Kim. 2010. Photolytic degradation of methylmercury enhanced by binding to natural organic ligands. Pages 473-476. Nature Geoscience.

Zhang, Y., C. Li, G. Yang, Y. Wang, Z. Tao, Y. Zhang, and A. Wang. 2017. Ontogenetic diet shift in Antarctic krill (Euphausia superba) in the Prydz Bay: a stable isotope analysis. Acta Oceanologica Sinica **36**:67-78.

Zheng, W., and H. Hintelmann. 2009a. Isotope Fractionation of Mercury during Its Photochemical Reduction by Low-Molecular-Weight Organic Compounds. Pages 4246-4253.

Zheng, W., and H. Hintelmann. 2009b. Mercury isotope fractionation during photoreduction in natural water is controlled by its Hg/DOC ratio. Geochimica Et Cosmochimica Acta **73**:6704-6715.

Zhong, H., and W. X. Wang. 2009. Controls of Dissolved Organic Matter and Chloride on Mercury Uptake by a Marine Diatom. Pages 8998-9003. Environmental Science & Technology.